

**RECOMBINANT EXPRESSION AND BAND-GAP ENGINEERING OF THE
BACTERIAL PHOTOSYNTHETIC REACTION CENTRE**

by

Daniel Young Jun

B.Sc., The University of British Columbia, 2011

A THESIS SUBMITTED IN PARTIAL FULFILLMENT OF
THE REQUIREMENTS FOR THE DEGREE OF

DOCTOR OF PHILOSOPHY

in

THE FACULTY OF GRADUATE AND POSTDOCTORAL STUDIES
(Microbiology and Immunology)

THE UNIVERSITY OF BRITISH COLUMBIA
(Vancouver)

April 2017

© Daniel Young Jun, 2017

Abstract

The *Rhodobacter sphaeroides* photosynthetic reaction centre (RC) is a pigment-protein complex that efficiently captures and converts photon energy into a charge-separated state. Given the conversion efficiency and the high electric potential of the electron, the major focus of my project was to deliver/extract electrons to/from various cofactors along the charge-separation pathway in the RC, including the special pair of bacteriochlorophylls (P), the bacteriopheophytin (H_A), the primary quinone (Q_A), and the secondary quinone (Q_B). An over-expression system was created to produce RCs, using the *R. sphaeroides* RCx strain, pIND4 plasmid, a modified culture medium, and changes to growth conditions. These changes resulted in a 35-fold increase in protein levels compared to the previous system. To extract electrons from the quinone region of the RC, this region was made more accessible to the solvent by deleting portions of the H subunit cytoplasmic globular domain. The results indicated that the truncated RC mutants assembled stably and thereby reduced the electron transfer distance between the quinone and an external electron acceptor. Photochronoamperometry measurements on mutant RCs designed to test the feasibility of delivering electrons from an electrode to P showed photocurrent generation and direction that were consistent with the binding of the RC P-side to the electrode surface. Similar experiments on the feasibility of extracting electrons from H_A, Q_A and Q_B, for delivery to highly ordered pyrolytic graphite (HOPG) or gold electrodes, also showed photocurrent generation and direction consistent with the binding of the RC H_A-side or Q-side to the electrode surface. Finally, the thermal stability of complexes was studied by *in vivo* addition of light harvesting complex 1 (LH1) from the thermophile *Thermochromatium tepidum* to the RC. A hybrid core complex consisting of an *R. sphaeroides* RC surrounded by *T. tepidum* TLH1 conferred greater tolerance to thermal energies, compared to the analogous *R. sphaeroides* RC-LH1 core complex, at temperatures up to 70 °C. The combination of these results show that, in principle, the RC can be modified to extract electrons at different energy levels, or band gaps, with possible applications in heat-stable biohybrid solar cell technologies.

Preface

The research presented in this thesis was designed by me with contributions from other coworkers and advice from my supervisor.

A version of sections 3.1 and 4.1 has been published. Jun, D., Saer, R.G., Madden, J.D., and Beatty, J.T. (2014). Use of new strains of *Rhodobacter sphaeroides* and a modified simple culture medium to increase yield and facilitate purification of the reaction centre. *Photosynth Res* 120, 197-205. I conducted the majority of the testing and analysis, and wrote most of the manuscript. A modified form of sections 2.4 and 3.1.3 were written by R.G. Saer.

The entirety of the project in section 3.2 was completed by me alone, including creating constructs, protein purification, and data analysis.

For the project in section 3.3, J. Rogalski (UBC Proteomics Core Facility) collected the mass spectrometry data in Figure 3.14 and wrote the procedure in section 2.9. This project was a collaboration with the Madden laboratory in the Department of Electrical and Computer Engineering at UBC. A. Mahmoudzadeh conducted and collected data for the electrochemistry experiments, including cyclic voltammetry and photochronoamperometry measurements.

In section 3.4, V. Huang contributed to the project by growing cultures, measuring cellular protein levels, mutagenesis, and creating sucrose gradients. A draft of the procedure in section 2.11 was written by V. Huang and revised by me.

Table of Contents

Abstract.....	ii
Preface.....	iii
Table of Contents	iv
List of Tables	viii
List of Figures.....	ix
List of Abbreviations	xii
Acknowledgements	xv
Chapter 1: Introduction	1
1.1 Types of photosynthesis.....	2
1.2 The photosynthetic pigment-protein complexes of <i>Rhodobacter sphaeroides</i>	3
1.3 Reaction centre structure and function.	6
1.4 Electron transfer driving forces and rate kinetics.	10
1.5 Regulation of production of the photosynthetic apparatus.	12
1.6 Comparison of the RC-LH1 core complex of <i>R. sphaeroides</i> and <i>Thermochromatium tepidum</i>	14
1.7 Heterologous expression of genes in <i>R. sphaeroides</i>	17
1.8 Use of photosynthesis proteins in biohybrid solar cells.....	19
1.9 Thesis aims and approach.	20
Chapter 2: Materials and Methods	23
2.1 Bacterial strains and plasmids.....	23
2.2 Genetic manipulations.	31
2.2.1 Creation of the suicide vector pZDJ.	31
2.2.2 Creating the <i>rshI</i> , <i>ppsR</i> , and <i>crtI</i> knockouts, and the <i>crtI^{Pa}</i> knock-in.....	32
2.2.3 Cloning of <i>puhA</i> and <i>pufQBALMX</i>	34
2.2.4 Site-directed mutagenesis.	35
2.2.5 Truncations of the <i>puhA</i> gene.	36
2.2.6 Cloning of <i>TpuhA</i> and <i>TpufBALM</i>	37
2.3 Measurement of LH1 in disrupted cell samples.	40
2.4 Measurement of LH1 in intact cells.....	41

2.5	Purification of the RC and RC-LH1.	41
2.6	Removal of detergent from RCs.	42
2.7	Binding of the ATTO MB2 dye.....	42
2.8	Pigment extraction from RCs and quantification.....	43
2.9	Mass spectroscopy of RCs.....	43
2.10	Electrode preparation for cyclic voltammetry or photochronoamperometry.	43
2.10.1	Cyclic voltammetry.....	44
2.10.2	Photochronoamperometry.....	44
2.11	UV mutagenesis of <i>R. sphaeroides</i>	45
2.12	Heat stability measurements of the core complex.	46
Chapter 3:	Results.....	47
3.1	Recombinant expression of the genes encoding the RC and LH1 photosystems using a modified strain of <i>R. sphaeroides</i>	47
3.1.1	Comparison of inducible expression plasmids for production of pigment-protein complexes.	47
3.1.2	Use of a <i>ppsR</i> gene knockout host strain to boost aerobic production of pigment-protein complexes.	49
3.1.3	Effects of divalent salts in a complex LB-based growth medium on pigment-protein content of cells.	51
3.1.4	Effects of combining the pIND4, <i>ppsR</i> KO, and RLB modifications.	54
3.2	Characterisation of RCs containing a truncated H subunit.....	57
3.2.1	Construction of the 45, 80, and 150 mutants.	57
3.2.2	<i>In vivo</i> measurements of the assembly of truncated RCs.	58
3.2.3	Selection of a secondary mutant and phototrophic growth.....	60
3.2.4	Effect of detergent on stability, and purification of truncated RC and RC-LH1 complexes.	62
3.3	Characterisation of RCs bound to a highly ordered pyrolytic graphite (HOPG) or gold electrode.....	66
3.3.1	Analysis of dye binding to the M256 mutant by SDS-PAGE and mass spectrometry.. ..	67

3.3.2	Surface analysis of an HOPG or gold electrode using cyclic voltammetry.....	71
3.3.3	Photochronoamperometry measurements of SbnI bound to an HOPG or gold electrode.....	77
3.3.4	Addition of Cys near the P region and photochronoamperometry measurements of the TM mutant bound to an HOPG or gold electrode.....	78
3.3.5	Addition of Cys near the H _A region and photochronoamperometry measurements of the M256-Cys and M256/L121-Cys mutants bound to an HOPG or gold electrode.....	83
3.3.6	Addition of Cys near the Q _A region of the truncated 45M RC and photochronoamperometry measurements of the 45M-M229 mutant bound to an HOPG electrode.....	89
3.3.7	Addition of Cys near the Q _B region of the truncated 45M RC and photochronoamperometry measurements of the 45M-L210 and 45M-L210/L213 mutants bound to a gold electrode.....	93
3.4	Recombinant expression of the genes encoding the <i>T. tepidum</i> photosystems using a modified strain of <i>R. sphaeroides</i>	96
3.4.1	Evaluation of a synthetic operon construct of the genes encoding the <i>T. tepidum</i> TRC, purification, and formation of a charge-separated state of the TRC.....	97
3.4.2	Evaluation of synthetic operon constructs and expression of the genes encoding combinations of the <i>R. sphaeroides</i> RC, <i>T. tepidum</i> TRC and TLH1.	100
3.4.3	Effect of the carotenoid spirilloxanthin on TLH1 assembly and levels.....	104
3.4.4	Increasing the levels of TLH1 by UV-mutagenesis and selection for improved phototrophic growth.....	106
3.4.5	Partial purification of RC-TLH1-X ⁺	109
3.4.6	Role of the PufX protein in hybrid core complexes.	110
3.4.7	Spectroscopic analysis of the heat stability of complexes containing <i>T. tepidum</i> pigment-protein complexes.....	112
Chapter 4: Discussion		116
4.1	Advantages of using the pIND4 plasmid, the strain RCx ^R , and the medium RLB for the homologous expression of genes.	116
4.2	Implications of the role of the H subunit in RC assembly and function.....	117

4.2.1	<i>In vivo</i> assembly of the LM, 45, 80, and 150 RC mutants.....	118
4.2.2	Characterisation of the LM, 45, and 80 RC mutants and <i>in vitro</i> charge separation.....	120
4.2.3	Requirement of the H subunit for phototrophic growth.....	121
4.2.4	Role of the cytoplasmic domain of the H subunit.....	123
4.3	Evidence of direct electron transfer to or from multiple cofactor sites in the RC.	124
4.3.1	Electron transfer to and from the special pair P.....	124
4.3.2	Electron transfer from the H _A bacteriopheophytin.	127
4.3.3	Electron transfer from the quinone region.	131
4.4	Expression of <i>T. tepidum</i> TLH1 for the enhanced thermal stability of the core complex.	133
4.4.1	Characterisation of the TRC and <i>in vitro</i> charge separation.....	133
4.4.2	Reduced levels of TLH1 and selection of phototrophy-capable mutants.	135
4.4.3	The PufX protein may not be involved in the assembly of hybrid core complexes.....	136
4.4.4	Thermal stability of hybrid core complexes.	138
Chapter 5: Conclusion and Future Directions		140
References		142
Appendices.....		162
Appendix A.....		162
A.1	RC mutants and corresponding mutations used in the electron transfer studies.....	162
Appendix B.....		163
B.1	Chemical structure of the ATTO MB2 dye with a maleimide functional group.	163
Appendix C.....		164
C.1	CVs of different electron mediators in 1x PBS pH 7.2.....	164
Appendix D.....		165
D.1	Residual plots of the two-phase exponential decay fits.....	165

List of Tables

Table 2.1. Bacterial strains.....	23
Table 2.2. Plasmids.....	24
Table 2.3. Primers used to create pZDJ.....	32
Table 2.4. Primers used to create the <i>rshI</i> and <i>ppsR</i> knockouts, and <i>crtI</i> knock-in.....	33
Table 2.5. Primers used to clone <i>puhA</i> and <i>pufQBALMX</i>	34
Table 2.6. Primers used for site-directed mutagenesis.....	35
Table 2.7. Primers used for making <i>puhA</i> truncations.....	37
Table 2.8. Primers used to clone the <i>T. tepidum</i> genes.....	38
Table 2.9. LEDs used for action spectra measurements.....	45
Table 3.1. Summary of different detergents used to purify the 45 RC mutant.....	63
Table 3.2. Ratios of bacteriochlorophyll (BChl) to bacteriopheophytin (BPhe) of pigments extracted from the wild type (WT) and truncated RC H mutants.....	65
Table 3.3. Predicted and measured molecular weights of the RC subunits and ATTO MB2 dye.....	71
Table 3.4. Two-phase exponential decay fit parameters of the RC-LH1-X ⁺ , RC-LH1-X ⁻ , and RC-TLH1-X ⁺ at 70 °C.....	115

List of Figures

Figure 1.1. A schematic of the photosynthetic machinery in anoxygenic photosynthesis.	4
Figure 1.2. The protein structure of the RC.	7
Figure 1.3. The absorbance spectrum of a wild type RC.	8
Figure 1.4. The difference absorbance spectrum of a wild type RC.	10
Figure 1.5. The cofactors involved in the charge-separation process and their midpoint potentials.	11
Figure 1.6. The chemical structures of the spheroidene and spirilloxanthin and their ketone derivatives.	15
Figure 1.7. The Q_y transition absorbance spectra of the photosystems from <i>R. sphaeroides</i> and <i>T. tepidum</i> (produced in <i>R. sphaeroides</i>).	16
Figure 2.1. Map of the suicide plasmid pZDJ.	32
Figure 3.1. Comparison of LH1 levels using the plasmids pRS1 or pIND4-RC1.	49
Figure 3.2. Comparison of LH1 levels in cultures of <i>R. sphaeroides</i> Δ RCLH Δ rshI and RCx.	51
Figure 3.3. Comparison of LH1 levels due to the effects of divalent cations.	52
Figure 3.4. Comparison of LH1 levels due to the culture media LB and RLB (LB medium supplemented with 810 μ M MgCl ₂ and 510 μ M CaCl ₂).	53
Figure 3.5. Comparison of the growth kinetics and final yields of cell concentrations in different culture conditions.	55
Figure 3.6. Contributions of <i>R. sphaeroides</i> strain, expression plasmid, and culture conditions to the relative amounts of the LH1 complex.	56
Figure 3.7. Predicted structures of the 45, 80, and 150 truncation mutants of the RC H subunit.	58
Figure 3.8. Assembly and <i>in vivo</i> levels of RC truncation mutants.	59
Figure 3.9. Growth curves of the RC truncation mutants under photosynthetic conditions.	61
Figure 3.10. Assembly and formation of a charge-separated state in the RC truncation mutants.	65
Figure 3.11. Absorbance spectra of the 80RC-LH1 PS ⁺ and 150RC-LH1 PS ⁺ core complexes.	66
Figure 3.12. Absorbance spectra of the ATTO MB2 dye (red) and RC (blue).	68
Figure 3.13. SDS-PAGE of conditions tested for the binding of ATTO MB2 to the Cys on M256.	69
Figure 3.14. Mass spectroscopy of the M256 mutant bound to the ATTO MB2 dye.	70

Figure 3.15. CVs of 1 mM ferrocyanide in 10 mM Tris pH 8.0 or 1x PBS pH 7.2 buffer using an HOPG working electrode.....	72
Figure 3.16. CVs of 1 mM ferrocyanide in 1x PBS pH 7.2 buffer using an HOPG working electrode.....	74
Figure 3.17. Schematic of RC binding to an HOPG electrode using <i>N</i> -(1-pyrene)maleimide linkers.....	75
Figure 3.18. CVs of 1 mM ferrocyanide in 1x PBS pH 7.2 buffer using a gold working electrode.....	76
Figure 3.19. Photocurrents generated by SbnI on an HOPG or gold electrode.....	78
Figure 3.20. Structural modifications in the TM RC.....	79
Figure 3.21. Photocurrents generated by the TM mutant on an HOPG or gold electrode.....	81
Figure 3.22. External quantum efficiency (EQE) action spectra of the TM mutant on a gold electrode.....	82
Figure 3.23. Structural modifications in the M256-Cys and M256/L121-Cys mutants.....	84
Figure 3.24. Photocurrents generated by the M256-Cys and M256/L121-Cys mutants on an HOPG or gold electrode.....	87
Figure 3.25. External quantum efficiency (EQE) action spectra of the M256-Cys (A) and M256/L121-Cys (B) on an HOPG electrode.....	89
Figure 3.26. Structural modifications in the 45M-M229 and 45M-M229/M226 mutants.....	90
Figure 3.27. Photocurrents generated by the 45M-M229 mutant on an HOPG electrode.....	91
Figure 3.28. External quantum efficiency (EQE) action spectrum of the 45M-M229 mutant on an HOPG electrode.....	92
Figure 3.29. Structural modifications in the 45M-L210 and 45M-L210/L213 mutants.....	94
Figure 3.30. Photocurrents generated by the 45M-L210 (A) and 45M-L210/L213 (B) mutants on a gold electrode.....	95
Figure 3.31. Assembly and <i>in vivo</i> levels of the RC and TRC.....	99
Figure 3.33. Difference absorbance spectra of the Q _y transition region of the TRC.....	100
Figure 3.34. Schematic of the different <i>T. tepidum</i> and <i>R. sphaeroides</i> gene combinations for protein expression constructs.....	102
Figure 3.35. Assembly and <i>in vitro</i> levels of hybrid RC-TLH1 and TRC-TLH1 complexes. ...	104

Figure 3.36. Assembly and <i>in vitro</i> levels of hybrid RC-TLH1 and TRC-TLH1 complexes due to the carotenoid spirilloxanthin.	106
Figure 3.37. Assembly and <i>in vitro</i> levels of hybrid RC-TLH1 and TRC-TLH1 complexes capable of supporting phototrophic growth.	108
Figure 3.38. Absorbance spectra of RC-LH1-X ⁺ (blue) and RC-TLH1-X ⁺ (red).	110
Figure 3.39. Sucrose gradients of RC-LH1-X ⁺ , RC-LH1-X ⁻ , RC-TLH1-X ⁺ , and RC-TLH1-X ⁻	111
Figure 3.40. Changes in the absorbance profile of RC-LH1-X ⁺ due to thermal denaturation at 70 °C.	113
Figure 3.41. Decay kinetics of the LH1 875 nm peak and the TLH1 915 nm peak due to exposure to heat.	114
Figure 4.1. Proposed electron flow in the TM RC.	126
Figure 4.2. Proposed electron flow in the M256-Cys RC.	128
Figure 4.3. Distance relationship between the H _A bacteriopheophytin, F(L121)W, W(L100), and the electrode.	129
Figure 4.4. Exposure of the Trp at L100.	131
Figure 4.5. Proposed electron flow in the 45M-M229 RC.	132
Figure 4.6. Proposed electron flow in the 45M-L210 or 45M-L210/L213 RC.	133
Figure 4.7. Structures of ubiquinone and menaquinone.	134

List of Abbreviations

μE	Microeinstein
ADP	Adenosine 5' diphosphate
AFM	Atomic force microscopy
Ala	Alanine
Ap ^R	Ampicillin resistance
Arg	Arginine
ATP	Adenosine 5' triphosphate
<i>bch</i>	Operon encoding the bacteriochlorophyll biosynthesis proteins
BChl	Bacteriochlorophyll <i>a</i>
BPhe	Bacteriopheophytin <i>a</i>
BQ	Benzoquinone (cyclohexa-2,5-diene-1,4-dione)
<i>C.</i>	<i>Chloroflexus</i>
CHAPS	3-[(3-Cholamidopropyl)dimethylammonio]-1-propanesulfonate
<i>crt</i>	Operon encoding the carotenoid biosynthesis proteins
CV	Cyclic voltammetry
Cys	Cysteine
cyt	Cytochrome
DDM	<i>N</i> -dodecyl- β -D-maltoside
DMF	Dimethylformamide
DMSO	Dimethyl sulfoxide
DNA	Deoxyribonucleic acid
DNase A	Deoxyribonuclease A
<i>E.</i>	<i>Escherichia</i>
EQE	External quantum efficiency
ETC	Electron transport chain
FWHM	Full width at half maximum
Gn ^R	Gentamycin resistance
<i>hem</i>	Operon encoding the heme biosynthesis proteins
HOPG	Highly ordered pyrolytic graphite

HQ	Hydroquinone (benzene-1,4-diol)
IPTG	Isopropyl β -D-1-thiogalactopyranoside
IR	Infrared
kb	Kilobase
Kn ^R	Kanamycin resistance
LDAO	Lauryldimethylamine- <i>N</i> -oxide
LED	Light emitting diode
LH	Light harvesting
LH1	Light harvesting complex 1
LH2	Light harvesting complex 2
MW	Molecular weight
NADP/H	Nicotinamide adenine dinucleotide phosphate
NTA	Nitrilotriacetic acid
NIR	Near infrared
oPh	<i>o</i> -phenanthroline (1,10-phenanthroline)
PBS	Phosphate-buffered saline
PCR	Polymerase chain reaction
PDB	Protein databank
PGC	Photosynthesis gene cluster
PSI	Photosystem I
PSII	Photosystem II
<i>puc</i>	Operon encoding the LH2 complex proteins
<i>puf</i>	Operon encoding the RC L/M and LH1 complex proteins
<i>puhA</i>	Gene encoding the RC H protein
Q _x	Intermediate energy absorbance band for chlorins
Q _y	Low energy absorbance band for chlorins
<i>R.</i>	<i>Rhodobacter</i>
RC	Reaction centre
Rif ^R	Rifampicin resistance
RPM	Revolutions per minute

SDS-PAGE	Sodium dodecyl sulfate polyacrylamide gel electrophoresis
Ser	Serine
SHE	Standard hydrogen electrode
<i>T.</i>	<i>Thermochromatium</i>
TCEP	3,3',3''-phosphanetriyltripropanoic acid
Tc ^R	Tetracycline resistance
TLH1	<i>Thermochromatium tepidum</i> light harvesting complex 1
TRC	<i>Thermochromatium tepidum</i> reaction centre
Trp	Tryptophan
Tyr	Tyrosine
UPLC	Ultra high performance liquid chromatography
WT	Wild type
X	PufX

Acknowledgements

There are numerous people I would like to thank during my time at UBC, especially in particular, my supervisor Dr. J. Thomas Beatty. He has provided me the opportunity to start my research career back in my undergraduate years and to pick up an ambitious project. Further, he fostered an environment that gave me the freedom to explore and pursue questions for the sake of curiosity. I also thank Jeanette Beatty for her highly thorough and meticulous management of the lab, and patience training me starting from the basics.

I would like to thank my committee members, Drs. Dan Bizzotto, Lindsay Eltis, and Michael Murphy, for their guidance over the years. Your guidance and suggestions have been greatly appreciated, given the high-risk nature and broad, multi-disciplinary aspect of my project.

I am grateful to my colleagues who provided scientific advice and guidance, especially Dr. Rafael Saer, who took me on as his first undergraduate student. I also thank Drs. Hao Ding, Alexander Westbye, Cedric Brimacombe, Marek Kobylarz, Paul Fogg, and Paul Jaschke. I have enjoyed our non-scientific discussions that would make me look forward to each day.

I thank Dr. William Ramey for having introduced me to scientific research and Dr. Thomas Beatty during my undergraduate years. Without this connection, I'm sure life will have led me on a completely different track.

To the biophotovolatics group, I thank Dr. John Madden and his laboratory for access to resources and expertise, in particular, Drs. Ali Mahmoudzadeh, Ashwin Usgaocar, and Jo Slotanewson. I am grateful for your patience working with finicky biological proteins that never really ever behaved properly.

I am deeply indebted to Julie Hemily, Michelle Dunn, Angele Arrieta, and Rebecca Smyth, for their continued emotional and mental support, especially in times of difficulty.

To the late Dr. Neil Mackenzie – thank you for sharing your Monday mornings where we swapped stories from our weekend adventures and planned new ones. Life is too short and fleeting, and you are a constant reminder to pursue our passions.

I also thank my family, and friends who have joined me on numerous adventures for taking me away from the lab at the most opportune times.

Chapter 1: Introduction

With environmental issues stemming from the extraction and use of fossil-fuelled energy sources, many research groups have been developing alternative and sustainable energies including solar technologies (Dresselhaus and Thomas, 2001). Sunlight is an abundant and reliable source of energy, with more than enough energy in one hour of solar illumination to meet the demands of global energy usage in a year (Barber, 2009), but it is dilute and varies in intensity depending on geographical location, seasonal fluctuations, and weather. Among the possible improvements of solar cells is to increase the efficiency of devices that capture photons and produce electrical energy (Alharbi and Kais, 2015; Blankenship et al., 2011). One approach is to create a hybrid biological photovoltaic (*i.e.*, biohybrid) device that couples biological components to electrodes (Kim et al., 2014; Ravi and Tan, 2015). Therefore, some research has focused on photosynthetic proteins in bacteria. Phototrophic microorganisms have optimised systems to capture light at multiple wavelengths and low intensities, including the photosynthetic reaction centre (RC) of *Rhodobacter sphaeroides*. This purple non-sulphur bacterium is a model organism used widely for photosynthesis studies: the genome sequence is available (Kontur et al., 2012; Mackenzie et al., 2001), there is a rich history of spectroscopic data of wild type and mutant RCs (Martin et al., 1986; Williams et al., 1992; Zhu et al., 2013), and several high resolution crystal structures of photosynthesis-related proteins exist (Allen et al., 1987a, b; Koepke et al., 2007).

Over billions of years and a constant supply of photons bombarding the planet every day, through natural selection driving evolutionary change, Nature has arrived at a variety of efficient photosystems to capture light and create high energy bonds that are used to drive cellular reactions for metabolism. This process, called photosynthesis, is one of the most fundamental processes that support life as we see today. One definition of photosynthesis is the fixation of inorganic carbon, primarily CO₂, coupled with the splitting of water catalysed by light energy, to produce carbohydrates and gaseous oxygen as the carbon source for growth and waste by-product, respectively (Calvin and Benson, 1948). Chemically reductive carbon fixation through photosynthesis is balanced against oxidative cellular respiration, and this constant reduction and oxidation of carbon drives life on Earth (Falkowski et al., 2000).

1.1 Types of photosynthesis.

Despite the common definition of photosynthesis described above, the term photosynthesis is also used in a looser sense to describe life that can use light as the major form of energy to drive cellular metabolism without the actual “synthesis” of reduced carbon (*i.e.*, phototrophic growth) (Gest, 1993). Using the broader definition, organisms that can photosynthesise are divided into two categories of photosynthesis: oxidative photophosphorylation and anoxygenic photophosphorylation.

As the name implies, in oxidative photophosphorylation, oxygen is evolved in the process that results in the phosphorylation of ADP. Organisms that use this process, such as plants, algae, and cyanobacteria, are photoautotrophs and use light energy to produce ATP and reducing power to produce NADPH for reduction of CO₂ to create glucose. There are two pigment-protein supramolecular complexes, called Photosystem I (PSI) and Photosystem II (PSII), that carry out the light energy transduction reactions. The core of these photosystems is a photochemical reaction centre (RC). In what is termed the light-dependent reactions, the main function of PSII is to absorb light and to split a water molecule as a source of electrons for an electron transport chain (ETC) that creates a proton gradient to synthesise ATP; PSI obtains electrons from PSII and reduces NADP⁺ to form NADPH. ATP and NADPH are used in the light-independent reactions of the Calvin-Benson cycle to fix CO₂ and generate carbohydrate for cellular metabolism and energy storage (Allen, 2003).

Anoxygenic photophosphorylation, a process in which oxygen is not evolved, is carried out by a variety of bacteria including the purple sulphur and non-sulphur bacteria. Unlike in oxygenic photophosphorylation, water is not required as an electron source by the RC pigment-protein complex. Instead, during photoautotrophic growth an inorganic substance such as H₂, H₂S or Fe²⁺ is oxidised as a source of electrons, and CO₂ is the source of cellular carbon. During photoheterotrophic growth, an organic compound is oxidized to provide both electrons and carbon for metabolic intermediates. The RC will be described in more detail in a subsequent section, but in short, the RC captures light to drive electron transfer reactions. A key distinction is that in oxidative photophosphorylation the flow of electrons is linear from H₂O to NADP⁺, whereas in anoxygenic photophosphorylation electrons may cycle between the RC and the ETC. The outcome, nonetheless, is similar in that electrons are transported through an ETC to

translocate protons from the cytoplasm to the periplasm and create an electrochemical gradient for ATP generation (Hu et al., 2002; McEwan, 1994).

In both oxygenic and anoxygenic photophosphorylation, the heart is the RC complex of proteins, pigments, and other cofactors. The fundamental drive behind the photochemistry, irrespective of the type of RC, is due to Gibbs free energy. Because of finely-tuned systems of slight dielectric, electrostatic, and conformational differences in the surrounding protein environment, each cofactor in the complex has a higher affinity for electrons than the preceding cofactor (Guo et al., 2012; Pan et al., 2016; Pan et al., 2013; Saggu et al., 2014); in other words, successive electron acceptors are more electronegative (*i.e.*, have a more positive midpoint potential). Hence, the free energy change, ΔG , is negative and therefore the reaction spontaneously is favoured in the forward direction, towards the separation of charge and ultimately, the reduction of the terminal electron acceptor (Jones, 2009).

1.2 The photosynthetic pigment-protein complexes of *Rhodobacter sphaeroides*.

The metabolically versatile α -proteobacterium *R. sphaeroides* can respire aerobically as well as carry out anoxygenic photophosphorylation. Under decreasing oxygen concentrations the organism responds through tightly regulated processes by undergoing physiological changes, characterised by the invagination of the cytoplasmic membrane to form vesicle-like structures that, upon release from cells after cell disruption, are called chromatophores (Niederman, 2016).

Within the lipid bilayer and lumen of each spherical chromatophore are proteins that contribute to anoxygenic photophosphorylation, including the RC, light harvesting complexes 1 (LH1) and 2 (LH2), cytochrome c_2 (cyt c_2), cytochrome bc_1 (cyt bc_1), and ATP synthases (Geyer and Helms, 2006; Scheuring et al., 2014). The cell membrane invaginations that give rise to the chromatophore pseudo-organelle increase the available surface area for the capture of light, facilitated initially by the LH1 and LH2 complexes that enhance photon capture and transfer the energy to the RC via a Förster resonance energy transfer mechanism (Strumpfer and Schulten, 2009). The subsequent conversion of light energy into a charge-separated state in the RC, followed by the translocation of protons from the cytoplasm through the cyt bc_1 complex into the periplasmic space, forms an electrochemical gradient that is used to create ATP for cellular processes. A schematic of the photosynthetic membrane and machinery is shown in Figure 1.1.

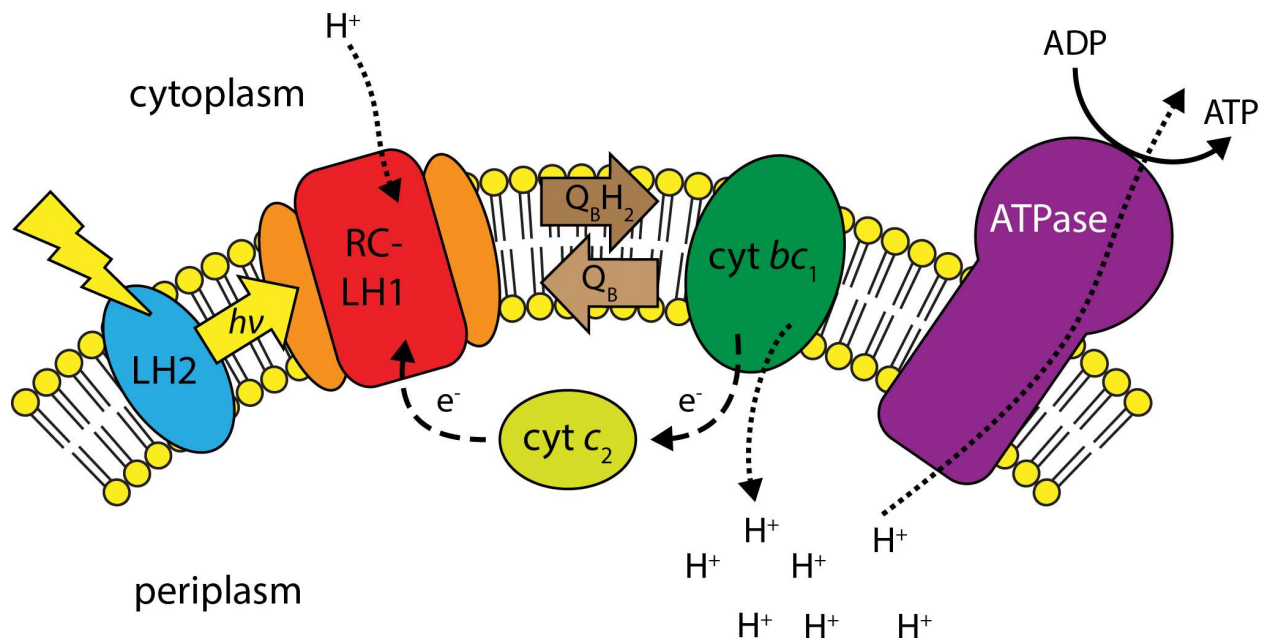


Figure 1.1. A schematic of the photosynthetic machinery in anoxygenic photosynthesis. Light is absorbed by LH1 and LH2, which transfer the energy to the RC. A charge-separated state is formed within the RC that results in the reduction of Q_B and the uptake of two protons after two cycles. Q_BH_2 diffuses into the Q-pool in the membrane, where it is taken up by *cyt bc₁*, which translocates the protons across the membrane, forming a proton gradient that drives the phosphorylation of ADP.

LH2 is an antenna complex that functions solely to increase the spectrum of light that can be absorbed and to pass excitation energy to the RC-LH1 complex. Comprised of eight or nine pairs of $\alpha\beta$ polypeptide subunits, these heterodimers form the ring structure of LH2, in which each pair binds three bacteriochlorophylls and a carotenoid. Two of the bacteriochlorophylls are in close contact and absorb maximally at 850 nm, and the third bacteriochlorophyll absorbs at 800 nm (Olsen et al., 2008). LH2 rings are independent of other light-absorbing complexes, and are the predominant component of chromatophores obtained from cells grown under low light intensity and in the absence of oxygen (Woronowicz et al., 2012).

Similarly, LH1 is another antenna complex that extends the absorbance spectrum of *R. sphaeroides*. LH1, too, functions to absorb light and transfer the energy to the RC, but it

additionally is a relay for energy transfer between LH2 and the RC. The LH1 $\alpha\beta$ polypeptide subunits bind a pair of interacting bacteriochlorophylls that absorb at 875 nm and a single carotenoid, but do not form independent ring structures like LH2. Rather, LH1 assembles a ring of 12 to 14 heterodimers around each RC, in concert with the PufX protein to form an S-shaped structure, resulting in a dimeric structure called the RC-LH1 core complex (Qian et al., 2005; Qian et al., 2013). The exact function of PufX is unclear, but it is proposed that PufX is necessary to form the dimeric form of the core complex, as without it the monomeric form is produced (Holden-Dye et al., 2008). Furthermore, the dimeric form is needed for photosynthetic growth, and it is thought that PufX enables quinones to diffuse in and out of the core complex (Qian et al., 2013). Most of the protein components of the core complex are transcribed as part of the *pufBALMX* operon, and the presence of an intercistronic stem-loop between the genes encoding LH1 (*pufBA*) and the RC (*pufLM*) in the mRNA transcript is an important component in maintaining the correct ratio of LH1 to RC message segments, and therefore the correct ratio of LH1 to RC proteins (Chen et al., 1988).

The structure and function of the RC will be described in greater detail in the next section, but in brief, this complex is at the heart of photosynthesis and its role is to convert light energy into a chemical form. As energy is passed from LH2 and LH1 to the RC, the energy is absorbed by a special pair of RC bacteriochlorophylls, resulting in the excitation of an electron. The electron initiates a series of redox reactions that ultimately results in the reduction of the secondary quinone, coupled with the uptake of a proton. The cycle occurs twice to reduce the secondary quinone and begin the process of translocating protons across the membrane (Okamura et al., 2000).

After the doubly-reduced quinone diffuses out of the RC and into the quinone pool in the membrane, the molecule makes its way to cyt *bc*₁. The cyt *bc*₁ multi-subunit complex is an oxidoreductase that reduces and oxidises quinones to pump protons across the intracytoplasmic membrane into the periplasm via a Q-cycle mechanism, thus forming a proton gradient. The complex also reduces cyt *c*₂, an electron carrier that cycles between being reduced by cyt *bc*₁ and reducing the RC special pair (Brandt and Trumpower, 1994; Esser et al., 2008). *Rhodobacter* species may contain a membrane-bound cytochrome *c*_γ that compensates for the absence of cyt *c*₂ (Daldal et al., 2001), but because this is not relevant to my work I will refer to cyt *c*₂ as the

electron carrier from cyt bc_1 to the RC in the following pages. The continuous translocation of protons by light-driven electron transfer processes during photoheterotrophic growth maintains a proton-motive force across the intracytoplasmic membrane. The F_0F_1 -ATP synthase uses the proton gradient across the membrane to synthesise ATP, completing the process involved in anoxygenic photophosphorylation (Feniouk et al., 2002).

1.3 Reaction centre structure and function.

The fundamental role of the RC is to convert light energy into chemical potential energy with a $\sim 100\%$ quantum efficiency (Blankenship, 2002), and therefore has been the focus of many structural, functional, and electron transfer studies in the past decades. Some of the work done previously has investigated the effects of electron transfer due to mutations that exclude (Khatypov et al., 2005; McAuley et al., 2000; Watson et al., 2005a) or substitute cofactors (Katilius et al., 1999; Kirmaier et al., 1991; van Brederode et al., 1999), and those that promote electron transfer down the usually inactive B-branch (Wakeham and Jones, 2005). Mutations that impede proton transfer in existing pathways in the protein have also been studied (Adelroth et al., 2001; Paddock et al., 2003b). Other groups have focused on studying the structural side of the protein by genetically making larger-scale mutations that replaced several transmembrane helices (Robles et al., 1990) or swapped domains (Tehrani et al., 2003), or used biochemical techniques to remove entire subunits (Agalidis and Reiss-Husson, 1983).

The RC complex is comprised of three individual polypeptides, called H, L and M, for heavy, light and medium, respectively. The naming scheme was a result of the apparent masses on the basis of protein band migration in SDS-PAGE, but later data showed that the apparent masses do not correspond to the genuine masses (Michel et al., 1986); nonetheless, the naming convention remains. The H subunit consists of two domains: an N-terminal non-cleaved signal-like sequence that forms a transmembrane helix, and a cytoplasmic globular domain. In contrast, the homologous L and M subunits are composed of five transmembrane helices arranged in a two-fold symmetry, that form a matrix in which the cofactors are held (Allen et al., 1987b). The cofactors consist of a dimer of bacteriochlorophylls, termed the special pair (P), two accessory bacteriochlorophylls (B_A and B_B), two bacteriopheophytins (H_A and H_B), two quinones (Q_A and Q_B), one non-heme iron, and one carotenoid. These cofactors function in using light energy to

mediate a charge-separated state through a series of redox reactions that are well-insulated by the surrounding RC protein; the pigments, excluding the carotenoid, are arranged symmetrically between two branches, A and B, with the special pair located on the P-side (periplasmic side) of the RC and the quinones at the Q-side (cytoplasmic side). Despite the symmetry, only the A-branch is active (Allen et al., 1987a). The cartoon representation of the RC subunits and cofactors based on the crystal structure from PDB 2J8C is displayed in Figure 1.2.

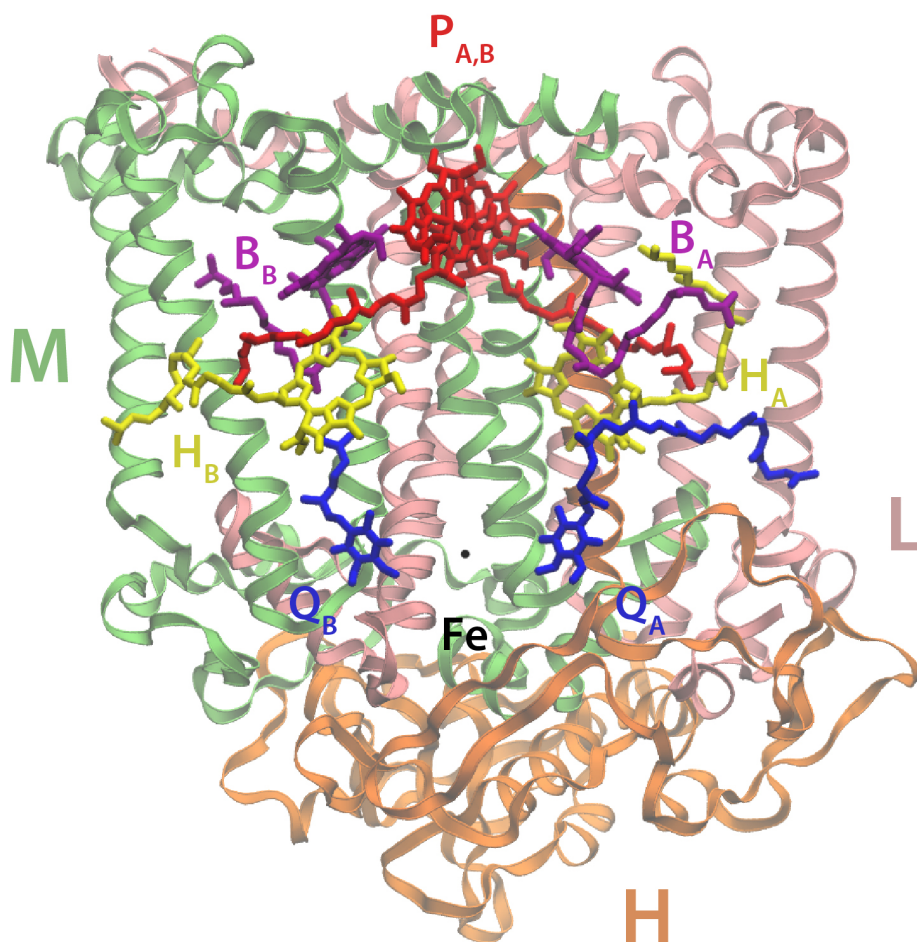


Figure 1.2. The protein structure of the RC. Three subunits make up the complex: H (orange), L (pink) and M (green). Within the RC are ten cofactors: special pair bacteriochlorophylls, P (red); accessory bacteriochlorophylls, B_A and B_B (purple); bacteriopheophytins, H_A and H_B (yellow); quinones, Q_A and Q_B (blue); and a non-heme iron (black). The carotenoid is not shown. The figure is based on PDB 2J8C.

The RC cofactors produce a characteristic absorbance spectrum, shown in Figure 1.3. There are seven major peaks that correspond to different components of the RC. The protein subunits absorb primarily at 280 nm, mainly due to contributions from aromatic amino residues, such as Trp, Tyr, and Phe (Goodwin and Morton, 1946). All the bacteriochlorophylls and bacteriopheophytins absorb at 370 nm, producing the Soret band. The 500 to 650 nm region is termed the Q_x transition region. The bacteriopheophytins (H_A , H_B) absorb around 540 nm and the bacteriochlorophylls (P , B_A , B_B) around 600 nm. There is a minor contribution due to the spheroidenone carotenoid at 500 nm. The near-infrared (NIR) region of 700 to 950 nm is known as the Q_y transition region, where the H_A and H_B bacteriopheophytins absorb primarily at 760 nm. The bacteriochlorophylls absorb farther to the red, where the accessory bacteriochlorophylls (B_A and B_B) contribute to the dominant peak at 804 nm and the special pair P absorb around 865 nm (Jones, 2009).

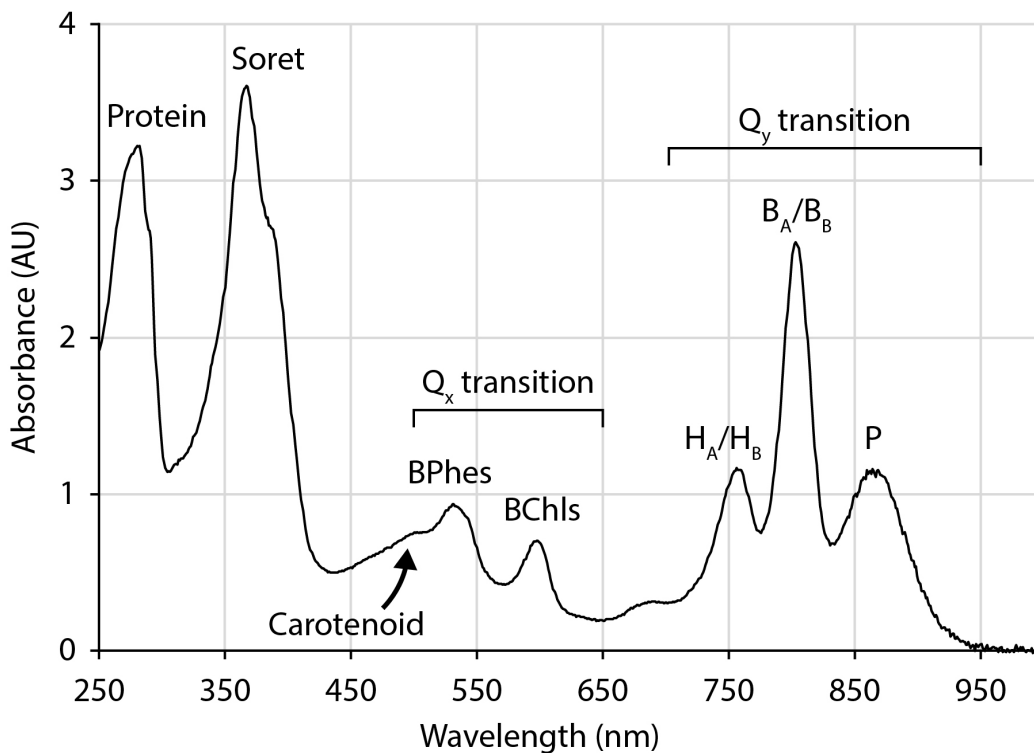


Figure 1.3. The absorbance spectrum of a wild type RC. The characteristic absorbance peaks are due to the contributions from the embedded pigments. The Q_x transition region spans from 500 to 650 nm and the Q_y region from 700 to 950 nm.

The pathway through which the RC converts light energy into a charge-separated state has been investigated thoroughly (Savikhin and Jankowiak, 2014; Warshel et al., 1988). The RC harnesses photons initially in the special pair on the P side where photon energy is transformed into an electron-excited state, called P*. The strongly reducing electron of ~ -1 V versus the Standard Hydrogen Electrode (SHE) is transferred from P* down the A branch in the L subunit, in a series of oxidation and reduction reactions, as it passes through the accessory bacteriochlorophyll (B_A), followed by the bacteriopheophytin (H_A), before reaching the primary quinone (Q_A) on the Q side of the RC, resulting in the charge-separated state. The electron moves from Q_A⁻ to the secondary quinone (Q_B), forming P⁺Q_B⁻, followed by a subsequent proton uptake to neutralise the radical state of Q_B⁻. The cycle repeats after P⁺ is reduced by an electron from cyt *c*₂. Research groups have investigated and determined the proton and electron transfer pathways, in which Q_B is doubly reduced upon receiving two electrons and two protons to form Q_BH₂ that diffuses out of the RC (Adelroth et al., 2000; Ishikita and Knapp, 2005; Paddock et al., 2003a). The formation of a charge-separated state can be measured by difference absorbance spectroscopy (Figure 1.4), where the P-band at 865 nm is completely bleached, and an electrochromic absorbance change results from a blue-shift of the B-band at 804 nm and the red-shift of the 760 nm H-band (Tiede et al., 1996).

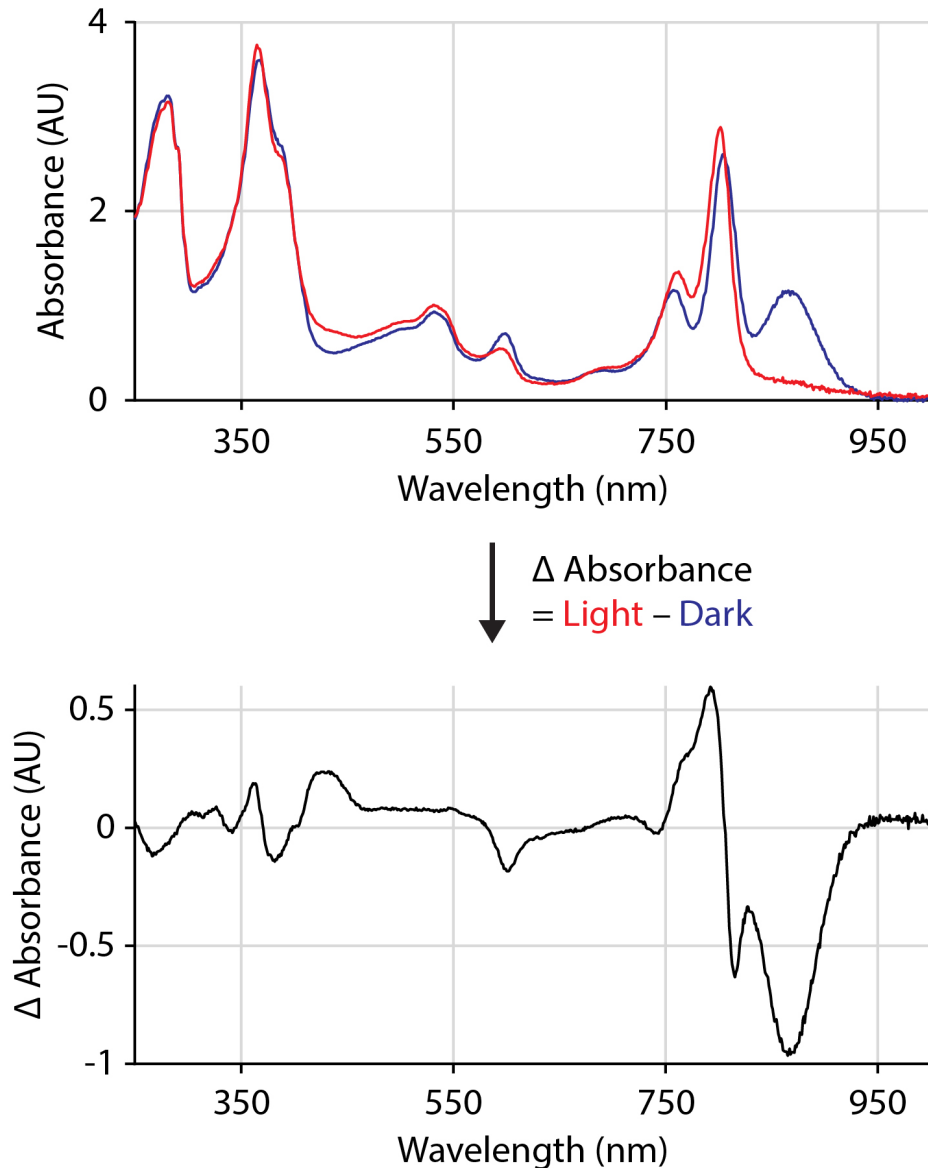


Figure 1.4. The difference absorbance spectrum of a wild type RC. The absorbance changes depending on whether it is in the ground dark-adapted state (blue) or excited light-adapted state (red). The difference absorbance spectrum (black) is created by subtracting the dark-adapted state from the light-adapted state.

1.4 Electron transfer driving forces and rate kinetics.

Naturally, the question that arises is how electron transfer redox reactions occur, especially when the bacteriochlorophylls have the same reduction potential in solution, and the same pigments are arranged symmetrically in two branches. The general understanding is that

the protein milieu and other cofactors surrounding the pigments, namely the dielectric, electrostatic and hydrogen bonding forces are responsible for shifting the midpoint potential, therefore the free energies, and driving the reaction forward towards the charge-separated state with a near unity quantum efficiency (Guo et al., 2012; Jankowiak et al., 2016). A visual schematic of the electron transfer pathways and relationship between the midpoint potentials are shown in Figure 1.5. Furthermore, electron transfer is predominantly down the A-branch, as the redox potential of B_B is higher (*i.e.*, more electropositive) than that of P, making the reaction thermodynamically unfavourable (Dylla et al., 2016; Frolov et al., 2005).

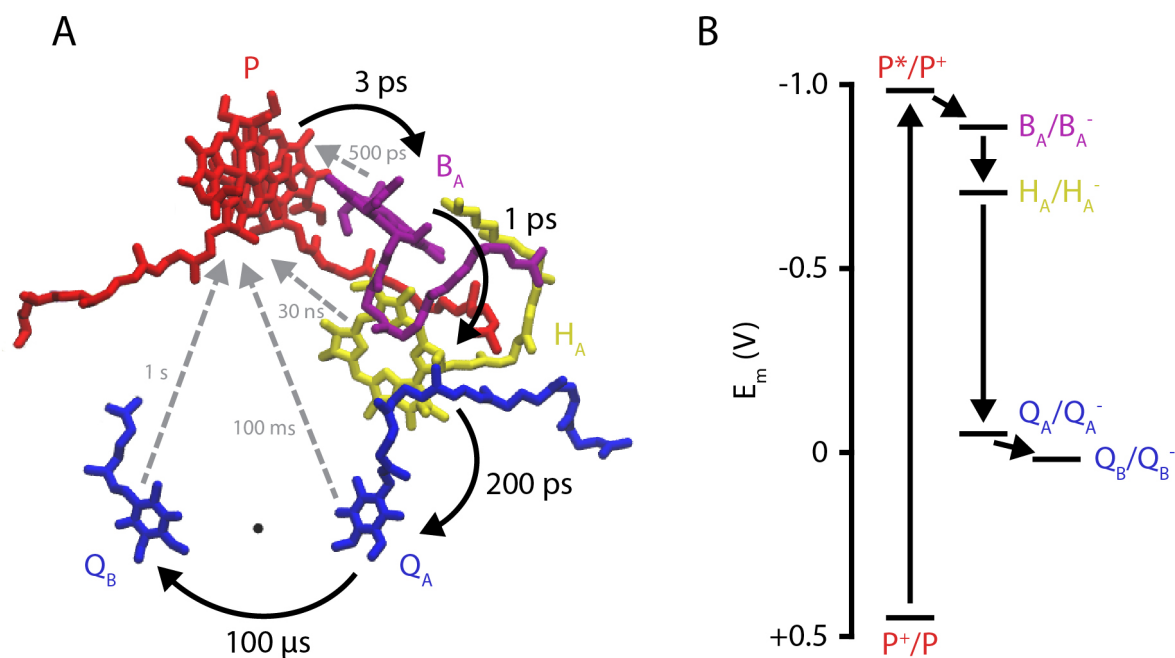


Figure 1.5. The cofactors involved in the charge-separation process and their midpoint potentials. A) Only the pigments involved in the charge-separation process are shown. The experimentally-derived rate constants are denoted with black arrows; and the reverse recombination rates from each cofactor to ground state are shown in grey. B) The approximate midpoint potentials of the different cofactors in the A-branch of the RC.

However, thermodynamics alone does not describe the electron transfer rates. For this, Marcus theory is used to elucidate the rates of biological electron transfer between the donor and acceptor molecules in proteins (Marcus, 1992). In short, the equation can be simplified to

$$k_{\text{ET}} \propto ce^{-\beta\delta} \exp\left(-\frac{(\Delta G + \lambda)^2}{4\lambda k_{\text{B}}T}\right)$$

where k_{ET} describes the rate of an electron tunnelling event. The parameters in the equation show how electron rates decrease exponentially through a medium, β , across a distance, δ , and the relationship between the driving force of the reaction, ΔG , and the reorganisation energy, λ (Winkler and Gray, 2014). In terms of the electron transfer events in the RC, the near-perfect quantum yield in forming a charge-separated state is thought to occur because the forward reactions out-compete the recombination reactions, because the latter reactions are in the inverted regime. The inverted regime is a phenomenon where electron rates begin to decrease with increasingly more negative ΔG values (Moser et al., 1992). Furthermore, the amino acids Trp and Tyr have been used to bridge the distance between an electron donor and acceptor, thus accelerating electron flow through a protein (Reeder et al., 2012; Shih et al., 2008).

1.5 Regulation of production of the photosynthetic apparatus.

The photosynthesis pigment and protein biosynthesis genes are arranged in a 66.7 kb photosynthesis gene cluster (PGC) on chromosome 1 of *R. sphaeroides*. The LH1, RC L and M subunits, and PufX are encoded in the *puf* operon. The gene encoding the RC H subunit, *puhA*, is found 38 kb away. The LH2 genes are expressed as part of the *puc* operon, located even further from the *puf* operon, and genes for the biosynthesis of carotenoid (*crt*) and bacteriochlorophylls (*bch*) are located in several operons in the PGC between the *puf* and *puhA* genes (Choudhary and Kaplan, 2000; Naylor et al., 1999).

Expression of the genes in the PGC is controlled by redox-sensing, which is affected by oxygen levels in the cell. Several systems have been well-characterised, including the two-component signal transduction system of RegB/RegA (Elsen et al., 2004), which controls the expression of photosystem protein and pigment components. Other regulators, such as PpsR,

largely control pigment synthesis (Elsen et al., 2005), and Fnr controls the metabolic processes in the transition between aerobic respiration and anoxygenic photophosphorylation (Arai et al., 2008; Zeilstra-Ryalls and Kaplan, 1995). Of these three systems, only the mechanism of PpsR will be discussed, because I created and exploited a *ppsR* mutation in my work.

PpsR negatively represses the expression of bacteriochlorophyll (*bch*), heme (*hem*), and carotenoid (*crt*) biosynthetic genes under aerobic conditions. In other words, biosynthesis of photosynthesis pigments increases with decreasing oxygen tension, which is thought to have arisen from natural selection because the interaction between bacteriochlorophyll, light and oxygen results in the production of reactive oxygen species, potentially causing oxidative damage to the cell (Elsen et al., 2005; Pemberton et al., 1998). It appears that PpsR can “sense” oxygen and heme in the cell (Yin et al., 2012). Under aerobic conditions, PpsR adopts a conformation that favours binding to the promoter region of *bch*, *hem* and *crt* genes, and prevents RNA polymerase from binding and initiating transcription. The exact mechanism is unclear, but the latest data suggest that under aerobic conditions PpsR forms a dimer of tetramers and tightly binds to DNA as an octamer (Elsen et al., 2005; Winkler et al., 2013). The protein contains an intramolecular disulphide bond and it has been proposed that the reduced or oxidised state of the bond depends on cytoplasmic oxygen levels (Cho et al., 2004). It is under debate whether the Cys react directly with oxygen and heme, or if PpsR also responds to another signal of the cytoplasmic redox potential by interaction with the blue-light-sensing flavoprotein AppA (Kim et al., 2006).

As the concentration of oxygen decreases, levels of PpsR decrease and the blue-light sensing AppA protein levels increase. AppA forms a complex with a dimer of PpsR, and recent research shows that this complex has a higher affinity for promoter DNA sequences that may displace the PpsR octamer in the dark and prevent transcription initiation. Upon illumination under anaerobic conditions, absorption of light by the AppA-PpsR complex results in allosteric structural changes that decrease the affinity of the complex for DNA, which allows for induction of the transcription of photosynthesis pigment biosynthesis genes (Winkler et al., 2013).

1.6 Comparison of the RC-LH1 core complex of *R. sphaeroides* and *Thermochromatium tepidum*.

Thermochromatium tepidum is a thermophilic purple sulphur γ -proteobacterium, first isolated from a hot spring in Yellowstone US National Park that grows optimally at 50 °C, in comparison to 30 °C for the mesophile *R. sphaeroides* (Madigan, 1984). As *T. tepidum* is capable of phototrophic growth, there has been some interest and a few studies elucidating the mechanisms that confer heat tolerance to the photosynthetic machinery, which would enhance the lifetime of proteins operating at elevated temperatures, and could be exploited in applications such as solar cells.

Like *R. sphaeroides*, *T. tepidum* produces an RC (called the TRC hereon), but the TRC is more similar to that from *Blastochloris viridis* (Roszak et al., 2012). Like the *R. sphaeroides* RC the TRC is comprised of three polypeptides (H, L, M) and ten cofactors (bacteriochlorophylls, bacteriopheophytins, quinones, carotenoid, and non-heme iron), but is also associated with a tightly-bound, membrane associated tetra-heme cyt *c* on the periplasmic side. Additionally, like *B. viridis*, *T. tepidum* produces two different quinones, such that ubiquinone is found in the Q_B pocket, whereas menaquinone binds in the Q_A pocket. Lastly, a different type of carotenoid, spirilloxanthin/2,2'-diketo-spirilloxanthin, is produced and assembled in the TRC, in lieu of the spheroidene/spheroidenone present in *R. sphaeroides* (Niwa et al., 2014). The ketone form is synthesised under aerobic conditions by the monooxygenase CrtA (Lee et al., 2010). The structure of spirilloxanthin is similar to spheroidene, but contains an extra carbon to lengthen the molecule and three additional double bonds (10 versus 13) or four in the ketone form (11 versus 15) (Chi et al., 2015), thus further conjugating the π -orbital electrons and red-shifting the absorbance bands. The 2-D structures of these carotenoids are shown in Figure 1.6.

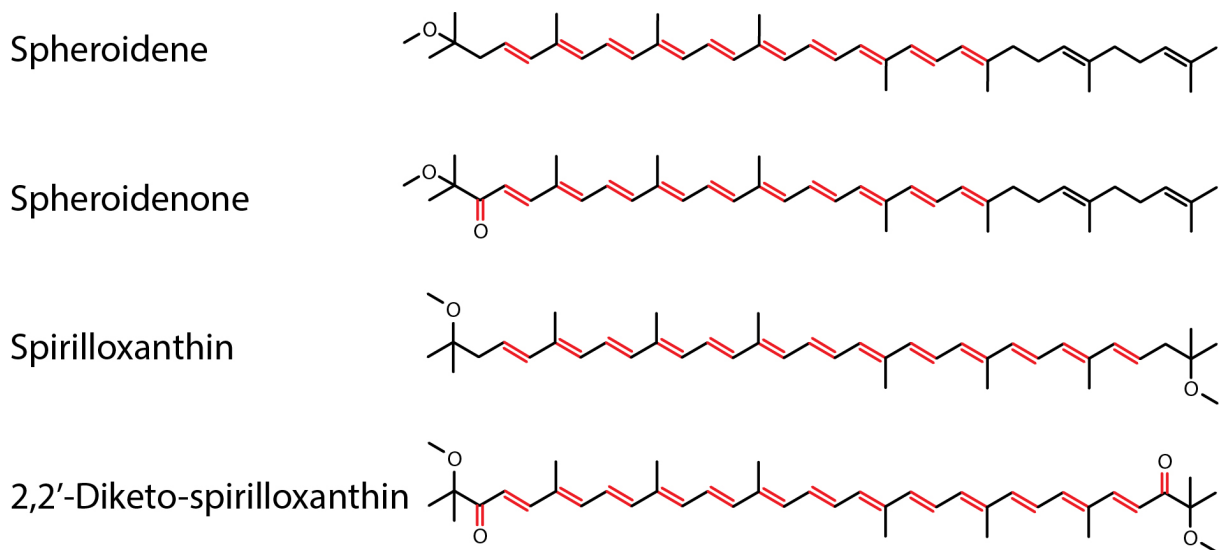


Figure 1.6. The chemical structures of the spheroidene and spirilloxanthin and their ketone derivatives. The conjugated double bonds are shown in red.

The *T. tepidum* LH1 (called TLH1 from hereon) is comprised of α and β polypeptide subunits and forms a core complex with the TRC, similar to that of *Rhodospseudomonas palustris* (Roszak et al., 2003). Unlike the core complex of *R. sphaeroides*, there is no PufX homologue and therefore the core complex is a single TRC surrounded by 16 TLH1. As noted above, it is thought that the role of PufX in RC-LH1 core complexes is to permit quinones to diffuse in and out of the supracomplex. Without a PufX-like or protein W-like (in *R. palustris*) polypeptide to allow for quinones to diffuse through the LH1 ring, a different mechanism appears to be used by *T. tepidum*. The crystal structure of the *T. tepidum* core complex was recently solved and shows that the TLH1 ring contains channels between each $\alpha\beta$ pair through which quinones are thought to diffuse (Niwa et al., 2014).

The dark-adapted absorbance spectra of the RC and TRC in the Q_y transition region are nearly identical, other than a red-shift of the P-band from 865 nm, as typically measured in the *R. sphaeroides* RC, to 870 nm in the TRC. The accessory bacteriochlorophyll B-band absorbance peaks in the TRC are slightly blue-shifted from 804 to 800 nm and the bacteriopheophytins remain at 760 nm. The TLH1 is greatly red-shifted from 875 to 915 nm. A comparison of the differences between the photosystem absorbance peaks is shown in Figure 1.7. The addition of Ca^{2+} ions to the purified TLH1 red-shifts the spectral peak from 880 nm to 915 nm (Ma et al.,

2008). Other divalent cations, such as Mn^{2+} and Sr^{2+} , have been used to modulate the absorbance shift, but none shifted the peak as much as Ca^{2+} (Jakob-Grun et al., 2012; Kimura et al., 2012). The cause of the shift by the binding of Ca^{2+} may be due to the result of the bacteriochlorophyll macrocycle distortion and increase in strength of a H-bond between the β -polypeptide and the bacteriochlorophyll (Jakob-Grun et al., 2012; Ma et al., 2009).

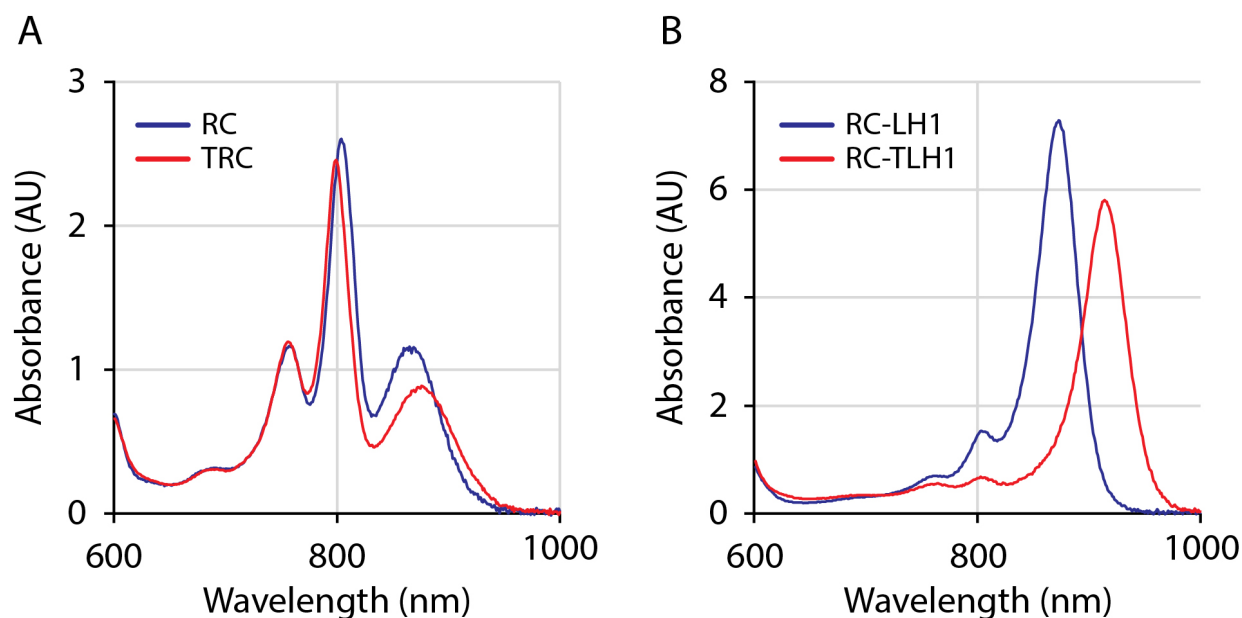


Figure 1.7. The Q_y transition absorbance spectra of the photosystems from *R. sphaeroides* and *T. tepidum* (produced in *R. sphaeroides*). A) The spectra show the RC (blue) and the TRC (red) with the shift of the TRC accessory bacteriochlorophyll B-band to 800 nm and special pair bacteriochlorophyll P-band to 870 nm. B) The RC-LH1 core complex is displayed in blue and the RC-TLH1 in red with the TLH1 peak shifted to 915 nm.

Despite the fact that *T. tepidum* is a thermophile, the stability of the TRC in isolation from other proteins has not been found to be significantly higher than the RC from *R. sphaeroides*; this indicates that the heat tolerance of the TRC is not due solely to the complex itself, but perhaps a contribution of several factors such as membrane lipid composition and interaction with other protein complexes (Kobayashi et al., 2005). It was surmised that the presence of charged Arg residues at the interface between the TRC and the phosphate group of the phospholipid contributes to the heat stability of the pigment-protein complex (Nogi et al.,

2000), but this speculation was disproven recently when similar homologous mutations were made in the RC and did not increase tolerance to heat (Watson et al., 2005b). It was suggested that the interaction of the TRC with the surrounding TLH1 is the biggest contributing factor to the stability of the core complex at temperatures up to 50 °C (Kobayashi et al., 2005); further analysis indicated that Ca²⁺ ions within the TLH1 structure also improve stability (Kimura et al., 2009).

It is difficult to perform genetic work on *T. tepidum*, in contrast to *R. sphaeroides*, as there are no plasmids described in the literature that the organism will maintain; furthermore, *T. tepidum* is an obligate anaerobe and requires 50 °C for optimal growth, making it technically difficult to work on. Hence, making site-directed mutations to study structural and functional aspects of the protein or even adding a His-tag to expedite purification was cumbersome and time-consuming, if not impossible. In order to overcome these difficulties in the genetic study of the *T. tepidum* photosystem, it was decided to express the system in the genetically tractable organism *R. sphaeroides* (Jun et al., 2014).

1.7 Heterologous expression of genes in *R. sphaeroides*.

Given that the overexpression of genes encoding membrane proteins can be challenging, there is a need for new techniques and approaches to obtain a more efficient system amenable to DNA cloning, cell transformation, and protein isolation (Bernaudat et al., 2011; Freigassner et al., 2009; Schlegel et al., 2014). *R. sphaeroides* provides a tractable platform for the production of modified native and foreign membrane proteins. In particular, due to the naturally-occurring and large membrane surface area provided by the invaginations of the intracytoplasmic membrane, yielding chromatophores upon cell disruption, there is considerable interest in optimising the expression of genes encoding integral and peripheral membrane proteins (Laible et al., 2004). Furthermore, chromatophores can be readily isolated and proteins solubilised through the use of several different types of detergents (Feher, 1971; Qian et al., 2005; Reed and Clayton, 1968); for example, depending on the type and strength of the detergent, RCs lacking one or both LH complexes can be isolated.

The native photosynthesis protein-encoding genes in *R. sphaeroides* have previously been expressed using a broad host-range vector, such as plasmid pRK404 or pRK415. The

expression plasmid pRS1 was derived from pRK415, and places the control of the *puhA* and *pufQBALMX* genes under the hypoxia-inducible *puc* promoter (Jaschke et al., 2011). However, there are several issues with the use of the pRS1 protein expression system. Primarily, the low plasmid copy number of 4 to 7 in *E. coli* and *R. sphaeroides* and its large size of approximately 16 kb make DNA isolation and cloning difficult, as well as the fact that the plasmid is somewhat unstable (Keen et al., 1988). Additionally, the use of the *puc* promoter requires cultures to be grown in low oxygen or anaerobic, photoheterotrophic conditions for induction, which make it more difficult to cultivate and obtain biomass compared to culture growth under aerobic conditions. These drawbacks apply to other pRK404- and pRK415-derived plasmids that utilise *puc* and/or *puf* promoters for transcription of genes.

The gene expression plasmid pIND4 contains an IPTG-inducible, T7-derived promoter (Ind et al., 2009). This narrow-host-range vector was created from the naturally occurring plasmid pMG160 of *Rhodobacter blasticus* and technical advantages over pRK-derived plasmids are attained given its smaller size of approximately 8 kb, copy number of 18 to 23 versus 4 to 7 for pRK415, and the IPTG-inducible promoter (Inui et al., 2003). However, the frequency of conjugal transfer of pIND4 and derivatives from *E. coli* to *R. sphaeroides* is very inefficient compared to plasmids such as pRS1 that contain the RK2 origin of transfer (*oriT*), due to the lack of compatible plasmid mobilising genes (Simon et al., 1983). Electroporation or chemical transformation may be used to introduce plasmids into *R. sphaeroides* (Donohue and Kaplan, 1991), but the presence of the restriction endonuclease, RshI, places limits on sequences containing the enzyme recognition sequence 5'-CGATCG-3' (Lynn et al., 1979).

Another benefit of using a *R. sphaeroides* system to produce membrane proteins is the increased lipid bilayer content of the intracytoplasmic membrane. The increase in membrane content and chromatophore biogenesis of the intracytoplasmic membrane is believed to be due to the synthesis and insertion of the photosynthetic pigment-protein complexes (Chandler et al., 2008; Niederman, 2013). Any strategies that involve the incorporation of foreign membrane-integral proteins into the intracytoplasmic membrane should take photosystems into account, to find the balance between maximum surface area of the intracytoplasmic membrane and level of the protein of study. In fact, data show that a strain lacking just LH2 (*i.e.*, RC⁺, LH1⁺, LH2⁻) produced similar levels of heterologously expressed protein as a strain lacking all photosystems

(*i.e.*, RC⁻, LH1⁻, LH2⁻); (Hanson et al., 2009); this enables the flexibility of growing cultures under aerobic or anaerobic and phototrophic conditions when trying to synthesise proteins sensitive to oxygen. Finally, the purification of membrane proteins has been facilitated by the use of protein-tag affinity chromatography (Goldsmith and Boxer, 1996).

1.8 Use of photosynthesis proteins in biohybrid solar cells.

Due to the near unity internal quantum efficiency of RC-catalysed conversion of a photon absorption into a charge-separated state (Blankenship, 2002), there has been considerable interest in harnessing this efficiency for use of photosynthesis proteins in solar cells and light sensors. As Nature has already created a highly efficient system, this can be used to our advantage in creating a device that separates charge over a large physical distance and maximises the charge-recombination time (*i.e.*, minimises the probability of charge-recombination, which lowers overall efficiency). Generally, research has focused on PSI and PSII of plants and cyanobacteria, or RCs and LH complexes of bacteria (Blankenship et al., 2011; Kim et al., 2014; Operamolla et al., 2015; Ravi and Tan, 2015; Yehezkeli et al., 2014).

Many different approaches have been used to create biological photoelectrochemical cells: 1) free-floating RCs in the electrolyte (Takshi et al., 2010); 2) RCs bound to electrodes directly (den Hollander et al., 2011; Mirvakili et al., 2014; Yaghoubi et al., 2012) or with a linker (Kondo et al., 2012; Kondo et al., 2007; Mahmoudzadeh et al., 2011; Trammell et al., 2006; Trammell et al., 2004); 3) RCs embedded in nanoporous structures (Lu et al., 2005; Oda et al., 2010); 4) RCs coated onto an electrode using the Langmuir-Blodgett method (Kamran et al., 2014; Kamran et al., 2015); and 5) RCs in a completely solid-state device without any charge mediators (Das et al., 2004). The diversity of these configurations and different techniques indicate the huge number of options and potential challenges in optimising the best conditions for using RCs in biohybrid solar cells, with some of the approaches and strategies described below. Chiefly, the goal is to maintain protein structure and function, and efficiently extract charges upon formation of the charge-separated state.

Most of the early work focused on the RC, due to its versatility and plasticity, and strategies in the last 10 years focused on different aspects of the biohybrid cell. For example, due to the narrow absorbance spectrum range of the RC, more light can be absorbed by using the RC-

LH1 core complex (Yaghoubi et al., 2015). Another key factor in photocurrent generation is the electron transfer rate between the RC and electrode. Generally, electron transfer rates increase exponentially with linear decreases in the distance between an electron donor and acceptor, hence there continues to be work on binding the RC closer to an electrode to accelerate the rate of electron flow (den Hollander et al., 2011). Other approaches involve modifying the electrodes or electrolyte by using selective semiconductor electrodes or charge mediators with optimal redox potentials to minimise parasitic side-reactions (Tan et al., 2012; Tan et al., 2013). Lastly, better protein loading or multi-layers of proteins are other methods explored to increase photocurrents (Giustini et al., 2012; Zhao et al., 2002). The latest results of using RC-LH1 complexes bound to a semi-porous, nanostructured electrode have shown currents of up to 416 $\mu\text{A}/\text{cm}^2$, the largest reported in the literature (Friebe et al., 2016).

1.9 Thesis aims and approach.

Much of the previous research on RC has focused predominantly on either the internal electron transfer processes within the RC or the engineering aspect of attaching wild type RCs to an electrode to create a biohybrid solar cell. Little research has explored bridging the two paths, such as genetically modifying the RC to generate photocurrents by extracting charges at different regions of the protein. Given that two-thirds of the electron energy is lost by the time it reaches Q_B (Figure 1.5), greater electrical potential would be gained by extracting the electron at an earlier cofactor in the charge-separation pathway, leading to greater photovoltages during photocurrent generation upon illumination.

Biohybrid solar cells could be created with RC mutants containing artificial electron transfer pathways in the RC that would improve the efficiency of electron transfer from the cofactors buried within the RC to and/or from electrodes. For example, it might be possible to redirect the electron pathway from H_A to Q_A such that direct electron transfer from H_A to an external electrode is favoured over transfer to Q_A . Also, because direct electron transfer is several orders of magnitude faster than the diffusion of charge mediators (Frew and Hill, 1988), the strategy of minimising distance from a cofactor to an electrode could increase the device efficiency in converting light into electrical current. The focus of my research was to answer the question of whether electrons within the RC could be extracted at different energy levels

associated with the cofactors at P, H_A, Q_A, and Q_B, to an external electron acceptor – in other words, band-gap engineering of the RC.

I also aimed to increase the levels of the RC complex in the bacterial cell by using genetic techniques and culture medium optimisation. This was multi-pronged approach and involved using the IPTG-inducible plasmid pIND4, making the new strain *R. sphaeroides* RCx (by knocking out the restriction endonuclease RshI, and the pigment synthesis repressor PpsR), supplementing LB medium with divalent salts, and changing growth from semi-aerobic to aerobic conditions.

My research investigated the feasibility of creating artificial electron transfer pathways in several regions of the RC. An RC lacking all the native Cys was used as starting material, and Cys were added back to the particular regions of study. Cys contains a thiol moiety that can be used for sulphur chemistry, such as forming a covalent thiol-ether bond to a linker adsorbed onto an electrode surface. For studying the P or H_A regions of the RC, Cys was added back to each region in order to minimise the distance between the electron donor or acceptor and electrode to ideally less than 10 Å. The pathways were further modified by introducing Trp residues to bridge the distance between donor and acceptor, to possibly increase transfer rates, using a rationale based on the work of Harry Gray (Shih et al., 2008). Several types of electrodes were evaluated, and cyclic voltammetry and photochronoamperometry measurements were used to characterise electrode surfaces and the response of biohybrid solar cells to illumination.

The Q_A and Q_B RC regions studied required drastic modification of the RC by removing portions of the cytoplasmic globular domain of the H subunit. The truncations were made to decrease the distance between the Q_A and Q_B RC regions and the protein surface. Although these RC H truncations resulted in large changes to the RC structure, I discovered which portions of the H subunit were required for assembly of the RC under aerobic, heterotrophic conditions or under anaerobic, phototrophic conditions. I used the same techniques to study the light-dependent responses of biohybrid solar cells that incorporated these H-truncated RCs. The results from these experiments provided insight on whether these RC mutants could be used in applications, such as creating a light-dependant biosensor, or fabricating a biohybrid solar cell.

Finally, given that proteins would be subject to thermal and light denaturation when a biohybrid solar cell is exposed to sunlight under actual working conditions, I started initial work

on using my mesophilic *R. sphaeroides* system as a way to express photosynthesis genes from a thermophile. An RC-LH1 core complex resistant to heat was designed by heterologously expressing in *R. sphaeroides* the genes encoding the RC and LH1 photosystems from the thermophilic purple sulphur bacterium, *T. tepidum*.

Chapter 2: Materials and Methods

2.1 Bacterial strains and plasmids.

A list of strains is given in Table 2.1. *E. coli* DH5 α was used for cloning and site-directed mutagenesis, and *E. coli* DH5 α λ pir to propagate the suicide plasmid pZDJ; *E. coli* S17-1 and *E. coli* S17-1 λ pir were used as conjugative plasmid donors; and *R. sphaeroides* Δ RCLH, which lacks all phototrophic pigment-protein complexes, was used as the background strain for several gene knockouts.

E. coli was grown at 37 °C in lysogeny broth (LB), defined as 1% tryptone, 0.5% yeast extract, and 1% NaCl. The media were supplemented as appropriate with 150 μ g/mL ampicillin for the pTZ18U/pTZ19U cloning vectors, 10 μ g/mL gentamicin for the suicide plasmid pZDJ, 10 μ g/mL tetracycline for maintenance of plasmid pRS1, or 50 μ g/mL kanamycin for pIND4 derivatives.

R. sphaeroides was grown at 30 °C in LB or a modified medium RLB, which is LB with the addition of 810 μ M MgCl₂ and 510 μ M CaCl₂ (Jun et al., 2014). Liquid cultures of *R. sphaeroides* were grown in Erlenmeyer flasks shaken at 150 RPM and filled to 80% (for semi-aerobic growth) or 20% (for aerobic growth) of the nominal capacity for the pIND4 IPTG-induction studies. For anaerobic, photoheterotrophic growth, cultures were inoculated in 16.5 mL screw-cap tubes or plates in anaerobic jars, and grown in temperature controlled aquariums at 30 °C and 75 μ E M⁻² s⁻¹ light intensity with illumination provided by tungsten filament lamps. Large scale aerobic cultures for protein purification were grown Erlenmeyer flasks filled to 25% of the nominal capacity with RLB and shaken at 200 RPM. Media were supplemented as appropriate with 20 μ g/mL gentamicin for the suicide plasmid pZDJ, 2 μ g/mL tetracycline for maintenance of plasmid pRS1, 25 μ g/mL kanamycin for pIND4 derivatives, or 10 μ g/mL rifampicin for the *R. sphaeroides* RCx^R strain.

Table 2.1. Bacterial strains.

Strain	Description	Reference
<i>E. coli</i>		
DH5 α	Chemically competent	(Hanahan, 1983)
DH5 α λ pir	Chemically competent, <i>pir</i>	Biomedal (Spain)

Strain	Description	Reference
S17-1	Chemically competent	(Simon et al., 1983)
S17-1 λ pir	Chemically competent, <i>pir</i>	Biomedal (Spain)
<i>R. sphaeroides</i>		
Δ RC ⁻ LH1 ⁻ LH2 ⁻	RC ⁻ , LH1 ⁻ , LH2 ⁻	(Tehrani and Thomas Beatty, 2004)
Δ RC ⁻ LH1 ⁻ LH2 ⁻ <i>rshI</i>	RC ⁻ , LH1 ⁻ , LH2 ⁻ , RshI ⁻	This study
RCx	RC ⁻ , LH1 ⁻ , LH2 ⁻ , RshI ⁻ , PpsR ⁻ , Rif ^S	This study
RCx ^R	RC ⁻ , LH1 ⁻ , LH2 ⁻ , RshI ⁻ , PpsR ⁻ , Rif ^R	This study
RCx ^R Δ <i>crtI</i>	RC ⁻ , LH1 ⁻ , LH2 ⁻ , RshI ⁻ , PpsR ⁻ , Rif ^R , CrtI ⁻	This study
RCx ^R Δ <i>crtI::crtI^{Pa}</i>	RC ⁻ , LH1 ⁻ , LH2 ⁻ , RshI ⁻ , PpsR ⁻ , Rif ^R , CrtI ⁻ , CrtI ^{Pa+} (expresses the <i>crtI</i> gene of <i>Pantoea agglomerans</i>)	This study

A list of plasmids used is given in Table 2.2. The plasmid pRS1 containing the *puhA* gene and *pufQBALMX* operon encoding the RC and LH1 protein structural subunits (Jaschke et al., 2011), was introduced into *R. sphaeroides* strain Δ RC⁻LH1⁻LH2⁻ by conjugation. The pIND4 derivatives were mobilised into *R. sphaeroides* Δ RC⁻LH1⁻LH2⁻*rshI*, RCx, RCx^R, or RCx^R Δ *crtI::crtI^{Pa}* by electroporation using a 2 mm electroporation cuvette, and a single shock of 2.5 kV, 25 μ F, and 400 Ω (Donohue and Kaplan, 1991).

Table 2.2. Plasmids.

Plasmid	Description	Reference
pTZ18U	Cloning vector, Ap ^r	Pharmacia (USA)
pTZ19U	Cloning vector, Ap ^r	Pharmacia (USA)
pTZN	pTZ18U with the SphI site changed to NcoI	This study
pZDJ	Suicide vector with the <i>tetA</i> promoter driving <i>sacB</i> , R6K <i>oriV</i> , Gm ^R	(Brimacombe et al., 2013)

Plasmid	Description	Reference
pZDJ:: Δ <i>rshI</i>	pZDJ containing the flanking regions of <i>rshI</i>	This study
pZDJ:: Δ <i>ppsR</i>	pZDJ containing the flanking regions of <i>ppsR</i>	This study
pZDJ:: Δ <i>crtI</i>	pZDJ containing the flanking regions of <i>crtI</i>	This study
pZDJ:: Δ <i>crtI</i> :: <i>crtI</i> ^{Pa}	pZDJ with the coding region of <i>crtI</i> replaced with <i>crtI</i> ^{Pa}	This study
pTZN:: <i>puhA</i>	pTZN containing the <i>R. sphaeroides puhA</i> gene (0.8 kb) as a NcoI-BamHI fragment with a 6-His tag on the C-terminus	This study
pTZN:: <i>cys</i> ⁻ <i>puhA</i>	pTZN:: <i>puhA</i> containing C156A, and C234S mutations	This study
pTZN:: <i>cys</i> ⁻ A51C <i>puhA</i>	pTZN:: <i>cys</i> ⁻ <i>puhA</i> containing an A51C mutation	This study
pTZN:: <i>45puhA</i>	pTZN containing the first 135 bases of the <i>R. sphaeroides puhA</i> gene as a NcoI-BamHI fragment with a 6-His tag on the C-terminus	This study
pTZN:: <i>45,6H</i> ⁻ <i>puhA</i>	pTZN:: <i>45puhA</i> with the 6-His tag removed	This study
pTZN:: <i>80puhA</i>	pTZN containing the first 240 bases of the <i>R. sphaeroides puhA</i> gene as a NcoI-BamHI fragment with a 6-His tag on the C-terminus	This study
pTZN:: <i>80,6H</i> ⁻ <i>puhA</i>	pTZN:: <i>80puhA</i> with the 6-His tag removed	This study
pTZN:: <i>150puhA</i>	pTZN containing the first 450 bases of the <i>R. sphaeroides puhA</i> gene as a NcoI-BamHI fragment with a 6-His tag on the C-terminus	This study
pTZN:: <i>TpuhA</i>	pTZN containing the <i>T. tepidum TpuhA</i> gene (0.8 kb) as a NcoI-BamHI fragment with a 6-His tag on the C-terminus	This study
pTZ18U:: <i>puf</i>	pTZ18U containing the <i>R. sphaeroides pufQBALMX</i> operon (3.2 kb) as a BamHI-HindIII fragment	This study

Plasmid	Description	Reference
pTZ19U:: <i>puf</i>	pTZ18U containing the <i>R. sphaeroides</i> <i>pufQBALMX</i> operon (3.2 kb) as a BamHI-HindIII fragment	This study
pTZ18U:: <i>pufLM</i>	pTZ18U containing the <i>R. sphaeroides</i> <i>pufLM</i> genes (1.7 kb) as a BamHI-HindIII fragment	This study
pTZ18U:: <i>cys⁻pufLM</i>	pTZ18U:: <i>pufLM</i> containing C(L92)C, C(L108)S, and C(L247)S mutations	This study
pTZ18U::TGA,6H <i>pufLM</i>	pTZ18U:: <i>pufLM</i> containing a stop codon upstream of <i>pufL</i> and a 6-His tag on the C-terminus of <i>pufM</i>	This study
pTZ18U::12H <i>pufLM</i>	pTZ18U:: <i>pufLM</i> with a 12-His tag on the C-terminus of the M subunit	This study
pTZ18U:: <i>cys⁻12H<i>pufLM</i></i>	pTZ18U::12H <i>pufLM</i> containing C(L92)C, C(L108)S, and C(L247)S mutations	This study
pTZ18U::TM	pTZ18U:: <i>cys⁻pufLM</i> containing E(L72)C, N(L274)C, and E(M100)C mutations	This study
pTZ18U::M256	pTZ18U:: <i>cys⁻pufLM</i> containing W(M252)F, M(M256)C, A(M260)W mutations	This study
pTZ18U::M256-Cys	pTZ18U::M256 containing a W(L59)C mutation	This study
pTZ18U::M256/L121	pTZ18U::M256 containing an F(L121)W mutation	This study
pTZ18U::M256/L121-Cys	pTZ18U::M256/L121 containing a W(L59)C mutation	This study
pTZ18U::M229	pTZ18U:: <i>cys⁻12H<i>pufLM</i></i> containing an F(M229)C mutation	This study
pTZ18U::M229/M226	pTZ18U::M229 containing a V(M226)W mutation	This study

Plasmid	Description	Reference
pTZ18U::L210	pTZ18U::cys ^{-12H} <i>pufLM</i> containing a D(L210)C mutation	This study
pTZ18U::L210/L213	pTZ18U::L210 containing a D(L213)W mutation	This study
pTZ19U:: <i>TpufL</i>	pTZ19U containing the <i>T. tepidum</i> <i>TpufL</i> gene (0.8 kb) as a BamHI-XbaI fragment	This study
pTZ19U:: <i>TpufM</i>	pTZ19U containing the <i>T. tepidum</i> <i>TpufM</i> gene (1.0 kb) as a XbaI-HindIII fragment	This study
pTZ19U::B- <i>TpufM</i>	pTZ19U:: <i>TpufM</i> with an internal BamHI site removed	This study
pTZ19U:: <i>TpufLM</i>	pTZ19U containing the BamHI-XbaI fragment from pTZ19U:: <i>TpufL</i> and the XbaI-HindIII fragment from pTZ19U::B- <i>TpufM</i>	This study
pTZ19U::5' <i>TpufBALM</i>	pTZ19U:: <i>TpufLM</i> containing <i>TpufBA</i> (0.6 kb) upstream of <i>TpufL</i> with <i>T. tepidum</i> ribosomal binding sites	This study
pTZ19U::rbs <i>TpufBALM</i>	pTZ19U::5' <i>TpufBALM</i> with artificial ribosomal binding sites	This study
pTZ19U::Rs <i>TpufBA pufLMX</i>	pTZ19U containing the <i>R. sphaeroides</i> <i>pufQBALMX</i> operon (3.2 kb) as a BamHI-HindIII fragment with <i>pufBA</i> replaced with <i>T. tepidum</i> <i>TpufBA</i>	This study
pTZ19U::Rs <i>TpufBA pufLM</i>	pTZ19U containing the <i>R. sphaeroides</i> <i>pufQBALM</i> operon (2.9 kb) as a BamHI-HindIII fragment with <i>pufBA</i> replaced with <i>T. tepidum</i> <i>TpufBA</i>	This study

Plasmid	Description	Reference
pTZ19U::Rs <i>TpufBALM</i> <i>pufX</i>	pTZ19U containing the <i>R. sphaeroides</i> <i>pufQBALMX</i> operon (3.2 kb) as a BamHI-HindIII fragment with <i>pufBALM</i> replaced with <i>T. tepidum TpufBALM</i>	This study
pTZ19U::Rs <i>TpufBALM</i>	pTZ19U containing the <i>R. sphaeroides</i> <i>pufQBALM</i> operon (2.9 kb) as a BamHI-HindIII fragment with <i>pufBALM</i> replaced with <i>T. tepidum TpufBALM</i>	This study
pRK415	Broad-host-range expression vector, Tc ^R	(Keen et al., 1988)
pATP19P	pRK415 containing the <i>R. sphaeroides puc</i> promoter as a 0.75 kb HindIII fragment	(Tehrani and Thomas Beatty, 2004)
pRS1	pATP19P containing the <i>R. sphaeroides puhA</i> gene (1.3 kb) as a BamHI-SacI fragment with a 6-His tag on the C-terminus and the <i>pufQBALMX</i> operon (3.6 kb) as a SacI-EcoRI fragment	(Jaschke et al., 2011)
pIND4	<i>R. sphaeroides</i> expression vector, Kn ^R	(Ind et al., 2009)
pIND4-RC	pIND4 containing the NcoI-BamHI fragment from pTZN:: <i>puhA</i> and the BamHI-HindIII fragment pTZ18U:: <i>pufLM</i>	This study
pIND4-RC1	pIND4 containing the NcoI-BamHI fragment from pTZN:: <i>puhA</i> and the BamHI-HindIII fragment pTZ18U:: <i>puf</i>	This study
pIND4-LM	pIND4 containing the BamHI-HindIII fragment pTZ18U::TGA,6H <i>pufLM</i>	This study
pIND4-45	pIND4 containing the NcoI-BamHI fragment from pTZN:: <i>45puhA</i> and the BamHI-HindIII fragment pTZ18U:: <i>pufLM</i>	This study

Plasmid	Description	Reference
pIND4-45M	pIND4 containing the NcoI-BamHI fragment from pTZN::45,6H $\overline{}$ <i>puhA</i> and the BamHI-HindIII fragment pTZ18U::12H <i>pufLM</i>	This study
pIND4-80	pIND4 containing the NcoI-BamHI fragment from pTZN::80 <i>puhA</i> and the BamHI-HindIII fragment pTZ18U:: <i>pufLM</i>	This study
pIND4-80M	pIND4 containing the NcoI-BamHI fragment from pTZN::80,6H $\overline{}$ <i>puhA</i> and the BamHI-HindIII fragment pTZ18U::12H <i>pufLM</i>	This study
pIND4-150	pIND4 containing the NcoI-BamHI fragment from pTZN::150 <i>puhA</i> and the BamHI-HindIII fragment pTZ18U:: <i>pufLM</i>	This study
pIND4-45RC1	pIND4 containing the NcoI-BamHI fragment from pTZN::45 <i>puhA</i> and the BamHI-HindIII fragment pTZ18U:: <i>puf</i>	This study
pIND4-80RC1	pIND4 containing the NcoI-BamHI fragment from pTZN::80 <i>puhA</i> and the BamHI-HindIII fragment pTZ18U:: <i>puf</i>	This study
pIND4-150RC1	pIND4 containing the NcoI-BamHI fragment from pTZN::150 <i>puhA</i> and the BamHI-HindIII fragment pTZ18U:: <i>puf</i>	This study
pIND4-TM	pIND4 containing the NcoI-BamHI fragment from pTZN:: <i>cys</i> $\overline{}$ <i>puhA</i> and the BamHI-HindIII fragment pTZ18U::TM	This study
pIND4-M256	pIND4 containing the NcoI-BamHI fragment from pTZN:: <i>cys</i> $\overline{}$ <i>puhA</i> and the BamHI-HindIII fragment pTZ18U::M256	This study

Plasmid	Description	Reference
pIND4-M256-Cys	pIND4 containing the NcoI-BamHI fragment from pTZN:: <i>cys</i> ⁻ <i>puhA</i> and the BamHI-HindIII fragment pTZ18U::M256-Cys	This study
pIND4-M256/L121	pIND4 containing the NcoI-BamHI fragment from pTZN:: <i>cys</i> ⁻ <i>puhA</i> and the BamHI-HindIII fragment pTZ18U::M256/L121	This study
pIND4-M256/L121-Cys	pIND4 containing the NcoI-BamHI fragment from pTZN:: <i>cys</i> ⁻ <i>puhA</i> and the BamHI-HindIII fragment pTZ18U::M256/L121-Cys	This study
pIND4-45M-M229	pIND4 containing the NcoI-BamHI fragment from pTZN:: <i>45,6H</i> ⁻ <i>puhA</i> and the BamHI-HindIII fragment pTZ18U::M229	This study
pIND4-45M-M229/M226	pIND4 containing the NcoI-BamHI fragment from pTZN:: <i>45,6H</i> ⁻ <i>puhA</i> and the BamHI-HindIII fragment pTZ18U::M229/M226	This study
pIND4-45M-L210	pIND4 containing the NcoI-BamHI fragment from pTZN:: <i>45,6H</i> ⁻ <i>puhA</i> and the BamHI-HindIII fragment pTZ18U::L210	This study
pIND4-45M-L210/L213	pIND4 containing the NcoI-BamHI fragment from pTZN:: <i>45,6H</i> ⁻ <i>puhA</i> and the BamHI-HindIII fragment pTZ18U::L210/L213	This study
pIND4-TRC	pIND4 containing the NcoI-BamHI fragment from pTZN:: <i>TpuhA</i> and the BamHI-HindIII fragment pTZ19U::TRC	This study
pIND4-rbsTRCT1	pIND4 containing the NcoI-BamHI fragment from pTZN:: <i>TpuhA</i> and the BamHI-HindIII fragment pTZ19U::5'rbsTRCT1	This study

Plasmid	Description	Reference
pIND4-RCT1X ⁺	pIND4 containing the NcoI-BamHI fragment from pTZN:: <i>puhA</i> and the BamHI-HindIII fragment pTZ19U:: <i>RCT1X</i> ⁺	This study
pIND4-RCT1X ⁻	pIND4 containing the NcoI-BamHI fragment from pTZN:: <i>puhA</i> and the BamHI-HindIII fragment pTZ19U:: <i>RCT1X</i> ⁻	This study
pIND4-TRCT1X ⁺	pIND4 containing the NcoI-BamHI fragment from pTZN:: <i>TpuhA</i> and the BamHI-HindIII fragment pTZ19U:: <i>TRCT1X</i> ⁺	This study
pIND4-TRCT1X ⁻	pIND4 containing the NcoI-BamHI fragment from pTZN:: <i>TpuhA</i> and the BamHI-HindIII fragment pTZ19U:: <i>TRCT1X</i> ⁻	This study

2.2 Genetic manipulations.

2.2.1 Creation of the suicide vector pZDJ.

The new suicide vector, pZDJ, was derived from the plasmid pZDJ29a (J. Jiang and C.E. Bauer, unpublished). The *Rhodobacter capsulatus puc* promoter driving transcription of the *sacB* gene was replaced with a *tetA* promoter from the broad-host-range vector pRK415, allowing for constitutive expression of the *sacB* gene and for use of this vector in other Gram-negative bacteria (Larsen et al., 2002), such as *R. sphaeroides*.

A list of primers used to create pZDJ is shown in Table 2.3. The plasmid pZDJ29a was linearized with ApaI and inverse PCR-amplified using the primer set sacB:accC1 ApaLI-MfeI F and sacB:accC1 ApaLI-MfeI R. This reaction yielded an ApaLI-MfeI fragment, with the *R. capsulatus puc* promoter removed. The *tetA* promoter from the broad-host-range vector pRK415 was PCR-amplified using the primers tetAp MfeI-ApaLI F and tetAp MfeI-ApaLI R, generating an MfeI-ApaLI fragment. These two PCR fragments were digested with ApaLI and MfeI, ligated together, and transformed into *E. coli* DH5 α λ pir, resulting in the 4.8 kb suicide vector pZDJ (Figure 2.1).

Table 2.3. Primers used to create pZDJ.

Primer Name	Sequence (5' → 3')
sacB:accC1 ApaLI-MfeI F	GAATTCGTGCACATGAACATCAAAAAGTTTGC
sacB:accC1 ApaLI-MfeI R	GAATTCCAATTGTTAGGTGGCGGTACTTG
tetAp MfeI-ApaLI F	GAATTCCAATTGATGATTCTCCGCCAGCAT
tetAp MfeI-ApaLI R	GAATTCGTGCACCCTCCGGACCAGC

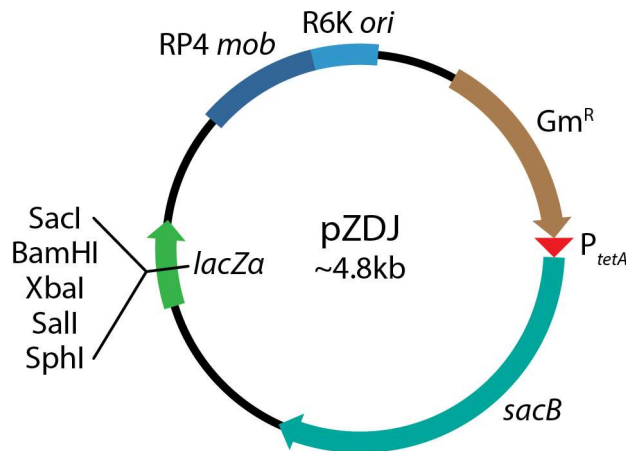


Figure 2.1. Map of the suicide plasmid pZDJ.

2.2.2 Creating the *rshI*, *ppsR*, and *crtI* knockouts, and the *crtI*^{Pa} knock-in.

A list of primers used to create the *rshI* and *ppsR* knockouts is shown in Table 2.4. The strain *R. sphaeroides* Δ RCLH Δ *rshI* was created by making a translationally in-frame deletion of the *rshI* gene in *R. sphaeroides* Δ RCLH. The flanking regions of the *rshI* gene were PCR-amplified as XbaI-RsrII and RsrII-SacI fragments, and cloned into the suicide plasmid pZDJ, resulting in pZDJ:: Δ *rshI*, transformed into *E. coli* DH5 α λ pir, conjugated with the recipient *R. sphaeroides* Δ RCLH, and selected for the first recombination event by growth in the presence of 20 μ g/mL gentamicin. The second recombination event was selected for by spreading serial dilutions of the cell culture on LB plates containing 10% sucrose.

The strain *R. sphaeroides* RCx was constructed similarly, by making an in-frame null mutant of *ppsR* using pZDJ:: Δ *ppsR* in a *R. sphaeroides* Δ RCLH Δ *rshI* background. The RCx^R strain is a derivative that developed a spontaneous mutation conferring resistance to rifampicin.

The *crtI* gene in *R. sphaeroides* RCx^R was knocked out using the pZDJ:: Δ *crtI*, resulting in the strain *R. sphaeroides* RCx^R Δ *crtI*. The *crtI* gene from *Pantoea agglomerans* (formerly called *Erwinia herbicola*) was PCR-amplified from the plasmid pERWI2 (Garcia-Asua et al., 2002) using the *crtI*-Pa FC primer set. The plasmid pZDJ:: Δ *crtI* was inverse PCR-amplified using the pZDJ::*crtI* FC primer ses. Using the FastCloning technique (Li et al., 2011), the PCR products were annealed to create pZDJ:: Δ *crtI*::*crtI*^{Pa}, and subsequently used to transform *E. coli* DH5 α . The resulting strain was called *R. sphaeroides* RCx^R Δ *crtI*::*crtI*^{Pa}.

Table 2.4. Primers used to create the *rshI* and *ppsR* knockouts, and *crtI* knock-in.

Primer Name	Sequence (5' → 3')
rshI KO up F	AATTGTCTAGATGCGCTGCCTGAACAACG
rshI KO up R	AATTCGGACCGATCAGCCATTTACCACA
rshI KO down F	TCTATCGGTCCGGCATCTATCGTTTGTCC
rshI KO down R	TAAGTGAGCTCCCAGACTCAATGCCGTGT
ppsR KO up F	AATTGTCTAGACTACATCCCCGAGGTCG
ppsR KO up R	AATTCGGACCGGGCCAGCATGTCTCTTC
ppsR KO down F	TCTATCGGTCCGTGAACAAGGACGAGTGAC
ppsR KO down R	TAAGTGAGCTCAAGCTCCCTGAGCTTCTC
<i>crtI</i> KO up F	AATTGTCTAGACACGTCCTTGTTCCGGC
<i>crtI</i> KO up R	AATTCGGATCCCATGGCGCGAACTCC
<i>crtI</i> KO down F	TCTATGGATCCCGCCGCGAGGCCGAAC
<i>crtI</i> KO down R	TAAGTGAGCTCAGGACGCACATCATCGC
<i>crtI</i> -Pa FC F	GGAGTTCGCGCCATGAAAAAACC GTT
<i>crtI</i> -Pa FC R	GGCCTCGCGGCGTCATTGCAGATCCTCAATCATCAGGCTGGCG GTGG
pZDJ:: <i>crtI</i> FC F	CCGCCAGCCTGATGATTGAGGATCTGCAATGACGCCGCGAGG CCGAAC
pZDJ:: <i>crtI</i> FC R	GGTTTTTTTCATGGCGCGAACTCCTGC

2.2.3 Cloning of *puhA* and *pufQBALMX*.

A list of primers used to clone *puhA* and *pufQBALMX* (and various derivatives) is shown in Table 2.5. The *puhA* gene of pRS1 was PCR-amplified using a forward primer containing a NcoI restriction site at the start codon and a reverse primer containing a 6-His tag followed immediately by a stop codon and a BamHI restriction site, yielding a 0.8 kb DNA product (*puhA* NcoI-BamHI primer set). This product was cloned into the plasmid pTZN, a derivative of pTZ18U in which the SphI site had been replaced with an NcoI site (Section 2.2.4). Similarly, the 3.2 kb *pufQBALMX* operon of pRS1 was amplified using a forward primer containing a new BamHI site introduced 299 bases upstream of the *pufQ* start codon and a reverse primer containing a HindIII site after the *pufX* stop codon, and cloned into pTZ18U (*puf* BamHI-HindIII primer set). The pIND4-RC1 plasmid was created from pIND4 by first inserting *puhA* as an NcoI to BamHI fragment, followed by the *pufQBALMX* operon as a BamHI to HindIII fragment, resulting in a synthetic operon driven by the IPTG-inducible P_{A1/04/03} promoter (Ind et al., 2009).

The same procedure was used to amplify and clone: *pufLM* (*pufLM* BamHI-HindIII primer set), *pufQBALMX* lacking *pufX* to produce an RC-LH1 monomer (*pufQBALMX* BamHI-HindIII primer set), *pufLM* with a stop codon preceding the start codon of *pufL* to produce the LM RC mutant (*pufLM* BamHI-TGA-HindIII primer set), and 12H*pufLM* with a 12-His tag on the C-terminus of the M subunit (12H*pufM* BamHI-HindIII primer set).

Table 2.5. Primers used to clone *puhA* and *pufQBALMX*.

Primer Name	Sequence (5' → 3')
<i>puhA</i> NcoI-BamHI F	TCTAACCATGGTTGGTGTGACTGCTT
<i>puhA</i> NcoI-BamHI R	GAATAGGATCCTCAGTGGTGGTGGTGGTG
<i>puf</i> BamHI-HindIII F	TAACTGGATCCGAAGTTTGCAACGCCCT
<i>puf</i> BamHI-HindIII R	CCATAAAGCTTTCAGACGAGATGCTTG
<i>pufLM</i> BamHI-HindIII F	ATAGCGGGATCCGTTGGGCCGACTGCAAGC
<i>pufLM</i> BamHI-HindIII R	ATAGCGAAGCTTTCAGTTCAGCGGCCCATG
<i>pufQBALM</i> BamHI-HindIII F	TAACTGGATCCGAAGTTTGCAACGCCCT
<i>pufQBALM</i> BamHI-HindIII R	TCTAGAAAGCTTTCAGTTCAGCGGCCCATG
<i>pufLM</i> BamHI-TGA-HindIII F	ATAGCGGGATCCTGAGTTGGGCCGACTGCAAGC

Primer Name	Sequence (5' → 3')
pufLM BamHI-TGA-HindIII R	ATAGCGAAGCTTTCAGTTCAGCGGGCGCCATG
12HpufM BamHI-HindIII F	ATAGCGGGATCCGTTGGGCCGACTGCAAGC
12HpufM BamHI-HindIII R	ATAGCGGGATCCGTTGGGCCGACTGCAAGC

2.2.4 Site-directed mutagenesis.

A list of primers used to create various site-directed mutations is shown in Table 2.6. This approach allowed for the changing of one, two, or three base-pair changes. Since pIND4 contains an NcoI site and pTZ18U does not, the SphI site was converted into an NcoI site in pTZ18U, resulting in the plasmid pTZN (pTZ SphI2NcoI primer set). The primer set TpufM antiBam was used with the plasmid pTZ19U::*TpufM* to introduce silent mutations in a BamHI site within the coding region of *TpufM*, resulting in the plasmid pTZ19U::B*TpufM*.

The other primer sets were used to make amino acid changes. The primer name contains the protein, residue number, amino acid prior to mutation, and amino acid after mutation. For example, the primer set pufL C92S indicates a PufL (RC L) Cys to Ser change at residue 92.

Table 2.6. Primers used for site-directed mutagenesis.

Primer Name	Sequence (5' → 3')
pTZ SphI2NcoI F	AGTCGACCTGCAGCCATGGAAGCTTGGCACTG
pTZ SphI2NcoI R	CAGTGCCAAGCTTCCATGGCTGCAGGTCGACT
pufL C92S F	CAGATCATCACGATCTCGGCCACTGGTGCCTTC
pufL C92S R	GAAGGCACCAGTGGCCGAGATCGTGATGATCTG
pufL C108S F	CGCGAAGTCGAAATCAGCCGTAAGCTGGGCATC
pufL C108S R	GATGCCCAGCTTACGGCTGATTTGACTTCGCG
pufL C247S F	TTCTTCAGCGCCCTCAGCATGATCATTACCGGC
pufL C247S R	GCCGGTAATGATCATGCTGAGGGCGCTGAAGAA
pufL E72C F	ACCCGCCGGCCCTTTGCTATGGCCTGGGAGGT
pufL E72C R	ACCTCCCAGGCCATAGCAAAGGGCCGGCGGGT
pufL N274C F	TGCCGTGGTGGGCGTGCATCCCGGGAGGCA
pufL N274C R	TGCCTCCCAGGGATGCACGCCACCACGGCA

Primer Name	Sequence (5' → 3')
pufM E100C F	AGCCGCCGGCACCCTGCTACGGTCTGTCCTTC
pufM E100C R	GAAGGACAGACCGTAGCAGGGTGCCGGCGGCT
pufM A260W F	ACCATGGGTTTCAACTGGACGATGGAAGGCATC
pufM A260W R	GATGCCTTCCATCGTCCAGTTGAAACCCATGGT
pufM W252F F	GCCGCCCTCTTCTTCCGCTGGACCATG
pufM W252F R	CATGGTCCAGCGGAAGAAGAGGGCGGC
pufL F121W F	ACATCCCGTTCGCCTGGGCGTTCGCCATCCTG
pufL F121W R	CAGGATGGCGAACGCCAGGCGAACGGGATGT
pufM M256C F	TTCTTCCGCTGGACCTGCGGTTTCAACTGGACG
pufM M256C R	CGTCCAGTTGAAACCGCAGGTCCAGCGGAAGAA
pufL D210C F	AAATGCGGACGCCGTGCCACGAGGATACGTTCTC
pufL D210C R	GAGAACGTATCCTCGTGGCACGGCGTCCGCATTT
pufL D210C D213W F	ACGCCGTGCCACGAGTGGACGTTCTTCCGCGATC
pufL D210C D213W R	GATCGCGGAAGAACGTCCACTCGTGGCACGGCGT
pufM F229C F	TCGCGGTCTCCCGCTGCGGGCGGCGAGCGCG
pufM F229C R	CGCGCTCGCCGCCGCAGCGGGAGACCGCGA
pufM V226W F229C F	GCGACCATCCTCGCGTGGTCCCGCTGCGGGCGGC
pufM V226W F229C R	GCCGCCGCAGCGGGACCACGCGAGGATGGTCGC
pufL W59C F	CCGTACTCCAGGGTACCTGCAACCCCCAACTCATCTC
pufL W59C R	GAGATGAGTTGGGGGTTGCAGGTACCCTGGAGTACGG
puhA A51C F	CGGCACCCCGGCCTGCAACCAGGGCCCGTTC
puhA A51C R	GAACGGGGCCCTGGTTGCAGGCCGGGGTGCCG
TpufM antiBam F	ACGGCGGGGATCGGAATACTTCTGAGCGGGAC
TpufM antiBam R	GTCCCGCTCAGAAGTATTCCGATCCCCGCCGT

2.2.5 Truncations of the *puhA* gene.

A list of primers used to create the *puhA* truncations is shown in Table 2.7. Using pTZN::*puhA* as starting material, the plasmid was inverse PCR-amplified with various primer pairs (the numerical value in the names correspond to length of the truncated H subunit). The

primers contained sticky ends to anneal the PCR product onto itself to form a nicked plasmid, which was subsequently used for transformation. The removal of the 6-His tag is denoted as “6H”.

Table 2.7. Primers used for making *puhA* truncations.

Primer Name	Sequence (5' → 3')
45puhA F	AACGAGCACCACCACCACCACCTGA
45puhA R	GTGGTGCTCGTTCTCCAGCGGATAG
80puhA F	GAAAGCCACCACCACCACCACCTGA
80puhA R	GTGGTGGCTTTCCGGGCCGGGC
150puhA F	ATCGGCCACCACCACCACCACCTGA
150puhA R	GTGGTGGCCGATCGGGTTCTTGCC
45,6H-puhA F	AACGAGTGAGGATCCCCGGGTACCG
45,6H-puhA R	TCCTCACTCGTTCTCCAGCGGATAG
80,6H-puhA F	GAAAGCTGAGGATCCCCGGGTACCG
80,6H-puhA R	TCCTCAGCTTTCCGGGCCGGGCACG

2.2.6 Cloning of *TpuhA* and *TpufBALM*.

A list of primers used to clone the *T. tepidum* genes is shown in Table 2.8. Similar to the cloning of *puhA*, *TpuhA* was PCR-amplified from *T. tepidum* chromosomal DNA and cloned into pTZN as an NcoI-BamHI fragment. A 6-His tag was introduced at the C-terminus of the *TpuhA* gene. *TpufL* and *TpufM* were similarly amplified from chromosomal DNA and cloned into pTZ19U, resulting in pTZ19U::*TpufL* and pTZ19U::*TpufM*, respectively. Artificial ribosomal binding site sequences were introduced for both *TpufL* and *TpufM*. The BamHI site in pTZ19U::*TpufM* was removed using site-directed mutagenesis (Section 2.2.4), resulting in pTZ19U::B-*TpufM*.

To create pTZ19U::*TpufLM* (and all subsequent constructs), the FastCloning method was used (Li et al., 2011). The pTZ19U::*TpufL* plasmid was inverse PCR-amplified and *TpufM* amplified from pTZ19U::B-*TpufM*.

Creating pTZ19U::rbs*TpufBALM* utilised a two-step approach. The plasmid pTZ19U::5' *TpufBALM* was created first. *TpufBA* was amplified from *T. tepidum* chromosomal DNA using the 5*TpufBA* FC primer set (containing *T. tepidum* ribosome binding sites). pTZ19U:: *TpufLM* was inverse PCR-amplified using the 5pTZ *TpufL*:lacZ FC primer set (containing artificial ribosomal binding sites). Another round of PCR amplification was required to exchange the *T. tepidum* ribosomal binding sites with artificial ones. The plasmid pTZ19U::rbs*TpufBALM* was created by amplifying pTZ19U::5' *TpufBALM* with the 5rbs*TpufB* FC and 5rbs*TpufA*:lacZ FC primer sets.

The pTZ19U::Rs *TpufBA pufLMX* was created by inverse PCR-amplifying pTZ19U::*puf* with the Rs *pufL*:lacZ primer set. *TpufB* and *TpufA* were PCR-amplified using Rs *TpufB* and Rs *TpufA* primer sets, respectively. Similarly, pTZ19U::Rs *TpufBALM pufX* was a further iteration by inverse PCR-amplifying pTZ19U::Rs *TpufBA pufLMX* with the Rs *pufX*:*TpufA* primer set, and *TpufL* and *TpufM* with the Rs *TpufL* FC and Rs *TpufM* FC primer sets, respectively.

The *pufX* was removed by inverse PCR-amplifying pTZ19U::Rs *TpufBA pufLMX* and pTZ19U::Rs *TpufBALM pufX* with pTZ RC TLH X⁻ and pTZ TRC TLH X⁻ primer sets, respectively. This resulted in the products pTZ19U::Rs *TpufBA pufLM* and pTZ19U::Rs *TpufBALM*.

Table 2.8. Primers used to clone the *T. tepidum* genes.

Primer Name	Sequence (5' → 3')
<i>TpufA</i> NcoI-BamHI F	TCTAACCATGGCTGCTGGCATACT
<i>TpufA</i> NcoI-BamHI R	GAATAGGATCCTCAGTGGTGGTGGTGGTGGTGCAGCAGGG GACCG
<i>TpufL</i> BamHI-XbaI F	TCTAAGGATCCGAGGAGAAATTAACCATGGCCATGCTCAG
<i>TpufL</i> BamHI-XbaI R	GAATATCTAGATTACCACAGCGGGA
<i>TpufM</i> XbaI-HindIII F	TCTAATCTAGAGAGGAGAAATTAACCATGCCAGAATATCA AAAT
<i>TpufM</i> XbaI-HindIII R	GAATAAAGCTTTCATTGCATCACCTCC
pTZ: <i>TpufL</i> FC F	TGCAATGAAAGCTTGGCACTGGCC
pTZ: <i>TpufL</i> FC R	TTCTCCTCTCTAGATTACCACAGCGGG

Primer Name	Sequence (5' → 3')
TpufM FC F	TGTGGTAATCTAGAGAGGAGAAATTAACCATGC
TpufM FC R	CCAGTGCCAAGCTTTCATTGCATCAC
5TpufBA FC F	GGTACCCGGGGATCCAGTGCGGCGTAACCTGAGGCTCAAC TCCTT
5TpufBA FC R	GGTTAATTTCTCCTCTGGGGAGGTGCTCTATGATGCTCTAT
5pTZ TpufL:lacZ FC F	TAGAGCACCTCCCCAGAGGAGAAATTAACCATGGCCATGC TCA
5pTZ TpufL:lacZ FC R	AGGTTACGCCGCACTGGATCCCCGGGTACCGAGCTCG
5rbsTpufB FC F	TCAACTCCTTAGTTTGAGGAGAAATTAACCATGGCTGAAC AGAAG
5rbsTpufB FC R	ATTCATCGTGAACATGGTTAATTTCTCCTCCAAAATTAATG GGCC
5rbsTpufA:lacZ FC F	GGCCCATTAATTTTGGAGGAGAAATTAACCATGTTACACGA TGAAT
5rbsTpufA:lacZ FC R	CTTCTGTTTCAGCCATGGTTAATTTCTCCTCAAATAAGGAG TTGA
Rs TpufB FC F	GATCCGGAGGATAGCATGGCTGAACAGAAG
Rs TpufB FC R	AACATGATCTTGTTCTCCTTACAGCCAAGGACG
Rs TpufA FC F	TGTAAGGAGAACAAGATCATGTTACGATGAAT
Rs TpufA FC R	GGGCCGGCCCGATTATTTCTTGCCCAGCGC
Rs pufL:lacZ FC F	GCGCTGGGCAAGAAATAATCGGGCCGGCCCTCCGTCGCG
Rs pufL:lacZ FC R	CTTCTGTTTCAGCCATGCTATCCTCCGGATCGTAAGACTG
Rs TpufL FC F	CGGAGAGGGAAGCATGGCCATGCTCAG
Rs TpufL FC R	TCCCGGGATGTTGCCCCACCACGTTACCACAGCGGGA
Rs TpufM FC F	GGCGAACATCCCGGGAGGCATCAATGCCAGAATATCAAA AT
Rs TpufM FC R	CATTGTGATCGCTCCTCATTGCATCACCTCC
Rs pufX:TpufA FC F	GGAGGTGATGCAATGAGGAGCGATCACAATG
Rs pufX:TpufA FC R	CTGAGCATGGCCATGCTTCCCTCTCCG

Primer Name	Sequence (5' → 3')
pTZ RC TLH X ⁻ F	GCGCCGCTGAACTGAAAGCTTCCCTATAGTGAGTCGTAT TAGAG
pTZ RC TLH X ⁻ R	CTATAGGGAAAGCTTTCAGTTCAGCGGCCATGC
pTZ TRC TLH X ⁻ F	GAGGTGATGCAATGAAAGCTTCCCTATAGTGAGTCGTAT TAGAG
pTZ RC TLH X ⁻ R	CTATAGGGAAAGCTTTCATTGCATCACCTCCGCCGC

2.3 Measurement of LH1 in disrupted cell samples.

Because the concentration of RC in cells is proportional to the peak amplitude of LH1 (Abresch et al., 2005), the LH1 peak height at 875 nm was used as a metric for the relative RC expression between samples. For the plasmid induction, growth of the *ppsR* knockout strain and time course of growth studies, cells were grown aerobically in the dark (chemotrophically) to 0.2 AU at 700 nm in triplicate and induced with 1 mM IPTG. For semi-aerobic conditions, cultures were grown in 200 mL of medium in 250 mL flasks, whereas for aerobic conditions, cultures were grown in 200 mL in 1 L flasks, all shaken at 150 RPM; however, for the growth kinetics studies, cultures were grown in twice these liquid volume and flask sizes. For each measurement at 0, 6, 12, 18, 24, 36, and 48 h, a volume of culture was removed such that the density was approximately 0.6 AU at 700 nm after concentration or dilution in a final volume of 1 mL; cells were disrupted by sonication with a Microson Ultrasonic Cell Disruptor for 30 s at a power output setting of 5 W. Following centrifugation at 14,000 x g for 1 minute the supernatant liquid was retained for absorbance measurements, using a StellarNet BLACK-Comet-SR spectrophotometer with an integration time of 36 ms, and a pixel boxcar smoothing level of 4, or a Hitachi U-3010 spectrophotometer. Spectra were normalised to 0.1 AU at 700 nm, 5 spectral measurements of each culture were averaged, and the spectra of three cultures averaged again; the population standard deviation of the mean was the calculated error. Subtractions were accomplished by using the average of the negative control spectrum and errors after each subtraction were calculated in quadrature of the two spectra.

2.4 Measurement of LH1 in intact cells.

The relative RC expression in intact cells was measured as a function of LH1 absorbance and cell culture density. For the experiment using the new medium RLB, there were a few changes to the general protocol described above. One mL of semi-aerobically grown *R. sphaeroides* was used to seed triplicate cultures in 250 mL flasks containing 200 mL, which were grown with shaking at 150 RPM in the dark. One mL of these cultures was removed for each measurement after 0, 48, 72, 96, and 120 h of growth. Each sample was briefly centrifuged to pellet the cells, the supernatant was removed, the cells were washed once in a buffer consisting of 10 mM Tris, pH 8.0, 150 mM NaCl, and finally resuspended in the same buffer. For each sample, an absorbance spectrum was obtained from 600 to 1000 nm using a Hitachi U-3010 spectrophotometer. The relative amount of the RC in whole cells between samples was compared by calculating a scatter-subtracted LH1 absorbance value, and multiplying this value by the culture density (measured at 700 nm) according to the following equation,

$$\text{LH1 output} = A_{700} \times \left(A_{875} - \left(\frac{A_{825} + A_{925}}{2} \right) \right)$$

where the changes in absorbance due to cell scatter in the near IR region are assumed to be linear over this small wavelength range.

2.5 Purification of the RC and RC-LH1.

Purification of the photosystems followed a modified published protocol of using a His tag and Ni²⁺-NTA affinity chromatography to purify proteins (Goldsmith and Boxer, 1996). For pIND4-derived plasmids, cells were inoculated with 50 mL of overnight starter culture into 2 L Erlenmyer flasks with 500 mL RLB medium, 50 µg/mL kanamycin, and 1 mM IPTG. Cultures were grown at 30 °C, shaken at 200 RPM, and grown to the late logarithmic growth phase (approximately 18-21 h).

Cells were centrifuged at 7000 x g and the supernatant discarded. The cell pellet was suspended in 10 mM Tris pH 8.0, 150 mM NaCl – for every gram of cell paste, 2 mL of buffer were added, as well as 1 µL of 1 M MgCl₂ and a few crystals of DNase I. Cells were broken in a

French press at 20,000 to 25,000 PSI and centrifuged at 10,000 x *g* for 20 minutes to pellet cell debris and unbroken cells.

Chromatophore proteins were solubilised using detergent and 5 mM imidazole for 15 to 20 min at room temperature in the dark. LDAO was used at 1% to solubilise RCs, unless otherwise indicated. The H subunit truncation mutant RCs and core complexes were solubilised in 1% DDM. The RC-LH1-X⁺ core complexes were solubilised in 1% DDM and RC-LH1-X⁻ core complexes solubilised in 0.8% LDAO. The *T. tepidum* hybrid core complexes were solubilised in 1% Deriphat 160C.

The solubilised proteins were centrifuged at 40,000 RPM for 20 min at 4 °C in a Beckman-Coulter Type 70 Ti rotor to pellet insoluble materials. The protein mixture supernatant was subsequently bound to a Ni²⁺-NTA chromatography column equilibrated with 10 mM Tris pH 8.0, 150 mM NaCl, 0.03% LDAO (or 0.04% DDM) at 4 °C. The column was washed with this buffer until the 280 nm absorbance was less than 0.02 AU. The RCs bound to the column were eluted with 10 mM Tris pH 8.0, 150 mM NaCl, 0.03% LDAO (or 0.04% DDM), 100 mM imidazole. The eluted product was exchanged into a buffer containing 10 mM Tris pH 8.0, 0.03% LDAO (or 0.04% DDM).

2.6 Removal of detergent from RCs.

Bio-Beads SM-2 (Bio-Rad) resin is an adsorbent material that can be used to remove detergent molecules from the RC without denaturing the protein (Gast et al., 1994; Gast et al., 1996; Rigaud et al., 1998). Protein samples were diluted with 10 mM Tris pH 8.0 such that the absorbance at 804 nm was around 5 AU and 1 to 2 mL of beads were added to the sample. The mixture was rocked until precipitation was visible and/or agitation of the sample did not result in foaming. The precipitate was separated from the SM-2 resin with a pipette.

2.7 Binding of the ATTO MB2 dye.

Detergent-less RCs were used in the solid-phase form to bind the ATTO MB2 dye. The dye is soluble predominantly in polar, aprotic solvents, such as DMSO or DMF, hence the volume of the solvent had to be minimised to reduce any adverse effects on the protein. Different conditions were tested: 3- or 10-fold molar excess dye; 30 °, 37 °, or 45 °C incubation

temperatures; pH 6.5 (10 mM Bis-Tris), pH 7.2 (1x PBS), or pH 8.0 (10 mM Tris); and 30 min, 2 h, and 24 h incubation times.

After binding, the sample was diluted with 10 mM Tris pH 8.0, spun down to pellet the RCs, and the supernatant removed. This procedure was repeated until the supernatant did not contain any dye. The pellet was resuspended in 50 to 100 μ L 10 mM Tris pH 8.0, and 0.1% LDAO was titrated until the proteins were resolubilised, indicated by a visible decrease in the amount of precipitated proteins. Insoluble proteins were removed with a final centrifugation step.

2.8 Pigment extraction from RCs and quantification.

Pigments of RCs were extracted using a 7:2 solution of acetone:methanol. The protein subunits that aggregated upon addition of the organic solvent were pelleted by centrifugation. The supernatant containing the pigments was measured using UV-vis absorbance spectroscopy and quantified (van der Rest and Gingras, 1974).

2.9 Mass spectroscopy of RCs.

Protein were denatured using a 1:1 chloroform:methanol mixture collected as a pellet after centrifugation, and solvated in a mixture of 50% formic acid, 25% acetonitrile, 15% isopropanol, and 10% H₂O (Feick and Shiozawa, 1990).

For electrospray ionisation intact protein mass spectrometry, 1 mg/mL samples were diluted 1:250 in a solution containing 5% acetonitrile and 0.1% formic acid in H₂O. Five μ L of the diluted sample were injected into a 5 mm C4 column connected to a Waters Xevo GS-2 QToF mass spectrometer using a NanoAquity UPLC system. Samples were eluted over 2 min in a gradient from 5 to 100% acetonitrile (0.1% formic acid in H₂O) at 20 μ L/min. Mass spectra were summed and deconvoluted using the Waters MaxEnt algorithm.

2.10 Electrode preparation for cyclic voltammetry or photochronoamperometry.

HOPG electrodes were mechanically cleaved to produce a clean surface, then immersed in a 5 mM solution of *N*-(1-pyrene)maleimide in DMSO, incubated for 1 h at room temperature, and dipped in H₂O to remove excess DMSO and linker. Gold electrodes were cleaned by sonicating, washing the electrode with ethanol and H₂O, and flaming using a Bunsen burner until

the electrode turned pink in colour. Protein samples (10 μM in 1x PBS pH 7.2, 0.03% LDAO or 0.04% DDM, and 1 mM TCEP) were subsequently incubated for 1-2 h at 4 $^{\circ}\text{C}$ on HOPG or gold.

2.10.1 Cyclic voltammetry.

Cyclic voltammetry measurements utilised the Autoab PGSTAT101 potentiostat in a three-electrode setup in 10 mM Tris pH 8 or 1x PBS pH 7.2 with a Pt counter electrode, an Ag/AgCl reference electrode, and HOPG or gold working electrode. Voltage sweeps were in the positive direction at 10 or 100 mV/s. All potentials are with respect to the Standard Hydrogen Electrode (SHE).

2.10.2 Photochronoamperometry.

Photoelectrochemical measurements utilised the Solartron SI 1287 potentiostat in a three-electrode setup in 1x PBS pH 7.2 with a Pt counter electrode, an Ag/AgCl reference electrode, and HOPG or gold working electrode in a plastic 10 mm cuvette. No electronic filtering was applied.

The electrode setup was placed in black box with a shutter to minimise stray ambient light. A Newport 150 W solar simulator was used for illumination, resulting in 140 mW/cm^2 light intensity at the distance where the electrode was located without the cell in place. The photocurrent was measured at an applied voltage equal to the dark open circuit potential (*i.e.*, a potential at which no current was generated in the dark). The current polarity was such that cathodic current was negative and anodic current positive.

External quantum efficiency action spectra measurements were collected by using the setup described above, but using a seven LED array instead of the solar simulator. The LEDs used are shown in Table 2.9. For each LED, a photon counts spectrum and light intensity at the distance where the electrode was located without the cell in place were measured. Assuming that the measured light intensity was the sum of the contribution of each wavelength in the photon counts spectrum, the measured photocurrents were also the sum of the contribution of each wavelength. External quantum efficiency action spectra were plotted by calculating the photocurrent contribution of the wavelengths corresponding to the major peaks (758, 804, and

865 nm) and valleys (777 and 844 nm) of the RC Q_y transition region. Outlier external quantum efficiency data points were discarded.

Table 2.9. LEDs used for action spectra measurements.

Peak Wavelength (nm)	Bandwidth (nm, FWHM)	Catalogue Number (DigiKey)
680	30	1125-1089-ND
740	30	1125-1084-ND
770	25	1125-1081-ND
810	40	1125-1158-ND
860	30	1125-1100-ND
870	45	1125-1019-ND
935	50	365-1579-ND

2.11 UV mutagenesis of *R. sphaeroides*.

Semi-aerobically grown *R. sphaeroides* cultures were centrifuged, supernatant removed, and pellet resuspended in ice-chilled 0.1 M sterile $MgSO_4$, followed by an additional centrifugation step. A volume of cold 0.1 M $MgSO_4$ was added such that the final cell density was 300 Klett units (KU), using a Klett-Summerson Photoelectric Colorimeter. Cells were chilled for 15 min prior to placing 8 mL cultures in a Bio-Rad GS Gene Linker UV Chamber for UV irradiation of 0, 10, 20, and 30 s. Samples of 2 mL were taken from the irradiated cultures and inoculated into 2 mL of RLB medium supplemented with 25 $\mu g/mL$ kanamycin in aluminum foil-wrapped tubes. The cultures were incubated at 30 °C and 150 RPM for 4 h. Afterwards, an additional 4 mL of RLB were added and incubated overnight at 30 °C and 150 RPM. The overnight cultures were diluted to 50 KU, induced with 1 mM IPTG and incubated overnight again. Four mL from the 0, 10, 20, and 30 s cultures were transferred into 16.5 mL screw-cap tubes of RLB medium, 25 $\mu g/mL$ kanamycin, and 1 mM IPTG (and 10 μM menadione if the construct produced TRCs). The cultures were grown in temperature-controlled aquariums at 30 °C and 75 $\mu E M^{-2} s^{-1}$ light intensity to select for phototrophy-capable mutants. Mutants were streaked on RLB agar plates with 25 $\mu g/mL$ kanamycin, and 1 mM IPTG (and 10

μM menadione if the construct produced TRCs) and grown in anaerobic jars to isolate individual colonies.

2.12 Heat stability measurements of the core complex.

Core complexes were normalised to a concentration such that the absorbance at 875 nm (LH1) or 915 nm (TLH1) was approximately 0.2 AU. Protein samples, in triplicate, were subjected to temperatures of 30 °, 50 °, 70 °, and 90 °C for 2, 4, 8, 15, 30, and 60 min. A StellarNet BLACK-Comet-SR spectrophotometer was used to measure single absorbance spectra from 600 to 1000 nm with an integration time of 70 ms, and a pixel boxcar smoothing level of 4. The standard deviation of the mean was the calculated error.

Chapter 3: Results

3.1 Recombinant expression of the genes encoding the RC and LH1 photosystems using a modified strain of *R. sphaeroides*.

The *R. sphaeroides* strain Δ RCCLH(pRS1) had been used previously for the expression of photosynthetic RC and LH1 complexes (Jaschke et al., 2011). However, that system is time-consuming, taking up to six days to grow large-scale cultures under semi-aerobic (chemotrophic) conditions, and resource intensive with low RC yields of 0.2 to 0.3 mg/L culture from a 24 L culture. Furthermore, the existing protocol for the transfer of plasmid from *E. coli* into *R. sphaeroides* is conjugation, which takes up to a week or more to obtain a clean isolate.

To reduce delays associated with conjugation, another technique of transferring a plasmid is to transform *R. sphaeroides*. Both electrical and chemical transformation procedures have been used with success previously (Donohue and Kaplan, 1991), but the major genetic barrier is the presence of an endogenous restriction enzyme, RshI (Lynn et al., 1979) in *R. sphaeroides* 2.4.1. Any plasmid containing the sequence 5'-CGATCG-3' would therefore be restricted. The plasmid pBR322, which lacks the RshI restriction sequence, has been used in the past for transformation (Fornari and Kaplan, 1982); however, the restriction issue still remains with any additional DNA sequences cloned into pBR322. To circumvent this problem, I developed a silent, in-frame knockout of the *rshI* gene in *R. sphaeroides* Δ RCCLH. This knockout resulted in the creation of the strain *R. sphaeroides* Δ RCCLH Δ *rshI*, which was capable of being transformed with plasmids (e.g. pIND4) containing RshI restriction sequences. By having solved this issue, *R. sphaeroides* Δ RCCLH Δ *rshI* could be transformed electrically and form isolated colonies in ~3 days – saving about half to a week of time. The next sections describe several different strategies I used to increase RC and LH1 levels using the new strain *R. sphaeroides* Δ RCCLH Δ *rshI*.

3.1.1 Comparison of inducible expression plasmids for production of pigment-protein complexes.

The host strain used to compare the relative expression of LH1 and RC complexes was *R. sphaeroides* Δ RCCLH Δ *rshI*, which has deletions in the genes encoding the RC, LH1, and LH2 protein complexes, as well as the restriction endonuclease RshI. The plasmid expressing the IPTG-inducible RC-LH1 core complex, pIND4-RC1, was created by ligation of the *puhA* gene

followed by the *pufQBALMX* genes as a synthetic operon into the plasmid pIND4 (Ind et al., 2009). Production of pigment-protein complexes was initiated by addition of 1 mM IPTG when the cell culture density reached 0.2 AU at 700 nm, to induce expression of the *puhA* and *pufQBALMX* genes. Absorbance spectra were measured after sonication of cells, and the amplitude of the LH1 peak at 875 nm, identical to that found in the wild type bacterium, was used as an indication of protein expression levels, because the LH1 signal is stronger than those of the RC by a factor of ~5 (Abresch et al., 2005). Furthermore, because the ratio of LH1 to RC is constant, changes in LH1 amounts indicate changes in RC amounts.

After IPTG-induction of pIND4-RC1-expressed genes in cultures grown under semi-aerobic conditions, the maximum level of LH1 per cell was reached after about 24 h, as shown in Figure 3.1. In contrast, the plasmid pRS1 yielded an increase in LH1 levels by about 2- to 4-fold relative to the level at the start of cultivation, which plateaued after 18 hours. About 8 times more LH1 was produced by pIND4-RC1 than pRS1 in *R. sphaeroides* Δ RC1H Δ rshI under semi-aerobic conditions. Therefore, the IPTG-inducible promoter of pIND4-RC1 produced greater levels of RCs when compared to the hypoxia-inducible *puc* promoter of pRS1 under these experimental conditions.

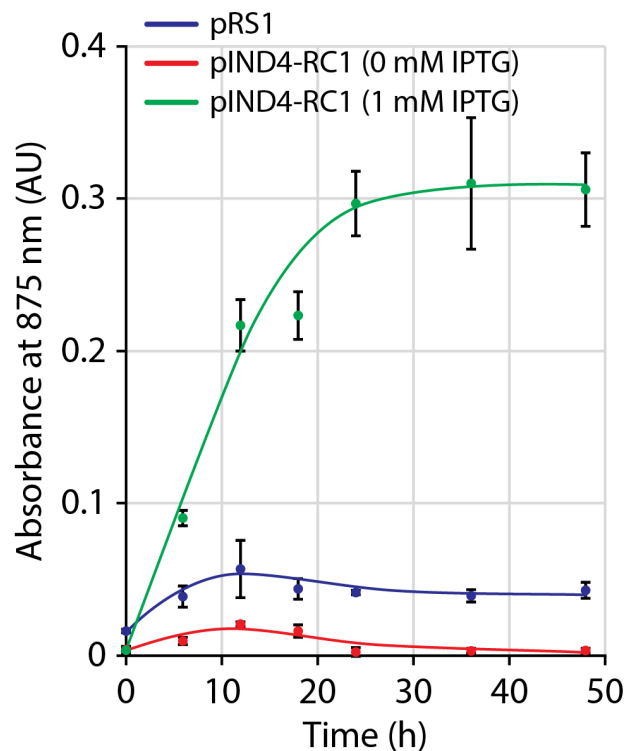


Figure 3.1. Comparison of LH1 levels using the plasmids pRS1 or pIND4-RC1. The *R. sphaeroides* Δ RCLH(pRS1) (blue) and Δ RCLH Δ rshI(pIND4-RC1) were grown semi-aerobically for 48 h. Δ RCLH Δ rshI(pIND4-RC1) induced with 1 mM IPTG (green); and Δ RCLH Δ rshI(pIND4-RC1) not induced (red). Error bars represent the standard deviation (n = 3). Lines drawn to represent approximate trends.

3.1.2 Use of a *ppsR* gene knockout host strain to boost aerobic production of pigment-protein complexes.

In *R. sphaeroides* Δ RCLH Δ rshI(pIND4-RC1), the amounts of bacteriochlorophyll, bacteriopheophytin, and carotenoid pigments made are dependent on the hypoxia-induced promoters driving transcription of their respective biosynthetic genes on the chromosome. A knockout of the *ppsR* gene encoding the pigment repressor protein PpsR was explored to further increase the levels of pigment-protein complexes. The PpsR protein is a global regulator of the photosynthesis gene cluster that functions by repressing synthesis of pigments and proteins in the presence of oxygen (Elsen et al., 2005). A knockout of *ppsR* would, in theory, result in constitutive expression of the *bch* and *crt* genes, and increased pigment levels. An additional

benefit of a *ppsR* knockout would be the ability to grow the organism under fully aerobic conditions, resulting in faster growth and higher densities than under semi-aerobic conditions. However, the risk of oxidative stress increases with simultaneous exposure to light and oxygen.

A silent, in-frame knockout of the *ppsR* gene in $\Delta RCLH\Delta rshI$ was constructed, generating the new strain *R. sphaeroides* RCx. The parallel strain RCx^R was also obtained as a spontaneous mutant that is resistant to the antibiotic rifampicin. The amounts of pigment-protein complexes synthesised in the strain RCx were evaluated to determine whether levels could be increased beyond what was obtained with the $\Delta RCLH\Delta rshI$ strain containing the plasmid pIND4-RC1. As in the previous section comparing the plasmids pIND4-RC1 and pRS1, cultures were induced with 1 mM IPTG at a density of 0.2 AU at 700 nm. Additionally, the RCx strain was evaluated whether high levels of pigment-protein complex could be produced during growth under aerobic conditions.

As shown in Figure 3.2, the *R. sphaeroides ppsR* mutant RCx containing pIND4-RC1 grown aerobically showed a marked increase in LH1 levels compared to *R. sphaeroides* $\Delta RCLH\Delta rshI$ (pIND4-RC1) by approximately 1.2-fold. Cultures of the RCx strain yielded maximal amounts of pigment-protein complexes after ~12 hours of aerobic growth, whereas the $\Delta RCLH\Delta rshI$ strain did not reach these levels and plateaued after 24 hours. The advantages of using a *ppsR* knockout are clear in that higher levels of LH1 are produced per cell and in half the time when grown aerobically.

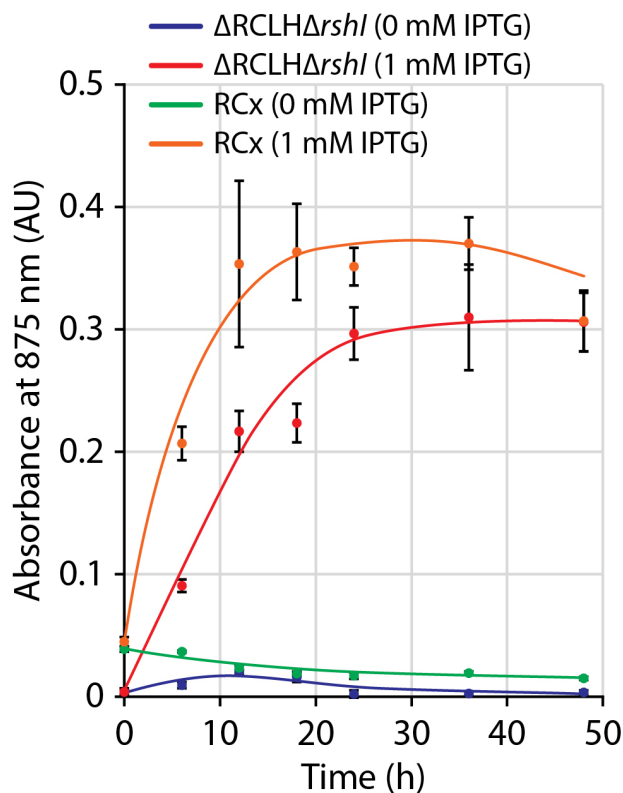


Figure 3.2. Comparison of LH1 levels in cultures of *R. sphaeroides* Δ RCLH Δ rshI and RCx. The *R. sphaeroides* Δ RCLH Δ rshI was grown semi-aerobically for 48 h, whereas the RCx strain was grown aerobically. *R. sphaeroides* RCx(pIND4-RC1) induced with 1 mM IPTG and grown aerobically (orange); strain RCx(pIND4-RC1) not induced and grown aerobically (green); Δ RCLH Δ rshI(pIND4-RC1) induced with 1 mM IPTG and grown semi-aerobically (red); and strain Δ RCLH Δ rshI(pIND4-RC1) not induced and grown semi-aerobically (blue). Error bars represent the standard deviation ($n = 3$). Lines drawn to represent approximate trends.

3.1.3 Effects of divalent salts in a complex LB-based growth medium on pigment-protein content of cells.

A comparison of *R. sphaeroides* cultures grown semi-aerobically in the synthetic RCV medium (Beatty and Gest, 1981) versus the complex LB medium indicated that one or more components of the RCV medium may result in an increase in the amount of pigment-protein complex gene expression, as measured by LH1 peak amplitude of intact cell preparations. One or a small number of stimulatory substances present in the RCV medium could be added to the LB

medium to enhance the production of pigment-protein complexes and thereby allow the use of a relatively simple medium to obtain maximal levels of LH1 and RC complexes.

To identify the components of RCV medium that might stimulate pigment-protein complex synthesis, each of the selected constituents of the RCV medium was added to LB at the same final concentration as in RCV. This study was performed under semi-aerobic conditions using *R. sphaeroides* Δ RCLH(pRS1). It was discovered that the addition of two salts, 810 μ M $MgCl_2$ and 510 μ M $CaCl_2$, resulted in an increased LH1 peak amplitude of cells grown in modified LB media (Figure 3.3). Adding both of these salts to the LB medium resulted in a stimulation of the amount of RC normalised per cell surpassing that of the RCV medium. The modified medium was termed RLB, which is defined as the rich medium LB supplemented with 810 μ M $MgCl_2$ and 510 μ M $CaCl_2$. Other components of RCV were found to produce little to no discernible differences in culture density (data not shown).

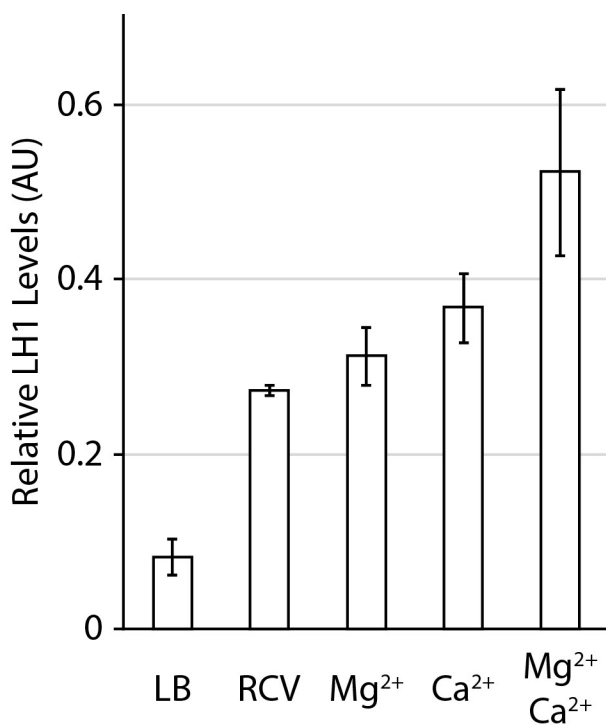


Figure 3.3. Comparison of LH1 levels due to the effects of divalent cations. Levels measured after *R. sphaeroides* Δ RCLH(pRS1) was grown semi-aerobically for 120 h. Error bars represent the standard deviation (n = 3).

Having constructed an improved medium for expressing pigment-protein complexes, *R. sphaeroides* RCx(pIND4-RC1) was grown in both LB and RLB, and LH1 levels compared in cells grown in these two media. As shown in Figure 3.4, it was evident that cultures produced more LH1 when grown in RLB than in LB after induction. With this particular modification, about 1.3-fold more LH1 per cell was detected in RLB, with the maximum plateauing around 24 h after induction.

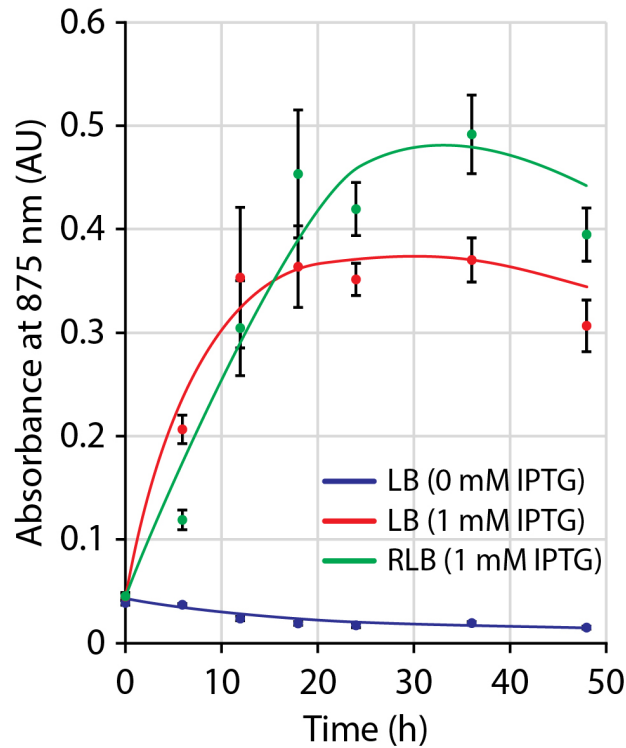


Figure 3.4. Comparison of LH1 levels due to the culture media LB and RLB (LB medium supplemented with 810 μM MgCl_2 and 510 μM CaCl_2). *R. sphaeroides* RCx(pIND4-RC1) induced with 1 mM IPTG and grown aerobically in RLB medium (green); RCx(pIND4-RC1) induced with 1 mM IPTG and grown aerobically in LB medium (red); and strain RCx(pIND4-RC1) not induced and grown aerobically in LB medium (blue). Error bars represent the standard deviation ($n = 3$). Lines drawn to represent approximate trends.

3.1.4 Effects of combining the pIND4, *ppsR* KO, and RLB modifications.

The individual changes of using an inducible plasmid, a PpsR knockout, and modifying the growth medium were combined to investigate the effect on the levels of the LH1 complexes per cell. Purified RC yields were also measured to calculate approximate protein levels per unit volume of culture.

Under aerobic growth in RLB medium, *R. sphaeroides* RCx(pIND4-RC1) reached a maximum of 4.5 AU at 700 nm about 36 h after induction, as shown in Figure 3.5. In contrast, the same strain reached a maximum density of 3 AU about 24 hours after induction in LB. Clearly, cultures grown aerobically in RLB medium with the addition of Mg^{2+} and Ca^{2+} result in a greater cell concentration in a shorter period of time than when grown in LB under the same conditions. Evidently, aerobic growth results in higher concentrations of cells, especially in the first 30 hours, than when cultures are grown semi-aerobically. The semi-aerobic growth of *R. sphaeroides* Δ RCLH(pRS1) did not plateau in 48 h of growth, as depicted in Figure 3.5, and its slower growth relative to *R. sphaeroides* RCx(pIND4-RC1) in RLB was evident as early as 6 h into the induction of RC-LH1. By 24 and 36 h, there were approximately two to three times as many cells per mL in cultures grown aerobically in either LB or RLB than semi-aerobically in LB. Because the semi-aerobic growth curve did not reach stationary phase in this experiment, the culture hypothetically could have reached higher cell concentrations, but this possibility was outweighed by the short time needed to obtain much greater amounts of cells and pigment-protein complexes using the combination of the new strain, *R. sphaeroides* RCx, and the new plasmid, pIND4-RC1.

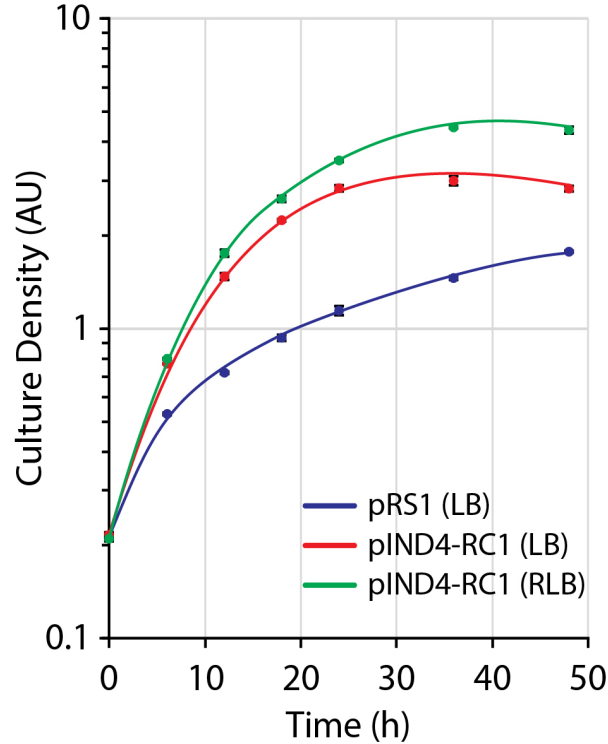


Figure 3.5. Comparison of the growth kinetics and final yields of cell concentrations in different culture conditions. *R. sphaeroides* RCx(pIND4-RC1) induced with 1 mM IPTG and grown in LB (red) and RLB (green) media aerobically; *R. sphaeroides* strain Δ RLCH(pRS1) grown in LB medium semi-aerobically (blue). Culture density was measured by measuring absorbance at 700 nm. Error bars represent the standard deviation ($n = 3$). Lines drawn to represent approximate trends.

Ultimately, the amount of RC purified, rather than using LH1 as a metric for RC levels, from a volume of culture grown for a short period of time is the best indication of whether the new and efficient protein expression system represents a useful advance for studies of the RC. Compared to earlier results, 8-fold more of the LH1 were detected using pIND4 than pRS1 under semi-aerobic growth; 1.2 times more of the LH1 were measured under aerobic growth in the new strain RCx; 1.3 times more in the new RLB medium than LB; and cultures contained 3 times more cells in RLB than when growing *R. sphaeroides* Δ RLCH(pRS1) in LB. Figure 3.6 shows the relative increases due to each progressive modification with an overall increase in LH1 yields by ~35-fold. As a method of verification, RCs were purified from cells grown under these

optimal conditions using the plasmid pIND4-RC (containing only the *puhA*, *pufL*, and *pufM* genes that code for the H, L, and M subunits, respectively) and yielded up to 15 mg/L culture, which corresponded to a 50-fold increase from the 0.2 to 0.3 mg/L culture typically purified from the original system.

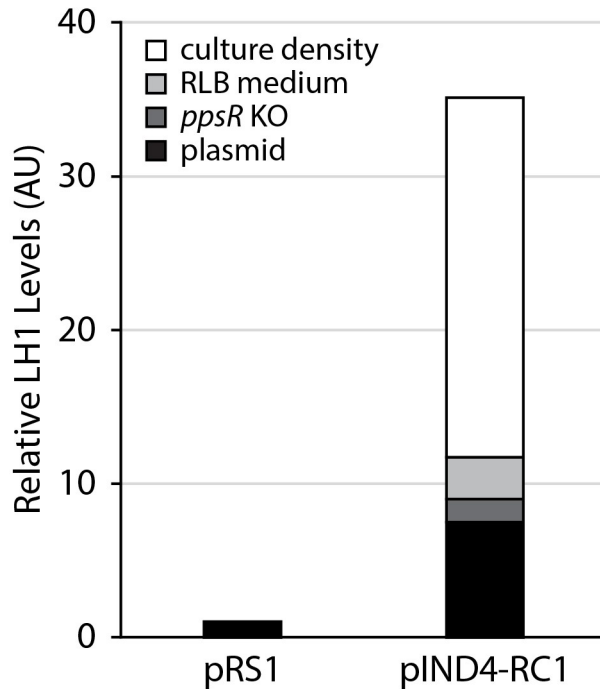


Figure 3.6. Contributions of *R. sphaeroides* strain, expression plasmid, and culture conditions to the relative amounts of the LH1 complex. The LH1 levels obtained in *R. sphaeroides* Δ RCLH(pRS1) grown in LB medium are indicated by the black bar over the pRS1 label, corresponding to the normalised value of 1. The 8-fold increase due to using the plasmid pIND4-RC1 is shown in black, with the value determined from Figure 3.1; the 1.2-fold contribution due to growth of the *ppsR* knockout strain RCx under aerobic conditions is shown in dark grey, with the value determined from Figure 3.2; the 1.3-fold contribution due to the effect of the new medium RLB is shown in light grey, with the value determined from Figure 3.4; and the 3-fold contribution of the increase in cell concentration in cultures is shown in white, reflecting the effect of aerobic growth over semi-aerobic growth, with the value determined from Figure 3.5.

3.2 Characterisation of RCs containing a truncated H subunit.

One of the goals of my research was to extract electrons directly from the Q_A and Q_B regions of the RC. The challenge of this aim is the presence of the large cytoplasmic globular domain of the H subunit. The size of this domain results in a distance of over 20 Å from Q_A or Q_B to the protein surface, where an electron acceptor may be located. Therefore, due to the long distances, the likelihood of a single electron jump from a Q_A or Q_B electron donor to an acceptor is highly improbable. Bridging this distance with multiple redox centres or Trp amino residues is unlikely due to the distance and because these modifications would have to be well-tuned to facilitate electron transfer. The alternative strategy used, in this attempt to extract electrons, was to minimise distances from Q_A to Q_B by removing the RC H cytoplasmic domain. The result of this should reduce the distance to the new surface of the protein to around 10 Å, a distance where electron transfer is more likely to occur (Winkler and Gray, 2014). In this section, I aimed to show the feasibility of creating truncated RCs, some of which supported photosynthetic growth, and show that these mutant RCs were still stable following purification for attachment to an electrode in downstream experiments.

3.2.1 Construction of the 45, 80, and 150 mutants.

Three mutants called 45, 80, and 150, were created by genetically truncating the *puhA* gene corresponding to the C-terminal region of the H subunit, resulting in smaller polypeptides that differ from the wild type length of 261 amino acids – now containing only the 45, 80, and 150 N-terminal residues, respectively. The 45 mutant consisted of the N-terminal periplasmic sequence and the membrane-spanning α -helix that anchors the H subunit into the membrane. The 80 mutant contained an additional 35 amino residues that form a portion of the cytoplasmic globular domain; and the 150 mutant is essentially a further extension of the 80 mutant with about half of the globular domain. The modified *puhA* segments were cloned into pIND4, along with the wild type *pufL* and *pufM* genes. Figure 3.7 shows the predicted structures of the truncated protein H subunits based on the wild type RC crystal structure and excluding the 6-His tag located at the C-terminus of the polypeptide. The cytoplasmic domain of each truncated protein is likely to fold differently than the corresponding segment of the full-length protein, but the figure gives a visual comparison of the amounts deleted.

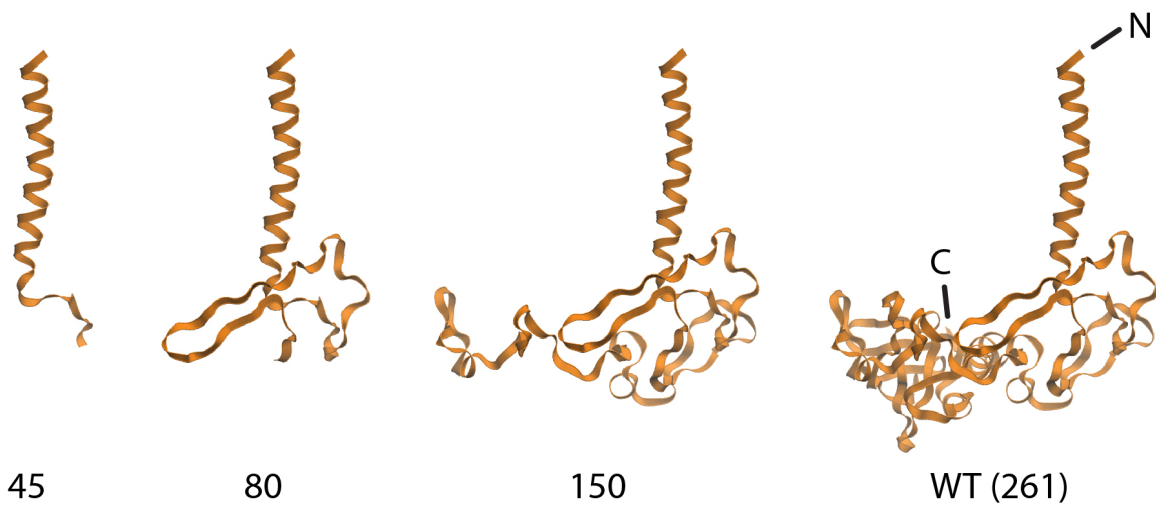


Figure 3.7. Predicted structures of the 45, 80, and 150 truncation mutants of the RC H subunit. Numbers indicate the number of residues, and the N- and C- termini of the H polypeptide is shown in the wild type. Structures are based on PDB 2J8C.

3.2.2 *In vivo* measurements of the assembly of truncated RCs.

Given the drastic changes to the protein structure, basically removing up to a third of the RC, the first thing was to determine whether the RCs assembled. Initially, the accessory bacteriochlorophyll peak at ~800 nm was used as a measure of correct assembly of protein subunits and cofactors. If RCs did not assemble properly, that would be observed as a lack of an 800 nm peak and perhaps accompanied by an increase in signal at 760 nm, due the absorbance of free bacteriochlorophylls in the event that RCs were unstable and released cofactors. An LM mutant was also created, which completely lacked the H subunit. Results of the broken cell absorbance spectra are shown in Figure 3.8.

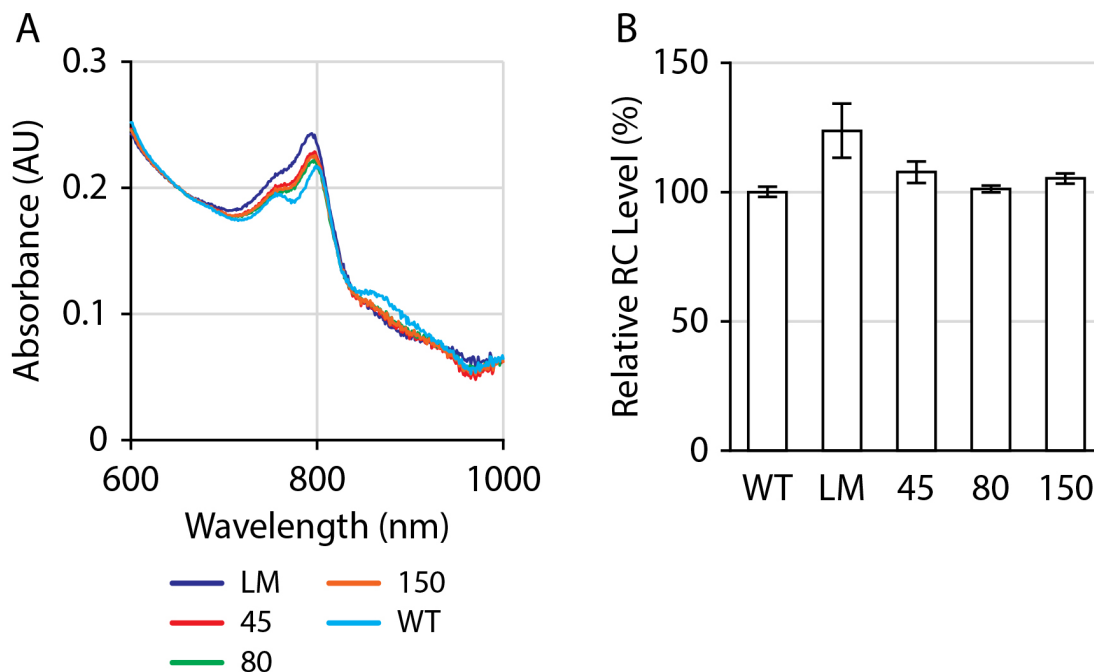


Figure 3.8. Assembly and *in vivo* levels of RC truncation mutants. The RC mutants LM, 45, 80, and 150 were expressed in *R. sphaeroides* RCx^R. A) Absorbance spectra of broken cells expressing: the LM RC lacking the H subunit (blue), the 45 mutant (red), the 80 mutant (green), the 150 mutant (orange). The wild type (WT) control is shown for peak reference (cyan); the 800 nm accessory bacteriochlorophyll peak blue-shifted with increasing truncation lengths of the H subunit. Spectra were normalised to $A_{650} = 0.2$. B) Relative levels of RC production compared to the wild type RC. Levels were calculated by subtracting the RCx^R baseline from the peak amplitude of the accessory bacteriochlorophylls ~800 nm and normalising the difference to the wild type RC. Error bars represent the standard deviation (n = 3).

All the mutants, including the LM mutant, showed a dominant peak at ~800 nm, with levels similar to that of the WT RC, if not slightly higher. This suggested that the RCs assembled with accessory bacteriochlorophylls at the B_A and B_B sites of the RC, irrespective of the complete or partial absence of the H subunit. Minor changes were observed, such as a slight blue-shift of the 800 nm peak with decreasing H subunit length. The cause of the shift is unclear, although denaturation resulting in the loss of pigments would have been observed as a decrease in the 800 nm absorbance band, rather than as an electrochromic shift. Therefore, it appears that

changes in the protein structure due to the partial deletions induced minor conformational changes in the protein milieu around the cofactors, which resulted in the shift of this peak.

The fact that all the RC mutants, including the LM RC lacking the H subunit entirely, assembled in the membrane was surprising. Past research suggested that the H subunit is necessary to recruit the L subunit to stably form the RC (Tehrani and Thomas Beatty, 2004); furthermore, when the cytoplasmic domain in the H subunit was swapped out for an equivalent domain from another similar photosynthetic bacterium, RC production levels dropped (Tehrani et al., 2003). Under these experimental conditions, the data from this experiment showed that the H subunit was not necessary for RC assembly *in vivo*.

3.2.3 Selection of a secondary mutant and phototrophic growth.

Although the truncated RCs were able to assemble *in vivo*, this assembly did not indicate whether the RCs were functional. One approach was to determine whether *R. sphaeroides* was capable of growing photosynthetically with these mutant RCs, which would indicate that charge-separation was occurring in the RC to support growth. Since the organism displays impaired growth under photosynthetic conditions with just the RC (Jones et al., 1992a; Jones et al., 1992b), the genes encoding the LH1 were added and expressed in pIND4. The wild type RC-LH1 core complex is sufficient for photosynthetic growth and, hence, used as the control.

None of the mutants, 45RC-LH1, 80RC-LH1, or 150RC-LH1, even with the addition of LH1, were able to grow photosynthetically. However, secondary mutants were selected that were phototrophy-capable. Presumably, these mutants carry one or more additional mutations that support growth under anaerobic, phototrophic conditions. Only the secondary mutants with core complexes containing the 80 and 150 RCs were capable of growing photosynthetically, and these mutants were named 80RC-LH1 PS⁺ and 150RC-LH1 PS⁺ (*i.e.*, the 45 mutant did not grow photosynthetically, even with the addition of LH1). To determine whether the secondary mutations were on the plasmid or chromosome, the plasmids expressing the 80RC-LH1 PS⁺ and 150RC-LH1 PS⁺ were extracted and transformed into a clean background, *R. sphaeroides* RCx^R. Since the complemented strains did not grow photosynthetically, it was likely that the secondary mutations were on the chromosome, as the plasmid from a phototrophy-capable strain did not result in a gain-of-function. For additional confirmation, DNA sequencing of the plasmids

expressing 80RC-LH1 PS⁺ and 150RC-LH1 PS⁺ did not show any mutations in the photosynthesis structural genes. The 80RC-LH1 PS⁺ and 150RC-LH1 PS⁺ secondary mutants did not grow as fast as the wild type RC-LH1, as shown in Figure 3.9.

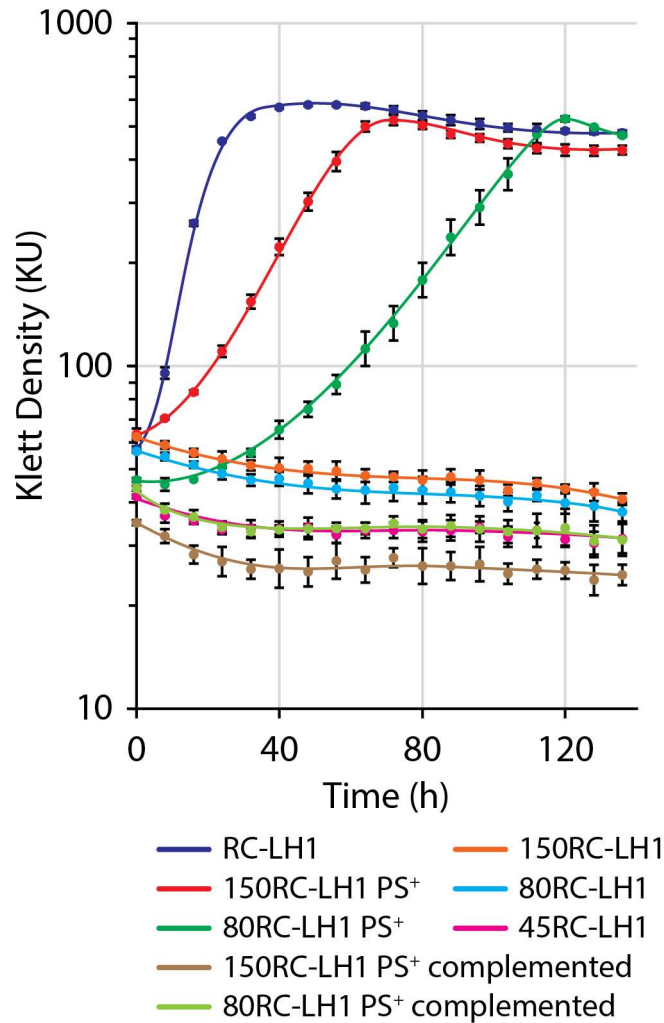


Figure 3.9. Growth curves of the RC truncation mutants under photosynthetic conditions. The mutants that were unable to grow photosynthetically were 45RC-LH1 (magenta), 80RC-LH1 (cyan), and 150RC-LH1 (orange). The plasmids from the 80RC-LH1 PS⁺ (green) and 150RC-LH1 PS⁺ (red) phototrophy-capable mutants were introduced into a “clean background”, *R. sphaeroides* RCx^R. The mutants, 80RC-LH1 PS⁺ complemented (light green) and 150RC-LH1 PS⁺ complemented (brown) did not grow, indicating that the secondary mutations in the strains

80RC-LH1 PS⁺ and 150RC-LH1 PS⁺ were on the chromosome. Error bars represent the standard deviation (n = 3). Lines drawn to represent approximate trends.

Although it was believed that the LM and 45 RC mutants assembled, by measure of the presence of the accessory bacteriochlorophyll at 800 nm, it was quite apparent that these mutants were unable to support photosynthetic growth in the presence of LH1. Evidently, the presence of the peak at 800 nm is not an accurate indication of the fully assembled and functional state of the RC because it is only a measure of the accessory bacteriochlorophyll and not of any other cofactors. Furthermore, although the LM and 45 mutants were able to assemble some components, it may not have been enough to support the cellular demands for quinone cycling. Past research with the LM mutant, where the H subunit was removed biochemically, showed a deficiency in the electron transfer to Q_B (Debus et al., 1985); additional recent data have indicated that the affinity for a quinone at Q_A is decreased and electron transfer rates reduced from H_A to Q_A in an RC lacking the H subunit (Sun et al., 2016; Sun et al., 2015). It might be possible that the affinity for quinones decreases with decreasing H subunit length, leading to a loss of the ability to photosynthesise, although this was not investigated further. The implications of the role of the H subunit and domains in RC assembly are interesting and have merit for further study, but the focus of my research was to investigate whether electrons could be extracted from the truncated RCs.

3.2.4 Effect of detergent on stability, and purification of truncated RC and RC-LH1 complexes.

The main point of working with the truncated RCs was to shorten the distance between Q_A or Q_B and the new protein surface that may facilitate electron transfer to an exogenous acceptor. The experiments in Section 3.2.2 showed that truncated RCs assembled in *R. sphaeroides*, whereas the subsequent experiments in this section describe the purification of the truncated RCs. Since the shortest truncated mutant, the 45 RC, assembled *in vivo*, the focus was to purify this particular mutant, as it provided the greatest accessibility to the Q_A and Q_B regions of the protein. Although the LM RC also assembled, yields were low, presumably due to the inherent instability of the complex outside of a membrane environment. Given the large-scale

modification of the RC, it was expected that the RC might be less stable and require a milder detergent for solubilisation.

Initially, as with the majority of RC mutants in my research, the 6-His tag was located at the C-terminus of the H subunit of the 45 mutant. As predicted, solubilisation with 1% of the zwitterionic LDAO detergent resulted in the immediate denaturation of the 45 mutant RC. Another zwitterionic, but milder, detergent, Deriphat 160C, was tested. The 45 mutant did not denature after solubilisation with 1% Deriphat 160C. However, none of the RCs bound to a Ni²⁺-NTA column. Since the 45 mutant contained a truncated H subunit, the C-terminal 6-His tag may not have projected through the detergent micelle to interact with the column matrix, and so the tag was moved to the C-terminus of the M subunit. A His tag at this location has been used previously with LDAO-solubilised RCs (Goldsmith and Boxer, 1996). Although a 6-His tag did not result in any binding, by extending the tag to 12 His, the 45 RC was able to bind to the column. Unfortunately, the binding appeared to be permanent, as the protein could not be eluted, even at 2 M imidazole. Similar results were obtained with the zwitterionic detergent CHAPS, where RCs were solubilised but could not be eluted from the column. Only by using the non-ionic detergent DDM were RCs able to be bound to and eluted from a Ni²⁺-NTA column. The results of these experiments are summarised in Table 3.1.

Table 3.1. Summary of different detergents used to purify the 45 RC mutant.

Detergent	Tag Length	Tag Location	Solubilisation	Binding	Elution
Deriphat 160C	6 His	H	Yes	No	No
	6 His	M	Yes	No	No
	12 His	M	Yes	Yes	No
CHAPS	6 His	M	Yes	1/2	No
	12 His	M	Yes	2/3	No
DDM	12 His	M	Yes	Yes	Yes

The 45 and 80 mutant RCs have been purified with a 12-His tag on the C-terminus of the M subunit, called 45M and 80M from hereon. The most obvious changes from the wild type RC spectrum are the diminished bacteriopheophytin peak at 760 nm, a diminished special pair bacteriochlorophyll peak at 865 nm, and an increased accessory bacteriochlorophyll peak at 800 nm in the case of the 45 and 80 mutants (Figure 3.10A). A possible reason for the decrease of these peaks may be due to the instability of the mutants or a change in the protein environment surrounding the cofactors. If the former is the case, then a pigment extraction may indicate whether a bacteriochlorophyll or bacteriopheophytin has been lost by calculating the ratios. Table 3.2 shows the ratios of bacteriochlorophyll and bacteriopheophytin in the wild type, LM, 45M, and 80M RCs. In the wild type RC, a ratio of two is expected that represents the four bacteriochlorophylls and two bacteriopheophytins. It was not readily apparent that a pigment was lost from the 45 and 80 truncated RCs. If a single bacteriopheophytin were removed, then a ratio of four would be expected, one and a half in the case of the loss of a single bacteriochlorophyll, or three if both a single bacteriochlorophyll and bacteriopheophytin were lost. For the LM mutant, the ratio of ~ 3 and the further loss of signal in the Q_y transition region probably indicate a loss of a bacteriochlorophyll and bacteriopheophytin. Since a ratio of around two was measured for the 45M and 80M mutants, it was unlikely that any chlorins were lost. Therefore, the most likely explanation for the changes in the absorbance profile compared to the wild type is due to the changes in the protein environment surrounding the cofactors resulting from the deletion of the H subunit cytoplasmic domain. Further, a partial charge-separated state was detected in the 45M and 80M mutants (Figure 3.10B), indicating the likelihood of an intact A-branch with the major bacteriochlorins in place.

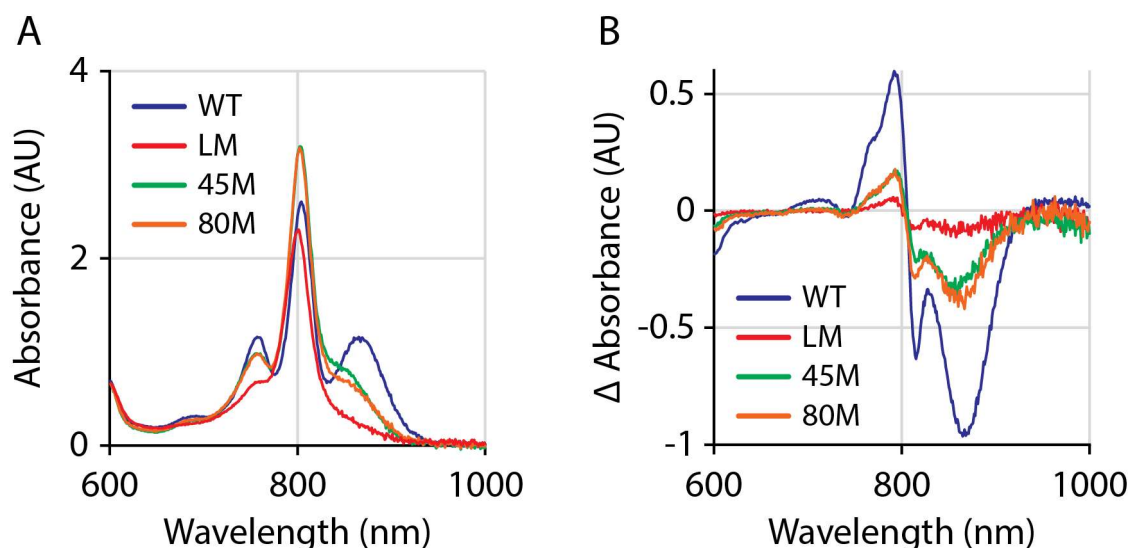


Figure 3.10. Assembly and formation of a charge-separated state in the RC truncation mutants. A) Absorbance spectra and B) difference absorbance spectra of purified wild type (WT; blue), LM (red), 45M (green), and 80M (orange) truncation mutants. The wild type spectrum was normalised to $A_{650} = 0.2$, and the other spectra normalised to the wild type Q_x bacteriochlorophyll peak at 596 nm.

Table 3.2. Ratios of bacteriochlorophyll (BChl) to bacteriopheophytin (BPhe) of pigments extracted from the wild type (WT) and truncated RC H mutants. Errors represent the standard deviation ($n = 3$).

RC	BChl:BPhe
WT	1.83 ± 0.03
LM	2.8 ± 0.1
45M	2.12 ± 0.09
80M	2.20 ± 0.04

In addition to purifying the 45M and 80M truncated RCs, the photosynthesis-capable 80RC-LH1 PS⁺ and 150RC-LH1 PS⁺ strains were grown under photosynthetic conditions and used to purify the respective core complexes. The DDM-solubilised membrane chromatophores showed an accentuated peak at 420 nm for the 80RC-LH1 PS⁺ and 150RC-LH1 PS⁺ mutants, compared to the wild type – the peak most likely corresponded to a cytochrome protein (Figure

3.11A). Upon elution of the core complexes from the Ni²⁺-NTA column, the 420 nm peak diminished, probably because this protein exists in the periplasmic space of cells, resulting in entrapment within chromatophore vesicles, rather than as part of the core complex. Interestingly, unlike the RC-only truncated variants, the 6-His tag on the C-terminus of the H subunit did not pose any issues in Ni²⁺-NTA chromatography. Additionally, the RC and LH1 peaks in the wild type RC-LH1, 80RC-LH1 PS⁺ and 150RC-LH1 PS⁺ mutants, were nearly identical (Figure 3.11B), suggesting that the truncated RC H proteins assembled properly into a core complex.

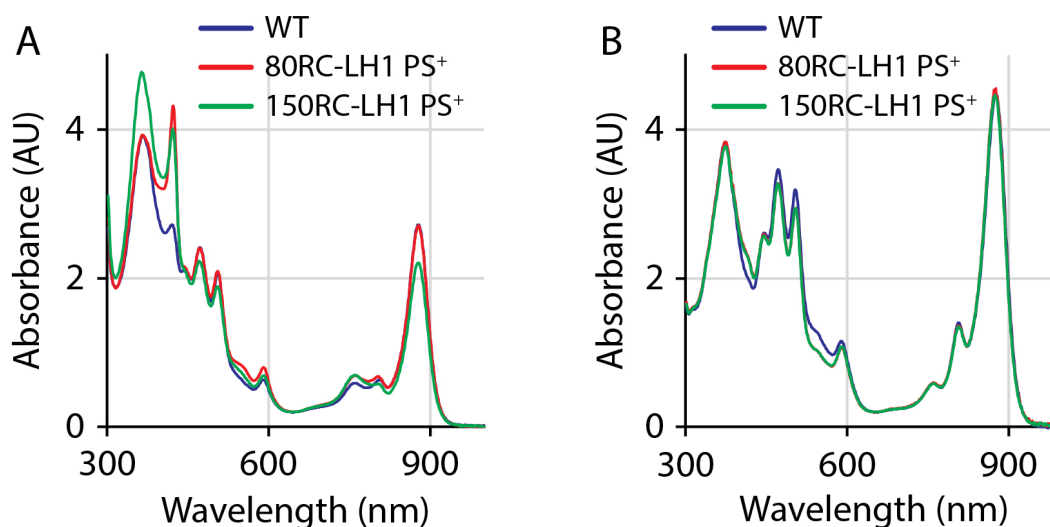


Figure 3.11. Absorbance spectra of the 80RC-LH1 PS⁺ and 150RC-LH1 PS⁺ core complexes. A) solubilised membrane chromatophores, and B) Ni²⁺-NTA column elution products of the 80RC-LH1 PS⁺ (red) and 150RC-LH1 PS⁺ (green) mutants. The spectra were normalised to A₆₅₀ = 0.2.

3.3 Characterisation of RCs bound to a highly ordered pyrolytic graphite (HOPG) or gold electrode.

Having established a high-yielding protein expression system and determined that truncated RCs were stable once purified in the detergent DDM, the next stage of my research focused on making further mutations in order to potentially promote electron transfer from different cofactors in the RC to an electrode, and attach RCs to a highly ordered pyrolytic graphite (HOPG) or gold electrode. To attach RCs to an HOPG electrode, a linker molecule, *N*-(1-pyrene)maleimide, was used. The pyrene group non-covalently binds to HOPG through π -orbital interactions and the maleimide functional group selectively reacts with the sulphur atom

on Cys sidechains. I aimed to show that by binding the RC in various orientations, electrons may be transferred to or from an electrode, depending on the cofactor of interest. Furthermore, since Trp has been shown to accelerate electron transfer in model proteins (Shih et al., 2008), much like a relay, Trp was added between a cofactor and the protein surface to possibly further enhance electron transfer.

3.3.1 Analysis of dye binding to the M256 mutant by SDS-PAGE and mass spectrometry.

Initially, one of the first goals was to show that the maleimide functional group was specific to thiol moieties in a chemical reaction that forms a covalent thioether bond. The M256 mutant was created with an M(M256)C substitution to assess accessibility and specificity of the Cys. Other additional residue substitutions to promote or block electron transfer in this mutant will be described in Section 3.3.5.

To show that the single Cys at M256 was the one binding to a maleimide group, all five native Cys were replaced with either Ser or Ala to eliminate reactions with other Cys. The following mutations were made, resulting in the Cys⁻ RC: C(H156)A, C(H234)S, C(L92)S, C(L108)S, and C(L247)S. The Cys⁻ RC was used as the starting material for additional mutations for each of the other RC mutants used in Section 3.3. A summary table listing the different mutants and corresponding mutations can be found in Appendix A.1. The Cys⁻ and wild type RCs were found to have the same cyt *c*₂ oxidation rate upon illumination (Dutta et al., 2014). Therefore, it was determined that the Cys⁻ mutant was functionally similar to that of the wild type RC, which was reasonable, as the native Cys are not involved in disulphide bonding, located near the cofactors, or known to be involved in electron transfer.

In the M256 mutant, the M(M256)C mutation was made in the vicinity of H_A; however, the location of the Cys was in a hydrophobic region of the RC and appeared to be shielded by a detergent micelle when the RC was solubilised in aqueous solutions. To access the Cys, the detergent was stripped by incubating the protein with Bio-Beads SM-2 resin. The beads are an adsorbent material that removes detergent molecules in solution; as more detergent molecules are removed from the solution, the equilibrium shifts the detergent from the micelles to the solution. The result was the aggregation and precipitation of the RCs.

In a solid-phase form, the proteins were stable and denaturation was not detected upon re-solubilisation by the addition of detergent. To determine the accessibility of the Cys at M256, a commercially available dye, ATTO MB2, was used (structure shown in Appendix B.1). This dye is a derivative of methylene blue with an absorbance peak at 660 nm, corresponding to an absorbance minimum of the RC spectrum (Figure 3.12). Using the ATTO MB2 dye was advantageous, as the dye binding could be monitored easily using UV-vis absorbance spectroscopy, as well as monitoring the specificity of binding by running the RCs on SDS-PAGE and visualising the labelling of the M subunit. After binding, the RCs were re-solubilised with 0.1% LDAO and proteins that denatured and aggregated were removed by centrifugation.

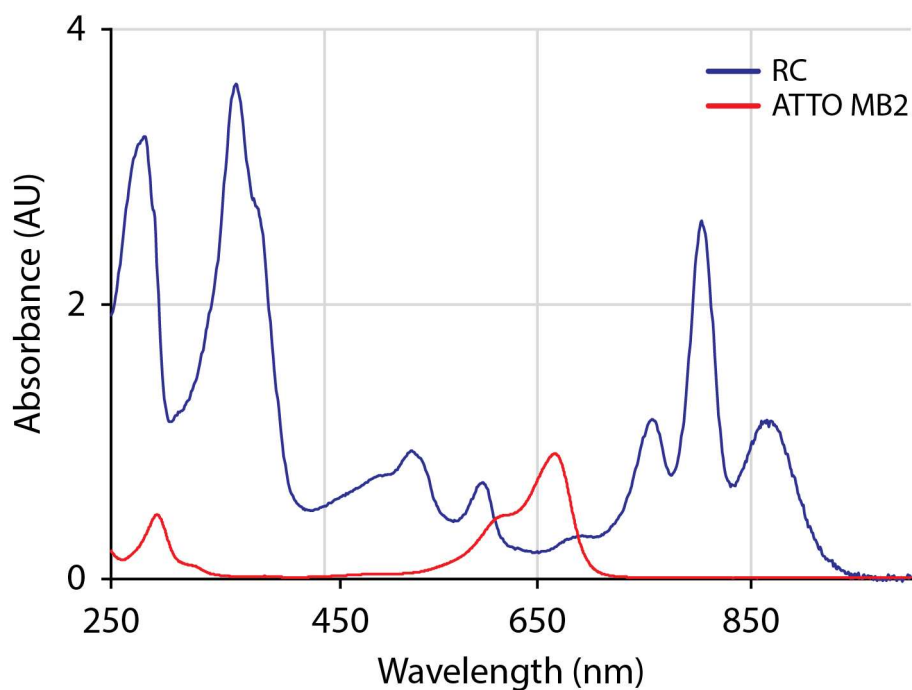


Figure 3.12. Absorbance spectra of the ATTO MB2 dye (red) and RC (blue). The RC spectrum was normalised to $A_{650} = 0.2$, and the ATTO MB2 dye normalised to the equivalent RC molar concentration.

Several conditions were tested, including temperature, pH, dye excess, and incubation time. The pH range of a maleimide cross-linking reaction occurs from a pH of 6.5 to 7.5. The RCs are stable at pH 8, but at this higher pH, the maleimide reacts non-specifically with primary amines and hydrolysis of the maleimide ring occurs, reducing efficiency (Khan, 1984). A pH of

7.2 in 1x PBS was found to be a good balance between reaction rate and reaction specificity. As expected with a typical chemical reaction, when the temperature was increased from 30 °C to 37 °C and 45 °C, the total binding increased as increased thermal energies increased rate kinetics; however, the downside was an increase in non-specific binding, as seen with the ATTO MB2 binding to the H subunit at higher temperatures. An incubation time of 2 h was generally preferred over overnight incubations, and a 10-fold molar excess dye resulted in more non-specific binding compared to that of 3-fold excess dye. The results of the different conditions can be found in Figure 3.13.

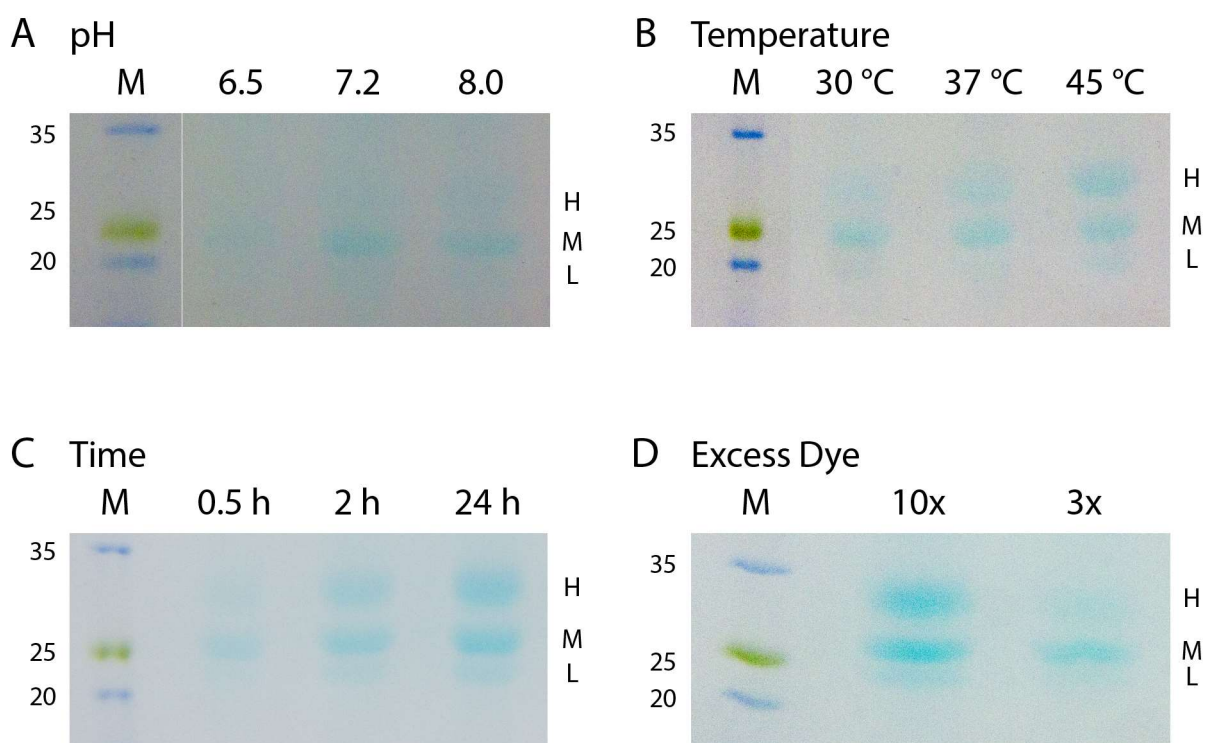


Figure 3.13. SDS-PAGE of conditions tested for the binding of ATTO MB2 to the Cys on M256. A) Different pH values were tested at 6.5 (10 mM Bis-Tris), 7.2 (1x PBS), and 8.0 (10 mM Tris). Samples were incubated at 30 °C for 2 h using 3-fold molar excess dye. B) Different incubation temperatures were tested at 30 °C, 37 °C, and 45 °C. Samples were incubated in 1x PBS pH 7.2 for 2 h using 3-fold molar excess dye. C) Different incubation times were tested for 30 min, 2 h, and 24 h. Samples were incubated in 1x PBS pH 7.2 at 30 °C using 3-fold molar excess dye. D) Different molar excesses of dye were tested using 10-fold and 3-fold molar excess. Samples were incubated in 1x PBS pH 7.2 for 2 h at 30 °C. The gels were unstained and

the visible cyan bands are due to the absorbance of ATTO MB2 bound to an RC subunit. The molecular-weight marker lane is indicated with the letter M.

As determined by SDS-PAGE, the ATTO MB2 dye bound to the M subunit M256 mutant, under the optimal conditions of a 2 h incubation at 30 °C in 1x PBS pH 7.2 using 3-fold molar excess dye. The binding specificity was further evidenced by mass spectroscopy, where an increase in the mass of the M subunit was detected, as shown in Figure 3.14. The mass increase of the M subunit is expected to be equal to the mass of the ATTO MB2 dye. The reaction was specific and bound minimally to the H or L subunits. Furthermore, since only a few unbound M subunits were detected in the mass spectrometry trace, it was presumed that the labelling was highly efficient and specific.

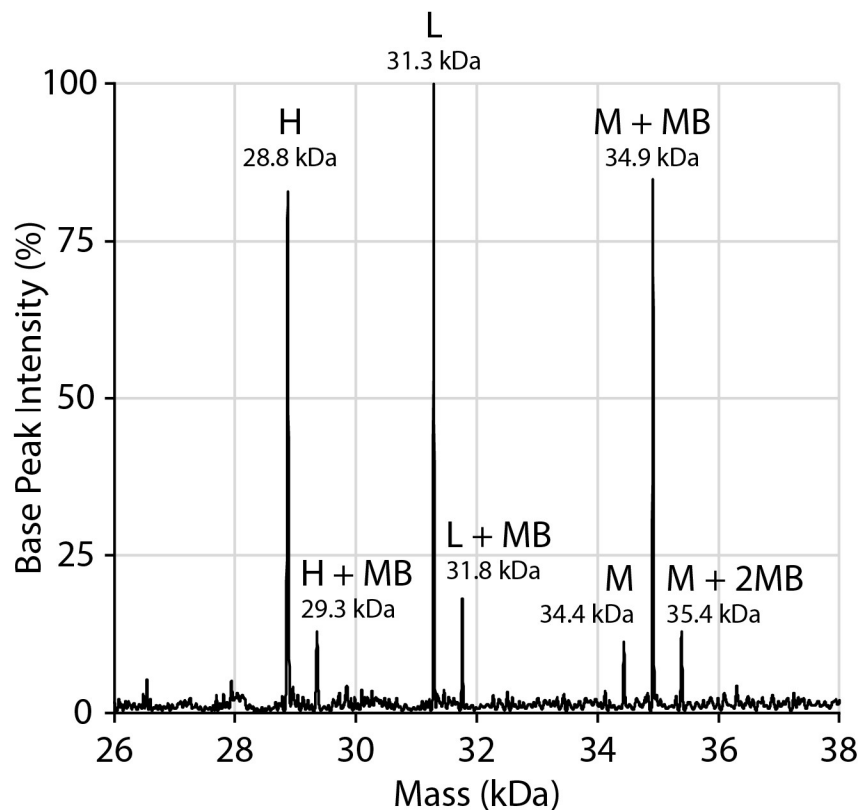


Figure 3.14. Mass spectroscopy of the M256 mutant bound to the ATTO MB2 dye. The vertical axis gives the percentage of base peak intensity.

The predicted and measured molecular weights of the protein subunits and ATTO MB2 dye are tabulated in Table 3.3. The majority of the dye bound to the M subunit, where the Cys is located on residue 256.

Table 3.3. Predicted and measured molecular weights of the RC subunits and ATTO MB2 dye.

Subunit	Predicted MW (kDa/mol)	Measured MW (kDa/mol)
H	28.8	28.8
L	31.4	31.3
M	34.5	34.4
ATTO MB2	0.5	0.5

3.3.2 Surface analysis of an HOPG or gold electrode using cyclic voltammetry.

The previous section characterised the chemical reaction specificity of the maleimide functional group to thiols, which is one part of the *N*-(1-pyrene)maleimide linker. The other part of the molecule contains a pyrene group and this functional group is used to non-covalently bind the linker to the HOPG electrode. Trying to determine surface coverage of the HOPG electrode with linker molecules or RCs is difficult and has not been well-documented in the literature. Most approaches are qualitative, such as the use of atomic force microscopy (AFM) to visualise protein structures on an electrode surface. Other techniques are indirect measurements, for example, using ellipsometry to show that a layer of protein was adsorbed onto the surface (Lebedev et al., 2006) or demonstrating using an action spectrum that the measured photocurrents were due to the presence of photosynthetic proteins on an electrode (den Hollander et al., 2011). The results described here using cyclic voltammetry (CV) was also a form of indirect measurement, but attempted to characterise the physical properties of both the linker layer and the RC layer, as a way of determining surface coverage.

RCs have conventionally been stored in 10 mM Tris pH 8, but the maleimide reaction chemistry was found to occur ideally at around pH 7.2 (Section 3.3.1). Tris is often used to buffer solutions between pH 7 and 9, and so Tris could have been used at pH 7.2 for the linking chemistry. However, it was found that Tris interacted with the surface of an HOPG electrode and

formed a blocking layer on the surface that decreased interactions of charge-transfer mediators with the electrode. To demonstrate this finding, CVs of a bare, clean HOPG electrode immersed in an aqueous solution of 1 mM ferrocyanide buffered with 10 mM Tris-HCl pH 8 were measured (Figure 3.15A). Additionally, CVs of the same setup but with 1 mM ferrocyanide in 1x PBS pH 7.2 were recorded (Figure 3.15B). In the first cycle of both buffers, the ferrocyanide oxidation and reduction peaks were present; however, in the case of the Tris buffer, the subsequent cycles showed a decrease of the ferrocyanide current peaks and broadening of the anodic and cathodic peak potential difference. This was a good indication that Tris interacted with the HOPG electrode and formed a partial blocking layer on the surface that reduced the interaction of ferrocyanide with the electrode (Kong et al., 2014; Nicholson, 1965). Conversely, the 1x PBS buffer did not show similar results and therefore, the reason for using 1x PBS instead of Tris when running experiments.

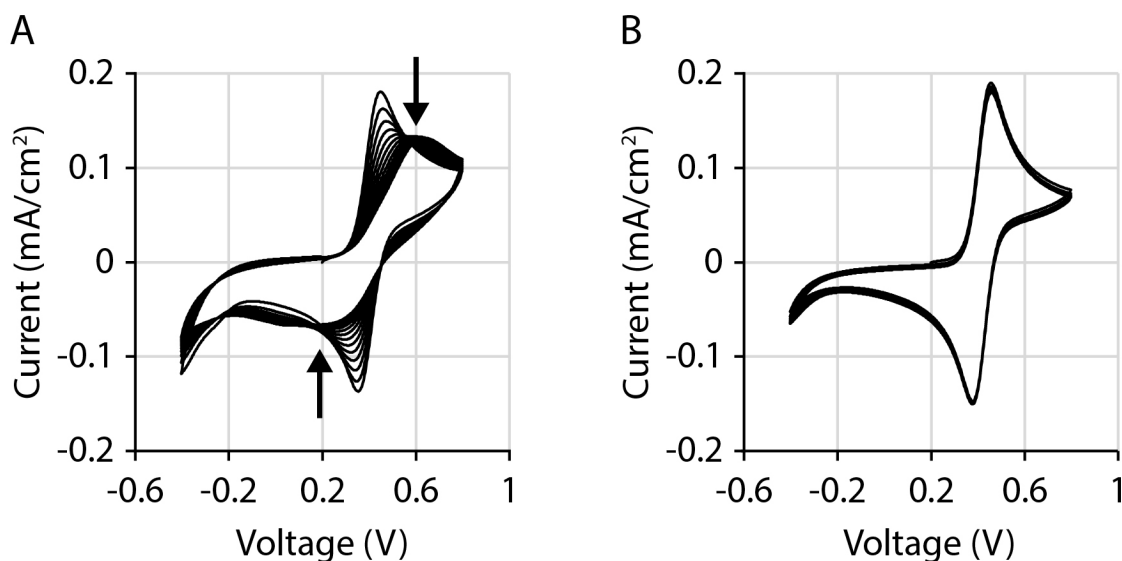


Figure 3.15. CVs of 1 mM ferrocyanide in 10 mM Tris pH 8.0 or 1x PBS pH 7.2 buffer using an HOPG working electrode. A) 25 cycles (only odd-numbered cycles shown) of 1 mM ferrocyanide in 10 mM Tris pH 8. Arrows indicate decreasing amplitude of adjacent ferrocyanide oxidation and reduction peaks with increasing cycle number. B) 10 cycles of 1 mM ferrocyanide in 1x PBS pH 7.2. Voltage swept at 100 mV/s. Potentials are with respect to the Standard Hydrogen Electrode (SHE).

The surface chemistry of HOPG changed after incubation with *N*-(1-pyrene)maleimide. To compare, CVs of clean, bare HOPG with 1 mM ferrocyanide in 1x PBS pH 7.2 buffer were measured. The peaks corresponding to the reduced and oxidised peaks of ferrocyanide on clean HOPG were observed (Figure 3.16). Evidently, as in the Figure 3.15A experiment, ferrocyanide was able to access the electrode and Faradaic electron transfer reactions occurred. After incubation in the presence of the linker, the CVs showed a decrease of the ferrocyanide peaks. Similar to the adsorption of Tris on an HOPG electrode, the *N*-(1-pyrene)maleimide appeared to cover the HOPG electrode surface and ferrocyanide electron exchange with the electrode was impeded. Therefore, it was likely that the *N*-(1-pyrene)maleimide linker formed a self-assembling layer on the surface of the HOPG electrode, to which a control SbnI protein or RCs could then be attached. The reduction peak at ~ -0.1 V appears to be an artefact that occurs due to a flaw in the assembly of the electrode, such as exposure of non-HOPG electrode components to the electrolyte; HOPG electrodes used in future experiments were tested to verify the absence of the peak before running photoelectrochemical measurements.

The soluble SbnI protein, purified from *E. coli*, was used as a control (generously provided by the Murphy laboratory in the Department of Microbiology and Immunology, UBC), because it naturally contains seven Cys on the protein surface and is neither redox active nor reactive to light illumination. From the results in Section 3.3.1 that showed the high efficiency and binding specificity of maleimides to thiols, it was therefore assumed that the binding of the maleimide functional group on *N*-(1-pyrene)maleimide was to the exposed thiols on SbnI. After incubation, CVs were measured again in the presence of 1 mM ferrocyanide. The ferrocyanide peaks were eliminated, indicating that the addition of SbnI likely bound to the linker and formed a blocking layer that prevented ferrocyanide from accessing the electrode surface.

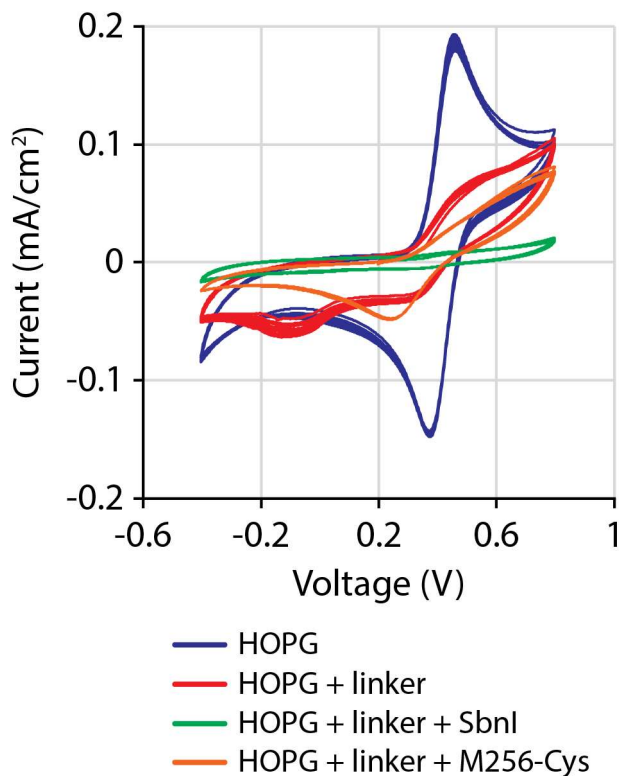


Figure 3.16. CVs of 1 mM ferrocyanide in 1x PBS pH 7.2 buffer using an HOPG working electrode. Several conditions were tested: bare HOPG (blue), HOPG with *N*-(1-pyrene)maleimide linker (red), HOPG with *N*-(1-pyrene)maleimide linker and bound SbnI (green), and HOPG with *N*-(1-pyrene)maleimide linker and bound M256-Cys RCs (orange). CVs were swept at 100 mV/s and cycled 5 times. Potentials are with respect to the Standard Hydrogen Electrode (SHE).

Interestingly, different results were obtained when the M256-Cys RC mutant was bound to the HOPG electrode. The M256-Cys mutant has two additional Cys compared to the M256 mutant. The additional Cys are located in a hydrophilic region at A(H51)C and W(L59)C, because it was found that the Cys at M(M256)C (in a hydrophobic region) appeared to be inaccessible due to the detergent micelle (see Section 3.3.1). A schematic of the M256-Cys binding to an HOPG electrode is shown in Figure 3.17. As shown in Figure 3.16, CV peaks were detected at 0.3 and 0.5 V, which could have been due to ferrocyanide. However, if the entire surface were covered with protein, as shown with the SbnI control, then it would be unlikely for the peaks to be have been due solely to ferrocyanide. A possible explanation and an indication

that RCs were bound to the electrode would be the contribution of the redox peaks of the RC special pair, with a similar midpoint potential to that of ferrocyanide of ~ 450 mV (Shuvalov et al., 1986; Yaghoubi et al., 2012), although, as will be shown later, the redox peaks were not apparent when the RC M256-Cys was bound to gold. Another possibility is that the RCs are assisting in the transfer of electrons from ferrocyanide, perhaps due to open gaps between RC units, or RCs pulling the linker off and exposing the electrode.

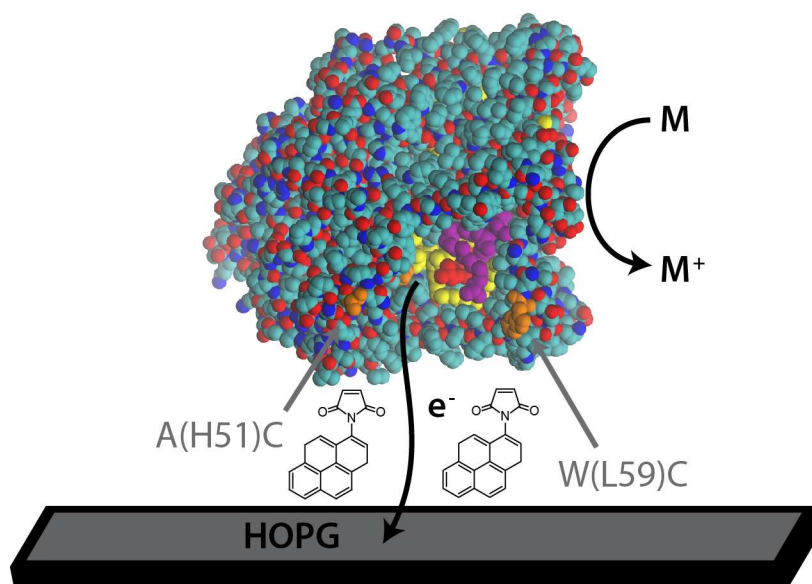


Figure 3.17. Schematic of RC binding to an HOPG electrode using *N*-(1-pyrene)maleimide linkers. The M256-Cys mutant is shown, with the Cys substitutions at A(H51)C and W(L59)C (orange), which are assumed to bind to *N*-(1-pyrene)maleimide on an HOPG electrode. The diagram shows how electrons might be extracted from the H_A (yellow) region of the RC and the P⁺ state reduced with a charge-transfer mediator in solution ($M \rightarrow M^+ + e^-$). Structure is based on PDB 2J8C.

Gold electrodes can also be used to bind RCs via Cys thiol moieties, as Au–S bonds form spontaneously. However, one of the major issues working with gold electrodes is the propensity for proteins and other molecules to non-specifically adsorb onto the surface (Moulton et al., 2003). Techniques to overcome this issue include coating the surface with a self-assembling

monolayer to prevent non-specific interactions (Yu et al., 2016) or reducing electrode exposure time to proteins (Iranpour, 2012). To ensure that PBS buffer components did not adsorb onto the electrode surface and interfere with electron transfer to gold, CVs were run with a solution of 1 mM ferrocyanide in 1x PBS pH 7.2 (Figure 3.18). Similar to the earlier results on an HOPG electrode (Figure 3.15), no adsorption was detected, as the ferrocyanide peaks did not shift or decrease, which would have indicated formation of a blocking layer on the electrode surface. This is largely in agreement with results in literature (Moulton et al., 2003). Upon addition of the SbnI protein, the ferrocyanide peaks disappeared, similar to the results obtained using an HOPG electrode. When M256-Cys was added, the ferrocyanide peaks also disappeared, which is in contrast to the data measured with an HOPG electrode. The loss of the Faradaic redox peaks is a good indication that a protein blocking layer was formed on the surface and prevented ferrocyanide from accessing the electrode. Whether the binding was specific or not could not be determined further, and other results, such as direction of current and action spectra would be required to determine whether a population of the RCs was oriented properly.

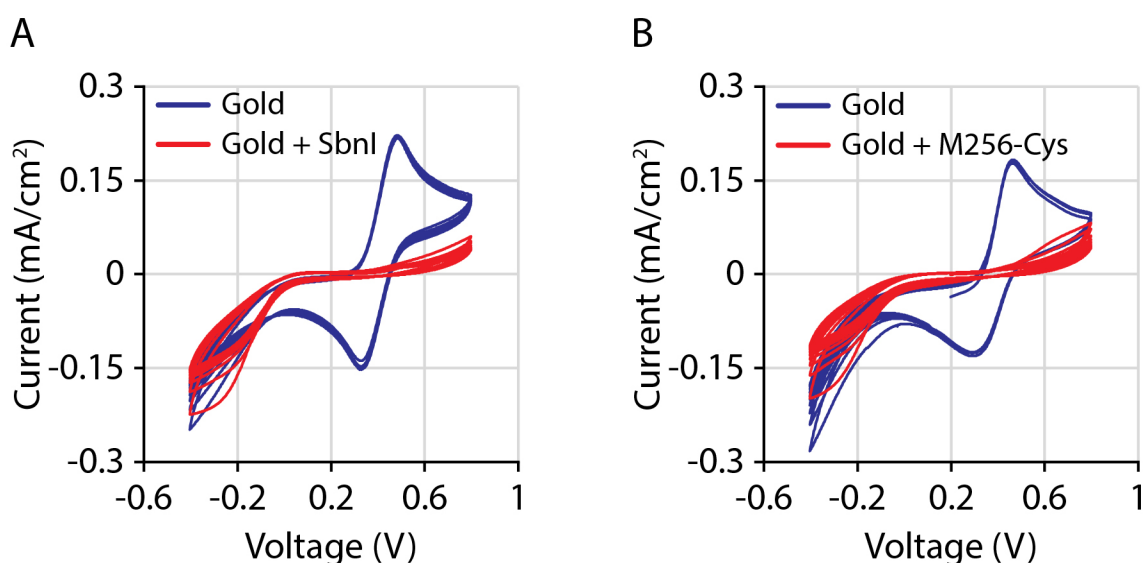


Figure 3.18. CVs of 1 mM ferrocyanide in 1x PBS pH 7.2 buffer using a gold working electrode. A couple conditions were tested: bare gold (blue) and gold with bound protein (red). A) The negative control SbnI and B) M256-Cys RC mutant. CVs were swept at 100 mV/s and cycled 10 times. Potentials are with respect to the Standard Hydrogen Electrode (SHE).

3.3.3 Photochronoamperometry measurements of SbnI bound to an HOPG or gold electrode.

The SbnI protein was used as a control, as it does not contain any photoactive chromophores, to determine whether the electrode and hydroquinone contributed to photocurrent generation upon illumination. When bound to an HOPG electrode by the *N*-(1-pyrene)maleimide linker illumination initiated a current of about 10 nA/cm² that drifted back to the dark current value in about 70 s (Figure 3.19A). The addition of 1 mM hydroquinone increased the photocurrent to around 20 nA/cm² with a slow decrease during the illumination period. The gold electrode also displayed current generation upon illumination of steady-state currents of less than 20 nA/cm² (Figure 3.19B). With this electrode setup, however, the addition of 1 mM hydroquinone did not increase photocurrents. Since the addition of hydroquinone did not change photocurrents, the interpretation was that SbnI formed a blocking layer on the electrode surface, in agreement with data from Section 3.3.2. The small increase in photocurrents on an HOPG electrode, however, may be attributed to the spacing of the *N*-(1-pyrene)maleimide linkers, resulting in small gaps between individual proteins, allowing hydroquinone to access the electrode. Further, both the gold and HOPG electrodes showed, steady state photocurrents of less than 20 nA/cm².

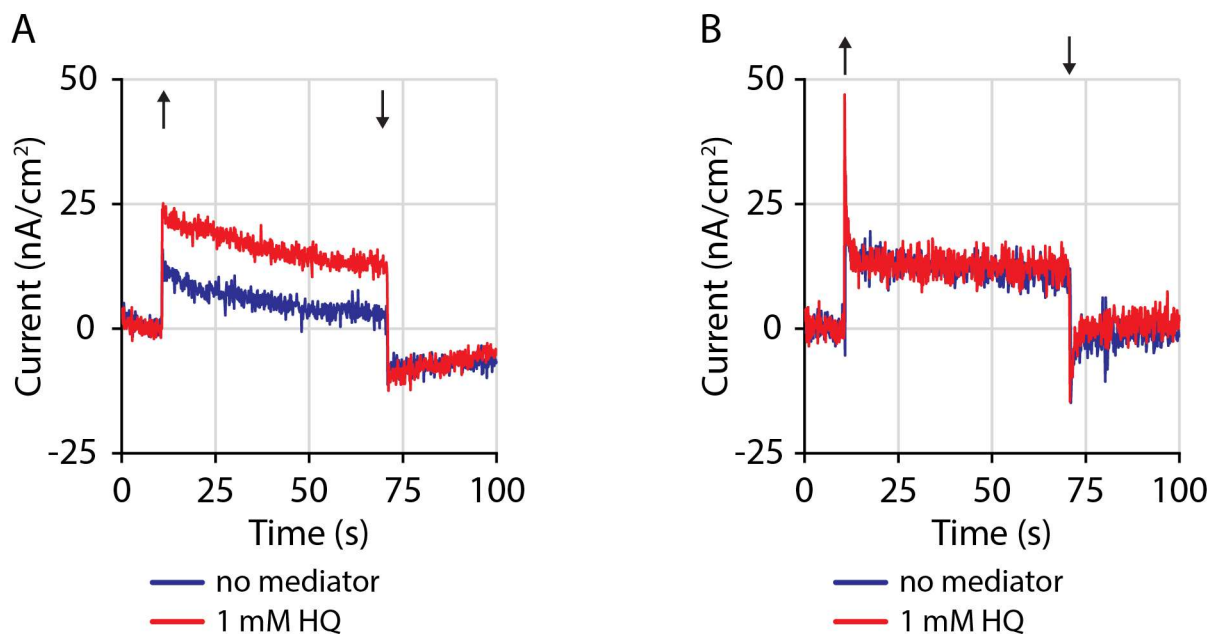


Figure 3.19. Photocurrents generated by SbnI on an HOPG or gold electrode. Arrows indicate light on (↑) and light off (↓). A) On an HOPG electrode, currents less than 15 nA/cm² were generated without hydroquinone (HQ) (blue), but the addition of 1 mM hydroquinone resulted in higher currents (red). B) On a gold electrode, steady-state currents of less than 20 nA/cm² were generated without hydroquinone (blue) and the addition of 1 mM hydroquinone did not result in a change in currents (red).

3.3.4 Addition of Cys near the P region and photochronoamperometry measurements of the TM mutant bound to an HOPG or gold electrode.

The special pair absorbs a photon upon illumination and subsequently an electron is excited, resulting in the excited state P*. The electron is then transferred to the accessory bacteriochlorophyll, bacteriopheophytin, and then the primary quinone at Q_A forming a charge-separated state, P⁺Q_A⁻. The P⁺ state is normally reduced by an electron donor in solution, such as cyt *c*₂, ascorbate, or ferrocyanide. However, by binding an RC with the P-side closest to the electrode surface, the electrode could also serve as an electron source and reduce the P⁺ state of the special pair.

In order to attach the RC to the electrode, three substitutions were made on the P-side in a Cys⁻ RC background: E(L72)C, N(L274)C, and E(M100)C. The resulting RC was called the

triple mutant, or TM. The three Cys were located around the periplasmic side on the rim of a “bowl”, as shown in Figure 3.20. The TM mutant was attached to a gold electrode directly without the use of a linker (Magis et al., 2011; Mahmoudzadeh et al., 2011) and to an HOPG electrode using the *N*-(1-pyrene)maleimide linker.

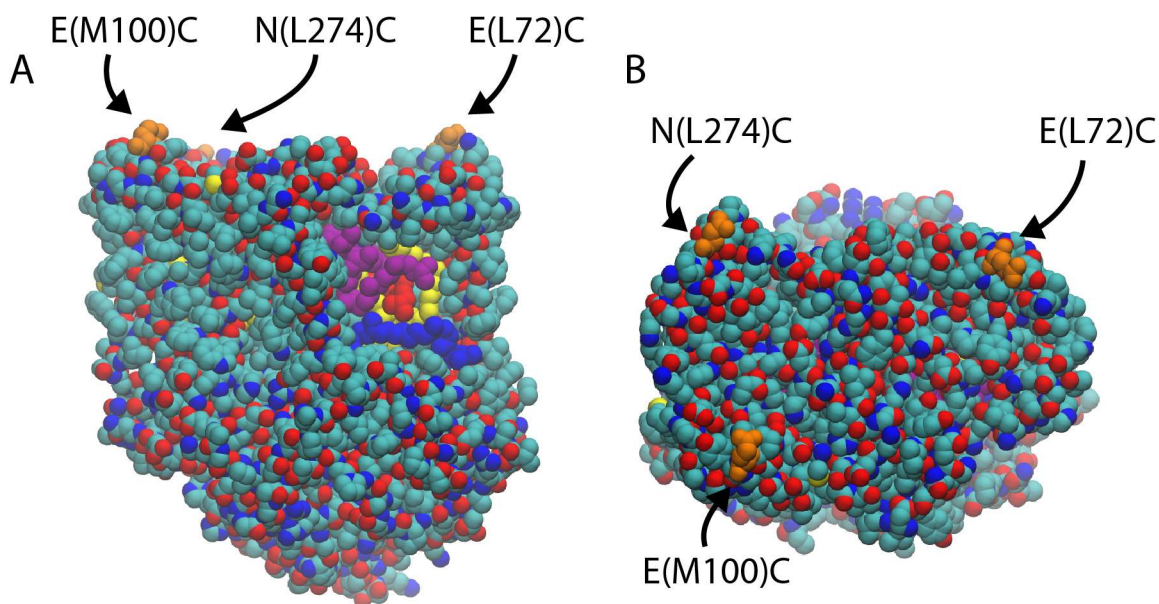


Figure 3.20. Structural modifications in the TM RC. Three substitutions were made to introduce Cys (orange) to the P-side of the RC: E(L27)C, N(L274)C, and E(M100)C. A) View of the TM RC from the side with the primary bacteriochlorophyll (red), accessory bacteriochlorophyll (purple), bacteriopheophytin (yellow), and quinone (blue). B) View from the top towards the cyt c_2 binding pocket. Structures are based on PDB 2J8C.

Photocurrents were generated upon illumination of the gold electrode-bound TM RC. Compared to previously published results, where maximum currents generated were approximately -5 nA/cm^2 (Mahmoudzadeh et al., 2011), currents this time were around -175 nA/cm^2 with 5 mM benzoquinone, as shown in Figure 3.21A. The increasing cathodic, negative currents with increasing concentration of benzoquinone indicated that the electrode supplied electrons to reduce the P^+ state. Benzoquinone was used as a charge mediator to shuttle electrons from Q_B to the counter electrode. The exact source of the large spike and steady-state positive photocurrents is unclear, but may possibly be attributed to electron extraction from the P region

(P* or B_A⁻ states), light-dependent oxidation of reduced benzoquinone on the electrode surface, or an instrumentation artifact. Similar large spikes have been reported, albeit in the opposite current direction (Mirvakili et al., 2014). If the positive photocurrents are due to electron extraction from the P region, then to verify this interpretation, *o*-phenanthroline, a non-redox-capable inhibitor of quinones at Q_B, was used to block electron transfer, as shown in Figure 3.21B (Diner et al., 1984; Wraight and Stein, 1980). A steady-state current of less than 10 nA/cm² was generated in the presence of 1 mM *o*-phenanthroline, similar to the currents generated with the SbnI control. With increasing concentrations of benzoquinone, increasing anodic, positive currents were measured, where at 1 mM benzoquinone, illumination resulted in an initial spike of 1.2 μA/cm² and steady state currents of 70 nA/cm². As suggested earlier, the generation of anodic, positive currents may be due to electron extraction from the P region, as electron transfer to Q_B is inhibited by *o*-phenanthroline. Reduction of the P⁺ state is likely mediated by the reduced form of benzoquinone; CVs showed that a freshly-prepared solution of benzoquinone is a mixture of the oxidised and reduced forms of the molecule, since an oxidation peak was measured in the first cycle, when voltages were ramped in the positive direction (Appendix C.1). Finally, binding of the TM mutant to an HOPG electrode resulted in the formation of positive photocurrents only, as shown in Figure 3.21C. A spike of 150 nA/cm² and steady state currents of 50 nA/cm² were measured. On HOPG, no negative photocurrents were detected, as would have been expected using 1 mM benzoquinone and without *o*-phenanthroline. In this configuration, the extraction of electrons of the P* state may be favoured over electron transfer to Q_B, resulting in anodic, positive photocurrents.

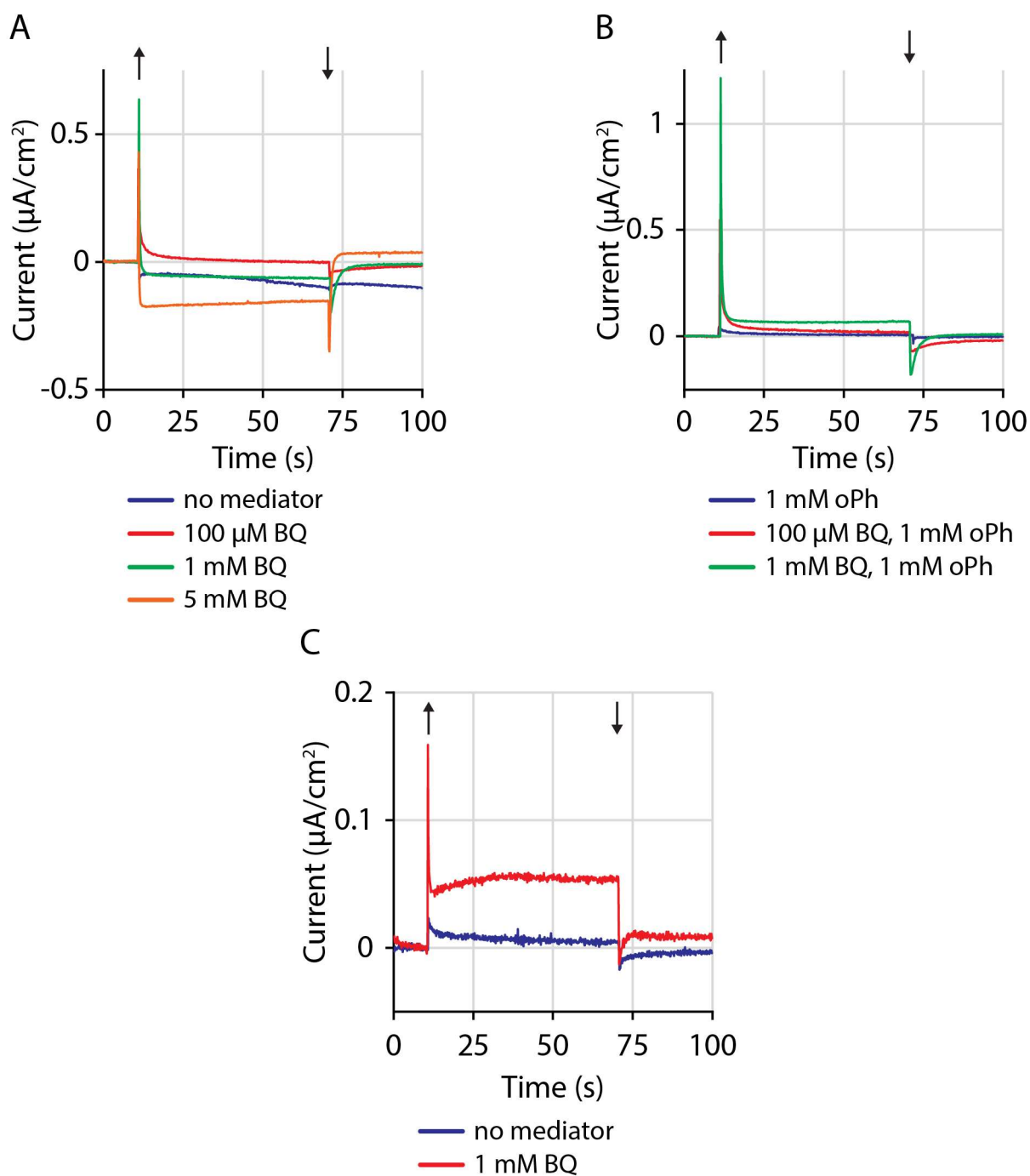


Figure 3.21. Photocurrents generated by the TM mutant on an HOPG or gold electrode. Arrows indicate light on (\uparrow) and light off (\downarrow). A) Different concentrations of benzoquinone (BQ) were used to generate photocurrents at 100 μM (red), 1 mM (green), and 5 mM (orange) on a gold electrode. B) 1 mM *o*-phenanthroline (oPh) was added as a control, as it is a competitive inhibitor of quinones, to block electron transfer to Q_B in the presence of benzoquinone at 100 μM

(red), and 1 mM (green) on gold. C) TM was bound to an HOPG electrode and 1 mM benzoquinone used to generate photocurrents.

To verify whether the observed photocurrents were indeed due to the RCs attached to the electrode, an external quantum efficiency action spectrum was calculated (Figure 3.22). Since the monochromator did not provide enough light intensity to measure a signal, stronger LEDs were used. Although the action spectrum is not identical to the TM absorbance spectrum, the major defining features, such as the higher absorbance peak of the accessory bacteriochlorophyll at 804 nm relative to the bacteriopheophytins at 760 nm and the special pair bacteriochlorophylls at 865 nm, are present. The action spectrum provides evidence that the currents produced under illumination were most likely due to the contributions of the TM bound to a gold electrode.

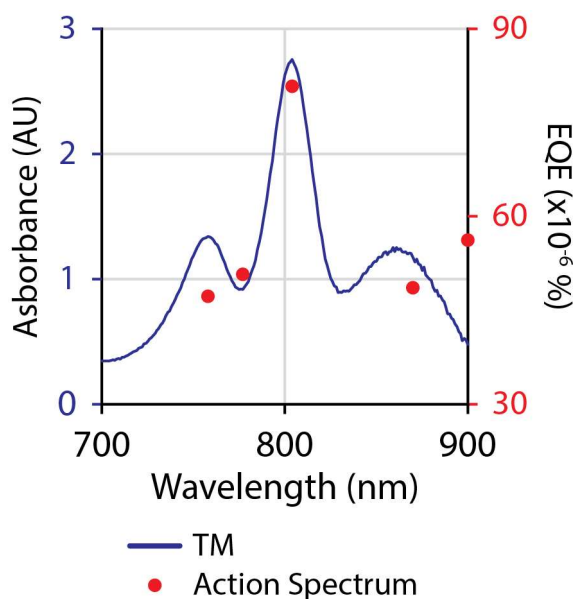


Figure 3.22. External quantum efficiency (EQE) action spectra of the TM mutant on a gold electrode. 1 mM benzoquinone was used as the electron acceptor. The absorbance spectrum of the TM mutant was normalised to $A_{650} = 0.2$.

3.3.5 Addition of Cys near the H_A region and photochronoamperometry measurements of the M256-Cys and M256/L121-Cys mutants bound to an HOPG or gold electrode.

After an electron is excited and begins the chain of redox events in the A-branch, the electron is transferred to the H_A bacteriopheophytin from the B_A bacteriochlorophyll. The electron is then transferred to the Q_A primary quinone. In order to extract electrons from H_A, the electron transfer to Q_A should be slowed or blocked completely. Earlier research showed that an A(M260)W mutation introduced a Trp residue in the Q_A binding pocket and prevented the Q_A quinone from assembling in the RC (McAuley et al., 2000; Ridge et al., 1999); consequently, the electron does not proceed to Q_A or Q_B. Furthermore, a Trp bridges the bacteriopheophytin and the quinone at Q_A, and replacement with non-aromatic amino residues resulted in a decrease in electron transfer to Q_A (Balabin and Onuchic, 2000; Stilz et al., 1994). An A(M260)W and W(M252)F substitution were combined to prevent electrons proceeding beyond the bacteriopheophytin in the H_A site. These mutations were created in the Cys⁻ RC and coupled with the M(M256)C mutation to result in the M256 mutant.

Earlier results in Section 3.3.1 assessed the specificity of maleimide binding to Cys thiols. However, due to the location of M(M256)C (in a hydrophobic region and presumably buried underneath a detergent micelle at the bottom of a depression as shown in Figure 3.23A) and the shortness of the *N*-(1-pyrene)maleimide linker, the Cys in this particular location could not be relied for attachment to an electrode. Two additional substitutions were created, A(H51)C and W(L29)C, resulting in the M256-Cys mutant. The locations of these Cys were on the protein surface and in hydrophilic regions.

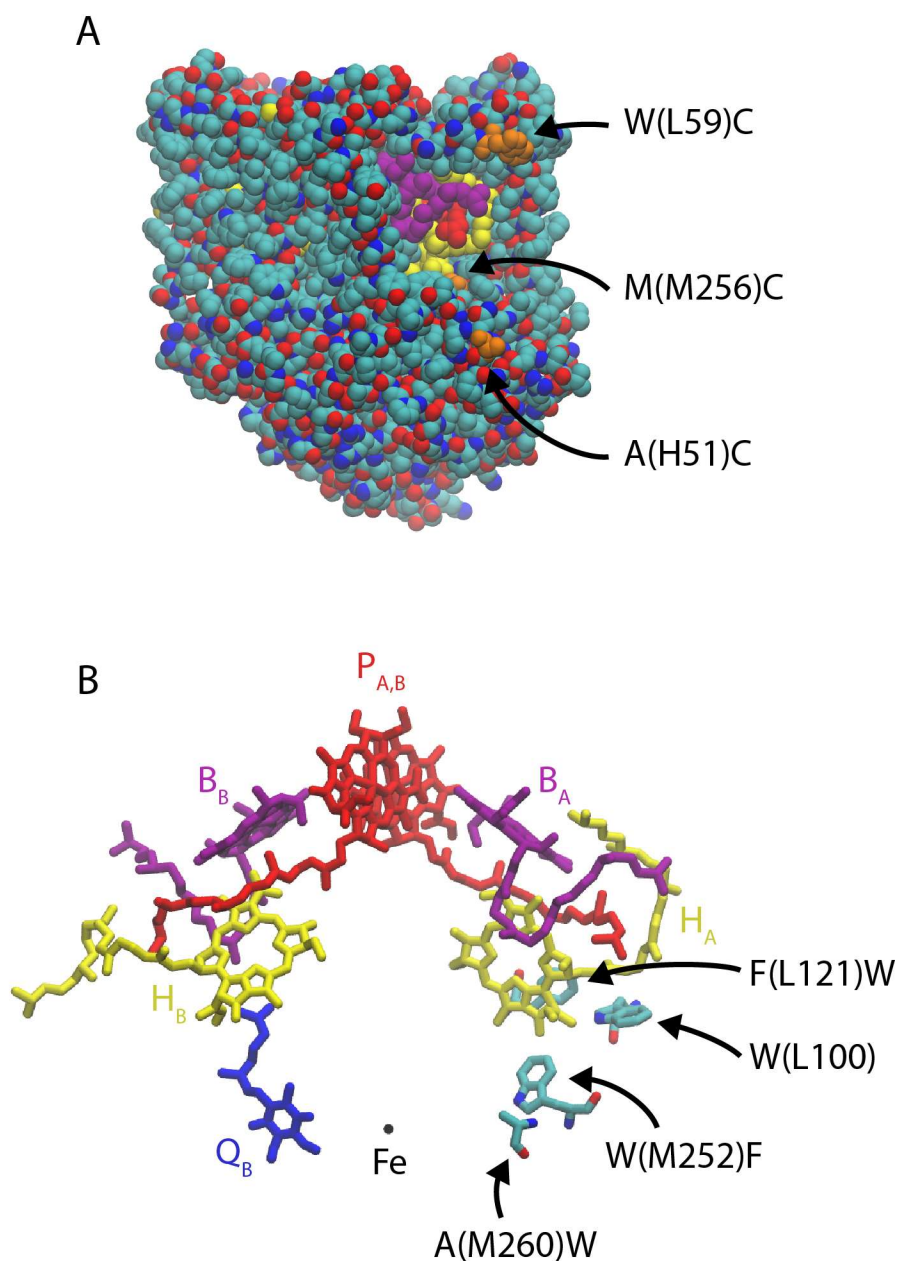


Figure 3.23. Structural modifications in the M256-Cys and M256/L121-Cys mutants. A) Arrangement of Cys in the M256-Cys and M256/L121-Cys mutants with the primary bacteriochlorophyll (red), accessory bacteriochlorophyll (purple), bacteriopheophytin (yellow), and quinone (blue). Three substitutions were made to introduce Cys (orange) in the vicinity of H_A : A(H51)C, W(L59)C, and M(M256)C. It is believed that only A(H51)C and W(L59)C participate in covalent bonding to the *N*-(1-pyrene)maleimide linker, as they are in exposed,

hydrophilic regions of the RC. B) Arrangement of the cofactors and amino acid residues in the M256-Cys and M256/L121-Cys mutants. The quinone at Q_A does not assemble due to a A(M260)W substitution. Arrows show the locations of F(L121)W and W(L100). Structures are based on PDB 2J8C.

A further mutation, F(L121)W, was made, resulting in M256/L121-Cys. It was hypothesised that the π orbitals of the H_A bacteriopheophytin macrocycle would interact with those at the L121 Trp. Another Trp at L100 would be within van der Waals distance for possible edge-to-edge electron transfer (Figure 3.23B).

The M256-Cys and M256/L121-Cys mutants were bound to an HOPG electrode via the *N*-(1-pyrene)maleimide linker. 100 or 500 μ M ascorbate was used to reduce the M256-Cys mutant (Figure 3.24A). Although some photocurrents were generated beyond that of the control, the rate of electron transfer from ascorbate to P^+ appeared to be slow and overall currents low. In other words, the maximal steady-state current obtained with 100 μ M ascorbate was reached at around 20 nA/cm^2 , which did not increase very much with a 5-fold molar increase in ascorbate to around 25 nA/cm^2 . In contrast, when 500 μ M hydroquinone was used with the M256-Cys, currents increased to around 50 nA/cm^2 (Figure 3.24B). Additionally, the diffusive-limited behaviour, observed as the initial spike and decay, was eliminated with excess 1 mM hydroquinone. The difference between the mediators may be due to the fact that ascorbate is not a fast electron donor compared to hydroquinone. CVs were run showing that hydroquinone has at least a 50-fold increase in the peak oxidation current compared to that of ascorbate (Appendix C.1).

The M256/L121-Cys mutant was designed with a F(L121)W mutation to determine whether the presence of this additional Trp would accelerate electron transfer from H_A to the electrode. It was presumed that the Trp would interact with the H_A bacteriopheophytin macrocycle and withdraw electrons away from the bacteriopheophytin as part of a relay. The results indicated that in fact the M256-Cys mutant created greater current, in the same experimental conditions of using 1 mM hydroquinone in 1x PBS pH 7.2 (Figure 3.24C). The shaded blue and red regions are the standard deviation of three samples.

Finally, the M256-Cys mutant was attached to a gold electrode. Here, the results were cleaner than on an HOPG electrode, with less drift masking the current baseline. Evidently, the addition of more hydroquinone resulted in higher currents, with the maximal steady-state current peaking with 2 mM hydroquinone at about 100 nA/cm^2 (Figure 3.24D). The initial spike observed to reach 200 nA/cm^2 may be attributed to rapid electron transfer that is faster than the diffusion of the mediator.

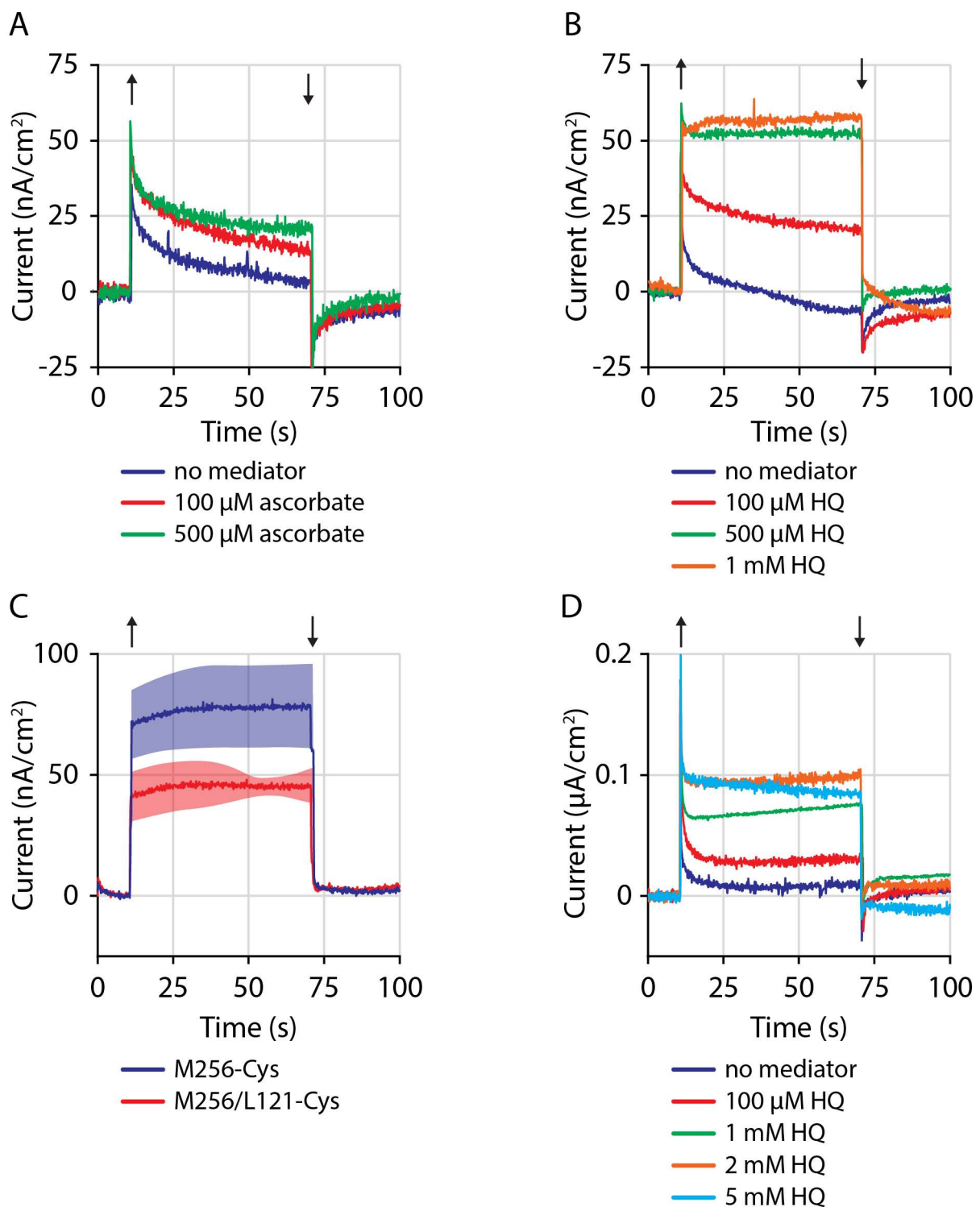


Figure 3.24. Photocurrents generated by the M256-Cys and M256/L121-Cys mutants on an HOPG or gold electrode. Arrows indicate light on (↑) and light off (↓). A) Different concentrations of ascorbate were used to generate photocurrents at 100 μM (red) and 500 μM

(green) on an HOPG electrode. B) Hydroquinone (HQ) was titrated at 100 μ M (red), 500 μ M (green), and 1 mM (orange), showing faster kinetics than ascorbate on an HOPG electrode, indicated by an increase in current. C) The average ($n = 3$) and standard deviation (shaded blue and red regions) of the M256-Cys (blue) and M256/L121-Cys (red) were plotted to determine whether the F(L121)W mutation resulted in accelerated electron flow on an HOPG electrode using 1 mM hydroquinone as the electron donor. D) M256-Cys was bound to a gold electrode and titrated with 100 μ M (red), 1 mM (green), 2 mM (orange), and 5 mM (cyan) hydroquinone.

External quantum efficiency action spectra of the M256-Cys and M256/L121-Cys mutants were calculated (Figure 3.25). In the case of the M256-Cys RC, the action spectrum showed a good correlation between the RC spectrum and the action spectrum. Although the spectra did not align perfectly, the major features, such as the peaks and valleys corresponded, as well as the greater contribution from the accessory bacteriochlorophyll at 804 nm than the other pigments. Similar results were observed with action spectrum of the M256/L121-Cys, though the accessory bacteriochlorophyll appeared to be depressed with respect to the bacteriopheophytin at 760 nm. Given that the absorbance spectrum also showed a decreased absorbance at 804 nm, relative to the M256-Cys mutant, the M256/L121-Cys mutant may not have been as stable. Regardless, the action spectra of both mutants provide evidence that the photocurrents were likely due to proteins bound to an HOPG electrode.

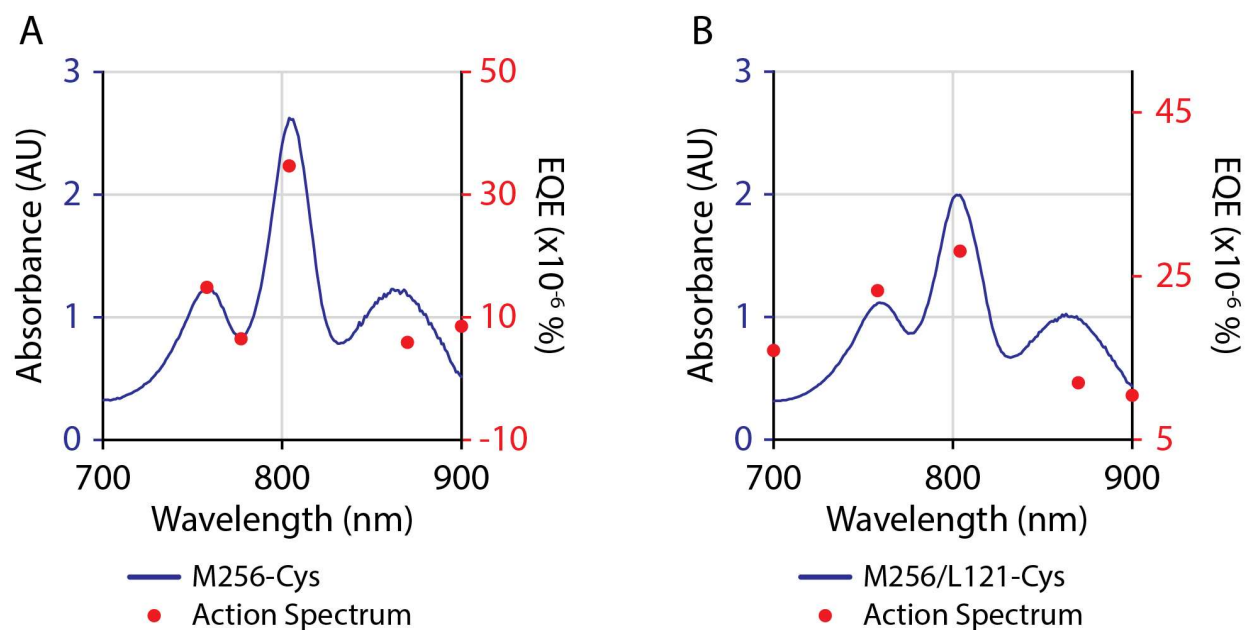


Figure 3.25. External quantum efficiency (EQE) action spectra of the M256-Cys (A) and M256/L121-Cys (B) on an HOPG electrode. 1 mM hydroquinone was used as the electron donor. The absorbance spectra of the M256-Cys and M256/L121-Cys mutants were normalised to $A_{650} = 0.2$.

3.3.6 Addition of Cys near the Q_A region of the truncated 45M RC and photochronoamperometry measurements of the 45M-M229 mutant bound to an HOPG electrode.

A Cys substitution at F(M229)C was made using a Cys⁻ variant of the 45M mutant, called 45M-M229, in order to bind the mutant to an electrode surface (Figure 3.26). A further mutation, V(M226)W, was made to introduce a Trp between Q_A and the protein surface, but this RC mutant did not assemble.

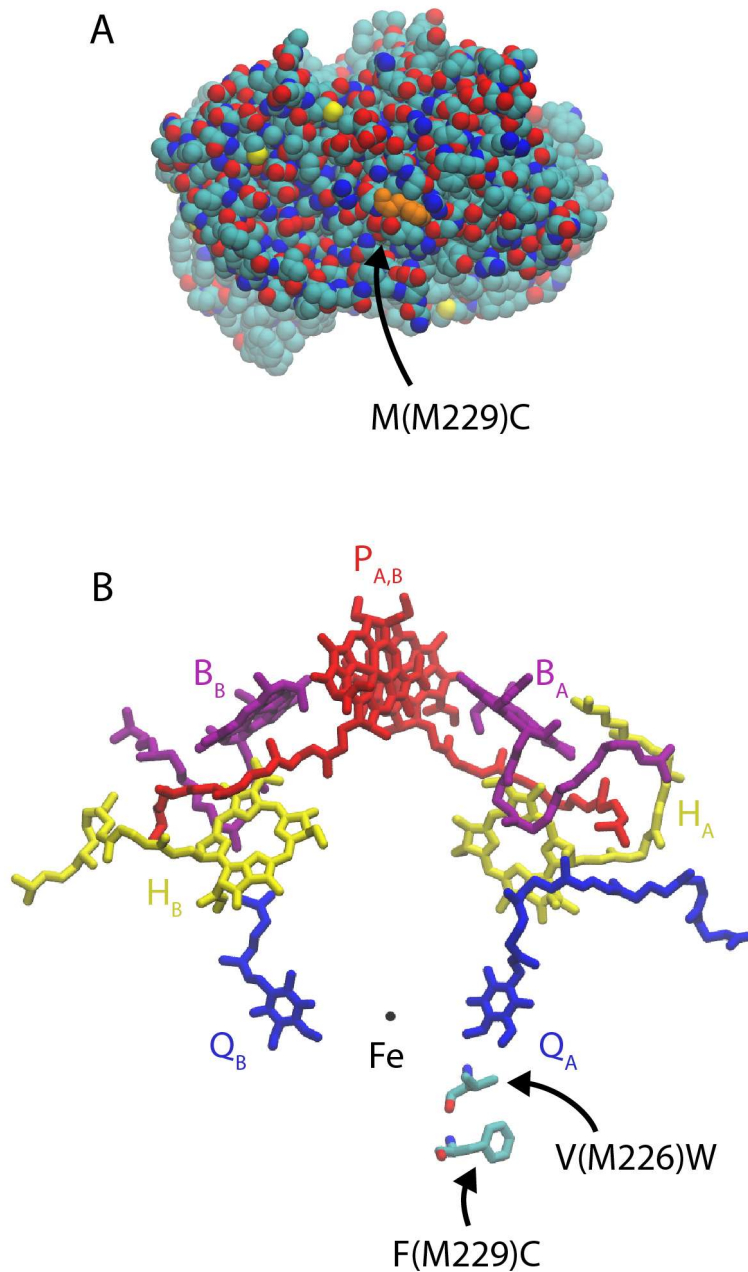


Figure 3.26. Structural modifications in the 45M-M229 and 45M-M229/M226 mutants. A) Arrangement of Cys in the 45M-M229 and 45M-M229/M226 mutants with the primary bacteriochlorophyll (red), accessory bacteriochlorophyll (purple), bacteriopheophytin (yellow), and quinone (blue). A single substitution, F(M229)C was made to introduce Cys (orange) in the vicinity of Q_A. View of the RC looking from below towards the quinones with the H subunit removed. B) Arrangement of the cofactors and amino acid residues in the 45M-M229 and 45M-M229/M226 mutants. Structures are based on PDB 2J8C.

Both ascorbate and hydroquinone were used as an electron donor to P^+ . Similar to the results observed with the M256-Cys mutant, ascorbate was not a very good electron donor, compared to hydroquinone. Using hydroquinone as the sole mediator consistently resulted in higher currents generated upon illumination (Figure 3.27). Currents of about 85 nA/cm^2 were achieved using 1 mM hydroquinone.

The role of *o*-phenanthroline has not been fully characterised. It is well-established that *o*-phenanthroline is an inhibitor and prevents quinones from binding at Q_B in a wild type RC. However, the 45M-M229 has a large structural truncation of the H subunit, and results in the literature suggest that in the absence of RC H, the primary and secondary quinones are loosely bound (Sun et al., 2015). Further, there is evidence that electron transfer is decreased 10^2 - 10^3 -fold from Q_A to Q_B and that sensitivity to the *o*-phenanthroline inhibitor is decreased by approximately 100-fold (Debus et al., 1985).

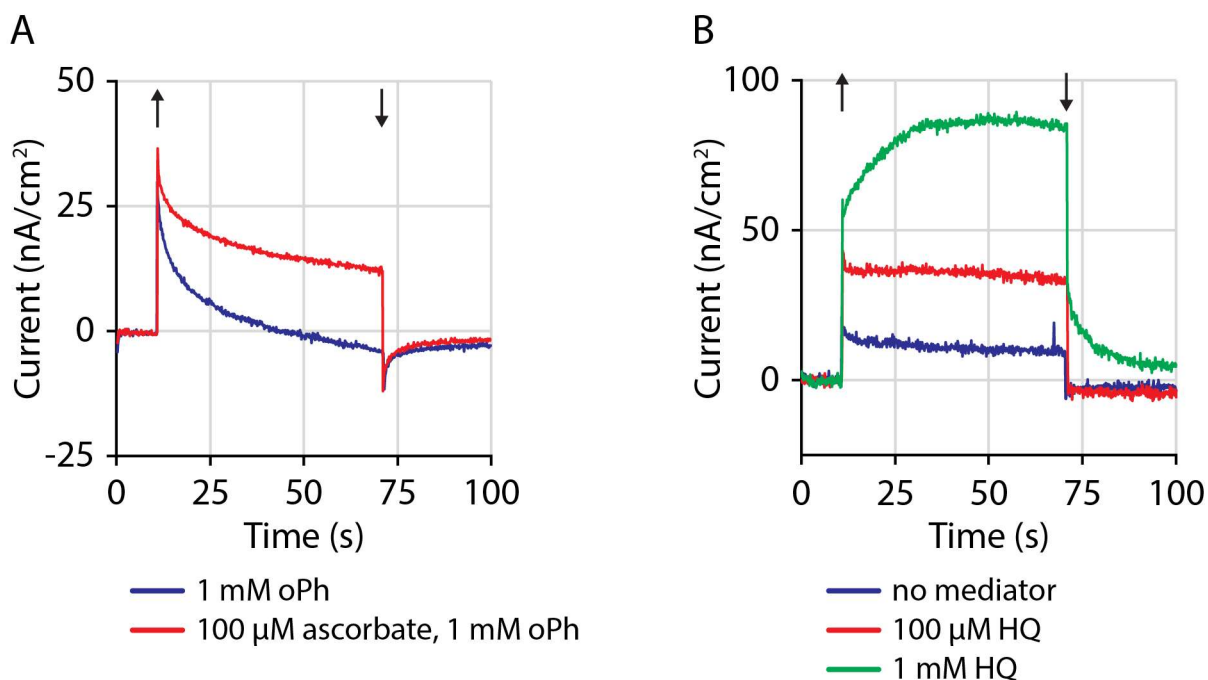


Figure 3.27. Photocurrents generated by the 45M-M229 mutant on an HOPG electrode. Arrows indicate light on (\uparrow) and light off (\downarrow). A) A control with only 1 mM *o*-phenanthroline (oPh) present in solution (blue) was compared to the same condition, but with the addition of $100 \mu\text{M}$ ascorbate (red). B) Hydroquinone (HQ) used in this experiment at $100 \mu\text{M}$ (red) and 1 mM (green). In the presence of 1 mM HQ, currents of 85 nA/cm^2 were generated.

The photocurrents at seven wavelengths were measured, using ascorbate as a reducing agent in order to calculate the external quantum efficiency action spectrum (Figure 3.28). An action spectrum similar to that of the RC absorbance spectrum would indicate that the RC pigments contributed to the generation of currents, but with the 45M-M229 mutant, there appears to be no correlation between the action and absorbance spectra. The photocurrents generated are likely due to contributions from proteins bound to the HOPG electrode, but there may be other factors that reduced photocurrent generation efficiency. For example, the use of ascorbate, which is a slow electron donor (Appendix C.1), may be limiting photocurrent contributions from the different pigments in the RC. Additionally, as the 45M-M229 mutant has large structural truncations, the bound form on an electrode may not be stable, further decreasing efficiency.

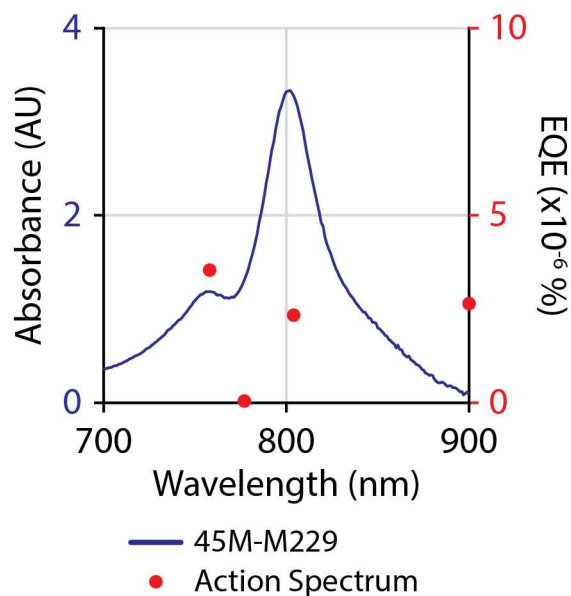


Figure 3.28. External quantum efficiency (EQE) action spectrum of the 45M-M229 mutant on an HOPG electrode. 100 μ M ascorbate was used as the electron donor and 1 mM *o*-phenanthroline to exclude quinones from Q_B . The absorbance spectrum of the 45M-M229 mutant was normalised to $A_{650} = 0.2$.

3.3.7 Addition of Cys near the Q_B region of the truncated 45M RC and photochronoamperometry measurements of the 45M-L210 and 45M-L210/L213 mutants bound to a gold electrode.

Another of the cofactors where electrons could be extracted from is Q_B. Although the quantum efficiency of forming a charge-separated state is near unity, the drawback is that the electron has lost two-thirds of its starting energy by the time it reaches Q_B (Jones, 2009). Electrons at this stage do not have as strong of a reducing potential compared to electrons at H_A.

Using the 45M as starting material, similar to the 45M-M229 mutant, and a Cys⁻ background, a D(L210)C mutation was made, resulting in 45M-L210. The newly introduced Cys is to bind to an electrode surface. A further mutation, D(L213)W, was made that introduced a Trp midway between Q_B and D(L210)C. The location of the residues and cofactors are shown in Figure 3.29. Both the 45M-L210 and 45M-L210/L213 mutants assembled and were purified.

Neither the 45M-L210 nor the 45M-L210/L213 mutant generated any photocurrent on an HOPG electrode and, because current was obtained using a gold electrode (see below), I assume that the mutants did not attach to an HOPG electrode (data not shown). This assumption was not investigated.

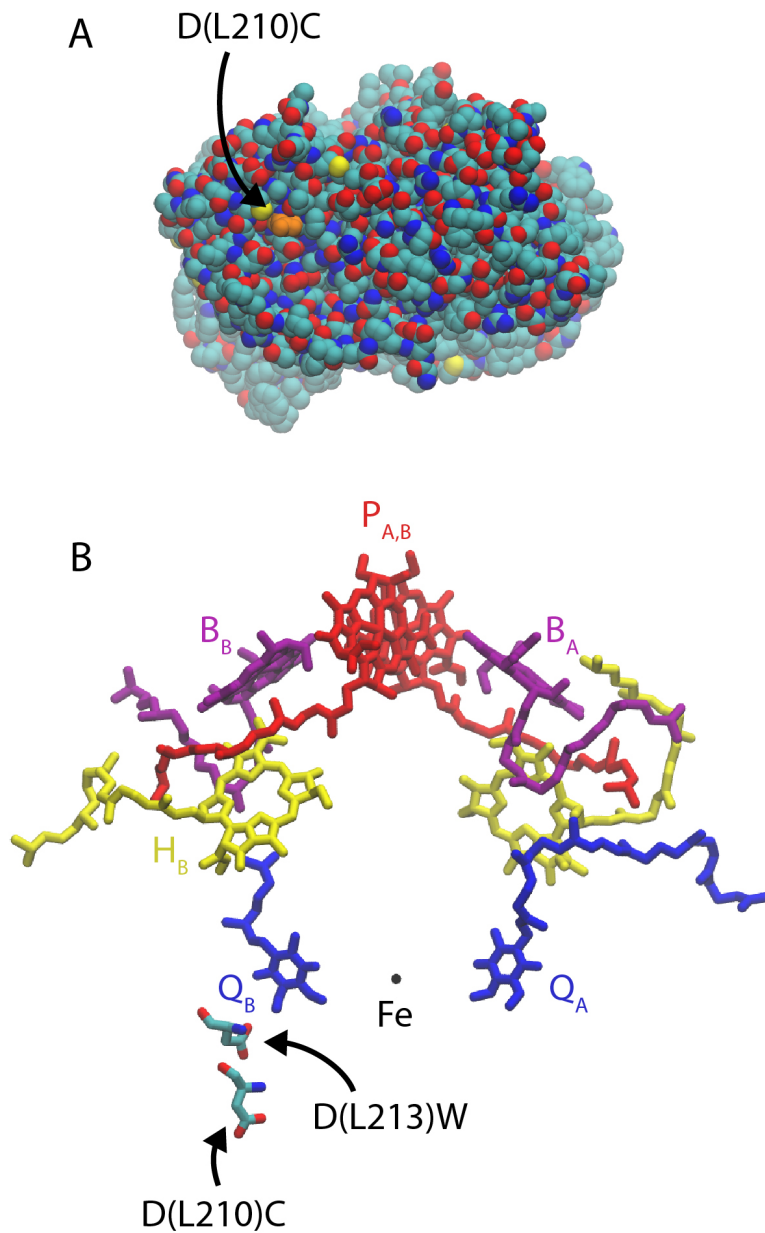


Figure 3.29. Structural modifications in the 45M-L210 and 45M-L210/L213 mutants. A) Arrangement of Cys in the 45M-L210 and 45M-L210/L213 mutants with the primary bacteriochlorophyll (red), accessory bacteriochlorophyll (purple), bacteriopheophytin (yellow), and quinone (blue). A single substitution, D(L210)C was made to introduce Cys (orange) in the vicinity of Q_B. View of the RC looking from below towards the quinones with the H subunit removed. B) Arrangement of the cofactors and amino acid residues in the 45M-L210 and 45M-L210/L213 mutants. In addition to the D(L210)C mutation, an additional D(L213)W substitution

was made to bridge the electron transfer distance from Q_B to the RC surface. Structures are based on PDB 2J8C.

The 45M-L210 mutant was bound to a gold electrode. Currents were generated upon illumination using hydroquinone as the sole mediator in the experimental setup. About 40 nA/cm^2 was generated using $100 \text{ }\mu\text{M}$ hydroquinone, and the current increased to around 80 nA/cm^2 when the concentration of the mediator was increased to 1 mM (Figure 3.30A). The illumination-dependent current obtained using the control without mediator indicated that the 45M-L210 RC bound to gold and was able to transfer electrons directly to the electrode. The 45M-L210/L213 mutant did not produce currents comparable to the 45M-L210 mutant.

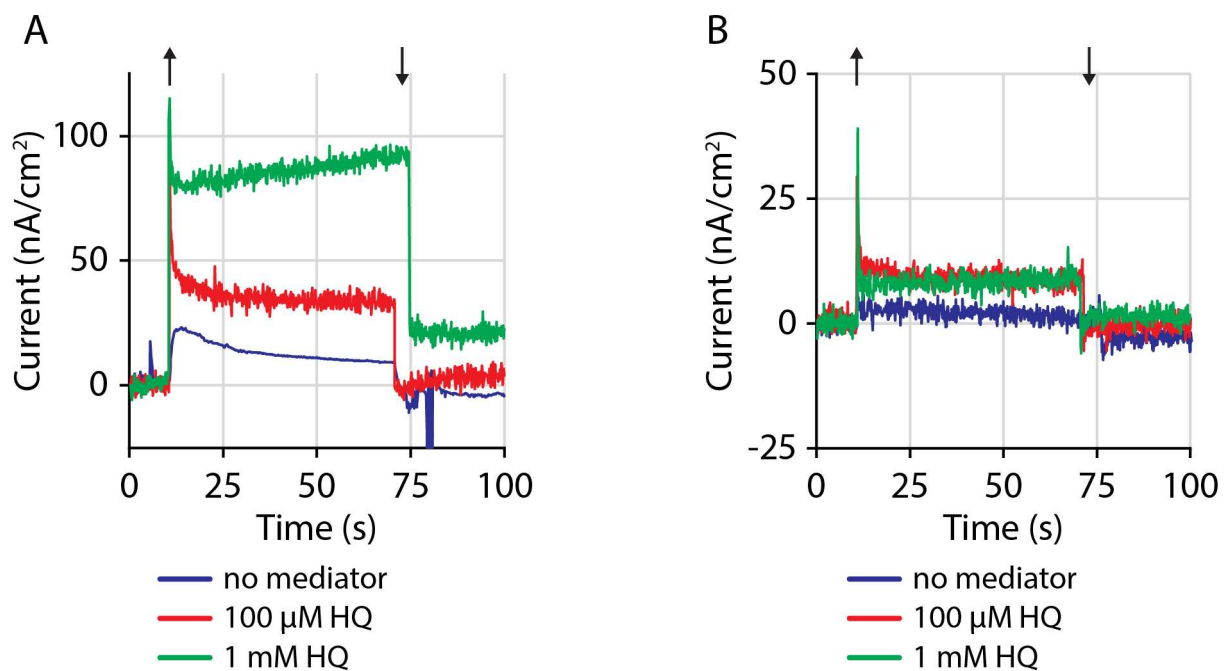


Figure 3.30. Photocurrents generated by the 45M-L210 (A) and 45M-L210/L213 (B) mutants on a gold electrode. Arrows indicate light on (↑) and light off (↓). A control with no mediator (blue) was compared to two different concentrations of hydroquinone (HQ) used in the experiment, $100 \text{ }\mu\text{M}$ (red) and 1 mM (green). Upon addition of 1 mM HQ, currents of 80 nA/cm^2 were generated with the 45M-L210 mutant.

3.4 Recombinant expression of the genes encoding the *T. tepidum* photosystems using a modified strain of *R. sphaeroides*.

If photosystems are to be used in solar cell applications, the proteins would be subjected to elevated temperatures under sunlight and the associated thermal energies may cause proteins to become non-functional by denaturing. Hence, I explored ways of increasing the longevity of proteins by using proteins naturally resistant to the denaturing effects of heat. I looked into the photosystems produced by *T. tepidum*, as it is a thermophile that grows at temperatures up to 58 °C (Madigan, 1984) and therefore its cellular machinery must be able to withstand those temperatures. Having established a rapid and high-yielding protein expression system, I wanted to see if I could express *T. tepidum* genes coding for the RC and LH1 (called TRC and TLH1 hereon) in *R. sphaeroides*, and measure the kinetics of protein denaturation at elevated temperatures.

There are several advantages of producing *T. tepidum* pigment-protein complexes in *R. sphaeroides*. One, there are genetic tools, such as expression plasmids, that can be used to generate synthetic operons with different *T. tepidum* gene combinations for expression in *R. sphaeroides*. Two, it is logistically simpler and faster to work with and culture *R. sphaeroides* in large volumes, as the organism is able to grow aerobically or anaerobically in facilities provided in the building; whereas, *T. tepidum* is an obligate anaerobe and requires 50 °C for optimal growth. If expression of *T. tepidum* genes in *R. sphaeroides* were successful, I will have created a tractable platform that could serve as a system to easily make genetic modifications in *T. tepidum* genes for future functional and structural studies. Finally, work on *T. tepidum* genes expressed in *R. sphaeroides* would serve as a model for expressing other genes from thermophiles, such as in metagenomic libraries from hot springs. The following sections describe the constructs I created, the effect of the carotenoid spirilloxanthin on pigment-protein complex assembly, purification of the *R. sphaeroides*/*T. tepidum* hybrid photosystems, and tolerance to heat.

3.4.1 Evaluation of a synthetic operon construct of the genes encoding the *T. tepidum* TRC, purification, and formation of a charge-separated state of the TRC.

The first goal was to determine if *R. sphaeroides* could synthesise and assemble the TRC genes from *T. tepidum*. Similar to pIND4-RC, where *puhA*, *pufL*, and *pufM* are synthesised on one transcript, the plasmid pIND4-TRC was created with *T. tepidum puhA*, *pufL*, and *pufM* genes (called *TpuhA*, *TpufL*, and *TpufM* hereon, respectively) with a 6-His tag on the C-terminus of the H subunit. However, since *R. sphaeroides* may not have been able to recognise the *T. tepidum* ribosome binding sites (containing the Shine-Dalgarno sequence), the synthetic Shine-Dalgarno sequence from pIND4 was used to drive translation of all three genes. Earlier induction experiments with pIND4-RC showed that the synthetic Shine-Dalgarno sequence in pIND4 was recognised by *R. sphaeroides* to translate *puhA* and assemble into the RC. Therefore, the 5'-**GAGGAGAAATTAACC**-3' sequence from pIND4 (with the Shine-Dalgarno sequence in bold) was cloned upstream of the start codons of *TpuhA*, *TpufL*, and *TpufM*.

Cell cultures of *R. sphaeroides* RCx^R(pIND4-RC) and RCx^R(pIND4-TRC) were grown under aerobic and chemotrophic conditions, and induced with 1 mM IPTG at a density of 1-2 AU at 700 nm. Expression of *T. tepidum* genes in *R. sphaeroides* resulted in impaired growth (data not shown), and induction in late-exponential phase minimised this effect. Figure 3.31 shows the comparison of cellular levels of the RC and TRC after cells were broken by sonication. The TRC assembled, though at levels lower than the RC, indicating that the artificial Shine-Dalgarno sequences were recognised to initiate translation of the TRC subunits, which assembled properly in the membrane as evidenced by the presence of the 800 nm peak corresponding to the accessory bacteriochlorophylls. Characteristic traits of an RC that did not assemble properly would have been observed as a low 800 nm peak and a relatively high 760 nm peak, indicating free bacteriochlorophylls (Hughes et al., 2006).

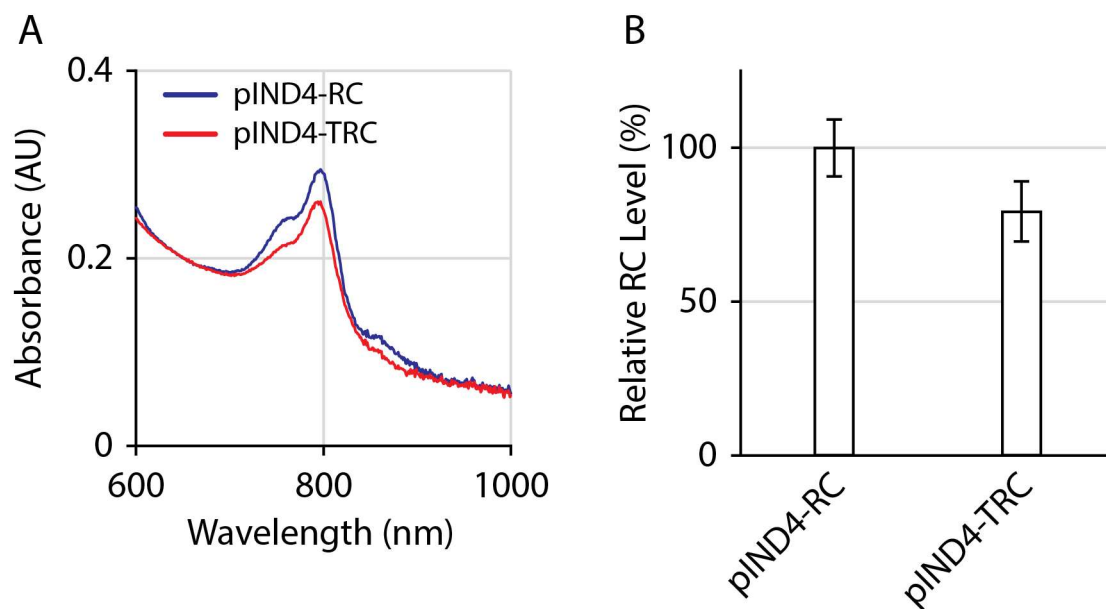


Figure 3.31. Assembly and *in vivo* levels of the RC and TRC. The plasmids pIND4-RC and pIND4-TRC were expressed in *R. sphaeroides* RC^R. A) Absorbance spectra of broken cells expressing RCs (blue) and TRCs (red). The spectra were normalised to $A_{650} = 0.2$. B) Relative levels of RC production compared to the wild type RC (pIND4-RC). Levels were calculated by subtracting the RC^R baseline from the peak amplitude and normalising the difference to the wild type RC. Error bars represent the standard deviation ($n = 3$).

T. tepidum TRCs were purified using DDM detergent to solubilise, although yields were low and not comparable to the 15 mg/L culture of wild type RCs. As TRCs contain menaquinone at Q_A and *R. sphaeroides* does not synthesise this cofactor, the RLB growth medium was supplemented with 10 μ M menadione. Not surprisingly, the spectrum of the purified TRC was similar to that of the RC (Figure 3.32). There were a few differences, such as the blue-shift of the accessory bacteriochlorophyll to 800 nm and the red-shift of the special pair bacteriochlorophyll to 870 nm; the amplitude and wavelength of the bacteriopheophytin at 760 nm appeared to be the same as in the RC.

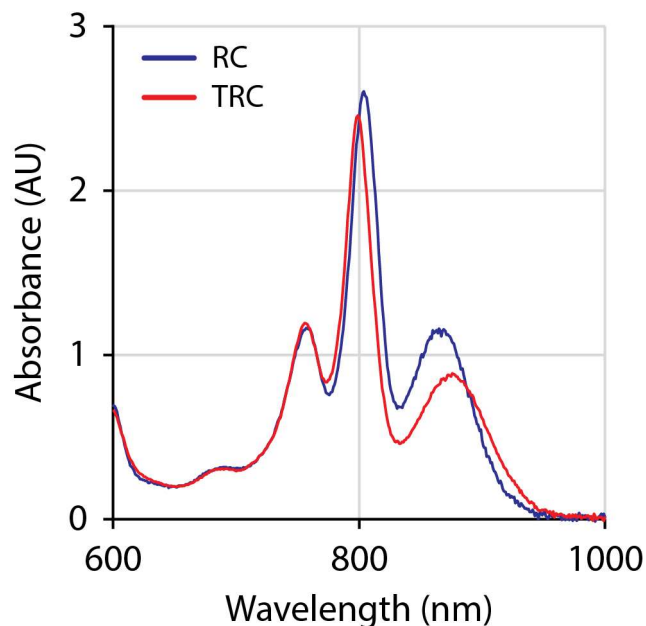


Figure 3.32. Absorbance spectra of the purified RC (blue) and TRC (red). The spectra were normalised to $A_{650} = 0.2$.

The easiest way of determining whether the TRC complex was functional was to measure the formation of a charge-separated state. Charge-separation occurs by the rapid transfer of an electron from the special pair to the primary and secondary quinones. The 870 nm P-band was illuminated with an 870 nm LED and the difference absorbance spectrum calculated, as shown in Figure 3.33. A charge-separated state was formed, as indicated by the large negative peak at 870 nm of the difference absorbance spectrum. Only a partial state was formed, indicating that perhaps the Q_A pocket was not fully populated with menadione and that supplementing the growth medium with 10 μM menadione was not sufficient. Addition of 5-fold molar excess menadione increased the charge-separated state further, and a 10-fold molar excess fully bleached the 870 nm special pair, indicating a complete charge-separation.

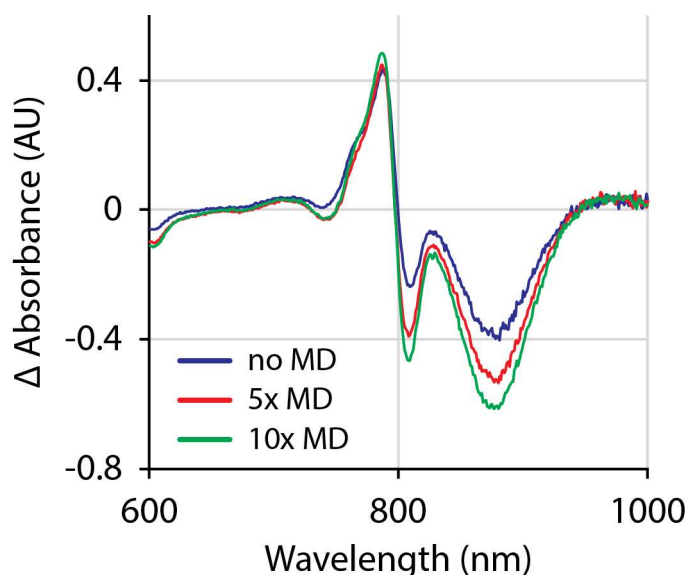


Figure 3.33. Difference absorbance spectra of the Q_y transition region of the TRC. An 870 nm LED was used for illumination to measure the charge-separated formation without additional menadione (MD) (blue), 5-fold molar excess menadione (red), and 10-fold molar excess menadione (green). The dark-adapted spectra were normalised to $A_{650} = 0.2$ and the light-adapted spectra were normalised using the same multiplier.

3.4.2 Evaluation of synthetic operon constructs and expression of the genes encoding combinations of the *R. sphaeroides* RC, *T. tepidum* TRC and TLH1.

The main purpose of utilising *T. tepidum* TRC was to take advantage of the thermophilic properties of the organism. However, it was found previously that the TRC has similar tolerance to heat as an RC from the mesophile *R. sphaeroides* (Kobayashi et al., 2005). Further studies showed that the thermal stability is in fact due to the presence of the *T. tepidum* TLH1 surrounding the TRC and Ca^{2+} ions in the TLH1 structure (Kimura et al., 2009; Kobayashi et al., 2005). Therefore, the most stable and the most heat-tolerant structure would be the TRC-TLH1 core complex. However, since many electron transfer studies have used the *Rhodobacter* RC as a paradigm, I decided to attempt to increase the stability of the existing RC, rather than using the TRC that has not been as well-studied and used for electron transfer studies of mutants. Therefore, given that TLH1 is believed to confer stability to the core complex, TLH1 was expressed in *R. sphaeroides* as a hybrid core complex with either the RC, as well as with the TRC.

Different combinations of genes from *T. tepidum* and *R. sphaeroides* were cloned into a synthetic operon in pIND4. The constructs are illustrated in Figure 3.34. The construct pIND4::*TpuhA* 5'*TpufBALM* was created by inserting the *TpufBA* DNA fragment, including 50 bases upstream of the *TpufB* start codon, the native *T. tepidum* Shine-Dalgarno sequences, and 151 bases downstream of the *TpufA* stop codon encoding the predicted intercistronic mRNA stem-loop, into pIND4-TRC between *TpuhA* and *TpufLM*. Furthermore, since it was unclear whether the *T. tepidum* Shine-Dalgarno sequences for *TpufB* and *TpufA* would be recognised in *R. sphaeroides*, the *T. tepidum* Shine-Dalgarno sequences were replaced with the artificial one from pIND4, similar to the strategy used in the construction of pIND4-TRC, as described above in Section 3.4.1; this replacement resulted in the construct pIND4-rbsTRCT1 with the same Shine-Dalgarno sequence initiating translation of *TpuhA*, *TpufB*, *TpufA*, *TpufL*, and *TpufM*.

The pIND4-rbsTRCT1 construct did not produce any TLH, as seen in Figure 3.35. TLH1 levels were measured at the peak absorbance at 915 nm, compared to 875 nm for LH1. The 915 nm peak is due to the pair of bacteriochlorophylls in each $\alpha\beta$ subunit, and it was assumed that the TLH1 complex did not assemble if the peak was not present. The data indicated, however, that the operon was transcribed and that the issues with TLH1 levels were associated with post-transcriptional processes. The evidence supporting the formation of a complete transcript was the fact that the TRC assembled and the genes encoding that protein (*TpuhA*, *TpufL*, and *TpufM*) were arranged such that *TpuhA* and *TpufM* were located on the 5' and 3' ends of the transcript, respectively, with *TpufB*, *TpufA*, and *TpufL* in between. The intercistronic stem loop between *TpufA* and *TpufL* should also increase TLH1 levels relative to the TRC by decreasing the rate of mRNA degradation of the *TpufB* and *TpufA* portion of the transcript (Chen et al., 1988). If the issue were not at the transcriptional level, then the next level would have been during translation. Since the translation of all the genes were initiated with the same Shine-Dalgarno sequence and given that the TRC polypeptides were produced and assembled into a functioning pigment-protein complex, it was assumed therefore that translation of the α and β polypeptides of TLH1 was initiated as well.

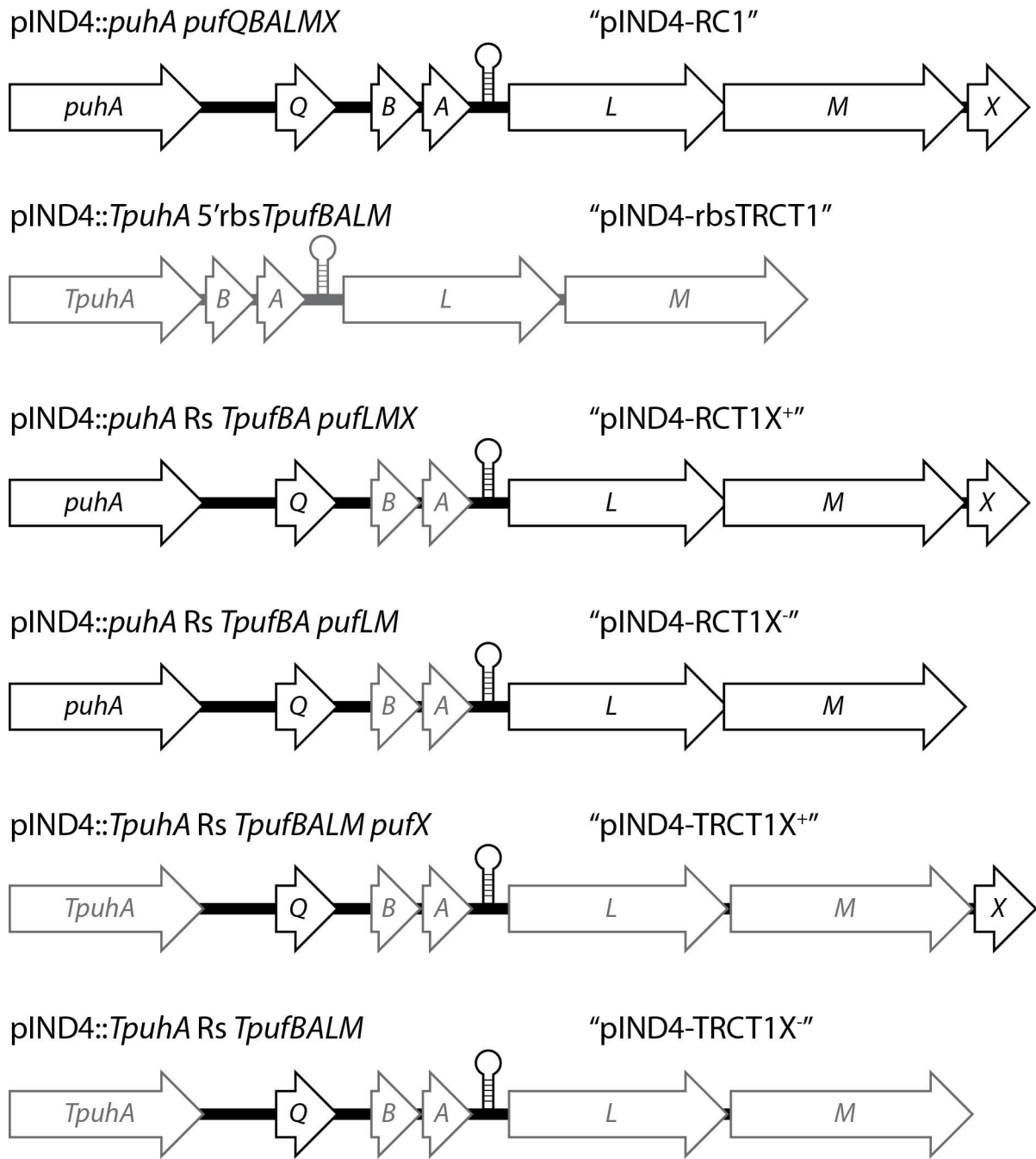


Figure 3.34. Schematic of the different *T. tepidum* and *R. sphaeroides* gene combinations for protein expression constructs. The *R. sphaeroides* genetic coding and non-coding elements are drawn in black and the *T. tepidum* components in grey.

The other approach of creating constructs utilised the existing and characterised pIND4-RC1 plasmid (Section 3.1), containing the *R. sphaeroides* *pufQBALMX* operon with all the

coding and non-coding genetic elements recognised by *R. sphaeroides*, and replace the coding regions with the equivalent from *T. tepidum*. Since this plasmid produced RC and LH1 at the correct ratios, then simply replacing the coding regions with *T. tepidum* genes, and maintaining the non-coding genetic material, should theoretically yield the correct level of TLH1. The plasmid pIND4-RCT1X⁺ was created by replacing the *R. sphaeroides pufB* and *pufA* coding sequences with *T. tepidum TpufB* and *TpufA*; this construct was designed to create a hybrid core complex containing the *R. sphaeroides* RC and *T. tepidum* TLH1. The construct pIND4-TRCT1X⁺ was a further iteration in which the *R. sphaeroides pufL* and *pufM* were replaced with *TpufL* and *TpufM*. The plasmids pIND4-RCT1X⁻ and pIND4-TRCT1X⁻ were created by removing *pufX* from the synthetic operon of both pIND4-RCT1X⁺ and pIND4-TRCT1X⁺. The PufX protein is believed to form a dimer of the RC-LH1 complex in *R. sphaeroides* and allow for the passage of quinones in and out of the core complex (Holden-Dye et al., 2008; Qian et al., 2013); however, in *T. tepidum*, no PufX homologue has been discovered and the core complex exists as a monomer (Niwa et al., 2014). The crystal structure does not show a PufX-like protein, confirming the genetic data that no homologue exists; instead there is a gap, or “channel” between the $\alpha\beta$ dimers in the TRC-TLH1 core complex (Niwa et al., 2014). Hence, the pIND4-RCT1X⁻ and pIND4-TRCT1X⁻ constructs lacking PufX were tested in case that this protein was interfering with the assembly of the TLH1 units in the core complex. A representation of the gene constructs is shown in Figure 3.34.

Despite simply replacing the coding regions of the *R. sphaeroides pufQBALMX* operon as the basis for the expression of TLH1 genes, the TLH1 protein levels remained significantly depressed compared to that of the RC-LH1 control (Figure 3.35). This indicated that the issue of low expression lay at the post-transcriptional level. In subsequent experiments, the four plasmids, pIND4-RCT1X⁺, pIND4-RCT1X⁻, pIND4-TRCT1X⁺, and pIND4-TRCT1X⁻, were used.

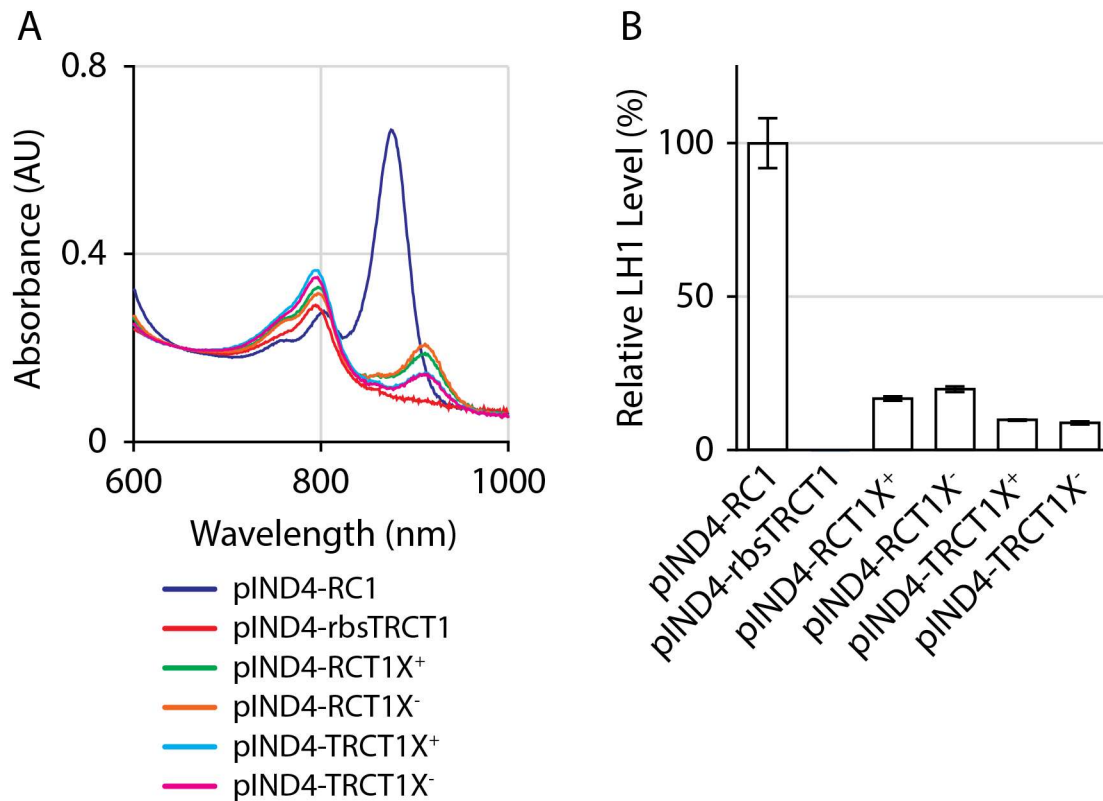


Figure 3.35. Assembly and *in vitro* levels of hybrid RC-TLH1 and TRC-TLH1 complexes. The constructs shown in Figure 3.34 were expressed in *R. sphaeroides* RCx^R. A) Absorbance spectra of broken cells expressing RC-LH1-X⁺ (blue), TRC-TLH1-X⁻ (red), RC-TLH1-X⁺ (green), RC-TLH1-X⁻ (orange), TRC-TLH1-X⁺ (cyan), and TRC-TLH1-X⁻ (magenta). The spectra were normalised to A₆₅₀ = 0.2. B) Relative levels of TLH1 production compared to the wild type LH1 (pIND4-RC1). Levels were calculated by subtracting the RCx^R baseline from the peak amplitude and normalising the difference to the wild type LH1. Error bars represent the standard deviation (n = 3).

3.4.3 Effect of the carotenoid spirilloxanthin on TLH1 assembly and levels.

In *T. tepidum*, after translation of the α and β polypeptides of TLH1, these subunits assemble in the membrane as α -helices, and coordinate a pair of bacteriochlorophylls and a spirilloxanthin carotenoid. However, in *R. sphaeroides*, the carotenoid spheroidene is synthesised (under anaerobic conditions; under aerobic conditions spheroidene is converted to spheroidenone (Lee et al., 2010)). There have been conflicting data on whether carotenoids are necessary for

light harvesting complex assembly. Some groups suggest that carotenoids are necessary for assembly (Lang and Hunter, 1994), whereas others have shown evidence of light harvesting complexes lacking carotenoids (Fiedor et al., 2004). Other evidence shows that carotenoids may not be necessary for assembly, but help stabilise the light harvesting complex or associate with other photosystems (Moskalenko et al., 2005). Some of these differences may be specific to LH2 versus LH1 or to a particular species. It is apparent that the interactions of carotenoid molecules with photosynthesis protein structures are complex. Therefore, an *R. sphaeroides* mutant producing spirilloxanthin was created to determine whether this would increase TLH1 levels by using the native carotenoid to stabilise the complex.

Other research groups have successfully produced spirilloxanthin in lieu of spheroidene in *R. sphaeroides* (Garcia-Asua et al., 2002; Hunter et al., 1994). Following on their work, the *crtI* gene encoding a three-step phytoene desaturase, was knocked out in *R. sphaeroides* RCx^R and replaced with a four-step phytoene desaturase from *Pantoea agglomerans* (Chi et al., 2015), creating *R. sphaeroides* RCx^R Δ *crtI*::*crtI*^{Pa}. The resultant strain produced spirilloxanthin as was confirmed by absorbance spectroscopy, because the carotenoid peaks were red-shifted. The RCx^R Δ *crtI*::*crtI*^{Pa} strain was transformed with the plasmids pIND4-RCT1X⁺ and pIND4-TRCT1X⁺ to see whether spirilloxanthin increased the amount of TLH1.

After inducing the cells with 1 mM IPTG and subsequent sonication, TLH1 levels were measured (Figure 3.36). This approach of replacing spheroidene with spirilloxanthin did not yield a significant increase in TLH1 levels. In fact, less TLH1 was detected, and therefore, the carotenoid spheroidene native to *R. sphaeroides* was maintained in subsequent work. This outcome is not entirely surprising, given that other LH1 complexes have assembled without a carotenoid. Furthermore, the structures of spheroidene and spirilloxanthin are quite similar, with the latter containing one additional double bond and an additional methoxy group.

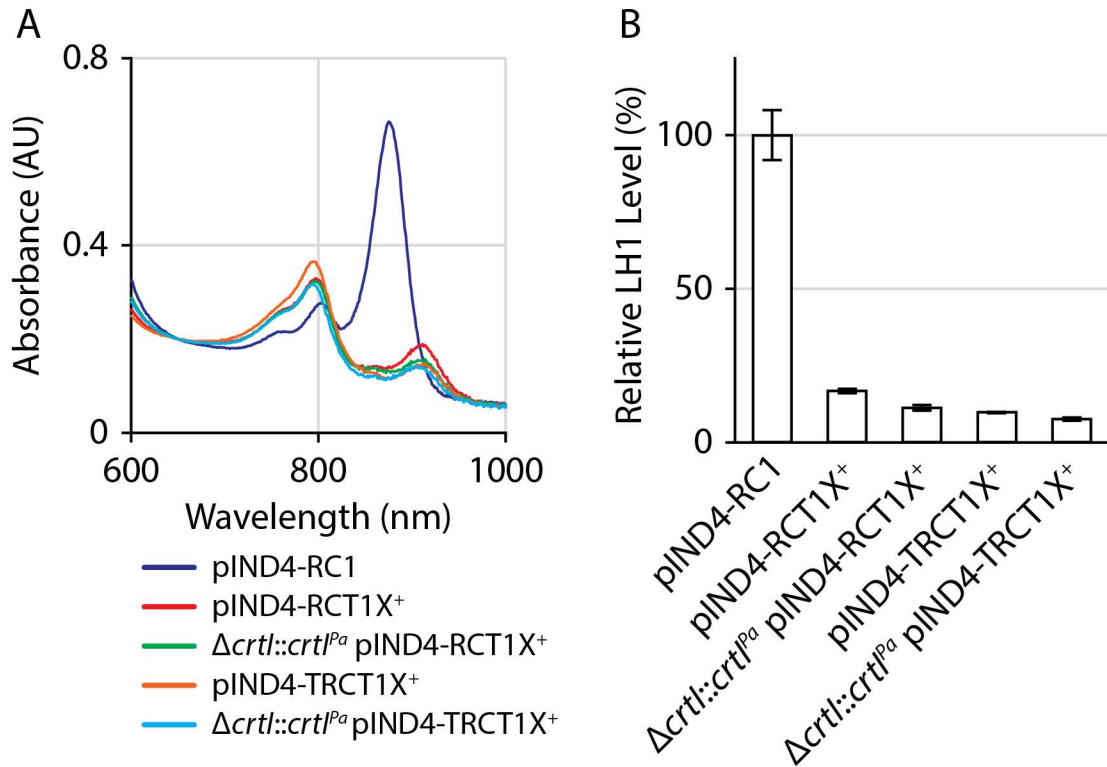


Figure 3.36. Assembly and *in vitro* levels of hybrid RC-TLH1 and TRC-TLH1 complexes due to the carotenoid spirilloxanthin. The constructs pIND4-RCT1X⁺ and pIND4-TRCT1X⁺ were expressed in *R. sphaeroides* RCx^R and RCx^R $\Delta crtI::crtI^{Pa}$. A) Absorbance spectra of broken cells expressing the carotenoid spheroidene in the strain RCx^R with RC-LH1-X⁺ (blue), RC-TLH1-X⁺ (red), or TRC-TLH1-X⁺ (orange). Absorbance spectra of broken cells expressing the carotenoid spheroidene in the strain RCx^R $\Delta crtI::crtI^{Pa}$ with RC-TLH1-X⁺ (green) or TRC-TLH1-X⁺ (cyan). The spectra were normalised to A₆₅₀ = 0.2. B) Relative levels of TLH1 production compared to the wild type LH1 (pIND4-RC1). Levels were calculated by subtracting the RCx^R baseline from the peak amplitude and normalising the difference to the wild type LH1. Error bars represent the standard deviation (n = 3).

3.4.4 Increasing the levels of TLH1 by UV-mutagenesis and selection for improved phototrophic growth.

Rather than genetically manipulating *R. sphaeroides* using rational design to produce more TLH1, it was decided to use directed evolution to have the organism “find” the suitable mutation(s) that improves its fitness for phototrophic growth. To accelerate “evolution”, cells

were irradiated with UV to mutate DNA and/or grown under the selective pressure of anaerobic, phototrophic conditions, to select for mutants. The mutagenesis approach was applied to the RC^xR strain containing one of the plasmids expressing the core complexes with the RC or TRC, and with or without PufX: pIND4-RCT1X⁺, pIND4-RCT1X⁻, pIND4-TRCT1X⁺, and pIND4-TRCT1X⁻.

After mutagenesis, the cells were placed under anaerobic, phototrophic conditions in liquid culture, then streaked on an RLB plate and grown again under anaerobic, phototrophic conditions to select for and isolate the fastest-growing mutant. Furthermore, for the constructs containing TRCs, the RLB medium was supplemented with 10 μ M menadione because the TRC requires a menadione at the Q_A pocket for complete assembly and charge-separation (*R. sphaeroides* produces only ubiquinone; Section 3.4.1). As shown in Figure 3.37, where the absorbance spectrum of a particular construct before mutagenesis is overlaid with the spectrum after selection (appended with the word “UV”) for a phototrophic-capable mutant, there was an increase in the *T. tepidum* peaks representing the core complex. However, the levels did not match the wild type *R. sphaeroides* levels of LH1, even though the mutants were able to grow photosynthetically. Clearly, despite the low TLH1 levels, there were enough light harvesting complexes to support growth under those conditions. The elevated levels of RC and TRC, relative to TLH1, would not have been able to contribute much to phototrophic growth, as strains lacking both LH1 and LH2 (*i.e.*, RC only) have impaired growth (Jones et al., 1992a; Jones et al., 1992b). DNA sequencing did not show any mutations in the photosynthesis genes expressed *in trans* on pIND4.

The suboptimal levels of TLH1 probably led to the over-abundance of RC in the membrane. It was not evident whether the TLH1 was even assembling with the RC to form a core complex. In other words, it was conceivable that empty or partial TLH1 rings formed, although there have been no reports of TLH1 rings forming independently of the TRC in *T. tepidum*. The most likely model would be two populations of an RC-only pool and an RC-TLH1 pool coexisting in the membrane. There is strong evidence that once LH1 units start assembling around an RC, the circularisation process continues until the ring is completed; there has been no evidence to date to support the formation of a partially-encircled RC core complex (Mothersole et al., 2016). If this interpretation is correct, it should be possible to isolate both the RC from the

core complex during purification of the photosystems (as described in Sections 3.4.5 and 3.4.6). At the time of writing, a photosynthesis-capable mutant with the plasmid pIND4-TRCT1X⁺ or pIND4-TRCT1X⁻ was not isolated.

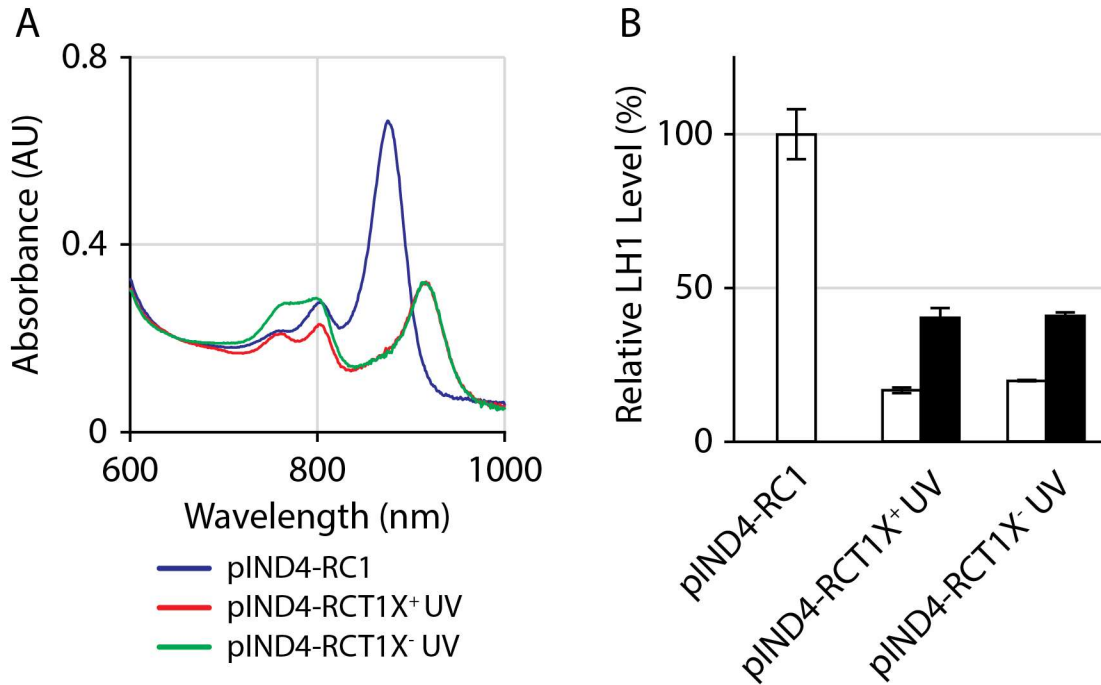


Figure 3.37. Assembly and *in vitro* levels of hybrid RC-TLH1 and TRC-TLH1 complexes capable of supporting phototrophic growth. The constructs pIND4-RCT1X⁺ UV, pIND4-RCT1X⁻ UV, and pIND4-TRCT1X⁺ UV were expressed in *R. sphaeroides* RCx^R. A) Absorbance spectra of broken cells expressing RC-LH1-X⁺ (blue), RC-TLH1-X⁺ (red), and RC-TLH1-X⁻ (green). The spectra were normalised to A₆₅₀ = 0.2. B) Relative levels of TLH1 production compared to the wild type LH1 (pIND4-RC1). White bars represent TLH1 levels prior to UV mutagenesis, whereas the black bars show TLH1 levels after a photosynthesis-capable mutant was isolated. Levels were calculated by subtracting the RCx^R baseline from the peak amplitude and normalising the difference to the wild type LH1. Error bars represent the standard deviation (n = 3).

3.4.5 Partial purification of RC-TLH1-X⁺.

The phototrophy-capable mutants were grown in large-scale cultures under anaerobic, phototrophic conditions for the purification of the core complexes. A typical purification of the RC utilises a Ni²⁺-NTA affinity chromatography and a 6-His tag located on the C-terminus of the H subunit. This procedure worked for the purification of RC from *R. sphaeroides*, and although a 6-His tag on the C-terminus of the H subunit worked for the purification of the RC-LH1 core complex, it was determined in Section 3.2.4 that a 12-His tag on the C-terminus of the M subunit facilitated better binding and purification of the complex using detergents other than LDAO, such as DDM. Unfortunately, this fact was not discovered until after all the constructs were made and mutants selected for phototrophic growth, and so the 6-His tag remained on the H subunit.

Initial attempts at purifying the core complexes using Ni²⁺-NTA affinity chromatography did not work, as it appeared that solubilising the membrane complexes with DDM shielded the tag from binding to the column. Furthermore, DDM was unable to solubilise the core complex (only the RC was solubilised), and so the detergent Deriphat 160C was used instead. A further complication was the fact that RC-only complexes may be purified as well as the respective core complexes. Only the RC-TLH1-X⁺ variant was purified as a core complex. Comparison with the RC-LH1-X⁺ showed a red-shift of the TLH1 peak to 915 nm, whereas the LH1 absorbs maximally at 875 nm (Figure 3.38).

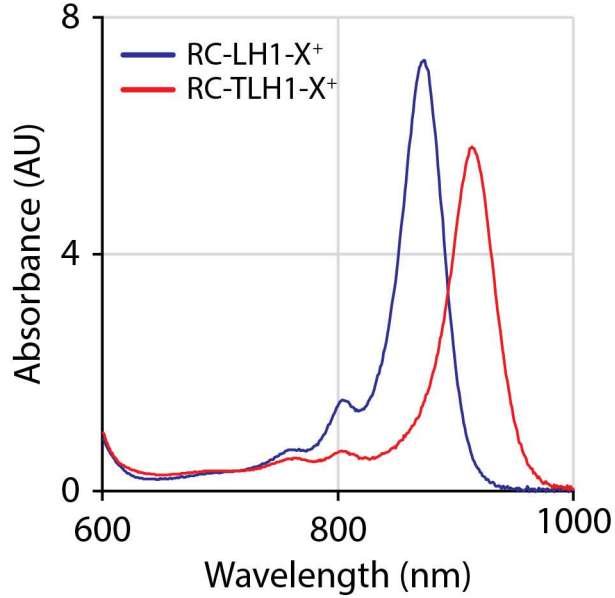


Figure 3.38. Absorbance spectra of RC-LH1-X⁺ (blue) and RC-TLH1-X⁺ (red). The *R. sphaeroides* LH1 absorbs maximally at 875 nm, whereas the *T. tepidum* TLH1 absorbs at 915 nm. The RC-LH1-X⁺ spectrum was normalised to $A_{650} = 0.2$ and the RC-TLH1-X⁺ normalised to the 592 nm peak of RC-LH1-X⁺.

3.4.6 Role of the PufX protein in hybrid core complexes.

The RC-LH1 core complex from *R. sphaeroides* assembles as a dimer, apparently due to the protein PufX. Without PufX, the monomeric form of the core complex predominates. Furthermore, PufX appears to create a break in the ring of LH1 surrounding the RC to permit the diffusion of quinone molecules in and out of the core. Studies of PufX null mutants have shown the loss of photosynthetic growth capability (Holden-Dye et al., 2008). In *T. tepidum*, there is no PufX equivalent in the TRC-TLH1 core complex, resulting in the monomeric form. Interestingly, despite having a completely enclosed ring of TLH1, *T. tepidum* is able to grow photosynthetically, perhaps because of a gap between the $\alpha\beta$ dimers of the TRC-TLH1 core complex (Niwa et al., 2014).

When expressing TLH1 in *R. sphaeroides*, it was unclear whether the TLH1 associated and assembled with an RC core, because the experiments in Section 3.4.4 showed that cellular levels of TLH1 relative to either RC or TRC were not similar to the wild type RC and LH1 ratio. From previous research, it has been suggested that LH1 complexes will form a complete ring

around an RC and leave free RCs in solution, rather than having a distribution of partially assembled core complexes (Mothersole et al., 2016). However, there was no indication whether the PufX-replete core complexes were in the dimer form. To help answer this question, sucrose gradients were run and are shown in Figure 3.39.

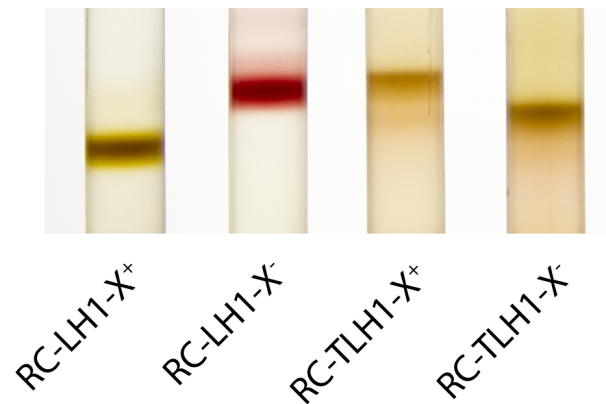


Figure 3.39. Sucrose gradients of RC-LH1-X⁺, RC-LH1-X⁻, RC-TLH1-X⁺, and RC-TLH1-X⁻. The RC-LH1-X⁺ was isolated from a strain lacking *crtD*, resulting in a green-coloured complex containing methoxyneurosporene as the primary carotenoid. The RC-LH1-X⁻ was grown aerobically where spheroidenone is produced, creating a red colour. The RC-TLH1-X⁺ and RC-TLH1-X⁻ complexes were grown anaerobically, where spheroidene is synthesised, resulting in a green colour similar to RC-LH1-X⁺.

The RC-LH1-X⁺ core complex from a “green” (*crtD*) mutant was run as a control to show the sedimentation of the dimer complex (Qian et al., 2013). The RC-LH1-X⁻ core complex from a *crtD*⁺ strain was run as a control to show the sedimentation of the monomer complex. The PufX-replete variant (RC-TLH-X⁺) of the TLH-containing core complex did not sediment at a similar rate as the *R. sphaeroides* RC-LH1-X⁺ dimer, but instead sedimented at a rate more similar to that of the RC-LH1-X⁻ monomer, as seen in Figure 3.39, indicating that the RC-TLH1-X⁺ is in a monomeric form and the PufX protein likely does not interact with the TLH1 $\alpha\beta$ units. Conversely, the *pufX* null mutant yielding RC-TLH1-X⁻ ran at a rate somewhere in between the RC-LH1-X⁺ and RC-LH1-X⁻. This was surprising because the RC-TLH1-X⁻ does not contain a PufX protein and was expected to run like the RC-LH1-X⁻.

3.4.7 Spectroscopic analysis of the heat stability of complexes containing *T. tepidum* pigment-protein complexes.

The purpose of having expressed *T. tepidum* TLH1 with an RC was to explore the feasibility of creating a core complex in *R. sphaeroides* highly tolerant of the damaging and denaturing effects of heat. As had been shown previously, the detergent-solubilised TRC-TLH1 core complex is capable of sustaining temperatures of 50 °C for over an hour or room temperature for days (Kimura et al., 2009). The enhanced stability was attributed to Ca²⁺ bound to the TLH1; hence, if it were possible to increase the stability of the RC with the simple addition of adding a TLH1 ring structure it could be highly advantageous in solar photovoltaic applications. A secondary benefit of using TLH1 in photovoltaic applications would be the increased absorbance spectrum range, especially in the far-red and near-IR range, which could be used to absorb photons and generate photocurrents (Blankenship et al., 2011; Yaghoubi et al., 2015).

All the protein constructs were purified and obtained in a final buffer containing DDM detergent. The proteins were subjected to temperatures of 30 °, 50 °, 70 °, and 90 °C in a buffer consisting of 10 mM Tris pH 8, 0.04% DDM, and 1 mM CaCl₂. The stability of the complex was measured by absorbance spectroscopy; a decrease in the LH1 875 nm or TLH1 915 nm peak amplitude indicated a loss of bacteriochlorophyll from the complex, along with an increase in absorbance of free bacteriochlorophyll in solution at 775 nm (Figure 3.40). The decay kinetics of each complex are shown in Figure 3.41 and parameters of the two phase exponential decay fits of the samples at 70 °C listed in Table 3.4.

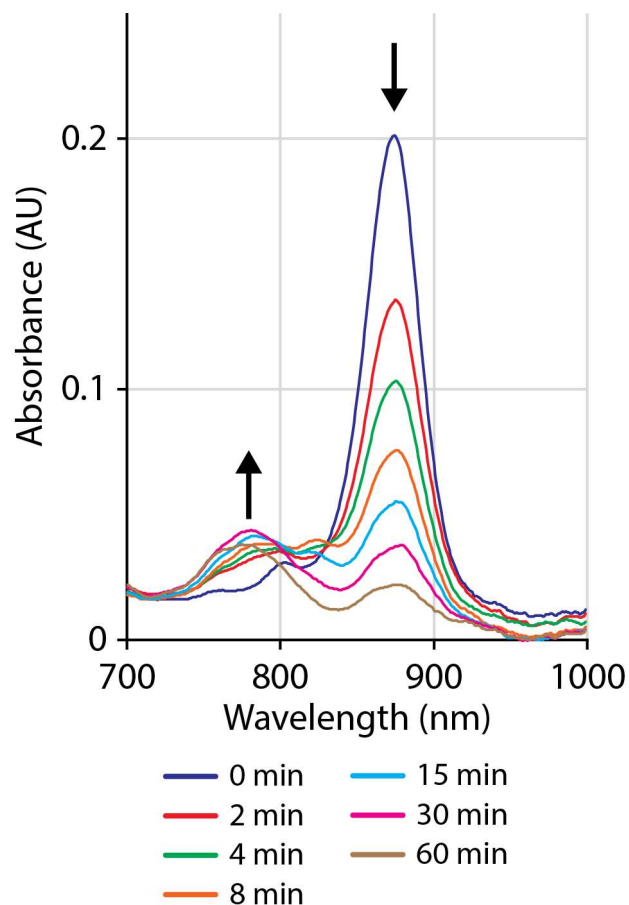


Figure 3.40. Changes in the absorbance profile of RC-LH1-X⁺ due to thermal denaturation at 70 °C. Characteristic changes in the absorbance due to denaturation is observed by a decrease of the LH1 875 nm peak and an increase in the 775 nm peak corresponding to free-floating bacteriochlorophylls and bacteriopheophytins in solution (arrows). Denaturation progress was measured at 0 min (blue), 2 min (red), 4 min (green), 8 min (orange), 15 min (cyan), 30 min (magenta), and 60 min (brown). Samples were normalised to the same starting concentration of $A_{875} = 0.2$ and are an average of three replicates.

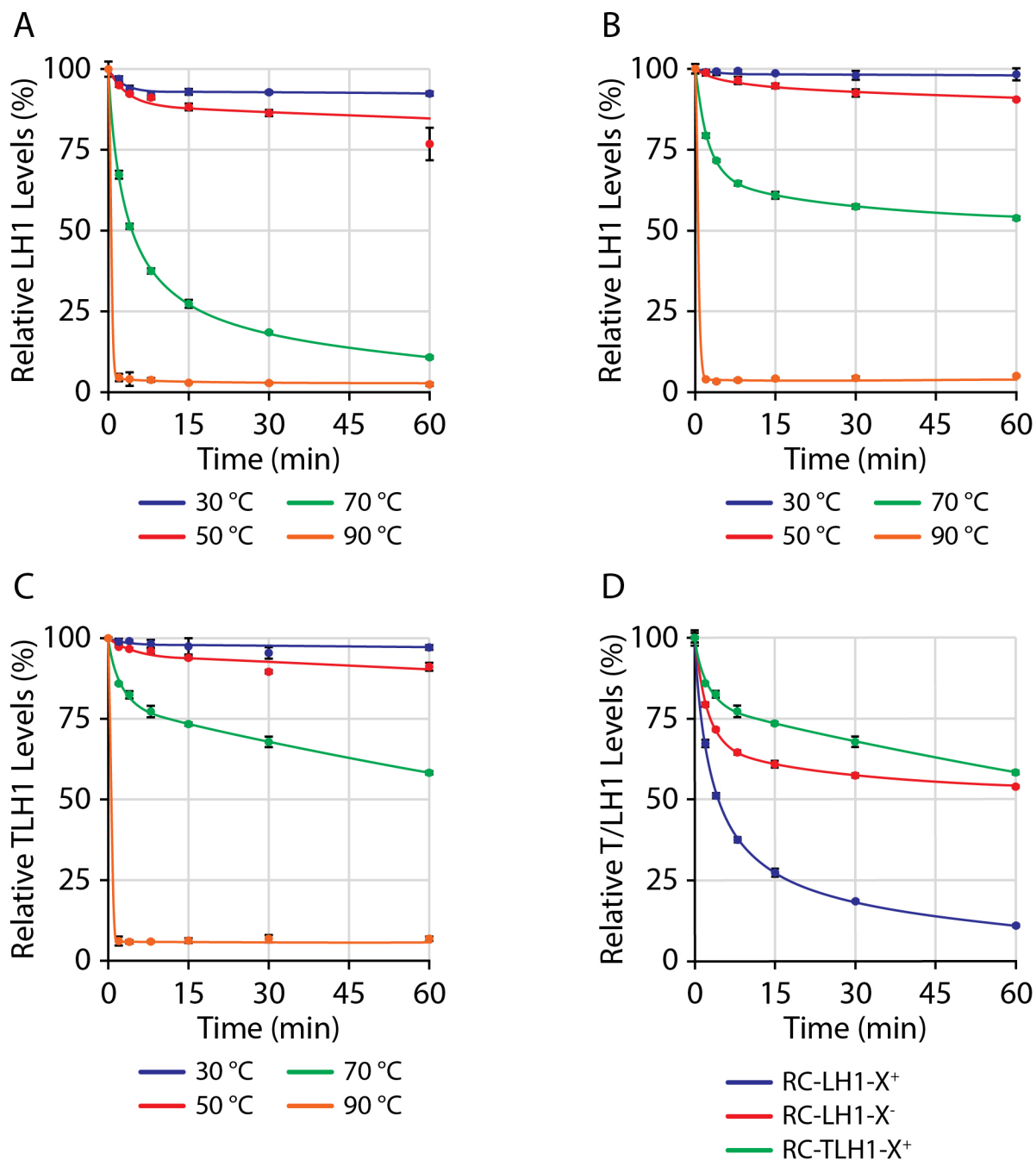


Figure 3.41. Decay kinetics of the LH1 875 nm peak and the TLH1 915 nm peak due to exposure to heat. The protein samples were subjected to temperatures of 30 °C (blue), 50 °C (red), 70 °C (green), and 90 °C (orange) for up to an hour; A) RC-LH1-X⁺, B) RC-LH1-X⁻, and C) RC-TLH1-X⁺. D) The decay profiles of RC-LH1-X⁺ (blue), RC-LH1-X⁻ (red), and RC-TLH1-X⁺ (green) exposed to 70 °C are shown. Lines are exponential decay fits. Error bars represent the standard deviation (n = 3).

Table 3.4. Two-phase exponential decay fit parameters of the RC-LH1-X⁺, RC-LH1-X⁻, and RC-TLH1-X⁺ at 70 °C.

Mutant	y ₀	A ^{fast}	t _{1/2} ^{fast} (min)	A ^{slow}	t _{1/2} ^{slow} (min)	R ²
RC-LH1-X ⁺	9 ± 2	53 ± 4	1.7 ± 0.2	38 ± 3	15 ± 3	0.99773
RC-LH1-X ⁻	53 ± 1	31 ± 2	1.5 ± 0.2	16 ± 2	17 ± 6	0.99544
RC-TLH1-X ⁺	43 ± 12	18 ± 2	1.2 ± 0.2	39 ± 10	44 ± 23	0.98881

The hybrid core complex RC-TLH1-X⁺ consisting of an RC core and TLH1 showed the highest tolerance to heat during the 1 h incubation time, as at 70 °C, as the RC-TLH1-X⁺ only decayed to 58% of the initial starting amount, compared to 11 and 53% for the RC-LH1-X⁺ and RC-LH1-X⁻, respectively. Further, the exponential decay can be broken into an initial fast decay followed by a slow decay (the residual plots are shown in Appendix D.1). The RC-TLH1-X⁺ shows the longest slow phase half-time, indicating greater stability. The RC-LH1-X⁻ showed higher stability than the RC-LH1-X⁺, as the latter resulted in a near-complete degradation by the end of the heat incubation, possibly indicating that a smaller, compact monomer is more stable than the dimer complex. As seen in the sucrose gradients in Section 3.4.6, the RC-TLH1-X⁺ appears to be a monomer and this form may contribute most to overall stability. The further increase in stability over the RC-LH1-X⁺ monomer is attributed to contributions from TLH1. Although these results indicate that the stability of the RC in a core complex is more complicated than solely substituting TLH1 in place of LH1, TLH1 produced in concert with the RC in *R. sphaeroides* appears to yield greater thermal stability of the core complex than the monomer and dimer forms of the *R. sphaeroides* native complex.

Chapter 4: Discussion

4.1 Advantages of using the pIND4 plasmid, the strain RCx^R, and the medium RLB for the homologous expression of genes.

One of the major challenges of working with membrane proteins is the low yield often associated with expression issues and limited membrane surface area (Schlegel et al., 2014). The system that was created was optimised for the expression of photosynthetic *R. sphaeroides* integral pigment-protein complexes, but could be used to express other membrane or soluble proteins. Under environments shifting to anoxygenic conditions, the intracytoplasmic membrane of the cell invaginates, facilitated by the insertion of pigment-protein complexes (Niederman, 2013), which increases the surface area into which other membrane proteins can be inserted. Additionally, by knocking out the gene encoding the restriction enzyme RshI, plasmids capable of replication in *R. sphaeroides* can be transformed rather than conjugated into the organism, reducing the time associated with isolating colonies from one to two weeks down to four days.

The pIND4 expression plasmid resulted in an 8-fold increase of RC-LH1 core complexes over using the previous pRS1 system (Jaschke et al., 2011) under semi-aerobic conditions. The pIND4 copy number of 18 to 23, versus 4 to 7 for pRK415-derived plasmids such as pRS1, most likely was one of a few determining factors in elevating mRNA transcript levels and thus protein levels. Another factor was the use of a IPTG-inducible, T7-derived promoter, which has been shown to be comparable or slightly stronger than the endogenous *puc* promoter previously used in *R. sphaeroides* protein expression systems (Ind et al., 2009).

The knockout of the PpsR regulatory protein meant that the biosynthesis genes for heme, bacteriochlorophyll, and carotenoid were constitutively expressed, regardless of the oxygen concentration levels in the culture medium. This ensured the maximal production of bacteriochlorins such that they were not the limiting factor in the assembly of RCs. The production of an excess of pigments resulted in a 1.2-fold increase in RC levels. More crucially, the requirement of not having to grow cultures under low oxygen or anaerobic conditions in darkness (to avoid selection for second site mutations that improve phototrophic growth) is important, because aerobic cultures grow faster via respiration and to higher densities.

It was discovered that the addition of Mg²⁺ and Ca²⁺ ions increased pigment-protein complex levels further by an additional 1.3-fold. Although the mechanism for the increase is

unclear, the addition of Mg^{2+} may improve incorporation into bacteriochlorophyll, and both Mg^{2+} and Ca^{2+} help to stabilise the outer membrane (Clifton et al., 2015; Onoda et al., 2000). Furthermore, as the PpsR protein was knocked-out, cultures could be grown aerobically and were about three times more dense than semi-aerobic cultures, and reached harvest density overnight, compared to four to five days of semi-aerobic growth.

The result of all the modifications was a system that produced 35-fold more pigment-protein complexes in less than half of the time than previously (Jaschke et al., 2011). Although the majority of the proteins expressed and purified using this system were RCs, other membrane or soluble proteins can be synthesised, although the greater advantage would be with the former, due to the large surface area of the intracytoplasmic membrane. Additionally, genes from other organisms can be heterologously expressed (Section 4.4).

4.2 Implications of the role of the H subunit in RC assembly and function.

The assembly of the reaction centre has been explored extensively in the past to determine which components are necessary for structural and functional integrity of this pigment-protein complex. Two distinct approaches have been used to study this question, one biochemical and the other genetic. Here, a genetic approach was used to modify the functionality of truncated RC mutants with further applications in biohybrid solar cells.

The H subunit from an intact RC had been removed previously using biochemical means to show that the resulting LM RC still maintained some charge separation to at least the primary quinone. Electron transfer from Q_A to Q_B was severely reduced by approximately 10^2 - 10^3 -fold, indicating transfer slowed from 100 μ s to 10-100 ms, and the quinones were found to bind with less affinity (Debus et al., 1985). More recently, using the same procedure to create an LM RC, the electron transfer rates from H_A^- to Q_A , as well as the recombination from Q_A to P^+ , were reduced by approximately four-fold (Sun et al., 2016). The likely cause for the decrease in electron transfer rates is increased conformational changes of the quinone binding pockets due to the removal of the H subunit (Sun et al., 2015).

Other groups have explored the assembly of RCs using genetic means. For example, a disruption of the *puhA* gene showed a 150-fold decrease in photooxidation activity of the LM RC – if it assembled at all (Sockett et al., 1989) – and high turnover of the individual polypeptides

(Varga and Kaplan, 1993). In other studies of the *R. sphaeroides* H subunit domains such as the N-terminal periplasmic sequence, membrane-spanning α -helix, and cytoplasmic globular domain were replaced with the equivalent from *Blastochloris viridis*. Replacement of the cytoplasmic domain showed significant decrease in RC assembly, possibly due to the inability of *R. sphaeroides* to fold a domain originating from another bacterium (Tehrani et al., 2003). Furthermore, based on data from individual H, L, and M subunit gene knockouts, the authors suggested that the H subunit is necessary for maximal RC production, and a strain lacking the H subunit contained lower levels of the L polypeptide relative to the M polypeptide (Tehrani and Thomas Beatty, 2004).

Given the results of other groups, I took a different genetic approach, where various deletions from the C-terminus of the H subunit were made to study the components necessary to form a stable RC or RC-LH1 complex.

4.2.1 *In vivo* assembly of the LM, 45, 80, and 150 RC mutants.

Using the *R. sphaeroides* RC^x strain, coupled with the pIND4 expression plasmid, the resulting system over-produces pigment-protein complexes. To facilitate electron transfer from the quinone region of the RC to an external acceptor such as an electrode, truncations of the H subunit were made progressively from the C-terminus of the polypeptide. Truncations containing only the N-terminal 45, 80, and 150 amino acid residues of the H subunit were created, as well as a mutant completely lacking the H subunit (Figure 3.7). The result was a decrease in the distance from Q_A or Q_B to the newly-exposed protein surface. However, given the earlier evidence of the lack of RC formation *in vivo* of an LM RC and domain swapping experiments (Sockett et al., 1989; Tehrani et al., 2003; Tehrani and Thomas Beatty, 2004; Varga and Kaplan, 1993), it was not clear whether the RC would assemble *in vivo* with such major truncations of the H subunit.

It was surprising, therefore, that the RC assembled *in vivo*, regardless of H subunit length and even the lack of an H subunit. This is contrary to earlier data published that showed little accumulation, if any, of the LM RC in the membrane (Sockett et al., 1989). Measurement of broken cell spectra, as in Figure 3.8, was a direct measure of RC assembly with respect to the accessory bacteriochlorophyll peak at ~800 nm. There is a possibility that only the accessory bacteriochlorophylls, and none of the other bacteriochlorins, assembled in the RC, but that

likelihood seems unlikely because no evidence has been provided to date that support the assembly of an RC lacking bacteriochlorins without further structural modifications (Jackson et al., 1997; Moore and Boxer, 1998; Ridge et al., 1999; Watson et al., 2005a). However, there is a greater probability that the primary and secondary quinones may have been lost during assembly, due to weaker binding interactions after the H subunit is removed or truncated (Debus et al., 1985; Sun et al., 2015). As a result, measuring broken cell spectra may be a better indication of mutant RC assembly *in vivo* than measuring photooxidative activity, as done in earlier experiments (Sackett et al., 1989), because photooxidation requires complete occupancy of the quinone binding pockets, at least Q_A, in order to create and measure a charge separated state over μ s timescales.

The broken cell spectra show a blue-shifting of the \sim 800 nm peak with decreasing H subunit length. Initially, it was thought that the truncated RCs were degrading. But since a typical signature of a degrading RC is a decrease of the 800 nm peak accompanied by an increase in 760 nm signal, corresponding to free bacteriochlorophyll (Hughes et al., 2006), it may be more likely that the absorbance band shift is due to changes in the environment surrounding the cofactors rather than a sign of protein degradation. As the H subunit is continually shortened, this may induce structural changes within the remaining protein complex that changes the environment around the accessory bacteriochlorophylls (the origin of the 800 nm peak). A further indication that the shift of the 800 nm peak was not degradation was the fact that most of the truncation mutants were produced at levels higher than the wild type RC (Figure 3.8); however, this is under the assumption that the extinction coefficient of the accessory bacteriochlorophylls did not change.

Given that the results here are contrary to published data, it is important to note that there were differences in experimental setup. One was the use of a pIND4 plasmid that over-produces RC complexes. The constant over-production of the L and M polypeptides might have compensated their short half-lives and rapid turnover in the membrane (Varga and Kaplan, 1993). The other modification was the use of the RCx^R strain, where the gene encoding the PpsR repressor of heme, bacteriochlorophyll, and carotenoid synthesis was knocked-out. This resulted in the constant production of bacteriochlorophyll and bacteriopheophytin with no mechanism to decrease synthesis. There are data suggesting that these bacteriochlorins are required for RC

assembly and subsequent stability, *i.e.*, apo-RC pigment-protein complexes are inherently unstable (Dierstein, 1983; Takemoto and Lascelles, 1973). Hence, the combination of a constant supply of L and M subunits and an over-abundance of bacteriochlorins may have resulted in a greater probability of protein complex formation and stabilisation of the truncated mutants *in vivo*.

4.2.2 Characterisation of the LM, 45, and 80 RC mutants and *in vitro* charge separation.

The LM, 45 and 80 mutants were purified using the non-ionic detergent DDM, because the zwitterionic detergent LDAO resulted in rapid degradation. As seen in Figure 3.10A, there were several changes in the Q_y transition region of the LM, 45, and 80 RC mutants, compared to the native RC. In particular, for the 45 and 80 mutants, there was a relative decrease in absorbance of the 760 nm and 865 nm peaks, corresponding to the bacteriopheophytins and the special pair bacteriochlorophylls, respectively, and an increase in absorbance of the 804 nm accessory bacteriochlorophylls peak. As for the LM mutant, there was a further decrease in the 760 nm bacteriopheophytins and 804 nm accessory bacteriochlorophylls peaks, and an absence of the 865 nm special pair bacteriochlorophylls peak. The LM absorbance spectrum contrasts with data where the LM RC was formed by the removal of the H subunit using biochemical means. In that work, the LM RC absorbance spectrum showed no difference from wild type (Sun et al., 2015). Apparently, the assembly of the LM RC *in vivo* and/or purification method most likely resulted in a loss of bacteriochlorins and subsequently, a decrease in the three major absorbance peaks of the Q_y transition region.

At first, due to the decrease in absorbance, it was thought that a bacteriochlorophyll and/or a bacteriopheophytin was lost. However, pigment extraction of the 45 and 80 mutants showed a ratio of bacteriochlorophyll to bacteriopheophytin of two for the wild type, 45, and 80 RCs, indicating that four bacteriochlorophylls and two bacteriopheophytins were maintained (Table 3.2). Two bacteriochlorophylls and one bacteriopheophytin could have been lost, giving the same ratio, but this observation would have been likely indicated as a lack of formation of a charge separated state, similar to the LM mutant described next (Figure 3.10B). Hence, the ratio was an indication that all the bacteriochlorins assembled in the 45 and 80 mutants. Conversely, in the case of the LM mutant the ratio increased to around three, which may be the result of a

loss of a bacteriochlorophyll and a bacteriopheophytin, leaving three bacteriochlorophylls and one bacteriopheophytin left in the RC, supported by the observation that there were further decreases in the absorbance bands in the Q_y transition region and the Soret band corresponding to all bacteriochlorins.

To assess function of an RC, a charge separated state can be measured, which indicates electron transfer through the A-branch to either the primary or secondary quinone, and forming a $P^+Q_A^-$ or $P^+Q_B^-$ state, respectively. As seen in Figure 3.10B, a partial charge separation was measured for the 45 and 80 mutants. The LM mutant showed almost no change between the dark- and light-adapted states of the RC. Due to the changes in the amplitude and peak wavelength of the special pair bacteriochlorophylls of the dark-adapted state of the 45 and 80 mutants, the profile of the difference absorbance spectrum corresponding to charge separation differs from the wild type. However, electrochromic shifts were detected and the 45 and 80 P-band showed a near complete or complete bleaching (data not shown), strongly indicative of electron transfer from P to at least Q_A and possibly Q_B .

The combination of the *in vivo* and *in vitro* data show that under these experimental conditions, the H subunit may not be necessary for structural assembly of the RC *in vivo*, but a minimum of the membrane-spanning α -helix of the H subunit is required to stably maintain the complex for purification and downstream applications.

4.2.3 Requirement of the H subunit for phototrophic growth.

Assembly of the truncation mutants *in vivo* and evidence of charge separation, does not indicate that the RCs are functional and useable by the organism. None of the truncation mutants, even with the addition of LH1, allowed for growth under phototrophic conditions. Conceivably, charge separation efficiency decreased due to reduced binding affinity of the quinones (Debus et al., 1985; Sun et al., 2015). For an LM RC mutant, electron transfer from H_A to Q_A was decreased by 4-fold (Sun et al., 2016) and electron transfer from Q_A to Q_B was decreased 10^2 - 10^3 -fold (Debus et al., 1985). In other words, instead of forming a charge separated state in about 100 μ s, charge separation would occur in 100-1000 ms. This rate may be too slow to support phototrophic growth of the 45 mutant, assuming that it is more similar structurally and kinetically to the LM mutant than the wild type.

Only when secondary mutants were selected under phototrophic conditions did *R. sphaeroides* grow using the 80RC-LH1 PS⁺ or 150RC-LH1 PS⁺ core complexes, assuming compensatory mutations were obtained (Figure 3.9). Even then, growth was slow with increasing doubling times correlating with decreasing H subunit length. Doubling time for the wild type was approximately 5 h, whereas the doubling time increased to about 20 and 30 h for 150RC-LH1 PS⁺ and 80RC-LH1 PS⁺, respectively. The fact that these mutants grew may indicate that the longer variants of the H subunit can stabilise the quinones enough to support phototrophic growth. Complementing the *R. sphaeroides* strain RCx^R with the plasmids from phototrophy-capable mutants did not result in phototrophic growth, indicating that the secondary mutations were on the chromosome, and DNA sequencing confirmed that the plasmids did not contain any mutations.

Interestingly, as shown in Figure 3.11, chromatophores containing the 80RC-LH1 PS⁺ and 150RC-LH1 PS⁺ core complexes showed an accentuated peak at 420 nm. It is possible that this peak corresponds to a cytochrome protein, as the peak is characteristic of the Soret band absorbance of heme. Furthermore, the peak was only present in the periplasmic space of the chromatophores and diminished after the core complexes were purified.

Is an increased up-regulation of cytochrome required for phototrophic growth using RCs containing C-terminally truncated RC H proteins? If charge separation efficiency is decreased as a result of electrons leaking to an external mediator, because the lack of a cytoplasmic domain no longer insulates the quinone region of the RC, or quinones diffusing away, due to weaker interactions, then higher amounts of cytochrome may be sufficient to reduce P⁺ and increase electron turnover events to inefficiently reduce Q_B fully.

Finally, there were no major spectral differences of the purified forms of the 80RC-LH1 PS⁺ and 150RC-LH1 PS⁺ compared to the wild type RC-LH1 core complex in the Q_y transition region. This is in contrast to the purified 80 RC mutant, where the 760 nm peak decreased and 804 nm peak increased. Presumably, the addition of LH1 stabilised the RC core and resulted in a spectrum more similar to wild type.

4.2.4 Role of the cytoplasmic domain of the H subunit.

Although my primary purpose of creating truncation mutants was for applications in biohybrid solar cells and attachment to electrodes, biological questions arise, especially around the function and necessity of the H subunit. The membrane-spanning α -helix assists in maintaining the overall structural integrity of the RC complex, but the function of the cytoplasmic domain is still unclear.

Of the phototrophy-capable mutants, the 80RC-LH1 PS⁺ mutant contains the shortest H subunit. With only the first 80 residues of the H subunit, it is worth noting that the Q_B proton uptake pathway beginning with the His at residues 126 and 128 is absent (Okamura et al., 2000; Paddock et al., 2003a). The proton uptake kinetics were not explored in this project, but my results raise questions for the necessity of maintaining a globular domain for proton uptake. Given the removal of the proton uptake pathway, the network of water molecules and H-bonding is also removed and the Asp at residues 210 and 213 on the L subunit, which have been shown to transfer protons to Q_B, are now supposedly directly exposed to the cytoplasmic solvent. Since the 80RC-LH1 PS⁺ grew phototrophically, albeit at reduced rates compared to wild type and with compensatory secondary mutations, evidently, the bulk of the cytoplasmic domain is not required for growth under anaerobic, phototrophic conditions. Perhaps the proton transfer pathways in the cytoplasmic domain are not as critical as the maintenance of efficient electron transfer from H_A to Q_A to Q_B, as no phototrophy-capable mutant with the 45 truncated RC was isolated. As suggested by others (Debus et al., 1985; Sun et al., 2016; Sun et al., 2015), the cytoplasmic domain appears to be required for efficient electron transfer between H_A, Q_A, and Q_B, which is absent in the LM mutant. Presumably, the cytoplasmic domain in large part exists to shield the quinones from the solvent and maintain efficient electron transfer; and secondarily, internal water channels and proton transfer pathways are built in for proton uptake by the quinone at Q_B.

The H subunit cytoplasmic domain also plays a role in the assembly of the core complex with LH1 and PufX. For the assembly of the RC-LH1 core complex, one model proposes that the PufX protein interacts with the C-terminus of the H subunit to promote dimerisation of the RC with LH1 (Mothersole et al., 2016; Qian et al., 2013). In the case of the 80RC-LH1 PS⁺ and 150RC-LH1 PS⁺, it was assumed a dimer complex was formed, because the monomeric form does not support phototrophic growth (Holden-Dye et al., 2008), and these mutant RCs

supported growth under anaerobic, phototrophic conditions. How did LH1 and PufX assembly occur if the C-terminus of the H subunit is a factor in dimerisation when it was deleted? Furthermore, absorbance spectra of the phototrophy-incapable 45 RC-LH1 mutant showed the same ratio of RC to LH1 as the wild type (data not shown). Evidently, LH1 assembles around the RC even without the cytoplasmic domain of the H subunit, but due to the lack of the native C-terminus of the H subunit, PufX may not dock in the proper area of the RC. The result is the inability for quinones to diffuse in and out of the complex core efficiently, which consequently reduces growth rate.

4.3 Evidence of direct electron transfer to or from multiple cofactor sites in the RC.

4.3.1 Electron transfer to and from the special pair P.

The question of whether electrons can be injected into the RC when the oxidised P⁺ state is formed has been explored quite extensively and successfully. In fact, publications that studied the RC in biohybrid photoelectrochemical cells tended to use the RC with the P-side attached to an electrode substrate (Mahmoudzadeh et al., 2011; Tan et al., 2012; Tan et al., 2013; Yaghoubi et al., 2015; Yaghoubi et al., 2012). Binding on the P-side is a common orientation for a couple of reasons: one, there is a natural tendency for the P-side to adsorb onto an electrode or via a linker, such as a cytochrome protein (den Hollander et al., 2011; Kamran et al., 2015); and two, due to the cytoplasmic domain of H shielding the quinones, direct electron transfer is unlikely to occur through the long distances of 20 Å or more that would be needed for direct electron transfer out of the RC.

The TM RC (Figure 3.20) was bound directly to a gold electrode to confirm whether this configuration yielded the same photocurrent direction as other work in which electron flow was from an electrode into the RC (den Hollander et al., 2011; Kamran et al., 2015; Mahmoudzadeh et al., 2011; Mirvakili et al., 2014). The data also served as a control to indicate proper electron flow in the other RC mutants.

In the presence of 5 mM benzoquinone as charge mediator, currents of -175 nA/cm² were measured (Figure 3.21A). The cathodic, negative current flow indicates that electrons were injected into the solution, presumably to reduce the P⁺ state of the RC. This current is 20-fold larger than the -5 nA/cm² we previously reported (Mahmoudzadeh et al., 2011). The increase in

current magnitude may be due to several things: a gold leaf electrode can be easily cleaned of contaminants by flaming, whereas the glass slides previously used cannot be flamed and therefore may not have allowed for thorough cleaning; additionally, 1x PBS pH 7.2 was used, which has been shown to not adsorb onto the surface, whereas the 10 mM Tris pH 8 used previously adsorbs and irreversibly forms a blocking layer on the gold surface, and may reduce the surface area available for RC binding, or block effective electron transfer (Iranpour, 2012); the slow rise time of about 5 s to reach only -5 nA/cm^2 in previous work may have been due to the use of $50 \text{ }\mu\text{M}$ ubiquinone versus 5 mM benzoquinone, resulting in low turnover of the Q_B quinone; and only $1 \text{ }\mu\text{M}$ TM RC was used previously, compared to $10 \text{ }\mu\text{M}$ which likely resulted in better surface loading.

The large initial positive spike may have been initially attributed to the gold electrode reacting to light (*i.e.*, an instrumentation artifact), as when SbnI was bound to gold there was a similar positive spike (Figure 3.19B), or possibly due to a light-dependent oxidation of reduced benzoquinone on the electrode surface. However, the amplitude of the spike after the TM was bound is about 10-fold larger and hence, there appears to be a contribution from the RC. Upon initial excitation of the special pair, an electron is promoted to P^* . Usually, the electron transitions to the accessory bacteriochlorophyll in 3 ps (Jones, 2009). However, because the distance between the electrode surface and the edge of the special pair is less than 5 \AA , single-step electron transfer rates are expected to be in the ns to ps range (Winkler and Gray, 2014). There may be two opposing electron transfer processes such that the electron transfer from the P region to the electrode initially out-competes the electron flow down the A-branch. As will be described in Section 4.3.2, the spike appears to be largely independent of mediator concentration and may be an intrinsic reaction between the RC and the gold electrode. A possible schematic of the anodic, positive electron flow is shown in Figure 4.1A and, similarly, the schematic displaying the cathodic, negative electron flow is shown in Figure 4.1B.

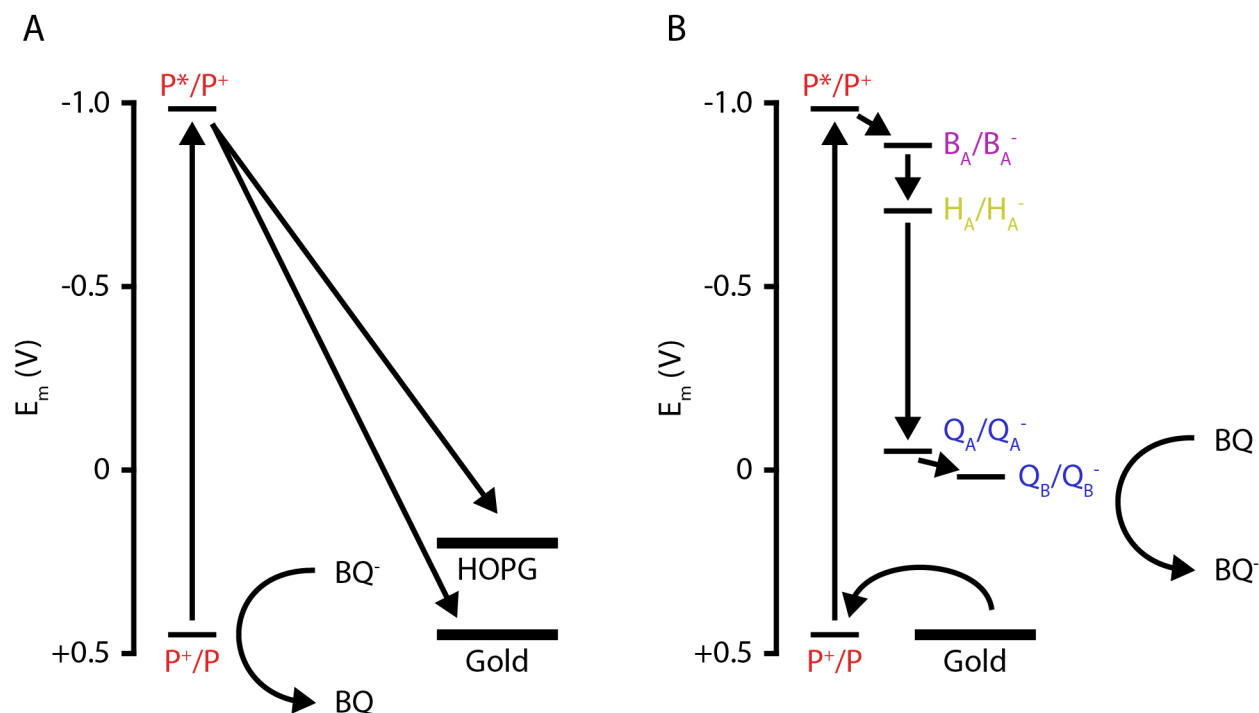


Figure 4.1. Proposed electron flow in the TM RC. A) Anodic, positive electron where electrons were extracted from the P region to an HOPG or gold electrode. The P^+ state was reduced by the reduced form of benzoquinone (BQ). B) Cathodic, negative electron flow where electrons likely flowed from the gold electrode into the P^+ state of the special pair bacteriochlorophylls. Benzoquinone was used as the quinone electron acceptor at Q_B .

The inhibitor *o*-phenanthroline is known to exclude the quinone at Q_B (Diner et al., 1984; Wraight and Stein, 1980). No steady-state currents larger than the currents generated with the SbnI control was detected in the presence of *o*-phenanthroline, further validating the model that electron transfer was blocked to the Q_B site of the RC. The addition of 1 mM benzoquinone resulted in a large initial positive spike of $1.2 \mu\text{A}/\text{cm}^2$, but more surprisingly, a positive steady-state of $70 \text{ nA}/\text{cm}^2$ was measured. This electron flow from the P region to the electrode, as shown in Figure 4.1A, is presumably mediated by the reduction of the P^+ state by the reduced form of benzoquinone – a solution of benzoquinone was found to be a mixture of both the oxidised and reduced forms of the molecule, despite the starting material used to create the solution (Appendix C.1). Depending on the presence of *o*-phenanthroline, TM RCs bound to

gold shows a dual-polarity current characteristic by producing both positive and negative photocurrents under illumination, which has not been previously reported in the literature.

Anodic, positive photocurrents were obtained when the TM was bound to an HOPG electrode with 1 mM benzoquinone (Figure 3.21C), despite the absence of *o*-phenanthroline. Since *o*-phenanthroline is required to block electron transfer to Q_B and produce positive steady-state photocurrents on a gold electrode, the formation of positive photocurrents without *o*-phenanthroline indicates that another mechanism is required to describe the results. The *N*-(1-pyrene)maleimide linker may be facilitating electron flow from the P region to the electrode at a rate faster than electron transfer down the A-branch of the RC, resulting in anodic current flow.

4.3.2 Electron transfer from the H_A bacteriopheophytin.

A major focus of my thesis research was to determine whether electrons could be extracted from the H_A region of the RC. There have been no reports of successful electron transfer from H_A . Although there is a report of the use of carotenoid-less RCs where sodium dithionite was used to reduce quinones at Q_A and Q_B (rendering them unable to accept electrons and participating in charge separation), and the resulting electron transfer from H_A was determined to be electron transfer from the triplet state of P^* (Lukashev et al., 2007). However, the RC mutants described here contain carotenoids that immediately quench the triplet state of P^* .

The M256-Cys RC mutant (Figure 3.23) was bound to both HOPG and gold electrodes (Figure 3.24). On an HOPG electrode, ascorbate or hydroquinone were used as electron donors to P^+ . With 100 μ M ascorbate, a small photocurrent spike was observed before decaying, although photocurrents were above the baseline without any mediator (this baseline was observed with the non-photoreactive SbnI control in Figure 3.19 as possibly attributed to light interacting with HOPG and/or the *N*-(1-pyrene)maleimide linker). Increasing the concentration to 500 μ M ascorbate did not reduce the initial spike and increased the steady-state current marginally. Parallel experiments on the same configuration, except with hydroquinone as the electron donor (Figure 3.24B), showed larger photocurrents than the equivalent ascorbate concentrations. Increasing the concentration of hydroquinone to 1 mM eliminated the photocurrent spike. Using CVs, hydroquinone shows faster and larger oxidation rates than

ascorbate (Appendix C.1), which may explain the larger photocurrents. Further, the initial spike is likely due to a fast, kinetic reaction that is diffusion limited, which is observed with the lower hydroquinone concentrations. With the highest concentration of hydroquinone, 1 mM, it appears that diffusion was not rate-limiting, as the spike was virtually eliminated. The positive direction of the current indicates that electrons transferred from the RC into the electrode, and measurements of the action spectra confirmed that the photocurrent generation was contributed by the RC mutants bound to the electrode. A schematic of possible electron flow is shown in Figure 4.2.

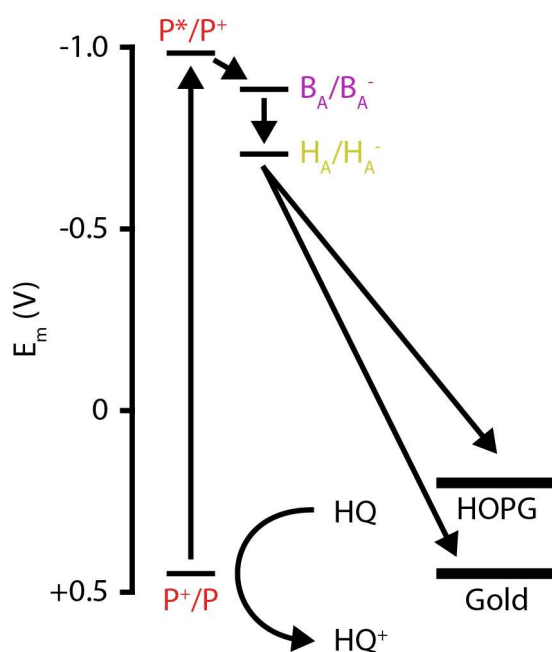


Figure 4.2. Proposed electron flow in the M256-Cys RC. Electrons likely flowed from the H_A bacteriopheophytin into an HOPG electrode or gold electrode. In this mutant, the Q_A quinone is absent. Hydroquinone (HQ) was used as the electron donor to P^+ .

The M256-Cys was also bound to gold (Figure 3.24D). Similar to the results on HOPG, the positive photocurrents indicate that electrons were injected into the electrode. The large initial spike was observed again, but now appears to be independent of mediator concentration. At 5 mM hydroquinone, the maximum steady-state current was achieved, but did not eliminate the spike in current; hence, the kinetics of the spike are faster than electron transfer from a

diffusible mediator. The decrease or elimination of this spike using the HOPG electrode may be because the *N*-(1-pyrene)maleimide linker slows electron rates by creating a blocking layer (Figure 3.16), allowing time for the transfer of charge by a diffusible mediator.

Another mutant, M256/L121-Cys, was tested using the hypothesis that replacing an insulating Phe with Trp might accelerate electron transfer (Shih et al., 2008), leading to higher photocurrents than its precursor. The Phe at L121 was substituted with Trp, but when compared with M256-Cys, the M256/L121-Cys generated less photocurrent (Figure 3.24C). This result may be explained by the fact that the F(L121)W is not directly in line between the electron donor H_A and the electrode electron acceptor (Figure 4.3). The indole plane of the Trp is believed to be within van der Waals distance of and coplanar to the H_A macrocycle, meaning the π -orbitals of both molecules are possibly interacting with each other, further delocalising and stabilising the electron cloud distribution.

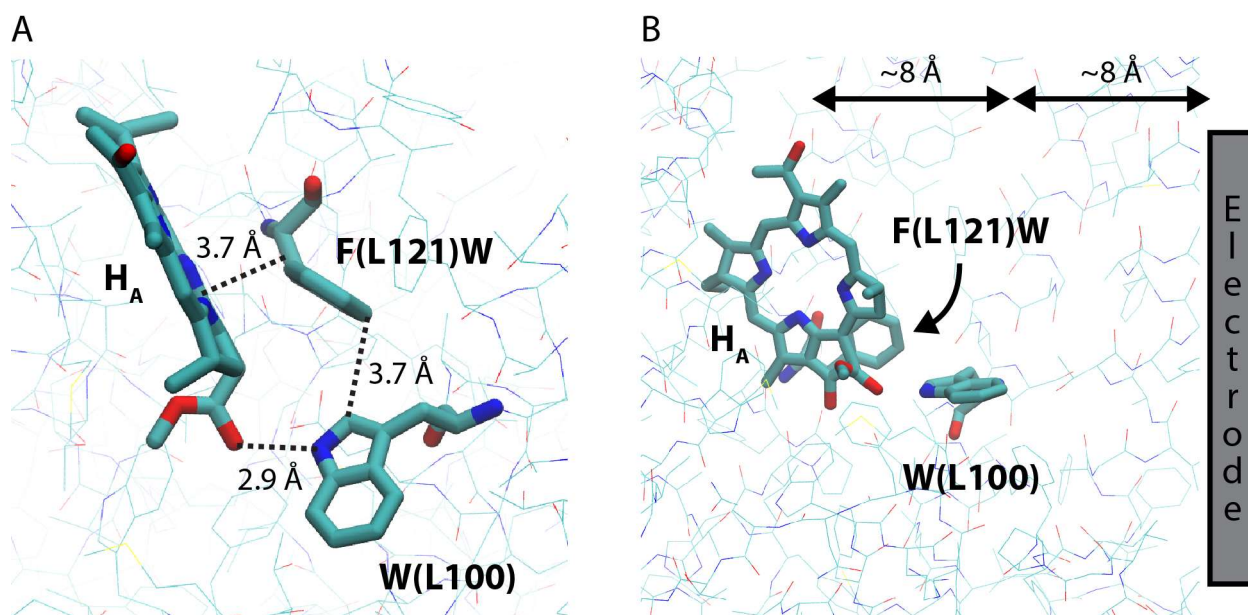


Figure 4.3. Distance relationship between the H_A bacteriopheophytin, F(L121)W, W(L100), and the electrode. The phytyl tail of H_A was removed for simplicity. Carbon atoms are teal, nitrogen atoms blue, and oxygen atoms red. A) Distances between H_A , F(L121)W, and W(L100). B) Distances between H_A , W(L100), and the electrode (grey). Structures based on PDB 2J8C.

In the M256-Cys mutant, the Q_A quinone is absent due to an A(M260)W mutation (Ridge et al., 1999). The immediate result is that electrons do not proceed beyond the H_A bacteriopheophytin. As shown above, attachment of this mutant to an electrode generates photocurrents. However, because the H_A region is hydrophobic and insulated, the question that arises is how the electrons are transferred from H_A through the dielectric to an electrode. Obviously, the forward must out-compete the reverse rate, which has been determined to be around 30 ns (Jones, 2009), indicating that the current electron transfer timescale is therefore faster than 30 ns across the estimated distance of 16 Å from the nearest edge of the H_A bacteriopheophytin to an electrode. A single electron tunnelling event through 16 Å of protein may be unlikely, electron tunnelling rates would be in the μ s range (Winkler and Gray, 2014), which is slower than the 30 ns back reaction from H_A^- to P^+ .

In the M256-Cys mutant that excludes a quinone from assembling in the Q_A pocket, in addition to losing the quinone head moiety, the isoprenoid tail is also lost. The isoprenoid tail of Q_A and phytol tails of the bacteriochlorophylls and bacteriopheophytin insulate the macrocycles of B_A and H_A , and the quinone from the external milieu, which prevents electrons from reacting with components in the solvent (Pan et al., 2013; Saer et al., 2013). Since the isoprenoid tail was removed in the M256-Cys mutant, the Trp at L100 became exposed to the interior of the detergent micelle (Figure 4.4). A solved crystal structure does not indicate the presence of a detergent or lipid molecule in the area where the Q_A isoprenoid tail used to be; in fact, the Phe at M258 has shifted to occupy the position corresponding to the first two isoprenoid units (McAuley et al., 2000). The Trp is believed to be H-bonded to the ester carbonyl group of ring V of the H_A bacteriopheophytin (Yeates et al., 1988) and may act as a relay between the bacteriopheophytin and the electrode in a Q_A -less configuration. Further experiments, such as substituting the Trp for a Phe to create a more insulating environment, might determine whether the Trp plays a role in electron transfer.

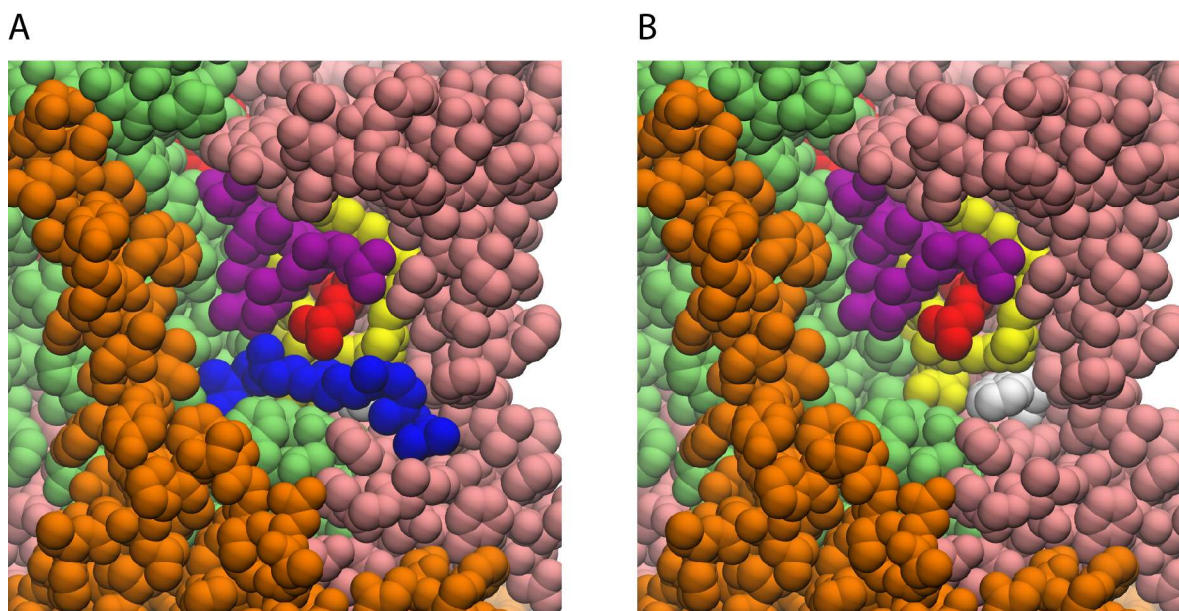


Figure 4.4. Exposure of the Trp at L100. A) The isoprenoid tail of the quinone (blue) at Q_A shields the Trp at L100 (not visible because it is located underneath the quinone tail) from the external solvent. B) Removal of the quinone, as in the M256-Cys mutant, exposes the Trp to the interior of the detergent micelle at L100 (white). The H subunit is shown in orange, L subunit in pink, and M subunit in green. The special pair is shown in red, the accessory bacteriochlorophyll in purple, and the bacteriopheophytin in yellow. Structures are based on PDB 2J8C.

4.3.3 Electron transfer from the quinone region.

One of the biggest difficulties in extracting electrons from the quinone region of the RC is the existence of the large, globular cytoplasmic domain of the H subunit that shields the quinones. As a result, direct electron transfer is not usually possible and photocurrent generation requires using quinones as a diffusible charge mediator. However, as discussed in Section 4.2, a novel approach of creating truncated RCs that removed the H subunit cytoplasmic domain enabled the extraction of electrons from the quinone region.

The first mutant, 45M-M229 (Figure 3.26), represents an attempt to extract electrons from the Q_A region. Earlier work indicated that electron transfer from Q_A to Q_B is impaired in an LM RC (H was removed from the purified RC) (Debus et al., 1985), and it was therefore assumed that most of the photocurrent obtained with 45M-M229 originated from the Q_A quinone. However, the photocurrents may underrepresent the rate of Q_A reduction, as there is a

possibility that electrons were transferred to Q_B and not to the electrode. With a distance of approximately 10 Å from the edge of the Q_A quinone headgroup to the protein surface, electron tunnelling rates would be in the ns range (Winkler and Gray, 2014), which is faster than the μ s range for the forward electron transfer to Q_B and ms range for the Q_A back reaction to P^+ in a wild type RC. Currents of up to 85 nA/cm² were measured in this configuration (Figure 3.27). A schematic of possible electron flow is shown in Figure 4.5.

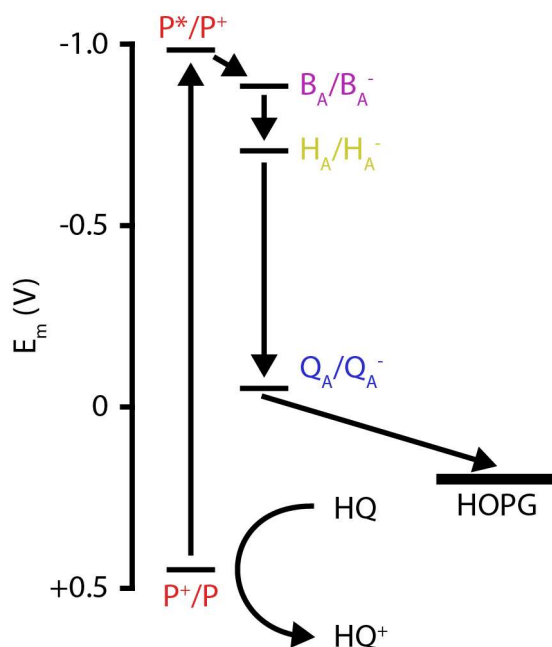


Figure 4.5. Proposed electron flow in the 45M-M229 RC. Electrons likely flowed from the Q_A primary quinone into the HOPG electrode. Hydroquinone (HQ) was used as the electron donor for P^+ .

A similar mutant, 45M-L210 (Figure 3.29), was made to extract electrons from Q_B . Because electron transfer from Q_A to Q_B could likely be impaired because of the truncation of the H subunit decreasing quinone occupancy of the Q_B site (Debus et al., 1985), currents were not expected to be large. Regardless, currents of around 80 nA/cm² were produced when bound to a gold electrode, though there may be a contribution from Q_A .

In the case of the 45M-L210/L213 mutant, a Trp was added between Q_B and D(L210)C (Figure 3.29) to investigate whether the addition of a Trp would accelerate electron transfer,

similar to the rationale used earlier for the M256/L121-Cys mutant. This was not the case, as photocurrents were lower than the 45M-L210 mutant. Some currents were generated, but it may be that the addition of a Trp at L213 caused structural changes in the Q_B pocket that resulted in even weaker binding of quinone. A schematic of possible electron flow is shown in Figure 4.6.

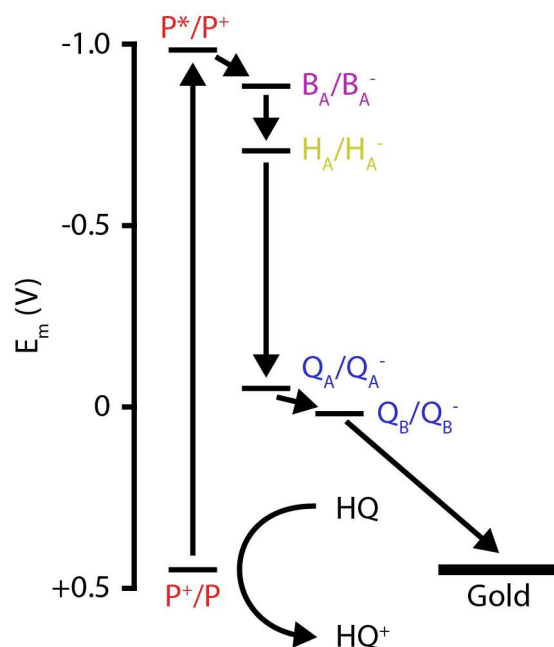


Figure 4.6. Proposed electron flow in the 45M-L210 or 45M-L210/L213 RC. Electrons likely flowed from the Q_B secondary quinone into the gold electrode. Hydroquinone (HQ) was used as the electron donor for P^+ .

4.4 Expression of *T. tepidum* TLH1 for the enhanced thermal stability of the core complex.

4.4.1 Characterisation of the TRC and *in vitro* charge separation.

The TRC was produced in and purified from *R. sphaeroides*; such heterologous expression of RC genes had not been reported in the literature previously. Although *T. tepidum* is a purple sulphur bacterium from the γ -proteobacteria class, the genes encoding the TRC subunits were recognised and assembled in *R. sphaeroides*. Figure 3.32 shows the Q_y transition region of the purified TRC, with the RC for comparison. The TRC shows the three dominant peaks in the near-IR range, with a few minor changes. The band corresponding to the accessory bacteriochlorophylls absorbs maximally at 800 nm versus 804 nm in *R. sphaeroides*. Similarly,

the special pair bacteriochlorophylls absorb at 870 nm in the TRC with a decrease in peak absorbance. These small divergences in the absorbance spectrum of the TRC from the RC are consistent with previously reported absorbance spectra. Furthermore, the TRC structure from *T. tepidum* is associated with a tetraheme cyt *c*-type protein bound to the P-side, which has been shown to increase the TRC stability (Kobayashi et al., 2005); however, this cyt was not expressed in my work on *R. sphaeroides*.

The charge-separated state of the TRC was measured, which indicates electron transfer through the A-branch to either the primary or secondary quinone. Recall that the TRC assembles with a menaquinone-8 at Q_A and an ubiquinone at Q_B (Nogi et al., 2000), and *R. sphaeroides* does not synthesis the former. As seen in Figure 3.33, a partial charge separation was detected, even without reconstituting the Q_A pocket with menadione. Perhaps the Q_A pocket was partially occupied due to the 10 μM menadione added to the culture medium during growth. Although possible, ubiquinone may have been inserted, but seems unlikely due to several differences in the headgroup (Figure 4.7). After reconstitution with 5-fold molar excess menadione, the charge separation was more complete, indicated by a further bleaching of the 875 nm P-band. At 10-fold molar excess, the bleaching was complete, as indicated by the complete loss of the P-band (data not shown). With the increasing concentrations of menadione, the Q_A pocket was likely reconstituted with menadione and/or replaced loosely bound ubiquinones (Graige et al., 1996).

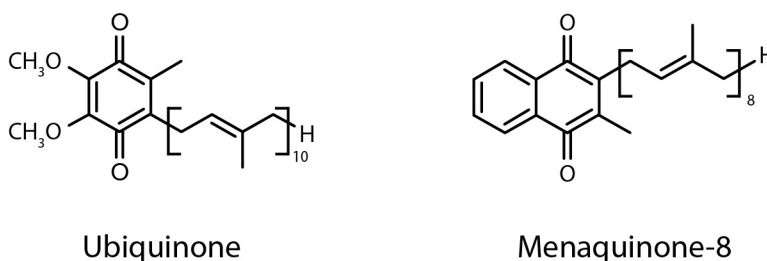


Figure 4.7. Structures of ubiquinone and menaquinone. Ubiquinone is derived from benzoquinone and has a tail with 10 isoprenoid units, whereas menaquinone is derived from naphthoquinone and has 8 isoprenoid units.

The successful expression, purification, and functional assembly of the TRC in *R. sphaeroides* now provides a platform for studying this pigment-protein complex without

resorting to the more complicated growth conditions of *T. tepidum* and the lack of a genetic manipulation system, such as the addition of a His-tag for purification, in this species.

4.4.2 Reduced levels of TLH1 and selection of phototrophy-capable mutants.

The largest contributing factor in core complex stability is TLH1 (Kimura et al., 2009), and so the genes encoding TLH1 were inserted into the pIND4 plasmid. Since the H, L, and M subunits were expressed and assembled into a TRC using the same ribosomal binding site containing the Shine-Dalgarno sequence, the same sequence was used to drive translation of the TLH1 $\alpha\beta$ polypeptides. No TLH1 was detected from pIND4-rbsTRCT1 (Figure 3.35), although there was evidence that the transcript was produced, as the TRC genes flanked the TLH1 genes, and TRCs were created. Furthermore, since all the genes had the same Shine-Dalgarno sequence, it was deduced that the $\alpha\beta$ polypeptides were translated, but did not assemble properly.

A different strategy involved using the *R. sphaeroides puf* operon, replacing the coding regions with *T. tepidum* sequences, and maintaining the *R. sphaeroides* non-coding genetic elements. This was chosen, since the analogous pIND4-RC1 is recognised by the host and produces high levels of RCs and LH1 complexes. Several different plasmids were constructed, with an RC, TLH1, and with or without PufX, a protein known to facilitate the formation of the core complex dimer. This approach yielded some TLH1, but at levels much less than the pIND4-RC1 control. Replacement of the spheroidene carotenoid with spirilloxanthin, typically found in *T. tepidum* did not result in increased TLH1 levels, and so it was concluded that the carotenoid is not essential in the assembly of TLH1. UV irradiation was used to select for mutants that could grow under anaerobic, phototrophic conditions; this approach was more promising as it yielded mutants that produced more TLH1. However, since reduction of the TRC requires a bound tetraheme cyt *c*-type protein under phototrophic growth, it was not known whether the *R. sphaeroides* cyt *c*₂ could be used as a viable replacement.

Despite selection of a phototrophic-capable mutant after UV irradiation, the levels of RC to TLH1 were not similar to that of the wild type RC to LH1. This presented an interesting case where there were not enough TLH1 units to encircle each RC. Recent data have shown that once LH1 units begin to assemble around a core RC, the assembly goes to completion (Mothersole et al., 2016). It was assumed, therefore, that there were two populations of RC-only, and RC-TLH1

pools. Sucrose gradients (Section 4.4.3) confirmed this assumption, because in the case of the RC-TLH1- X^+ a dominant, discrete band corresponding to the core complex was detected; this is in contrast to a smear or broad band in the gradient, which would be expected if there were a distribution of partially encircled RCs.

In *R. sphaeroides*, the assembly of LH1 and LH2 units is assisted by the assembly proteins LhaA and PucC, respectively; in the absence of either protein, phototrophic growth is impaired, but not abolished, suggesting that LhaA and PucC are not required for the formation of core complex (Mothersole et al., 2016). No *lhaA* homologue was found in the *T. tepidum* genome, although, a *pucC* homologue was found (genome sequence kindly provided by Dr. Wesley Swingley). Whether the *T. tepidum* PucC is specific for just LH2 or also assembles LH1 units is a question that was not explored; however, although the exact functions of LhaA and PucC are not known, both permit or assist in the assembly of the other light harvesting complex in *R. sphaeroides* (Mothersole et al., 2016). It is possible that in *R. sphaeroides*, LhaA and/or PucC did not recognise the *T. tepidum* $\alpha\beta$ polypeptides after translation, resulting in low-efficiency assembly of TLH1 around the RC. The heterologous expression of photosynthetic pigment-protein complex genes may be more complicated than initially believed, especially because the assembly of translated products may not be recognised well by the host. At least with the TLH1, there is a viable strategy of increasing levels by using UV mutagenesis to select for a mutant capable of phototrophic growth. Expression may also be improved by including the tetraheme cytochrome gene *TpufC*, and/or using as a platform the genetically tractable species *Rubrivivax gelatinosus* that assembles an RC that contains a bound tetraheme cyt *c*.

4.4.3 The PufX protein may not be involved in the assembly of hybrid core complexes.

In *R. sphaeroides*, the role of the PufX protein is believed to facilitate formation of the dimeric form of the RC-LH1 core complex, and produce a gap in the encircling LH1 assembly to allow quinones to diffuse in and out of the complex; the monomeric form is created in a *pufX* gene knockout, and does not support phototrophic growth, validating the observation that PufX is required for quinone diffusion (Holden-Dye et al., 2008). The *T. tepidum* core complex, however, is found as a monomer. Despite lacking a PufX homologue, the closed-ring monomeric

form still supports phototrophic growth and current crystallographic data show gaps between TLH1 $\alpha\beta$ dimers that are thought to allow for the passage of quinones (Niwa et al., 2014).

From Section 3.4.4, the data show that the RC-TLH1- X^+ and RC-TLH1- X^- variants were capable of phototrophic-growth after UV irradiation and/or selection under anaerobic, phototrophic conditions. Since PufX is required for phototrophic growth using the RC-LH1- X^+ core complex, the question was whether PufX played a role in the assembly of the hybrid core complexes; *i.e.*, was phototrophic growth and quinone exchange supported by the break in the TLH1 ring by PufX, as in the wild type RC-LH1- X^+ , or the gaps between the TLH1 $\alpha\beta$ dimers?

Sucrose gradients of the control RC-LH1- X^+ (dimer) and RC-LH1- X^- (monomer), show the relative differences in sedimentation (Figure 3.39). As expected, the RC-LH1- X^+ dimer form, which is twice the molecular weight of the monomer, sedimented farther than the monomer. Surprisingly, the predominant band of the RC-TLH1- X^+ migrated most similar to the RC-LH1- X^- monomer. The other faint bands are most likely contamination given that solubilised membranes of the hybrid core complexes were run in the gradient, rather than purified protein. Absorbance spectroscopy of the RC-TLH1- X^+ dominant band showed the characteristic RC and TLH1 peaks and ratio (data not shown). Perplexingly, the RC-TLH1- X^- , which does not have a gene encoding the PufX protein and expected to sediment similar to the RC-LH1- X^- monomer, did not sediment as either the monomer or dimer forms of the control.

Although it is not possible to discount PufX in the final assembled protein structure of RC-TLH1- X^+ , the sedimentation as a monomer form is indicative of a structure that lacks PufX. Furthermore, the encirclement of the RC by LH1 in the wild type begins with PufX associating with the LH1 α polypeptide (Mothersole et al., 2016). Given that a PufX homologue does not exist in *T. tepidum*, it was assumed that PufX would not associate well with TLH1 α and β polypeptides. The monomer form of the hybrid core complex supported phototrophic growth, which, therefore, indicates that the channels between the TLH1 $\alpha\beta$ dimers do permit the diffusion of quinones. Similar results have been found in *R. sphaeroides* and *Rhodobacter capsulatus*, where a knockout of *pufX* resulted in abolishment of phototrophic-growth and mutagenesis resulted in suppressor mutants that partially restored phototrophic growth; the mutations were in the LH1 α and β polypeptides, which may have produced enlarged holes for quinones to diffuse through the LH1 ring in the absence of PufX (Barz and Oesterhelt, 1994;

Lilburn et al., 1995). In the case of the RC-TLH1- X^+ , the DNA sequence of the *puf* genes *in trans* did not reveal any mutations, indicating no structural mutations were involved.

Note that although the RC-TLH1- X^+ is believed to be in the monomeric form and therefore lack a PufX protein, I use “ X^+ ” as a naming convention.

4.4.4 Thermal stability of hybrid core complexes.

The purpose of creating the different RC-TLH1- X^+ , RC-TLH1- X^- , TRC-TLH1- X^+ and TRC-TLH1- X^- mutants was to determine which would be most tolerant to heat compared to the native RC-LH1- X^+ . It was determined previously that the TRC has a similar tolerance to heat as the RC (Watson et al., 2005b), and the addition of TLH1 and Ca^{2+} ions were the components necessary to increase thermal stability (Kimura et al., 2009). Therefore, the relatively simple addition of adding a TLH1 ring structure around a core RC in theory could make it highly advantageous in solar photovoltaic applications, especially since the majority of electron transfer mutants have been studied in the RC.

The RC-LH1- X^+ (dimer) and RC-LH1- X^- (monomer) were used as controls. As shown in Figure 3.41, about half of the RC-LH1- X^+ core complex denatured within four minutes and showed essentially full denaturation after one hour. As generally expected with proteins from mesophiles, the RC-LH1- X^+ did not show great tolerance to heat above 30 °C, the ideal growth temperature. In contrast, the monomeric form, RC-LH1- X^- performed much better than its dimeric counterpart and did not sustain losses of more than 50%, even after one hour at 70 °C. This result may be due to the formation of a rigid core complex surrounded by a homogenous ring of LH1 and decreased flexibility possibly due to a single, planar core, rather than the larger, bent conformation of the dimer with a gap in the ring structure due to PufX (Qian et al., 2013), which might be more susceptible to increasing thermal energies.

The controls showed more stability than the published data of the TRC-TLH1 core complex at 70 °C. It would be expected that the TRC-TLH1 as from the native organism would be the most tolerant of heat, but the TRC-TLH1 showed complete denaturation within 20 min (Kimura et al., 2009), whereas the RC-LH1- X^+ denaturation took about an hour and the RC-LH1- X^- did not go below 50% during the same period. One possible reason for the increased thermal enhancement of the mesophilic complexes may be the use of the non-ionic DDM

detergent, whereas the zwitterionic detergent *n*-decylphosphocholine was used in the publication for TRC-TLH1. Previous reports suggest that DDM has a stabilising affect on the RC compared to other zwitterionic detergents, such as LDAO (Swainsbury et al., 2014).

The RC-TLH1- X^+ hybrid core complex was purified and assessed for its thermal stability. The RC-TLH1- X^+ complex showed even greater heat tolerance than the RC-LH1- X^- at 70 °C (Figure 3.41D). Granted, data from the sucrose gradient indicated that, despite the presence of a PufX protein, the monomeric form dominated. As seen from the RC-LH1- X^+ and RC-LH1- X^- controls, the monomeric form is more heat resistant than the dimeric form, presumably because the closed ring form provides greater stability. The additional higher heat tolerance over RC-LH1- X^- may be attributed to the TLH1 that substituted for LH1. The slow phase half-time constants suggest that the RC-TLH1- X^+ form was the least susceptible to heat degradation (Table 3.4). The results of these experiments show that, in principle, the strategy of adding heat stable TLH1 to an RC core can be used to improve the heat tolerance of the RC complex.

These early results open the way to investigating other changes to improve heat stability. A TRC-TLH1 that contains the bound cyt *c*, if it can be purified from *R. sphaeroides*, may yield even better tolerance to heat given that the protein-protein interactions between the TRC and TLH1 found naturally should be stronger than the hybrid complex of RC and TLH1. Furthermore, other groups have investigated the use of detergents, such as DDM, or non-detergent molecules, such as styrene maleic acid copolymer to stabilise the pigment-protein complexes in the presence of light or heat (Swainsbury et al., 2014). At the time of writing, in collaboration with Michael Carlson from the Duong laboratory in the Department of Biochemistry and Molecular Biology (UBC), nanodisc scaffold proteins were used in place of detergent, and we found that the heat-stability of the RC was increased (data not shown). Another approach would be to use complexes from other thermophilic species, such as *Chloroflexus aurantiacus*. Both the *R. sphaeroides* RC and *T. tepidum* TRC are not stable over 40 °C, whereas the RC from *C. aurantiacus* is able to withstand temperatures of 70 °C (Pierson et al., 1983). A combination of these different approaches may result in a heat-stabile complex, making it highly suitable to applications in solar technology, where degradation due to heat is an issue.

Chapter 5: Conclusion and Future Directions

The primary focus of my project was to determine whether electrons of different electric potentials could be extracted from the H_A, Q_A, and Q_B regions, or delivered into the P region of the RC. Answering this question involved several steps, such as creating a protein expression system capable of easily generating multiple RC mutants and purification with high yields. Although a 35-fold increase over the previous system was a welcome improvement, other additional improvements could be made to further increase yields or reduce cost, especially if proteins are to be isolated at large-scale industrial levels. For example, there are well-defined high-cell-density culture systems established for *E. coli*, which may be useful for *R. sphaeroides* to increase cell density. Also, using IPTG at 1 mM is about half the total cost of the culture media per unit volume, and so reducing the cost would be a high priority.

To extract electrons directly from the quinone region of the RC, the cytoplasmic domain of the H subunit was removed. Although a bit distant from my main focus, the question of whether this domain of H is necessary for RC assembly was nevertheless biologically and evolutionarily interesting. Though my data showed that most mutants were assembled and some capable of phototrophy, other questions remain. For example, what is the relationship between PufX and the H subunit of the RC? Do the core complexes with the truncated H subunit properly assemble the dimer form? Does the position of PufX change depending on the truncation length? How closely do the predicted structural changes correspond to a solved structure of the truncated mutants?

The photochronoamperometry measurements of the mutant RCs showed that electrons could be extracted directly from P, H_A, Q_A, and Q_B, or injected into P. Of particular interest is the extraction of electrons from H_A, as this is the first report of successful electron transfer from H_A to an electrode. The artificial electron pathway has not been fully characterised, although I presented a hypothesis that the Trp at L100 may be mediating electron transfer from H_A to the electrode. Further study is required, such as replacing the Trp with a Phe to demonstrate whether Trp plays a role in electron transfer, and results from this study would be a further validation of biological electron transfer mechanisms proposed by H. Gray. As a proof-of-principle, my results show that RC mutants can be bound in multiple orientations and that the mutants appear to donate electrons quite readily. The next step, on the engineering side, is to optimise

photocurrent generation. There are several different approaches, such as better coverage of the electrodes, a multi-protein-layer approach, or using mesoporous electrodes to increase surface area, naming a few, which may result in increased currents.

A system of heterologously expressing the *T. tepidum* genes was shown to assemble the TRC in *R. sphaeroides*. However, given the difficulty in purifying the core complex containing the TLH1, further work should include creating a more exposed His-tag for affinity chromatography by lengthening or moving the tag to a more accessible location. The hybrid core complex containing the *R. sphaeroides* RC and *T. tepidum* TLH1 had higher stability than the analogous *R. sphaeroides* RC-LH1 core complex. The results indicated that the addition of TLH1 did improve thermal stability overall, and other approaches could be used in conjunction to reduce the rate of denaturation further. For example, preliminary work on using nanodisc scaffold peptides (not shown) has shown greater stability of the RC compared to the RC solubilised in detergent.

References

- Abresch, E.C., Axelrod, H.L., Beatty, J.T., Johnson, J.A., Nechushtai, R., and Paddock, M.L. (2005). Characterization of a highly purified, fully active, crystallizable RC-LH1-PufX core complex from *Rhodobacter sphaeroides*. *Photosynth Res* 86, 61-70.
- Adelroth, P., Paddock, M.L., Sagle, L.B., Feher, G., and Okamura, M.Y. (2000). Identification of the proton pathway in bacterial reaction centers: both protons associated with reduction of QB to QBH₂ share a common entry point. *Proc Natl Acad Sci U S A* 97, 13086-13091.
- Adelroth, P., Paddock, M.L., Tehrani, A., Beatty, J.T., Feher, G., and Okamura, M.Y. (2001). Identification of the proton pathway in bacterial reaction centers: decrease of proton transfer rate by mutation of surface histidines at H126 and H128 and chemical rescue by imidazole identifies the initial proton donors. *Biochemistry* 40, 14538-14546.
- Agalidis, I., and Reiss-Husson, F. (1983). Several properties of the LM unit extracted with sodium dodecyl sulfate from *Rhodospseudomonas sphaeroides* purified reaction centers. *Biochimica et Biophysica Acta (BBA) - Bioenergetics* 724, 340-351.
- Alharbi, F.H., and Kais, S. (2015). Theoretical limits of photovoltaics efficiency and possible improvements by intuitive approaches learned from photosynthesis and quantum coherence. *Renewable and Sustainable Energy Reviews* 43, 1073-1089.
- Allen, J.F. (2003). Cyclic, pseudocyclic and noncyclic photophosphorylation: new links in the chain. *Trends Plant Sci* 8, 15-19.
- Allen, J.P., Feher, G., Yeates, T.O., Komiya, H., and Rees, D.C. (1987a). Structure of the reaction center from *Rhodobacter sphaeroides* R-26: the cofactors. *Proc Natl Acad Sci U S A* 84, 5730-5734.
- Allen, J.P., Feher, G., Yeates, T.O., Komiya, H., and Rees, D.C. (1987b). Structure of the reaction center from *Rhodobacter sphaeroides* R-26: the protein subunits. *Proc Natl Acad Sci U S A* 84, 6162-6166.
- Arai, H., Roh, J.H., and Kaplan, S. (2008). Transcriptome dynamics during the transition from anaerobic photosynthesis to aerobic respiration in *Rhodobacter sphaeroides* 2.4.1. *J Bacteriol* 190, 286-299.
- Balabin, I.A., and Onuchic, J.N. (2000). Dynamically controlled protein tunneling paths in photosynthetic reaction centers. *Science* 290, 114-117.

- Barber, J. (2009). Photosynthetic energy conversion: natural and artificial. *Chem Soc Rev* 38, 185-196.
- Barz, W.P., and Oesterhelt, D. (1994). Photosynthetic deficiency of a *pufX* deletion mutant of *Rhodobacter sphaeroides* is suppressed by point mutations in the light-harvesting complex genes *pufB* or *pufA*. *Biochemistry* 33, 9741-9752.
- Beatty, J.T., and Gest, H. (1981). Biosynthetic and bioenergetic functions of citric acid cycle reactions in *Rhodospseudomonas capsulata*. *J Bacteriol* 148, 584-593.
- Bernaodat, F., Frelet-Barrand, A., Pochon, N., Dementin, S., Hivin, P., Boutigny, S., Rioux, J.B., Salvi, D., Seigneurin-Berny, D., Richaud, P., et al. (2011). Heterologous expression of membrane proteins: choosing the appropriate host. *PLoS One* 6, e29191.
- Blankenship, R.E. (2002). *Molecular Mechanisms of Photosynthesis*, 1st Edition edn (Blackwell Science Ltd).
- Blankenship, R.E., Tiede, D.M., Barber, J., Brudvig, G.W., Fleming, G., Ghirardi, M., Gunner, M.R., Junge, W., Kramer, D.M., Melis, A., et al. (2011). Comparing photosynthetic and photovoltaic efficiencies and recognizing the potential for improvement. *Science* 332, 805-809.
- Brandt, U., and Trumpower, B. (1994). The protonmotive Q cycle in mitochondria and bacteria. *Crit Rev Biochem Mol Biol* 29, 165-197.
- Brimacombe, C.A., Stevens, A., Jun, D., Mercer, R., Lang, A.S., and Beatty, J.T. (2013). Quorum-sensing regulation of a capsular polysaccharide receptor for the *Rhodobacter capsulatus* gene transfer agent (RcGTA). *Molecular Microbiology* 87, 802-817.
- Calvin, M., and Benson, A.A. (1948). The Path of Carbon in Photosynthesis. *Science* 107, 476-480.
- Chandler, D.E., Hsin, J., Harrison, C.B., Gumbart, J., and Schulten, K. (2008). Intrinsic curvature properties of photosynthetic proteins in chromatophores. *Biophys J* 95, 2822-2836.
- Chen, C.Y., Beatty, J.T., Cohen, S.N., and Belasco, J.G. (1988). An intercistronic stem-loop structure functions as an mRNA decay terminator necessary but insufficient for *puf* mRNA stability. *Cell* 52, 609-619.
- Chi, S.C., Mothersole, D.J., Dilbeck, P., Niedzwiedzki, D.M., Zhang, H., Qian, P., Vasilev, C., Grayson, K.J., Jackson, P.J., Martin, E.C., et al. (2015). Assembly of functional

- photosystem complexes in *Rhodobacter sphaeroides* incorporating carotenoids from the spirilloxanthin pathway. *Biochim Biophys Acta* 1847, 189-201.
- Cho, S.H., Youn, S.H., Lee, S.R., Yim, H.S., and Kang, S.O. (2004). Redox property and regulation of PpsR, a transcriptional repressor of photosystem gene expression in *Rhodobacter sphaeroides*. *Microbiology* 150, 697-706.
- Choudhary, M., and Kaplan, S. (2000). DNA sequence analysis of the photosynthesis region of *Rhodobacter sphaeroides* 2.4.1. *Nucleic Acids Res* 28, 862-867.
- Clifton, L.A., Skoda, M.W., Le Brun, A.P., Ciesielski, F., Kuzmenko, I., Holt, S.A., and Lakey, J.H. (2015). Effect of divalent cation removal on the structure of gram-negative bacterial outer membrane models. *Langmuir* 31, 404-412.
- Daldal, F., Mandaci, S., Winterstein, C., Myllykallio, H., Duyck, K., and Zannoni, D. (2001). Mobile cytochrome c2 and membrane-anchored cytochrome cy are both efficient electron donors to the cbb3- and aa3-type cytochrome c oxidases during respiratory growth of *Rhodobacter sphaeroides*. *J Bacteriol* 183, 2013-2024.
- Das, R., Kiley, P.J., Segal, M., Norville, J., Yu, A.A., Wang, L., Trammell, S.A., Reddick, L.E., Kumar, R., Stellacci, F., et al. (2004). Integration of Photosynthetic Protein Molecular Complexes in Solid-State Electronic Devices. *Nano Letters* 4, 1079-1083.
- Debus, R.J., Feher, G., and Okamura, M.Y. (1985). LM complex of reaction centers from *Rhodospseudomonas sphaeroides* R-26: characterization and reconstitution with the H subunit. *Biochemistry* 24, 2488-2500.
- den Hollander, M.J., Magis, J.G., Fuchsenberger, P., Aartsma, T.J., Jones, M.R., and Frese, R.N. (2011). Enhanced photocurrent generation by photosynthetic bacterial reaction centers through molecular relays, light-harvesting complexes, and direct protein-gold interactions. *Langmuir* 27, 10282-10294.
- Dierstein, R. (1983). Biosynthesis of pigment-protein complex polypeptides in bacteriochlorophyll-less mutant cells of *Rhodospseudomonas capsulata* YS. *FEBS Letters* 160, 281-286.
- Diner, B.A., Schenck, C.C., and De Vitry, C. (1984). Effect of inhibitors, redox state and isoprenoid chain length on the affinity of ubiquinone for the secondary acceptor binding

- site in the reaction centers of photosynthetic bacteria. *Biochimica et Biophysica Acta (BBA) - Bioenergetics* 766, 9-20.
- Donohue, T.J., and Kaplan, S. (1991). Genetic techniques in rhodospirillaceae. *Methods Enzymol* 204, 459-485.
- Dresselhaus, M.S., and Thomas, I.L. (2001). Alternative energy technologies. *Nature* 414, 332-337.
- Dutta, P.K., Lin, S., Loskutov, A., Levenberg, S., Jun, D., Saer, R., Beatty, J.T., Liu, Y., Yan, H., and Woodbury, N.W. (2014). Reengineering the optical absorption cross-section of photosynthetic reaction centers. *J Am Chem Soc* 136, 4599-4604.
- Dylla, N.P., Faries, K.M., Wyllie, R.M., Swenson, A.M., Hanson, D.K., Holten, D., Kirmaier, C., and Laible, P.D. (2016). Species differences in unlocking B-side electron transfer in bacterial reaction centers. *FEBS Lett* 590, 2515-2526.
- Elsen, S., Jaubert, M., Pignol, D., and Giraud, E. (2005). PpsR: a multifaceted regulator of photosynthesis gene expression in purple bacteria. *Mol Microbiol* 57, 17-26.
- Elsen, S., Swem, L.R., Swem, D.L., and Bauer, C.E. (2004). RegB/RegA, a highly conserved redox-responding global two-component regulatory system. *Microbiol Mol Biol Rev* 68, 263-279.
- Esser, L., Elberry, M., Zhou, F., Yu, C.A., Yu, L., and Xia, D. (2008). Inhibitor-complexed structures of the cytochrome bc1 from the photosynthetic bacterium *Rhodobacter sphaeroides*. *J Biol Chem* 283, 2846-2857.
- Falkowski, P., Scholes, R.J., Boyle, E., Canadell, J., Canfield, D., Elser, J., Gruber, N., Hibbard, K., Hogberg, P., Linder, S., et al. (2000). The global carbon cycle: a test of our knowledge of earth as a system. *Science* 290, 291-296.
- Feher, G. (1971). Some chemical and physical properties of a bacterial reaction center particle and its primary photochemical reactants. *Photochem Photobiol* 14, 373-387.
- Feick, R.G., and Shiozawa, J.A. (1990). A high-yield method for the isolation of hydrophobic proteins and peptides from polyacrylamide gels for protein sequencing. *Analytical Biochemistry* 187, 205-211.

- Feniouk, B.A., Cherepanov, D.A., Voskoboynikova, N.E., Mulkidjanian, A.Y., and Junge, W. (2002). Chromatophore vesicles of *Rhodobacter capsulatus* contain on average one F(O)F(1)-ATP synthase each. *Biophys J* 82, 1115-1122.
- Fiedor, L., Akahane, J., and Koyama, Y. (2004). Carotenoid-induced cooperative formation of bacterial photosynthetic LH1 complex. *Biochemistry* 43, 16487-16496.
- Fornari, C.S., and Kaplan, S. (1982). Genetic transformation of *Rhodospseudomonas sphaeroides* by plasmid DNA. *J Bacteriol* 152, 89-97.
- Freigassner, M., Pichler, H., and Glieder, A. (2009). Tuning microbial hosts for membrane protein production. *Microb Cell Fact* 8, 69.
- Frew, J.E., and Hill, H.A. (1988). Direct and indirect electron transfer between electrodes and redox proteins. *Eur J Biochem* 172, 261-269.
- Friebe, V.M., Delgado, J.D., Swainsbury, D.J.K., Gruber, J.M., Chanaewa, A., van Grondelle, R., von Hauff, E., Millo, D., Jones, M.R., and Frese, R.N. (2016). Bioelectronics: Plasmon-Enhanced Photocurrent of Photosynthetic Pigment Proteins on Nanoporous Silver (*Adv. Funct. Mater.* 2/2016). *Adv Funct Mater* 26, 284-284.
- Frolov, D., Wakeham, M.C., Andrizhiyevskaya, E.G., Jones, M.R., and van Grondelle, R. (2005). Investigation of B-branch electron transfer by femtosecond time resolved spectroscopy in a *Rhodobacter sphaeroides* reaction centre that lacks the Q(A) ubiquinone. *Biochim Biophys Acta* 1707, 189-198.
- Garcia-Asua, G., Cogdell, R.J., and Hunter, C.N. (2002). Functional assembly of the foreign carotenoid lycopene into the photosynthetic apparatus of *Rhodobacter sphaeroides*, achieved by replacement of the native 3-step phytoene desaturase with its 4-step counterpart from *Erwinia herbicola*. *Mol Microbiol* 44, 233-244.
- Gast, P., Hemelrijk, P., and Hoff, A.J. (1994). Determination of the number of detergent molecules associated with the reaction center protein isolated from the photosynthetic bacterium *Rhodospseudomonas viridis*. *FEBS Letters* 337, 39-42.
- Gast, P., Hemelrijk, P.W., Van Gorkom, H.J., and Hoff, A.J. (1996). The Association of Different Detergents with the Photosynthetic Reaction Center Protein of *Rhodobacter sphaeroides* R26 and the Effects on its Photochemistry. *European Journal of Biochemistry* 239, 805-809.

- Gest, H. (1993). History of concepts of the comparative biochemistry of oxygenic and anoxygenic photosyntheses. *Photosynth Res* 35, 87-96.
- Geyer, T., and Helms, V. (2006). A spatial model of the chromatophore vesicles of *Rhodobacter sphaeroides* and the position of the Cytochrome bc1 complex. *Biophys J* 91, 921-926.
- Giustini, M., Autullo, M., Mennuni, M., Palazzo, G., and Mallardi, A. (2012). Polymer-photosynthetic protein multilayer architectures for herbicide optical detection. *Sensor Actuat B-Chem* 163, 69-75.
- Goldsmith, J.O., and Boxer, S.G. (1996). Rapid isolation of bacterial photosynthetic reaction centers with an engineered poly-histidine tag. *Biochimica et Biophysica Acta (BBA) - Bioenergetics* 1276, 171-175.
- Goodwin, T.W., and Morton, R.A. (1946). The spectrophotometric determination of tyrosine and tryptophan in proteins. *Biochem J* 40, 628-632.
- Graige, M.S., Paddock, M.L., Bruce, J.M., Feher, G., and Okamura, M.Y. (1996). Mechanism of Proton-Coupled Electron Transfer for Quinone (QB) Reduction in Reaction Centers of *Rb. Sphaeroides*. *Journal of the American Chemical Society* 118, 9005-9016.
- Guo, Z., Woodbury, N.W., Pan, J., and Lin, S. (2012). Protein dielectric environment modulates the electron-transfer pathway in photosynthetic reaction centers. *Biophys J* 103, 1979-1988.
- Hanahan, D. (1983). Studies on transformation of *Escherichia coli* with plasmids. *J Mol Biol* 166, 557-580.
- Hanson, D.K., Mielke, D.L., and Laible, P.D. (2009). Chapter 3 Harnessing Photosynthetic Bacteria for Membrane Protein Production. In *Current Topics in Membranes* (Academic Press), pp. 51-82.
- Holden-Dye, K., Crouch, L.I., and Jones, M.R. (2008). Structure, function and interactions of the PufX protein. *Biochim Biophys Acta* 1777, 613-630.
- Hu, X., Ritz, T., Damjanovic, A., Autenrieth, F., and Schulten, K. (2002). Photosynthetic apparatus of purple bacteria. *Q Rev Biophys* 35, 1-62.
- Hughes, A.V., Rees, P., Heathcote, P., and Jones, M.R. (2006). Kinetic analysis of the thermal stability of the photosynthetic reaction center from *Rhodobacter sphaeroides*. *Biophys J* 90, 4155-4166.

- Hunter, C.N., Hundle, B.S., Hearst, J.E., Lang, H.P., Gardiner, A.T., Takaichi, S., and Cogdell, R.J. (1994). Introduction of new carotenoids into the bacterial photosynthetic apparatus by combining the carotenoid biosynthetic pathways of *Erwinia herbicola* and *Rhodobacter sphaeroides*. *J Bacteriol* 176, 3692-3697.
- Ind, A.C., Porter, S.L., Brown, M.T., Byles, E.D., de Beyer, J.A., Godfrey, S.A., and Armitage, J.P. (2009). Inducible-expression plasmid for *Rhodobacter sphaeroides* and *Paracoccus denitrificans*. *Appl Environ Microbiol* 75, 6613-6615.
- Inui, M., Nakata, K., Roh, J.H., Vertes, A.A., and Yukawa, H. (2003). Isolation and molecular characterization of pMG160, a mobilizable cryptic plasmid from *Rhodobacter blasticus*. *Appl Environ Microbiol* 69, 725-733.
- Iranpour, B. (2012). Gold electrode electrochemistry in protein based solar cells. In *Electrical and Computer Engineering* (University of British Columbia).
- Ishikita, H., and Knapp, E.W. (2005). Energetics of proton transfer pathways in reaction centers from *Rhodobacter sphaeroides*. The Glu-H173 activated mutants. *J Biol Chem* 280, 12446-12450.
- Jackson, J.A., Lin, S., Taguchi, A.K.W., Williams, J.C., Allen, J.P., and Woodbury, N.W. (1997). Energy Transfer in *Rhodobacter sphaeroides* Reaction Centers with the Initial Electron Donor Oxidized or Missing. *The Journal of Physical Chemistry B* 101, 5747-5754.
- Jakob-Grun, S., Radeck, J., and Braun, P. (2012). Ca(2+)-binding reduces conformational flexibility of RC-LH1 core complex from thermophile *Thermochromatium tepidum*. *Photosynth Res* 111, 139-147.
- Jankowiak, R., Rancova, O., Chen, J., Kell, A., Saer, R.G., Beatty, J.T., and Abramavicius, D. (2016). Mutation-Induced Changes in the Protein Environment and Site Energies in the (M)L214G Mutant of the *Rhodobacter sphaeroides* Bacterial Reaction Center. *J Phys Chem B* 120, 7859-7871.
- Jaschke, P.R., Saer, R.G., Noll, S., and Beatty, J.T. (2011). Modification of the genome of *Rhodobacter sphaeroides* and construction of synthetic operons. *Methods Enzymol* 497, 519-538.

- Jones, M.R. (2009). The petite purple photosynthetic powerpack. *Biochem Soc Trans* 37, 400-407.
- Jones, M.R., Fowler, G.J., Gibson, L.C., Grief, G.G., Olsen, J.D., Crielaard, W., and Hunter, C.N. (1992a). Mutants of *Rhodobacter sphaeroides* lacking one or more pigment-protein complexes and complementation with reaction-centre, LH1, and LH2 genes. *Mol Microbiol* 6, 1173-1184.
- Jones, M.R., Visschers, R.W., van Grondelle, R., and Hunter, C.N. (1992b). Construction and characterization of a mutant of *Rhodobacter sphaeroides* with the reaction center as the sole pigment-protein complex. *Biochemistry* 31, 4458-4465.
- Jun, D., Saer, R.G., Madden, J.D., and Beatty, J.T. (2014). Use of new strains of *Rhodobacter sphaeroides* and a modified simple culture medium to increase yield and facilitate purification of the reaction centre. *Photosynth Res* 120, 197-205.
- Kamran, M., Delgado, J.D., Friebe, V., Aartsma, T.J., and Frese, R.N. (2014). Photosynthetic protein complexes as bio-photovoltaic building blocks retaining a high internal quantum efficiency. *Biomacromolecules* 15, 2833-2838.
- Kamran, M., Friebe, V.M., Delgado, J.D., Aartsma, T.J., Frese, R.N., and Jones, M.R. (2015). Demonstration of asymmetric electron conduction in pseudosymmetrical photosynthetic reaction centre proteins in an electrical circuit. *Nat Commun* 6, 6530.
- Katilius, E., Turanchik, T., Lin, S., Taguchi, A.K.W., and Woodbury, N.W. (1999). B-Side Electron Transfer in a *Rhodobacter sphaeroides* Reaction Center Mutant in Which the B-Side Monomer Bacteriochlorophyll Is Replaced with Bacteriopheophytin. *The Journal of Physical Chemistry B* 103, 7386-7389.
- Keen, N.T., Tamaki, S., Kobayashi, D., and Trollinger, D. (1988). Improved broad-host-range plasmids for DNA cloning in gram-negative bacteria. *Gene* 70, 191-197.
- Khan, M.N. (1984). Kinetics and mechanism of the alkaline hydrolysis of maleimide. *J Pharm Sci* 73, 1767-1771.
- Khatypov, R.A., Vasilieva, L.G., Fufina, T.Y., Bolgarina, T.I., and Shuvalov, V.A. (2005). Substitution of isoleucine L177 by histidine affects the pigment composition and properties of the reaction center of the purple bacterium *Rhodobacter sphaeroides*. *Biochemistry (Mosc)* 70, 1256-1261.

- Kim, S.K., Mason, J.T., Knaff, D.B., Bauer, C.E., and Setterdahl, A.T. (2006). Redox properties of the *Rhodobacter sphaeroides* transcriptional regulatory proteins PpsR and AppA. *Photosynth Res* 89, 89-98.
- Kim, Y., Shin, S.A., Lee, J., Yang, K.D., and Nam, K.T. (2014). Hybrid system of semiconductor and photosynthetic protein. *Nanotechnology* 25, 342001.
- Kimura, Y., Inada, Y., Numata, T., Arikawa, T., Li, Y., Zhang, J.P., Wang, Z.Y., and Ohno, T. (2012). Metal cations modulate the bacteriochlorophyll-protein interaction in the light-harvesting 1 core complex from *Thermochromatium tepidum*. *Biochim Biophys Acta* 1817, 1022-1029.
- Kimura, Y., Yu, L.J., Hirano, Y., Suzuki, H., and Wang, Z.Y. (2009). Calcium ions are required for the enhanced thermal stability of the light-harvesting-reaction center core complex from thermophilic purple sulfur bacterium *Thermochromatium tepidum*. *J Biol Chem* 284, 93-99.
- Kirmaier, C., Gaul, D., DeBey, R., Holten, D., and Schenck, C.C. (1991). Charge separation in a reaction center incorporating bacteriochlorophyll for photoactive bacteriopheophytin. *Science* 251, 922-927.
- Kobayashi, M., Fujioka, Y., Mori, T., Terashima, M., Suzuki, H., Shimada, Y., Saito, T., Wang, Z.Y., and Nozawa, T. (2005). Reconstitution of photosynthetic reaction centers and core antenna-reaction center complexes in liposomes and their thermal stability. *Biosci Biotechnol Biochem* 69, 1130-1136.
- Koepke, J., Krammer, E.-M., Klinge, A.R., Sebban, P., Ullmann, G.M., and Fritzsche, G. (2007). pH Modulates the Quinone Position in the Photosynthetic Reaction Center from *Rhodobacter sphaeroides* in the Neutral and Charge Separated States. *Journal of Molecular Biology* 371, 396-409.
- Kondo, M., Iida, K., Dewa, T., Tanaka, H., Ogawa, T., Nagashima, S., Nagashima, K.V.P., Shimada, K., Hashimoto, H., Gardiner, A.T., et al. (2012). Photocurrent and Electronic Activities of Oriented-His-Tagged Photosynthetic Light-Harvesting/Reaction Center Core Complexes Assembled onto a Gold Electrode. *Biomacromolecules* 13, 432-438.
- Kondo, M., Nakamura, Y., Fujii, K., Nagata, M., Suemori, Y., Dewa, T., Iida, K., Gardiner, A.T., Cogdell, R.J., and Nango, M. (2007). Self-assembled monolayer of light-harvesting

- core complexes from photosynthetic bacteria on a gold electrode modified with alkanethiols. *Biomacromolecules* 8, 2457-2463.
- Kong, N., Gooding, J.J., and Liu, J. (2014). Protein sensors based on reversible π - π stacking on basal plane HOPG electrodes. *Journal of Solid State Electrochemistry* 18, 3379-3386.
- Kontur, W.S., Schackwitz, W.S., Ivanova, N., Martin, J., Labutti, K., Deshpande, S., Tice, H.N., Pennacchio, C., Sodergren, E., Weinstock, G.M., et al. (2012). Revised sequence and annotation of the *Rhodobacter sphaeroides* 2.4.1 genome. *J Bacteriol* 194, 7016-7017.
- Laible, P.D., Scott, H.N., Henry, L., and Hanson, D.K. (2004). Towards higher-throughput membrane protein production for structural genomics initiatives. *J Struct Funct Genomics* 5, 167-172.
- Lang, H.P., and Hunter, C.N. (1994). The Relationship between Carotenoid Biosynthesis and the Assembly of the Light-Harvesting Lh2 Complex in *Rhodobacter-Sphaeroides*. *Biochemical Journal* 298, 197-205.
- Larsen, R.A., Wilson, M.M., Guss, A.M., and Metcalf, W.W. (2002). Genetic analysis of pigment biosynthesis in *Xanthobacter autotrophicus* Py2 using a new, highly efficient transposon mutagenesis system that is functional in a wide variety of bacteria. *Archives of Microbiology* 178, 193-201.
- Lebedev, N., Trammell, S.A., Spano, A., Lukashev, E., Griva, I., and Schnur, J. (2006). Conductive wiring of immobilized photosynthetic reaction center to electrode by cytochrome C. *J Am Chem Soc* 128, 12044-12045.
- Lee, P.C., Holtzapfle, E., and Schmidt-Dannert, C. (2010). Novel activity of *Rhodobacter sphaeroides* spheroidene monooxygenase CrtA expressed in *Escherichia coli*. *Appl Environ Microbiol* 76, 7328-7331.
- Li, C., Wen, A., Shen, B., Lu, J., Huang, Y., and Chang, Y. (2011). FastCloning: a highly simplified, purification-free, sequence- and ligation-independent PCR cloning method. *BMC Biotechnology* 11, 92.
- Lilburn, T.G., Prince, R.C., and Beatty, J.T. (1995). Mutation of the Ser2 codon of the light-harvesting B870 alpha polypeptide of *Rhodobacter capsulatus* partially suppresses the pufX phenotype. *J Bacteriol* 177, 4593-4600.

- Lu, Y., Yuan, M., Liu, Y., Tu, B., Xu, C., Liu, B., Zhao, D., and Kong, J. (2005). Photoelectric performance of bacteria photosynthetic proteins entrapped on tailored mesoporous WO₃-TiO₂ films. *Langmuir* 21, 4071-4076.
- Lukashev, E.P., Nadochenko, V.A., Permenova, E.P., Sarkisov, O.M., and Rubin, A.B. (2007). Electron phototransfer between photosynthetic reaction centers of the bacteria *Rhodobacter sphaeroides* and semiconductor mesoporous TiO₂ films. *Dokl Biochem Biophys* 415, 211-216.
- Lynn, S.P., Cohen, L.K., Gardner, J.F., and Kaplan, S. (1979). Characterization of a site-specific restriction endonuclease from *Rhodospseudomonas sphaeroides*. *J Bacteriol* 138, 505-509.
- Ma, F., Kimura, Y., Yu, L.J., Wang, P., Ai, X.C., Wang, Z.Y., and Zhang, J.P. (2009). Specific Ca²⁺-binding motif in the LH1 complex from photosynthetic bacterium *Thermochromatium tepidum* as revealed by optical spectroscopy and structural modeling. *FEBS J* 276, 1739-1749.
- Ma, F., Kimura, Y., Zhao, X.H., Wu, Y.S., Wang, P., Fu, L.M., Wang, Z.Y., and Zhang, J.P. (2008). Excitation dynamics of two spectral forms of the core complexes from photosynthetic bacterium *Thermochromatium tepidum*. *Biophys J* 95, 3349-3357.
- Mackenzie, C., Choudhary, M., Larimer, F.W., Predki, P.F., Stilwagen, S., Armitage, J.P., Barber, R.D., Donohue, T.J., Hosler, J.P., Newman, J.E., et al. (2001). The home stretch, a first analysis of the nearly completed genome of *Rhodobacter sphaeroides* 2.4.1. *Photosynthesis Research* 70, 19-41.
- Madigan, M.T. (1984). A novel photosynthetic purple bacterium isolated from a yellowstone hot spring. *Science* 225, 313-315.
- Magis, G.J., Olsen, J.D., Reynolds, N.P., Leggett, G.J., Hunter, C.N., Aartsma, T.J., and Frese, R.N. (2011). Use of engineered unique cysteine residues to facilitate oriented coupling of proteins directly to a gold substrate. *Photochem Photobiol* 87, 1050-1057.
- Mahmoudzadeh, A., Saer, R., Jun, D., Mirvakili, S.M., Takshi, A., Iranpour, B., Ouellet, E., Lagally, E.T., Madden, J.D.W., and Beatty, J.T. (2011). Photocurrent generation by direct electron transfer using photosynthetic reaction centres. *Smart Mater Struct* 20.
- Marcus, R.A. (1992). The Nobel Prize in Chemistry 1992. In *Nobelprizeorg* (Nobel Media AB).

- Martin, J.L., Breton, J., Hoff, A.J., Migus, A., and Antonetti, A. (1986). Femtosecond spectroscopy of electron transfer in the reaction center of the photosynthetic bacterium *Rhodospseudomonas sphaeroides* R-26: Direct electron transfer from the dimeric bacteriochlorophyll primary donor to the bacteriopheophytin acceptor with a time constant of 2.8 +/- 0.2 psec. *Proc Natl Acad Sci U S A* 83, 957-961.
- McAuley, K.E., Fyfe, P.K., Ridge, J.P., Cogdell, R.J., Isaacs, N.W., and Jones, M.R. (2000). Ubiquinone binding, ubiquinone exclusion, and detailed cofactor conformation in a mutant bacterial reaction center. *Biochemistry* 39, 15032-15043.
- McEwan, A.G. (1994). Photosynthetic electron transport and anaerobic metabolism in purple non-sulfur phototrophic bacteria. *Antonie Van Leeuwenhoek* 66, 151-164.
- Michel, H., Epp, O., and Deisenhofer, J. (1986). Pigment-protein interactions in the photosynthetic reaction centre from *Rhodospseudomonas viridis*. *EMBO J* 5, 2445-2451.
- Mirvakili, S.M., Slota, J.E., Usgaocar, A.R., Mahmoudzadeh, A., Jun, D., Mirvakili, M.N., Beatty, J.T., and Madden, J.D.W. (2014). Photoactive Electrodes Incorporating Electrospayed Bacterial Reaction Centers. *Adv Funct Mater* 24, 4789-4794.
- Moore, L.J., and Boxer, S.G. (1998). Inter-chromophore interactions in pigment-modified and dimer-less bacterial photosynthetic reaction centers. *Photosynthesis Research* 55, 173-180.
- Moser, C.C., Keske, J.M., Warncke, K., Farid, R.S., and Dutton, P.L. (1992). Nature of Biological Electron-Transfer. *Nature* 355, 796-802.
- Moskalenko, A.A., Makhneva, Z.K., Fiedor, L., and Scheer, H. (2005). Effects of carotenoid inhibition on the photosynthetic RC-LH1 complex in purple sulphur bacterium *Thiorhodospira sibirica*. *Photosynth Res* 86, 71-80.
- Mothersole, D.J., Jackson, P.J., Vasilev, C., Tucker, J.D., Brindley, A.A., Dickman, M.J., and Hunter, C.N. (2016). PucC and LhaA direct efficient assembly of the light-harvesting complexes in *Rhodobacter sphaeroides*. *Molecular Microbiology* 99, 307-327.
- Moulton, S.E., Barisci, J.N., Bath, A., Stella, R., and Wallace, G.G. (2003). Investigation of protein adsorption and electrochemical behavior at a gold electrode. *Journal of Colloid and Interface Science* 261, 312-319.
- Naylor, G.W., Adlesee, H.A., Gibson, L.C.D., and Hunter, C.N. (1999). The photosynthesis gene cluster of *Rhodobacter sphaeroides*. *Photosynthesis Research* 62, 121-139.

- Nicholson, R.S. (1965). Theory and Application of Cyclic Voltammetry for Measurement of Electrode Reaction Kinetics. *Analytical Chemistry* 37, 1351-1355.
- Niederman, R.A. (2013). Membrane development in purple photosynthetic bacteria in response to alterations in light intensity and oxygen tension. *Photosynth Res* 116, 333-348.
- Niederman, R.A. (2016). Development and dynamics of the photosynthetic apparatus in purple phototrophic bacteria. *Biochim Biophys Acta* 1857, 232-246.
- Niwa, S., Yu, L.J., Takeda, K., Hirano, Y., Kawakami, T., Wang-Otomo, Z.Y., and Miki, K. (2014). Structure of the LH1-RC complex from *Thermochromatium tepidum* at 3.0 Å. *Nature* 508, 228-232.
- Nogi, T., Fathir, I., Kobayashi, M., Nozawa, T., and Miki, K. (2000). Crystal structures of photosynthetic reaction center and high-potential iron-sulfur protein from *Thermochromatium tepidum*: thermostability and electron transfer. *Proc Natl Acad Sci U S A* 97, 13561-13566.
- Oda, I., Iwaki, M., Fujita, D., Tsutsui, Y., Ishizaka, S., Dewa, M., Nango, M., Kajino, T., Fukushima, Y., and Itoh, S. (2010). Photosynthetic electron transfer from reaction center pigment-protein complex in silica nanopores. *Langmuir* 26, 13399-13406.
- Okamura, M.Y., Paddock, M.L., Graige, M.S., and Feher, G. (2000). Proton and electron transfer in bacterial reaction centers. *Biochim Biophys Acta* 1458, 148-163.
- Olsen, J.D., Tucker, J.D., Timney, J.A., Qian, P., Vassilev, C., and Hunter, C.N. (2008). The organization of LH2 complexes in membranes from *Rhodobacter sphaeroides*. *J Biol Chem* 283, 30772-30779.
- Onoda, T., Enokizono, J., Kaya, H., Oshima, A., Freestone, P., and Norris, V. (2000). Effects of calcium and calcium chelators on growth and morphology of *Escherichia coli* L-form NC-7. *J Bacteriol* 182, 1419-1422.
- Operamolla, A., Ragni, R., Milano, F., Roberto Tangorra, R., Antonucci, A., Agostiano, A., Trotta, M., and Farinola, G. (2015). "Garnishing" the photosynthetic bacterial reaction center for bioelectronics. *Journal of Materials Chemistry C* 3, 6471-6478.
- Paddock, M.L., Feher, G., and Okamura, M.Y. (2003a). Proton transfer pathways and mechanism in bacterial reaction centers. *FEBS Lett* 555, 45-50.

- Paddock, M.L., Sagle, L., Tehrani, A., Beatty, J.T., Feher, G., and Okamura, M.Y. (2003b). Mechanism of proton transfer inhibition by Cd(2+) binding to bacterial reaction centers: determination of the pK(A) of functionally important histidine residues. *Biochemistry* 42, 9626-9632.
- Pan, J., Saer, R., Lin, S., Beatty, J.T., and Woodbury, N.W. (2016). Electron Transfer in Bacterial Reaction Centers with the Photoactive Bacteriopheophytin Replaced by a Bacteriochlorophyll through Coordinating Ligand Substitution. *Biochemistry* 55, 4909-4918.
- Pan, J., Saer, R.G., Lin, S., Guo, Z., Beatty, J.T., and Woodbury, N.W. (2013). The protein environment of the bacteriopheophytin anion modulates charge separation and charge recombination in bacterial reaction centers. *J Phys Chem B* 117, 7179-7189.
- Pemberton, J.M., Horne, I.M., and McEwan, A.G. (1998). Regulation of photosynthetic gene expression in purple bacteria. *Microbiology* 144 (Pt 2), 267-278.
- Pierson, B.K., Thornber, J.P., and Seftor, R.E.B. (1983). Partial purification, subunit structure and thermal stability of the photochemical reaction center of the thermophilic green bacterium *Chloroflexus aurantiacus*. *Biochimica et Biophysica Acta (BBA) - Bioenergetics* 723, 322-326.
- Qian, P., Hunter, C.N., and Bullough, P.A. (2005). The 8.5Å projection structure of the core RC-LH1-PufX dimer of *Rhodobacter sphaeroides*. *J Mol Biol* 349, 948-960.
- Qian, P., Papiz, M.Z., Jackson, P.J., Brindley, A.A., Ng, I.W., Olsen, J.D., Dickman, M.J., Bullough, P.A., and Hunter, C.N. (2013). Three-dimensional structure of the *Rhodobacter sphaeroides* RC-LH1-PufX complex: dimerization and quinone channels promoted by PufX. *Biochemistry* 52, 7575-7585.
- Ravi, S.K., and Tan, S.C. (2015). Progress and perspectives in exploiting photosynthetic biomolecules for solar energy harnessing. *Energy & Environmental Science* 8, 2551-2573.
- Reed, D.W., and Clayton, R.K. (1968). Isolation of a reaction center fraction from *Rhodospseudomonas spheroides*. *Biochem Biophys Res Commun* 30, 471-475.
- Reeder, B.J., Svistunenko, D.A., Cooper, C.E., and Wilson, M.T. (2012). Engineering tyrosine-based electron flow pathways in proteins: the case of *aplysia* myoglobin. *J Am Chem Soc* 134, 7741-7749.

- Ridge, J.P., van Brederode, M.E., Goodwin, M.G., Grondelle, R.v., and Jones, M.R. (1999). Mutations that modify or exclude binding of the QA ubiquinone and carotenoid in the reaction center from *Rhodobacter sphaeroides*. *Photosynthesis Research* 59, 9-26.
- Rigaud, J.L., Levy, D., Mosser, G., and Lambert, O. (1998). Detergent removal by non-polar polystyrene beads. *European Biophysics Journal* 27, 305-319.
- Robles, S.J., Breton, J., and Youvan, D.C. (1990). Partial symmetrization of the photosynthetic reaction center. *Science* 248, 1402-1405.
- Roszak, A.W., Howard, T.D., Southall, J., Gardiner, A.T., Law, C.J., Isaacs, N.W., and Cogdell, R.J. (2003). Crystal structure of the RC-LH1 core complex from *Rhodospseudomonas palustris*. *Science* 302, 1969-1972.
- Roszak, A.W., Moulisova, V., Reksodipuro, A.D., Gardiner, A.T., Fujii, R., Hashimoto, H., Isaacs, N.W., and Cogdell, R.J. (2012). New insights into the structure of the reaction centre from *Blastochloris viridis*: evolution in the laboratory. *Biochem J* 442, 27-37.
- Saer, R.G., Hardjasa, A., Rosell, F.I., Mauk, A.G., Murphy, M.E., and Beatty, J.T. (2013). Role of *Rhodobacter sphaeroides* photosynthetic reaction center residue M214 in the composition, absorbance properties, and conformations of H(A) and B(A) cofactors. *Biochemistry* 52, 2206-2217.
- Saggu, M., Carter, B., Zhou, X., Faries, K., Cegelski, L., Holten, D., Boxer, S.G., and Kirmaier, C. (2014). Putative hydrogen bond to tyrosine M208 in photosynthetic reaction centers from *Rhodobacter capsulatus* significantly slows primary charge separation. *J Phys Chem B* 118, 6721-6732.
- Savikhin, S., and Jankowiak, R. (2014). Mechanism of Primary Charge Separation in Photosynthetic Reaction Centers. In *The Biophysics of Photosynthesis*, J. Golbeck, and A. van der Est, eds. (New York, NY: Springer New York), pp. 193-240.
- Scheuring, S., Nevo, R., Liu, L.N., Mangenot, S., Charuvi, D., Boudier, T., Prima, V., Hubert, P., Sturgis, J.N., and Reich, Z. (2014). The architecture of *Rhodobacter sphaeroides* chromatophores. *Biochim Biophys Acta* 1837, 1263-1270.
- Schlegel, S., Hjelm, A., Baumgarten, T., Vikstrom, D., and de Gier, J.W. (2014). Bacterial-based membrane protein production. *Biochim Biophys Acta* 1843, 1739-1749.

- Shih, C., Museth, A.K., Abrahamsson, M., Blanco-Rodriguez, A.M., Di Bilio, A.J., Sudhamsu, J., Crane, B.R., Ronayne, K.L., Towrie, M., Vlcek, A., Jr., et al. (2008). Tryptophan-accelerated electron flow through proteins. *Science* 320, 1760-1762.
- Shuvalov, V.A., Shkuropatov, A.Y., Kulakova, S.M., Ismailov, M.A., and Shkuropatova, V.A. (1986). Photoreactions of bacteriopheophytins and bacteriochlorophylls in reaction centers of *Rhodospseudomonas sphaeroides* and *Chloroflexus aurantiacus*. *Biochimica et Biophysica Acta (BBA) - Bioenergetics* 849, 337-346.
- Simon, R., Priefer, U., and Puhler, A. (1983). A Broad Host Range Mobilization System for In Vivo Genetic Engineering: Transposon Mutagenesis in Gram Negative Bacteria. *Nat Biotech* 1, 784-791.
- Sockett, R.E., Donohue, T.J., Varga, A.R., and Kaplan, S. (1989). Control of photosynthetic membrane assembly in *Rhodobacter sphaeroides* mediated by *puhA* and flanking sequences. *J Bacteriol* 171, 436-446.
- Stilz, H.U., Finkle, U., Holzappel, W., Lauterwasser, C., Zinth, W., and Oesterhelt, D. (1994). Influence of M subunit Thr222 and Trp252 on quinone binding and electron transfer in *Rhodobacter sphaeroides* reaction centres. *Eur J Biochem* 223, 233-242.
- Strumpfer, J., and Schulten, K. (2009). Light harvesting complex II B850 excitation dynamics. *J Chem Phys* 131, 225101.
- Sun, C., Carey, A.-M., Gao, B.-R., Wraight, C.A., Woodbury, N.W., and Lin, S. (2016). Ultrafast Electron Transfer Kinetics in the LM Dimer of Bacterial Photosynthetic Reaction Center from *Rhodobacter sphaeroides*. *The Journal of Physical Chemistry B* 120, 5395-5404.
- Sun, C., Taguchi, A.T., Beal, N.J., O'Malley, P.J., Dikanov, S.A., and Wraight, C.A. (2015). Regulation of the Primary Quinone Binding Conformation by the H Subunit in Reaction Centers from *Rhodobacter sphaeroides*. *The Journal of Physical Chemistry Letters* 6, 4541-4546.
- Swainsbury, D.J., Scheidelaar, S., van Grondelle, R., Killian, J.A., and Jones, M.R. (2014). Bacterial reaction centers purified with styrene maleic acid copolymer retain native membrane functional properties and display enhanced stability. *Angew Chem Int Ed Engl* 53, 11803-11807.

- Takemoto, J., and Lascelles, J. (1973). Coupling Between Bacteriochlorophyll and Membrane Protein Synthesis in *Rhodospseudomonas spheroides*. *Proceedings of the National Academy of Sciences* 70, 799-803.
- Takshi, A., Madden, J.D.W., Mahmoudzadeh, A., Saer, R., and Beatty, J.T. (2010). A Photovoltaic Device Using an Electrolyte Containing Photosynthetic Reaction Centers. *Energies* 3, 1721-1727.
- Tan, S.C., Crouch, L.I., Mahajan, S., Jones, M.R., and Welland, M.E. (2012). Increasing the Open-Circuit Voltage of Photoprotein-Based Photoelectrochemical Cells by Manipulation of the Vacuum Potential of the Electrolytes. *Acs Nano* 6, 9103-9109.
- Tan, S.C., Yan, F., Crouch, L.I., Robertson, J., Jones, M.R., and Welland, M.E. (2013). Superhydrophobic Carbon Nanotube Electrode Produces a Near-Symmetrical Alternating Current from Photosynthetic Protein-Based Photoelectrochemical Cells. *Adv Funct Mater* 23, 5556-5563.
- Tehrani, A., Prince, R.C., and Beatty, J.T. (2003). Effects of photosynthetic reaction center H protein domain mutations on photosynthetic properties and reaction center assembly in *Rhodobacter sphaeroides*. *Biochemistry* 42, 8919-8928.
- Tehrani, A., and Thomas Beatty, J. (2004). Effects of Precise Deletions in *Rhodobacter sphaeroides* Reaction Center Genes on Steady-state Levels of Reaction Center Proteins: A Revised Model for Reaction Center Assembly. *Photosynthesis Research* 79, 101-108.
- Tiede, D.M., Vazquez, J., Cordova, J., and Marone, P.A. (1996). Time-resolved electrochromism associated with the formation of quinone anions in the *Rhodobacter sphaeroides* R26 reaction center. *Biochemistry* 35, 10763-10775.
- Trammell, S.A., Spano, A., Price, R., and Lebedev, N. (2006). Effect of protein orientation on electron transfer between photosynthetic reaction centers and carbon electrodes. *Biosens Bioelectron* 21, 1023-1028.
- Trammell, S.A., Wang, L.Y., Zullo, J.M., Shashidhar, R., and Lebedev, N. (2004). Orientated binding of photosynthetic reaction centers on gold using Ni-NTA self-assembled monolayers. *Biosens Bioelectron* 19, 1649-1655.

- van Brederode, M.E., van Stokkum, I.H., Katilius, E., van Mourik, F., Jones, M.R., and van Grondelle, R. (1999). Primary charge separation routes in the BChl:BPhe heterodimer reaction centers of *Rhodobacter sphaeroides*. *Biochemistry* 38, 7545-7555.
- van der Rest, M., and Gingras, G. (1974). The Pigment Complement of the Photosynthetic Reaction Center Isolated from *Rhodospirillum rubrum*. *Journal of Biological Chemistry* 249, 6446-6453.
- Varga, A.R., and Kaplan, S. (1993). Synthesis and stability of reaction center polypeptides and implications for reaction center assembly in *Rhodobacter sphaeroides*. *J Biol Chem* 268, 19842-19850.
- Wakeham, M.C., and Jones, M.R. (2005). Rewiring photosynthesis: engineering wrong-way electron transfer in the purple bacterial reaction centre. *Biochem Soc Trans* 33, 851-857.
- Warshel, A., Creighton, S., and Parson, W.W. (1988). Electron-transfer pathways in the primary event of bacterial photosynthesis. *The Journal of Physical Chemistry* 92, 2696-2701.
- Watson, A.J., Fyfe, P.K., Frolov, D., Wakeham, M.C., Nabdryk, E., van Grondelle, R., Breton, J., and Jones, M.R. (2005a). Replacement or exclusion of the B-branch bacteriopeophytin in the purple bacterial reaction centre: the H(B) cofactor is not required for assembly or core function of the *Rhodobacter sphaeroides* complex. *Biochim Biophys Acta* 1710, 34-46.
- Watson, A.J., Hughes, A.V., Fyfe, P.K., Wakeham, M.C., Holden-Dye, K., Heathcote, P., and Jones, M.R. (2005b). On the role of basic residues in adapting the reaction centre-LHI complex for growth at elevated temperatures in purple bacteria. *Photosynth Res* 86, 81-100.
- Williams, J.C., Alden, R.G., Murchison, H.A., Peloquin, J.M., Woodbury, N.W., and Allen, J.P. (1992). Effects of mutations near the bacteriochlorophylls in reaction centers from *Rhodobacter sphaeroides*. *Biochemistry* 31, 11029-11037.
- Winkler, A., Heintz, U., Lindner, R., Reinstein, J., Shoeman, R.L., and Schlichting, I. (2013). A ternary AppA-PpsR-DNA complex mediates light regulation of photosynthesis-related gene expression. *Nat Struct Mol Biol* 20, 859-867.
- Winkler, J.R., and Gray, H.B. (2014). Long-range electron tunneling. *J Am Chem Soc* 136, 2930-2939.

- Woronowicz, K., Olubanjo, O.B., Sung, H.C., Lamptey, J.L., and Niederman, R.A. (2012). Differential assembly of polypeptides of the light-harvesting 2 complex encoded by distinct operons during acclimation of *Rhodobacter sphaeroides* to low light intensity. *Photosynth Res* 111, 125-138.
- Wraight, C.A., and Stein, R.R. (1980). Redox equilibrium in the acceptor quinone complex of isolated reaction centers and the mode of action of O-phenanthroline. *FEBS Letters* 113, 73-77.
- Yaghoubi, H., Lafalce, E., Jun, D., Jiang, X., Beatty, J.T., and Takshi, A. (2015). Large photocurrent response and external quantum efficiency in biophotoelectrochemical cells incorporating reaction center plus light harvesting complexes. *Biomacromolecules* 16, 1112-1118.
- Yaghoubi, H., Li, Z., Jun, D., Saer, R., Slota, J.E., Beerbom, M., Schlaf, R., Madden, J.D., Beatty, J.T., and Takshi, A. (2012). The Role of Gold-Adsorbed Photosynthetic Reaction Centers and Redox Mediators in the Charge Transfer and Photocurrent Generation in a Bio-Photoelectrochemical Cell. *The Journal of Physical Chemistry C* 116, 24868-24877.
- Yeates, T.O., Komiya, H., Chirino, A., Rees, D.C., Allen, J.P., and Feher, G. (1988). Structure of the reaction center from *Rhodobacter sphaeroides* R-26 and 2.4.1: protein-cofactor (bacteriochlorophyll, bacteriopheophytin, and carotenoid) interactions. *Proc Natl Acad Sci U S A* 85, 7993-7997.
- Yehezkeili, O., Tel-Vered, R., Michaeli, D., Willner, I., and Nechushtai, R. (2014). Photosynthetic reaction center-functionalized electrodes for photo-bioelectrochemical cells. *Photosynth Res* 120, 71-85.
- Yin, L., Dragnea, V., and Bauer, C.E. (2012). PpsR, a Regulator of Heme and Bacteriochlorophyll Biosynthesis, Is a Heme-sensing Protein. *Journal of Biological Chemistry* 287, 13850-13858.
- Yu, Z.L., Yang, C.W., Triffaux, E., Doneux, T., Turner, R.F., and Bizzotto, D. (2016). Measuring and Remediating Nonspecific Modifications of Gold Surfaces Using a Coupled in Situ Electrochemical Fluorescence Microscopic Methodology. *Anal Chem*.
- Zeilstra-Ryalls, J.H., and Kaplan, S. (1995). Aerobic and anaerobic regulation in *Rhodobacter sphaeroides* 2.4.1: the role of the *fnrL* gene. *J Bacteriol* 177, 6422-6431.

Zhao, J.Q., Ma, N., Liu, B.H., Zhou, Y.L., Xu, C.H., and Kong, J.L. (2002).

Photoelectrochemistry of photosynthetic reaction centers embedded in Al₂O₃ gel. *J Photoch Photobio A* 152, 53-60.

Zhu, J., van Stokkum, I.H., Paparelli, L., Jones, M.R., and Groot, M.L. (2013). Early bacteriopheophytin reduction in charge separation in reaction centers of *Rhodobacter sphaeroides*. *Biophys J* 104, 2493-2502.

Appendices

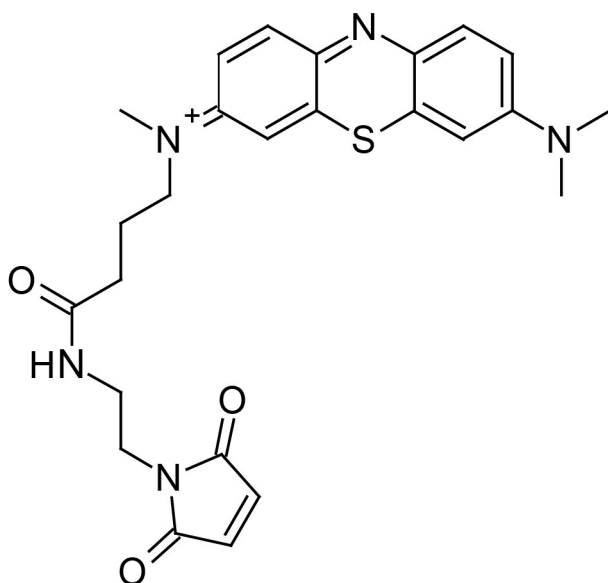
Appendix A

A.1 RC mutants and corresponding mutations used in the electron transfer studies.

RC	Mutations
Cys ⁻	C(H156)A, C(H234)S, C(L92)S, C(L108)S, C(L247)S
TM	Cys ⁻ , E(L27)C, N(274)C, E(M100)C
M256	Cys ⁻ , W(M252)F, M(M256)C, A(M260)W
M256-Cys	M256, A(H51)C, W(L59)C
M256/L121-Cys	M256-Cys, F(L121)W
45M-M229	Cys ⁻ , 45 H, F(M229)C
45M-M229/M226	45M-M229, V(M226)W
45M-L210	Cys ⁻ , 45 H, D(L210)C
45M-L210/L213	45M-L210, D(L213)C

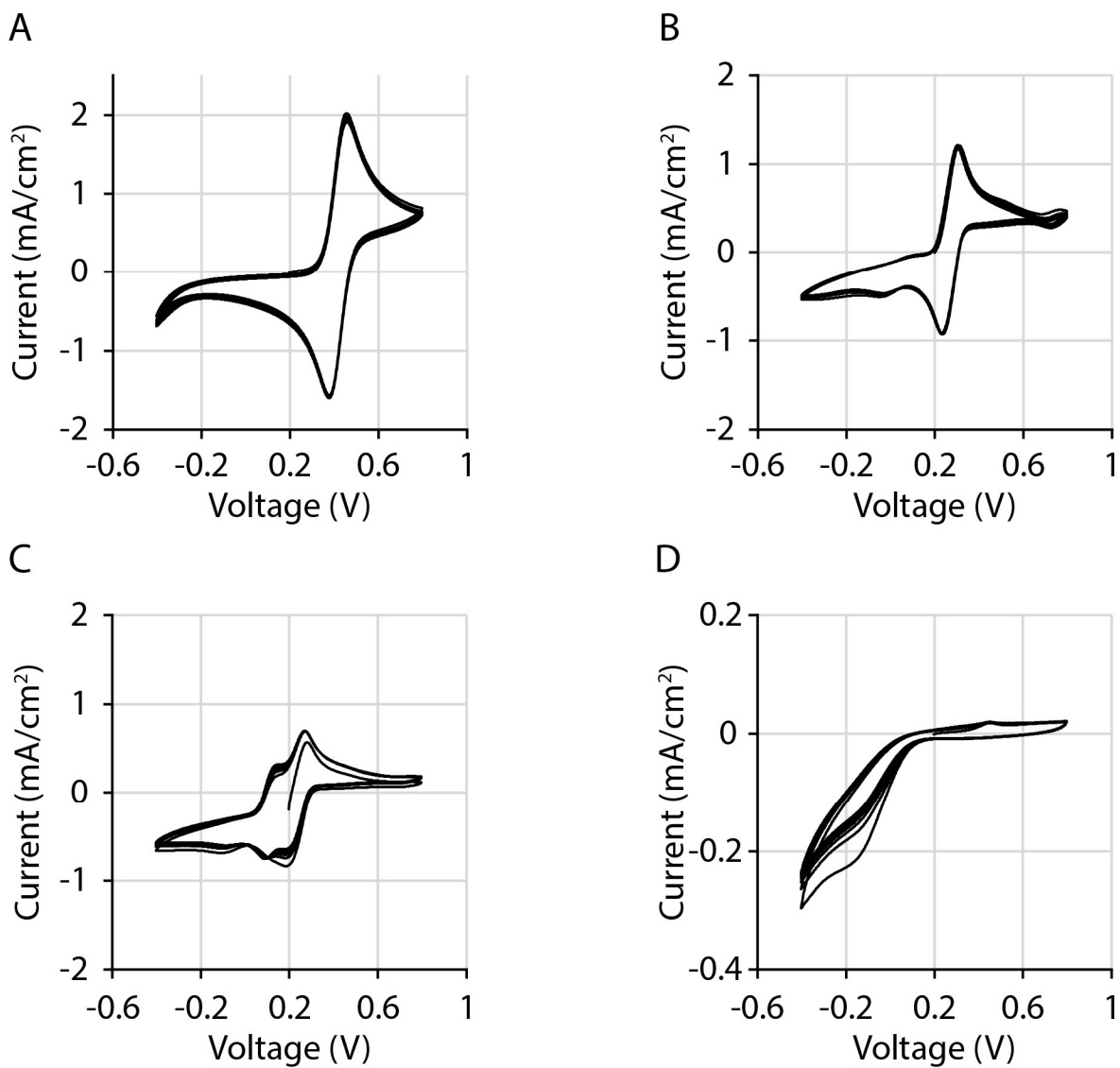
Appendix B

B.1 Chemical structure of the ATTO MB2 dye with a maleimide functional group.



Appendix C

C.1 CVs of different electron mediators in 1x PBS pH 7.2. A) 1 mM ferrocyanide, B) 1 mM hydroquinone, C) 1 mM benzoquinone, and D) 1 mM sodium ascorbate. CVs were swept at 100 mV/s and cycled 5 times. Potentials are with respect to the standard hydrogen electrode (SHE).



Appendix D

D.1 Residual plots of the two-phase exponential decay fits: A) RC-LH1- X^+ , B) RC-LH1- X^- , and C) RC-TLH1- X^+ .

